DOCTOR OF PHILOSOPHY

Novel di- and multitopic hydroxamate ligands towards discrete and extended network complexes

Mohammed, Baba Fugu

Award date:
2019

Awarding institution:
Bangor University

Novel di- and multitopic hydroxamate ligands towards discrete and extended network complexes

PRIFYSGOL
BANGOR
UNIVERSITY

Baba Fugu Mohammed

School of Natural Sciences

Bangor University

A thesis submitted to Bangor University
for the degree of Doctor of Philosophy

This work is dedicated to my parents,

wife and children.

Declaration and Consent

Details of the Work

I hereby agree to deposit the following item in the digital repository maintained by Bangor University and/or in any other repository authorized for use by Bangor University.

Author Name: Baba Fugu Mohammed

Title: Novel di- and multitopic hydroxamate ligands towards discrete and extended network magnetic complexes

Supervisor/Department: Dr Leigh F. Jones (SNS: Chemistry)

Funding body (if any): Petroleum Technology Development Fund (PTDF)

Qualification/Degree obtained: PhD in Chemistry

This item is a product of my own research endeavours and is covered by the agreement below in which the item is referred to as "the Work". It is identical in content to that deposited in the Library, subject to point 4 below.

Non-exclusive Rights

Rights granted to the digital repository through this agreement are entirely non-exclusive. I am free to publish the Work in its present version or future versions elsewhere.

I agree that Bangor University may electronically store, copy or translate the Work to any approved medium or format for the purpose of future preservation and accessibility. Bangor University is not under any obligation to reproduce or display the Work in the same formats or resolutions in which it was originally deposited.

Bangor University Digital Repository

I understand that work deposited in the digital repository will be accessible to a wide variety of people and institutions, including automated agents and search engines via the World Wide Web.

I understand that once the Work is deposited, the item and its metadata may be incorporated into public access catalogues or services, national databases of electronic theses and dissertations such as the British Library's EThOS or any service provided by the National Library of Wales.

I understand that the Work may be made available via the National Library of Wales Online Electronic Theses Service under the declared terms and conditions of use

(http://www.llgc.org.uk/index.php?id=4676). I agree that as part of this service the National Library of Wales may electronically store, copy or convert the Work to any approved medium or format for the purpose of future preservation and accessibility. The National Library of Wales is not under any obligation to reproduce or display the Work in the same formats or resolutions in which it was originally deposited.

Statement 1:

This work has not previously been accepted in substance for any degree and is not being concurrently submitted in candidature for any degree unless as agreed by the University for approved dual awards.

Signed …….. (candidate)

Date ……..

Statement 2:

This thesis is the result of my own investigations, except where otherwise stated. Where correction services have been used, the extent and nature of the correction is clearly marked in a footnote(s).Other sources are acknowledged by footnotes giving explicit references. A bibliography is appended.

Signed ……. (candidate)

Date …….

Statement 3:

I hereby give consent for my thesis, if accepted, to be available for photocopying, for inter-library loan and for electronic repositories, and for the title and summary to be made available to outside organisations.

Signed ……. (candidate)

Date …….

NB: Candidates on whose behalf a bar on access has been approved by the Academic Registry should use the following version of **Statement 3:**

Statement 3 (bar):

I hereby give consent for my thesis, if accepted, to be available for photocopying, for inter-library loans and for electronic repositories after expiry of a bar on access.

Signed …… (candidate)

Date ……

Statement 4:

Choose one of the following options

a) I agree to deposit an electronic copy of my thesis (the Work) in the Bangor University (BU) Institutional Digital Repository, the British Library ETHOS system, and/or in any other repository authorized for use by Bangor University and where necessary have gained the required permissions for the use of third party material.	
b) I agree to deposit an electronic copy of my thesis (the Work) in the Bangor University (BU) Institutional Digital Repository, the British Library ETHOS system, and/or in any other repository authorized for use by Bangor University when the approved bar on access has been lifted.	
c) I agree to submit my thesis (the Work) electronically via Bangor University's e-submission system, however I opt-out of the electronic deposit to the Bangor University (BU) Institutional Digital Repository, the British Library ETHOS system, and/or in any other repository authorized for use by Bangor University, due to lack of permissions for use of third party material.	

Options B should only be used if a bar on access has been approved by the University.

In addition to the above I also agree to the following:

1. That I am the author or have the authority of the author(s) to make this agreement and do hereby give Bangor University the right to make available the Work in the way described above.
2. That the electronic copy of the Work deposited in the digital repository and covered by this agreement, is identical in content to the paper copy of the Work deposited in the Bangor University Library, subject to point 4 below.

3. That I have exercised reasonable care to ensure that the Work is original and, to the best of my knowledge, does not breach any laws – including those relating to defamation, libel and copyright.

4. That I have, in instances where the intellectual property of other authors or copyright holders is included in the Work, and where appropriate, gained explicit permission for the inclusion of that material in the Work, and in the electronic form of the Work as accessed through the open access digital repository, or that I have identified and removed that material for which adequate and appropriate permission has not been obtained and which will be inaccessible via the digital repository.

5. That Bangor University does not hold any obligation to take legal action on behalf of the Depositor, or other rights holders, in the event of a breach of intellectual property rights, or any other right, in the material deposited.

6. That I will indemnify and keep indemnified Bangor University and the National Library of Wales from and against any loss, liability, claim or damage, including without limitation any related legal fees and court costs (on a full indemnity bases), related to any breach by myself of any term of this agreement.

Signature: ……

Date : …….

Table of Contents

Declaration and Consent 3

Table of Contents 7

List of Abbreviations 10

List of Figures 14

List of Schemes 17

List of Tables 18

Acknowledgements 19

Abstract 21

Chapter One 23

1.0 Introduction 24

1.1 Definition and history of magnetism 24

1.2 Magnetochemistry 27

1.2.1 Diamagnetism 27

1.2.2 Paramagnetism 27

1.2.3 Ferromagnetism 29

1.2.4 Antiferromagnetism 30

1.2.5 Ferrimagnetism 31

1.2.6 Pauli paramagnetism 32

1.3 Magnetization and magnetic susceptibility 32

1.3.1 Magnetic susceptibility for paramagnetic substances 34

1.3.2 Magnetic susceptibility of ferro-, ferri- and antiferromagnets 36

1.4 Molecular Magnetism 38

1.5 Single-Molecule Magnets 41

1.6 Single-Chain Magnets 43

1.7 Spin-crossover complexes 45

1.8 Coordination polymers 47
1.9 Magnetocaloric effect (MCE) 49
1.10 Hydroxamic acids: A brief history 50
1.10.1 Synthesis and reactivity of hydroxamic acids 51
1.10.2 Coordination chemistry of hydroxamic acids 53
1.11 Aims of the project 54
References 56
Chapter Two 66
2.0 Introduction 67
2.1 Results and Discussion 67
2.1.1 Ligand preparations 67
2.1.2 Metal complexations 69
2.13 Magnetic susceptibility studies 86
2.2 Concluding Remarks 91
2.3 Experimental Section 91
2.3.1 Single-crystal X-ray crystallography 92
2.3.2 Organic ligand preparation 93
2.3.3 Preparation of complexes **1**-**7**. 95
2.4 References 98
Chapter Three 100
3.1 Introduction 101
3.2 Result and Discussion 101
3.2.1 Ligands descriptions 102
3.2.2 Metal complexation 104
3.3 UV-Vis absorption and photoluminescence spectra of complex **9** 117
3.4 Magnetic studies 123
3.6 Experimental Section 125

3.6.2 Organic ligand preparation 127
3.6.3 Preparation of complexes **8-12**. 135
3.7 References 137
Chapter Four 140
4.1 General conclusion and summary 141
4.2 Recent results and future work 143
4.2.1 Hydroxamate bridged dimeric lanthanide complexes 144
4.3 Experimental Section 148
4.3.1 Single-crystal X-ray crystallography 148
4.3.2 Preparation of complexes **13** and **14** 148
4.4 References 149
Appendix A 150
Appendix B 158
4.5 References (appendices) 174

List of Abbreviations

Å	Ångström (unit of length equal to 10^{-10} m)
ac	Alternating current
B	Induced magnetic field
B_0	Externally applied magnetic field
br	Broad
C	curie constant
°C	Degrees Celsius
$CHCl_3$	Chloroform
$CDCl_3$	Deuterated chloroform
cm^{-1}	Wavenumbers
cm^3	Cubic centimetre
CPs	Coordination polymers
D	Zero field splitting parameter
d	Doublet
dc	Direct current
DCM	Dichloromethane
dd	Double doublet
DMC	Dynamic Monte-Carlo
DMF	Dimethylformamide
DMSO	Dimethyl sulfoxide
EA	Ethyl acetate
EI	Electron impact
EL	Electroluminescence
Et_2O	Diethyl ether
FRET	Fluorescence resonance energy transfer (Förster resonance energy transfer)
fwhm	Full width at half maximum
H	External magnetic field
hrs	Hours
HOMO	Highest occupied molecular orbital

HS	High spin
Hz	Hertz
ICT	Intramolecular charge transfer
IR	Infra-red
J	Coupling constant
K	Kelvin
kT	k is the Boltzmann constant and T is temperature
L	Total orbital angular momentum
L_1H_2	2-(acetoxy)phenyl hydroxamic
L_2H_2	4-amino-2-(acetoxy)phenyl hydroxamic acid
L_3H	2-mothoxybenzoate
L_4H_2	2-(methylamino)phenyl hydroxamic acid
L_5H_3	*N*-hydroxy-2-[(2-hydroxy-3-methoxybenzyl)amino]benzamide
L_6H_3	N-hydroxy-4-((2-hydroxy-3-methoxybenzyl)amino)benzamide
L_7H_3	N-hydroxy-4-((2-hydroxybenzyl)amino)benzamide
LUMO	Lowest unoccupied molecular orbital
LS	Low spin
LZ	Landau-Zener
m	Multiplet
M	Magnetization
MC	Metallacrowns
MeCN	Acetonitrile
Me	Methyl
MeOH	Methanol
min	Minute(s)
mmol	Millimolar
MS	Mass spectrometry, mass spectrum
m_s	Microstate
M_w	Weight average molecular weight
MS(EI+)	Mass spectra (electron impact, positive mode)
m/z	Mass to charge ratio
n	Number of unpaired electrons
$NEt_4(OH)$	Tetraethylammoniahydroxide
NMR	Nuclear magnetic resonance

pao	pyridine-2-aldoximate
phen	phenanthroline
Ph	Phenyl
PL	Photoluminescence
PLQY	Photoluminescence quantum yield
r.t	Room temperature
Ru	Ruthenium
S	Spin quantum number
$\hat{S}$	Spin operator
saltmen^{2-}	N,N′-(1,1,2,2-tetramethylethylene)
saoH_2	Salicyaldoxime ligand
SCM	Single-Chain Magnet
SCO	Spin crossover
s.e	Symmetry equivalent
SMM	Single-Molecule Magnet
SQUID	Superconducting Quantum Interference Device
TADF	Thermally activated delayed fluorescence
T_B	Blocking temperature
TBA(OH)	Tetrabutylammoniahydroxide
T_C	Curie temperature
TEA	Triethylamine
tert	Tertiary
THF	Tetrahydrofuran
TLC	Thin layer chromatography
TMS	Tetramethylsilane
T_N	Neel Temperature
UV	Ultraviolet
UV-Vis	Ultraviolet-visible electron absorption spectra (spectroscopy)
VBS	valence bond sum
XRD	X-ray data
pXRD	powdered X-ray data
δ	Chemical shift
χ	Magnetic susceptibility
χ_m	Molar susceptibility

χ_v	Volume susceptibility
μ_{eff}	effective magnetic moment
μ_{-n}	Number of metals involve in a bonding
μ_B	Bohr magneton
Δ	ligand field splitting energy
η	Bonding mode of a donor atom
τ	TAO value
λ_{abs}	Maxima of the bands in electron absorption spectra
λ_{PL}	Maxima of the bands in photoluminescence spectra
Φ_{PL}	Photoluminescence quantum yield
0-D	Zero dimensional
1-D	One dimensional
2-D	Two dimensional
3-D	Three dimensional

List of Figures

Figure 1.1 The Hans Christian Oersted statue at Oerstedsparken in Copenhagen, Denmark.

Figure 1.2 Schematic representation of diamagnetic and paramagnetic microscopic structures at rest in the presence of a magnetic field H.

Figure 1.3 Schematic diagram depicting the alignment of individual magnetic moments.

Figure 1.4 *Schematic showing Curie law behaviour of a paramagnet.*

Figure 1.5 *Number of unpaired electrons per atom, determined from Curie constants of transition metals and their 1:1 alloys.*

Figure 1.6 *Typical plots of* χ *vs. T and 1/*χ *vs. T for ferro-, ferri and antiferromagnet materials.* **Figure 1.7** Example of typical polymetallic magnetic cages constructed in the Jones group.

Figure 1.8 The molecular structure of the SMM $[Mn_6O_2(Et\text{-}sao)_6(O_2CPh)_2(EtOH)_4(H_2O)_2]$ and ChemDraw representation of Dysprocenium SMMs.

Figure 1.9 Hysteresis loops for the Single-Chain Magnet $[Mn(III)_2(saltmen)_2Ni(II)(pao)_2(py)_2](ClO_4)_2$.

Fig. 1.10 Diagram illustrating the dependence of the HS or LS state on the octahedral ligand field splitting (Δ_{Oct}) and the corresponding electronic configuration.

Figure 1.11 Adapted representation of spin transition curves of χ_{mT} vs temperature (K).

Figure 1.12 Crystal structure of the coordination polymer $[Cu(II)(L_6H_2)_2]_n$ (**11**).

Figure 1.13 Schematic highlighting the positions (binding locations A-C) situated around a phenylhydroxamic acid backbone.

Figure 2.1 Structure of **1** as viewed perpendicular (a) and parallel (b) to the plane.

Figure 2.2 Crystal packing representations of $[Cu(II)(L_1H)]_2]$ (**1**).

Figure 2.3 Powdered XRD pattern obtained from a crystalline sample of $[Cu(II)(L_1H)_2]$ (**1**) and the diffraction pattern of (**1**) as simulated by the Mercury software package.

Figure 2.4 Crystal structure of $[Fe(III)_2(L_1H)_4Cl_2]$.2MeCN (**2**) and its packing arrangement.

Figure 2.5 Crystal structure of $[Co(III)Co(II)_6(L_1H)_8(L_1)_2(MeOH)_4(NO_3)_2]NO_3.3.5H_2O{\cdot}14MeOH$ (**3**).

Figure 2.6 The crystal packing of $[Co(III)Co(II)_6(L_1H)_8(L_1)_2(MeOH)_4(NO_3)_2]NO_3{\cdot}3.5H_2O{\cdot}14MeOH$ (**3**).

Figure 2.7 Crystal structure of $[Mn(II)_6(L_3)_{12}]{\cdot}6MeCN$ (**4**).

Figure 2.8 Packing of the individual $\{Mn(II)_6\}$ units in **4** as viewed along the *b* direction (a) and *c* direction of the unit cell.

Figure 2.9 Crystal structure of $[Ni(II)(L_1H)(H_2O)(py)_3](NO_3){\cdot}MeCN$ (**5**).

Figure 2.10 A H-bonded dimer of $\{Ni(II)(L_1H)(H_2O)(py)_3\}^+$ units in **5.**

Figure 2.11 Space-fill represented packing diagram observed in the unit cell of **5.**

Figure 2.12 The crystal structure of the 1-D coordination polymer in $[Zn(II)_2(L_1H)_2(H_2O)_5](NO_3)_2]_n$ (**6**).

Figure 2.13 Packing arrangement observed in **6**.

Figure 2.14 The asymmetric unit in $\{[Cu(II)(L_2H)(H_2O)(NO_3)]\cdot H_2O\}_n$ (**7**).

Figure 2.15 The wave-like [4,4] net topology in **7.**

Figure 2.16 Overlay $\chi_M T$ versus T plots for polycrystalline sample of **2** and **3**.

Figure 3.17 Reduced magnetisation (M/μ_B) vs. B/T (T/K) data obtained from a polycrystalline sample of **3.**

Figure 3.1 The crystal structure in $[Cu(II)_5(L_4)_4(NO_3)_2]{\cdot}3H_2O$ (**8**).

Figure 3.2 Polyhedral packing arrangement in **8.**

Figure 3.3 (a) The asymmetric unit in $\{[Zn(II)(L_4H)_2]{\cdot}2MeOH\}_n$ (**9**).

Figure 3.4 A polyhedral representations of the 1D-chains as viewed along the equatorial (a) and axial (b) planes of the distorted octahedral Zn(II) centres in **9**. (c) The unit cell in **9** as viewed along the *c* direction.

Figure 3.5 The inorganic core in $[Cu(II)_5(L_5H)_4(MeOH)_2](NO_3)_2$ (**10**) along with the crystal structure and the bonding mode exhibited by the L_5H^{2-} ligands in **10**.

Figure 3.6 Packing arrangement in **10** as viewed down the *a*-axis of the unit cell.

Figure 3.7 Crystal structure of the coordination polymer in $[Cu(II)(L_6H_2)_2]_n$ (**11**).

Figure 3.8 A single ribbon 1D chain in **11** along with Space-fill represented and colour coded H-bonded stacks of chains in **11.**

Figure 3.9 (a) A single $\{[Cu(II)(L_7H_2)_2].2MeOH\}$ unit in **12**.

Figure 3.10 The coordination polymers in **11** (a and b) and **12** (c and d) highlighting significant differences in phenolic ring positions in relation to their conjoined hydroxamate fragments.
Figure 3.11 Powdered XRD pattern obtained from a crystalline sample of $[Cu(II)(L_6H_2)_2]_n$ (**11**).
Figure 3.12 Powdered XRD pattern obtained from a crystalline sample of $\{[Cu(II)(L_7H_2)].2MeOH\}_n$ (**12**).
Figure 3.13 UV-Vis absorption (a) and photoluminescence (b) spectra of complex **9** and ligand L_4H_2.
Figure 3.14 Solution of complex **9** in dichloromethane under ambient light (left) and under hand-held UV lamp irradiation, λ = 365 nm (right).
Figure 3.15 Thin films of complex **9** drop-casted on quarts disks from chloroform solution, under ambient light (left) and under hand-held UV lamp irradiation, λ = 365 nm (right).
Figure 3.16 Variable temperature $\chi_M T$ vs. T plot obtained from a polycrystalline sample of **10**.
Figure 3.17 Magnetisation (M / μB vs B (T) data obtained from a polycrystalline sample of **10**.
Figure 4.1 (a) Crystal structure of $[Ni(II)(L_1H)(H_2O)(py)_3](NO_3)\cdot MeCN$ (**5**).
Figure 4.2 (a) Crystal structures of $[Dy(III)_2(L_1H)_2(H_2O)_4(NO_3)_4]$ (**13**) and $[Gd(III)_2(L_1H)_2(H_2O)_4(NO_3)_4]$(**14**).
Figure 4.3 Packing arrangement in $[Dy(III)_2(L_1H)_2(H_2O)_4(NO_3)_4]$ (**13**) (top) and $[Gd(III)_2(L_1H)_2(H_2O)_4(NO_3)_4]$(**14**) (bottom) as viewed along *a* unit cell direction.

List of Schemes

Scheme 1.1 Three strategies towards the successful construction of a single-chain magnet.

Scheme 1.2 ChemDraw representations of the ligands 3,3′-azodibenzoic acid (a), 4,4′-azodibenzoic acid (b) discussed in reference 120 along with the ligands L_6H_3 and L_7H_3 employed in this work.

Scheme 1.3 General structure of a hydroxamic acid with R and R' as organic residues.

Scheme 1.4 The Z and E diastereomers commonly observed by hydroxamic acids.

Scheme 1.5 Synthesis of hydroxamic acid by the reaction hydroxylamine with esters.

Scheme 1.6 Preparation of hydroxamic acids from carboxylic acid derivatives.

Scheme 1.7 Preparation of hydroxamic acids from unactivated esters.

Scheme 1.8 Hydroxyaminolysis of an esters-link substrate using aqueous NH_2OH.

Scheme 1.9 Schematic representation of common chelating modes of hydroxamate ligands.

Scheme 2.1 ChemDraw representations of the ligands 2-(acetoxy)phenylhydroxamic acid (L_1H_2) and 4-amino-2-(acetoxy)phenylhydroxamic acid (L_2H_2).

Scheme 3.1 (a) ChemDraw representations of the ligands 2-(amino)phenylhydroxamic acid (2-am-phaH_2) and 2-(dimethylamino)phenylhydroxamic acid (2-dm-phaH_2) previously used in the production of a series of polynuclear 12-MC-4 [$M(II)_5$] (M = Ni, Cu) complexes and coordination polymers.[23,24] Two examples are given above. (Top right) ChemDraw representation of the ligand 2-(methylamino)phenylhydroxamic acid (L_4H_2) used in this work.

Scheme 3.2 (Left) The ligand o-[(E)-(2-hydroxy-3-methoxyphenyl)methylideneamino]benzohydroxamic acid (right) The novel ligand (N-hydroxy-2-((2-hydroxy-3-methoxybenzyl)amino)benzamide (L_5H_3) used in this work.

Scheme 3.3 ChemDraw representation of the ligands N-hydroxy-4-((2-hydroxy-3-methoxybenzyl)amino)benzamide (L_6H_3) and N-hydroxy-4-((2-hydroxybenzyl)amino)benzamide (L_7H_3) used in this work.

Scheme 4.1 ChemDraw representations of the ligands employed in this thesis.

List of Tables

Table 1.1 Néel temperature (T_N) values for some typical antiferromagnetic substances.

Table 1.2 Typical magnetic susceptibility (χ) values for a selection of metals, metal salts and metal alloys.

Table 2.1 Magnetic moment data obtained from a polycrystalline sample of **1**.

Table 2.2: BVS data on $[Fe(III)_2(L_1H)_4Cl_2].2MeCN$ (**2**)

Table 2.3: BVS data on $[Co(III)Co(II)_6(L_1H)_8(L_1)_2(MeOH)_4(NO_3)_2]NO_3 \cdot 3.5H_2O \cdot 14MeOH$ (**3**).

Table 2.4: BVS data on $[Mn(II)_6(L_3)_{12}].6MeCN$ (**4**)

Table 2.5 Selected crystal data obtained from **1-3**.

Table 2.6 Selected crystal data obtained from **4-7**.

Table 3.1 Magnetic moment data obtained from polycrystalline samples of **11** and **12**.

Table 3.2 Absorption and emission maxima of complex **9** in different solvents and in the solid state, together with data for ligand L_3H_2.

Table 3.3 Selected crystal data obtained from **8 - 10**.

Table 3.4 Selected crystal data obtained from **11** and **12**.

Table 4.1 Selected bond lengths and angles observed in compounds **13** and **14**.

Table 4.2 Selected crystal data obtained from **13** and **14**.

Table A1 Mononuclear complexes constructed with hydroxamic acids (valid at the time of writing).

Table A2 Dinuclear and polynuclear complexes constructed with hydroxamic acids (valid at the time of writing).

Table A3 Coordination polymers constructed with hydroxamic acids (valid at the time of writing).

Acknowledgements

I wish to offer my deepest gratitude is to Dr. Leigh F. Jones, whose advice, continued support and constant guidance have been fundamental for the completion of this thesis. I really appreciate his patient and enthusiasm. I would like to specially acknowledge my employer, the University of Maiduguri for the support and the fellowship. I am deeply grateful to Petroleum Technology Development Fund (PTDF) Nigeria, for providing me with a Scholarship from my third year all the way through to the end of my program (Sept. 2017-present), which fully covered my tuition fees and living expenses in UK, without which this success would not have been possible.

I would like to thank my progress committee, Professor Igor Perepichka, Dr. Lorrie Murphy and Dr. Patrick Murphy for their advice and encouragement throughout my research work. I am grateful to all the technicians at the Chemistry department (Bangor University): Mr. Gwynfor Davies, Mr. Glynne Evans, Dr. David Hughes and Mr. Nicholas Welsby.

I would like to thank the EPSRC National Crystallographic Service at the University of Southampton and the EPSRC UK National Mass Spectrometry Facility at Swansea University for their support. Many thanks to Professor Euan Brechin and his research team at the University of Edinburgh for performing magnetic measurement on some of my samples.

I would also like to express my gratitude to my colleague Mari Slater-Parry who shared with me the amazing experience of being a Ph.D. student. I am very grateful for her constant help. I thank all the students within the Jones group who have walked beside me during these years and helped me in one way or the other. You have all made the progress of my research faster. I would like to specially mention Isabella F. Dickinson, Rebecca J. Ellaby. Jordan Rickett, Jack Owen, Cameron Milne, Faizal Shaikh, Chotima Ratanasakprakan, Zahraa Al-Taie and Shayma Ahmad for all the good times we have had working together. I also want to thank all the staff of the 10th floor at the Chemistry tower. These are Dr Juma'a R. Al-Dulayymi, Dr Ahmed Al-Dulayymi, Dr Mark Bouillon and Dr Alison Jones, for some useful discussions and exchange of ideas.

I acknowledge the support and care of all my friends that helped me overcome setbacks and stay focused on my work. I would especially like to gratefully acknowledge the support and encouragement of my friend Junaidu Isa Bungudu towards my funding application to PTDF.

Finally, I would like to express my sincere appreciation to all members my family especially my Dad and Mom, my brothers and sisters, my wife Fatima Shettima and my Children (Ibrahim, Ali, Hauwa, Amma, Aisha, Kaltum, Sayyida and Husna) for their love and patient throughout my studies. Their trust in my abilities and constant encouragement motivated me to stay open-minded and to focus on my studies.

Abstract

A family of mono-, di- and multitopic hydroxamic acids have been employed in the synthesis, structural and physical characterisation of discrete (0-D) and (1- and 2-D) extended network coordination complexes. The majority of the complexes in this thesis have been synthesized using the ligands 2-methoxyphenylhydroxamic acid (L_1H_2), 4-amino-2-(acetoxy)phenyl hydroxamic acid (L_2H_2) and 2-(methylamino)phenyl hydroxamic acid (L_4H_2). More specifically, chapter 2 describes the synthesis and physical characterisation of the monomeric complexes $[Cu(II)(L_1H)_2]$ (**1**) and $[Ni(II)(L_1H)(H_2O)(py)_3](NO_3)\cdot MeCN$ (**5**) along with the dinuclear ferric complex $[Fe(III)_2(L_1H)_4Cl_2].2MeCN$ (**2**) and the heterovalent heptanuclear complex $[Co(III)Co(II)_6(L_1H)_8(L_1)_2(MeOH)_4(NO_3)_2]NO_3\cdot 3.5H_2O\cdot 14MeOH$ (**3**). We also present the novel 1-D Zn(II) coordination polymer $[Zn(II)_2(L_1H)_2(H_2O)_5](NO_3)_2]_n$ (**6**), also constructed with bridging 2-methoxyphenylhydroxamate ligands. Very recent investigations into the coordinating ability of L_1H_2 with Ln(III) ions gave rise to the dinuclear complexes $[Dy(III)_2(L_1H)_2(H_2O)_4(NO_3)_4]$ (**13**) and $[Gd(III)_2(L_1H)_2(H_2O)_4(NO_3)_4]$ (**14**) and are described in Chapter 4.

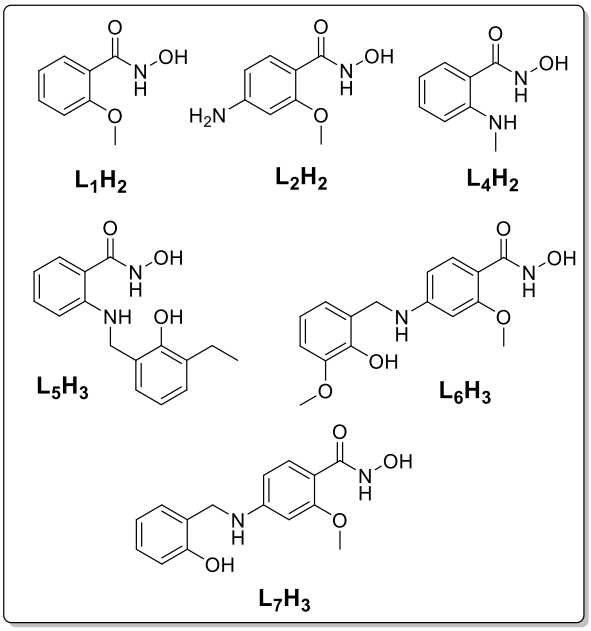

The introduction of an $-NH_2$ group at the 4th position of ligand L_1H_2 gives rise to the multitopic ligand 4-amino-2-(acetoxy)phenylhydroxamic acid (L_2H_2). Cu(II) ligation of this organic moiety leads to the 2-D extended network $\{[Cu(II)(L_2H)(H_2O)(NO_3)]\cdot H_2O\}_n$ (**7**), with a [4,4]-

net topology. Complexes **1-3** and **5-7** represent extremely rare examples of metal coordination of L_1H_2 and L_2H_2 and were therefore recently published in the RSC journal *Dalton Transactions*.[1]

We proceeded to replace the -OMe group at the 2-position in L_1H_2 with a methylamino (-NHMe) moiety, resulting in the synthesis of target ligand 2-(methylamino)phenyl hydroxamic acid (L_4H_2). This ligand was subsequently successfully incorporated into the pentanuclear MC-$4_{Cu(II)}$ metallacrown $[Cu(II)_5(L_4)_4(NO_3)_2]\cdot 3H_2O$ (**8**) and the 1-D coordination polymer $\{[Zn(II)(L_4H)_2]\cdot 2MeOH\}_n$ (**9**). In solution, the coordination polymer **9** exhibits a solvent dependent photoluminescent emission in the blue region ($\lambda_{PL} \approx 421 – 433$ nm) depending on the solvent. In the solid state, a bathochromic shift of ≈ 15 – 30 nm is observed, underlying the importance of inter-chain interactions on the excited state of the complex.

Chapter 3 described the design and synthesis of the more elaborate (and novel) multitopic hydroxamic acids: *N*-hydroxy-2-[(2-hydroxy-3-methoxybenzyl)amino]benzamide (L_5H_3), N-hydroxy-4-((2-hydroxy-3-methoxybenzyl)amino)benzamide (L_6H_3) and N-hydroxy-4-((2-hydroxybenzyl)amino)benzamide (L_7H_3). The latter two ligands were then successfully combined with Cu(II) nodes to form the unprecedented 1-D coordination polymers: $[Cu(II)(L_6H_2)_2]_n$ (**11**) and $\{[Cu(II)(L_7H_2)].2MeOH\}_n$ (1**2**). Interestingly, slight differences in the structures of L_6H_3 and L_7H_3 lead to significant connectivity and topology changes upon Cu(II) metalation. Complexes **11** and **12** will form the basis of a journal publication in the very near future.

The ligand L_5H_3 was produced via a one pot Schiff base reduction using sodium triacetoxyborohydride. The introduction of a phenolic moiety at the 2-position of the phenylhydroxamic acid framework deliberately forced non-planarity on the ligand topology. Upon Cu(II) metalation, the 12-MC-$4_{Cu(II)}$ metallacrown $[Cu(II)_5(L_5H)_4(MeOH)_2](NO_3)_2.4MeOH.4H_2O$ (**10**) was produced and represented the first complex to be constructed with such a ligand. Variable temperature magnetic susceptibility measurements on **10** indicates dominant antiferromagnetic exchange.

1. **M. B. Fugu,** R. J. Ellaby, H. M. O'Connor, M. Pitak, W. Klooster, P. N. Horton, S. J. Coles, M. H. Al-mashhadani, I. F. Perepichka, E. K. Brechin and L. F. Jones. *Dalton Trans.,* 2019, DOI 10.1039/C9DT01531K.

Chapter One

Introduction

1.0 Introduction

1.1 Definition and history of magnetism

Magnetism is a phenomenon associated with magnetic fields, which arise from the force caused by electric charges that attract or repel other objects. This force of attraction or repulsion arises due to motion of electrons in an atomic orbital, electric current or charge particles moving through a space.[1,2] The movement of magnetic force in the field which is perpendicular to both the velocity of the charge and the field itself indicates the presence of a magnetic field. Magnetism and electricity represent different aspects of electromagnetism, which is one part of nature's fundamental electroweak force.[3] The region in space that is penetrated by the imaginary lines of magnetic force describes a magnetic field. The strength of the magnetic field is determined by the number of lines of force per unit area of space.[4] Typical materials that are known to respond to a magnetic field are the elemental metals such as iron, cobalt and nickel and their alloys as well as solid solution materials.[5] The magnetic force field generated around magnetised materials differ from the fundamental force field of gravity, due to the polarity of the opposite signs at the two magnetic poles, which makes the field to be strongest at either pole of the magnet and weaker in the middle.[6]

The ancient Greek philosopher Thales of Miletus described the history of magnetism as early as 600 B.C., where the magnetic properties of the naturally magnetized mineral magnetite (Fe_3O_4) (a.k.a. lodestones) were first discovered. According to many historians, the term magnetism was named after a place in ancient Greece called Magnesia. In 1600 AD the English physicist Dr William Gilbert scientifically investigated static electricity by observing the behaviour of amber when near a magnet. He discovered that amber developed the ability to attract light pieces of material such as feathers, when lightly rubbed with a piece of fur.[7,8] Until then this strange effect remained a mystery for over 2000 years. Dr William Gilbert was also the first person to record the word 'electric' from the Latin electrum (literally "resembling amber") in a report on the theory of magnetism.[6] The term electron was also derived from the Greek word "elektron" meaning amber and this was the origin of the term "electricity".[9] Gilbert was also the first to proclaim that the earth was itself a magnet and composed of conductive molten iron. In addition, Gilbert discovered that magnets can lose strength when exposed to heat.[6] According to history, the Chinese were known to use a lodestone compass for navigations from as early as the 12th century. They discovered that when needle-like pieces

from lodestone were placed on the surface of water, one end of the needle always pointed south.[10]

In 1800, French man Charles Coulomb (1736-1806), established the inverse square law of force, which states that the attractive force between two magnetized objects is directly proportional to the product of their individual fields and inversely proportional to the square of the distance between them.[11] Hans Christian Oersted (1777-1851; Fig. 1.1), a physicist at the University of Copenhagen, was the first to suggest the relationship between electricity and magnetism (electromagnetism), when he realised that the force on a wire carrying an electric current caused a compass needle to move.[12] In 1820, a Frenchman Andre Marie Ampere discovered the relationship between magnetic field and electric field, known as electro-dynamic theory. He was the first person to attempt to theoretically explain and mathematically describe this phenomenon; hence, the unit of current (ampere) was named after him.[11]

Figure 1.1 *The Hans Christian Oersted statue at Oerstedsparken in Copenhagen, Denmark. Photograph taken by Leigh. F. Jones (Aug. 2016).*

Englishman Michael Faraday (1791-1869), was rightly credited with fundamental discoveries on electricity and magnetism; hence, an electric unit is named "Farad" in his honour. Michael Faraday was first to discover electromagnetic induction, invented magnetic rotary devices (first

electric motor), discovered the relationship between magnetism and light and named the peculiar behaviour of certain substance in strong magnetic field as diamagnetism.[13]

The Scottish scientist James Clerk Maxwell (1831-1879) demonstrated for the first time the intertwined relationship between electricity, magnetism and optics in the form of electromagnetic radiation. On the basis of Michael faraday's observation of induction, Maxwell formulated a series of simple equations that serves as a foundation of today's electromagnetic theory.[14,15] Maxwell demonstrated how electromagnetic waves created by the fluctuating electric and magnetic fields propagate at the speed of light and devised four partial differential equations which formulated relationships between electricity and magnetism.[16,17]

J. J. Thomson discovered the electron in 1897, more than thirty years after Maxwell introduced this remarkable idea in 1862. An electron is the central particle in the current understanding of both electricity and magnetism.[18] In the late 1960s, further studies on the fundamental forces were performed independently by Abdus Salam (1926- 1996) and Steven Weinberg (1933-) who merged electromagnetism and weak interaction forces into a unified electroweak force.[19-22]

The origin of the modern understanding of magnetic phenomena in condensed matter came from the work of Pierre Curie (1859-1906), Marie Curie (1867-1934) and Pierre Weiss (1865-1940). Pierre Curie studied magnetic property changes upon temperature variation and observed that above a certain critical temperature, materials like iron suddenly lost their magnetic behaviour. Weiss proposed a hypothetical concept based on an additional magnetic field coined an internal molecular field which was assumed to be proportional to the spontaneous magnetization in the magnetic matter.[23,24] The current understanding of quantum theory involving the interactions of charge particles with electromagnetic fields (quantum electrodynamics), originated from the work and theoretical models of Ernest Ising (1900- 1998) and Werner Heisenberg (1901-1976). Heisenberg was awarded the Nobel Prize in Physics in 1932 as one of the key pioneers of quantum mechanics.[23]

Today, after hundreds of years of research we not only know the attractive and repulsive nature of magnets, but also understand Magnetic Resonance Imaging (MRI) scans employed in the field of medicine, computer chips, television and telephones in electronics and even that certain birds, butterflies and other insects have a magnetic sense of direction.[24]

1.2 Magnetochemistry

Magnetochemistry is described as the study of the relationship between the chemical structure and resultant magnetic properties of magnetic materials. These materials comprise of numerous paramagnetic ions and such magnetic behaviour stems from the spin and orbital angular momentum of the unpaired electrons.[25]

When an isolated atom is placed in an external magnetic field, there is an interaction because each electron in the atom behaves like a tiny bar magnet. The electron therefore has a magnetic moment. There are two main types of interactions, diamagnetism and paramagnetism and classification depends on how a material responds to an external applied magnetic field. More specifically, paramagnetic materials are attracted to magnetic fields while diamagnetic species repel and actively move away from an external magnetic field.[26] Other magnetic behaviours such as ferromagnetism, antiferromagnetism, and ferrimagnetism are all considered as a special case of paramagnetic behaviour and are also described below.

1.2.1 Diamagnetism

Diamagnetism is a fundamental property of all materials as they are characterised by paired electrons and is a very weak form of magnetism. Indeed, in the presence of para- or ferromagnetism the stronger forces will easily overshadow diamagnetism contributions to the overall magnetic moment. A material is termed diamagnetic when it is the only contribution to the materials magnetic effect. Diamagnetic compounds have no net magnetic moment (net spin of zero). When exposed to a magnetic field, a negative magnetization is produced due to their non-cooperative behaviour and thus the resultant magnetic susceptibility product is negative and independent of temperature.

Any two electrons sharing the same orbital have different spin quantum numbers (m_s ±1/2). Whenever two electrons are paired together in an orbital, their total spin is zero and they are diamagnetic electrons and the material comprises diamagnetic atoms. Diamagnetic materials create an induced magnetic field in a direction opposite to an externally applied magnetic field and are therefore repelled by the applied magnetic field (Fig. 1.2).

1.2.2 Paramagnetism

The structural characteristic most noticeable to paramagnetic materials is the presence of unpaired electrons. Paramagnetic substances are drawn into the magnetic line of flux upon

application of an external magnetic field and are therefore attracted to a magnetic field (Fig. 1.2).

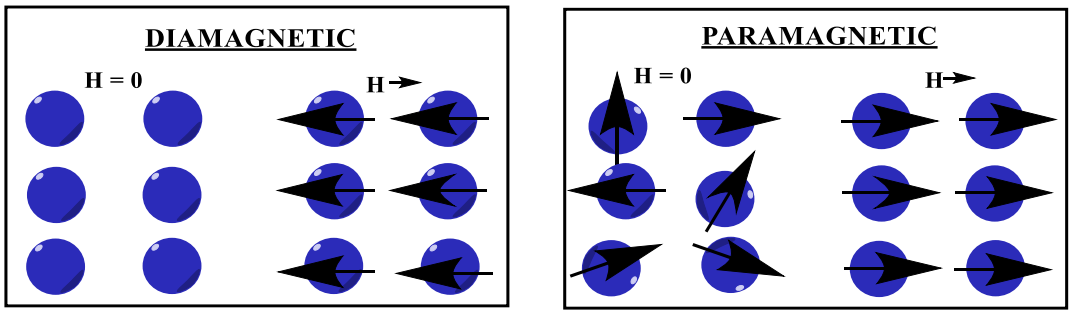

Figure 1.2 *Schematic representation of diamagnetic and paramagnetic microscopic structures at rest in the presence of a magnetic field H.*

Paramagnetic materials are slightly attracted to a magnetic field even if one orbital has a net spin. In the absence of a magnetic field the individual spins return to their original random orientations. This means that paramagnets do not retain any magnetization in the absence of an externally applied magnetic field, because thermal motion randomizes the spin orientations (Fig. 1.3A).[27] The magnitude of μ_{eff} for 1st row transition metals is, to a first approximation, a simple function of the number of unpaired electrons and can be quantified using the spin-only formula (Eqn. 1a and 1b). The magnitude of the paramagnetism is expressed as an effective magnetic moment, μ_{eff}. The formula used to calculate the spin-only magnetic moment of a paramagnetic compound can be written in two forms:

$$\text{Eqn. 1a:} \qquad \mu_{s.o.} = \sqrt{n(n+2)}$$

$$\text{Eqn. 1b:} \qquad \mu_{s.o.} = \sqrt{4S(S+1)}$$

where μ = effective magnetic moment, n = number of unpaired electrons and S = electron spin quantum number. For each unpaired electron, n = 1 and S = 1/2. For the heavier transition metals, lanthanides and actinides, spin-orbit coupling cannot be ignored. Exchange interaction can occur in clusters and infinite lattices, resulting in ferromagnetism, antiferromagnetism or ferrimagnetism depending on the relative orientations of the individual spins. The total magnetic susceptibility for both spin and orbital angular momenta is given by:

$$\textit{Eqn. 2:} \quad \mu = \{4S(S+1) + L(L+1)\}^{½}$$

where μ = effective magnetic moment, S = 1/2 for one unpaired electron, L = total orbital angular momentum. This equation applies only to high symmetry molecules where the unpaired electrons reside in degenerate energy orbitals. In case of very large splitting of orbital energy levels relative to kT, where k is the Boltzmann constant then the formula below is applied.

$$\textit{Eqn. 3:}\ \mu = g\{J(J+1)\}^{1/2}$$

$$\text{Where } g = \frac{1 + S(S+1) - L(L+1) + J(J+1)}{2J(J+1)}$$

and where $J = S + L$

The magnetization of a material is expressed in terms of density of net magnetic dipole moment in the material. We define a vector quantity called the magnetization M by:

$$\textit{Eqn. 4:}\ M = \mu_{total}/V$$

Then the total magnetic field B in the material is given by:

$$\textit{Eqn. 5:}\ B = B_0 + \mu_0 M$$

Where μ_0 is the magnetic permeability of space and B_0 is the externally applied magnetic field. The above formula is particularly useful for the heavier elements such as lanthanides and actinides. It is recommended to add a diamagnetic contribution in order obtain more accurate treatment as almost all elements contain a diamagnetic contribution from their paired electrons.

It should be noted here that using effective magnetic moments is considered supportive in describing the magnetic behaviour of molecules, due to the fact that it is a measure of the materials magnetic behaviour that do not depend on either the magnitude of the external field or the temperature. However, this formula cannot be set up as a convention for the materials that are either ferromagnetic, antiferromagnetic or ferrimagnetic due to the coupled magnetic behaviour.

1.2.3 Ferromagnetism

Ferromagnetism is a physical phenomenon in which certain electrically uncharged materials tend to stay magnetized to some extent after the applied external magnetic field is removed.

This phenomenon is known as magnetic hysteresis. Ferromagnetism results from interatomic electronic exchange forces that keep unpaired electrons aligned parallel to one another and this phenomenon is called ferromagnetic coupling. Such materials therefore comprise permanent atomic magnetic dipoles that are spontaneously oriented parallel to one another even in the absence of an external field (Fig. 1.3b). Ferromagnetic effects are very large; producing magnetizations sometimes orders of magnitude greater than the applied field and as such are much larger than either diamagnetic or paramagnetic effects. Materials such as iron, cobalt, nickel and some alloys as well as some rare-earth elements such as neodymium, samarium and gadolinium exhibit ferromagnetic behaviour.

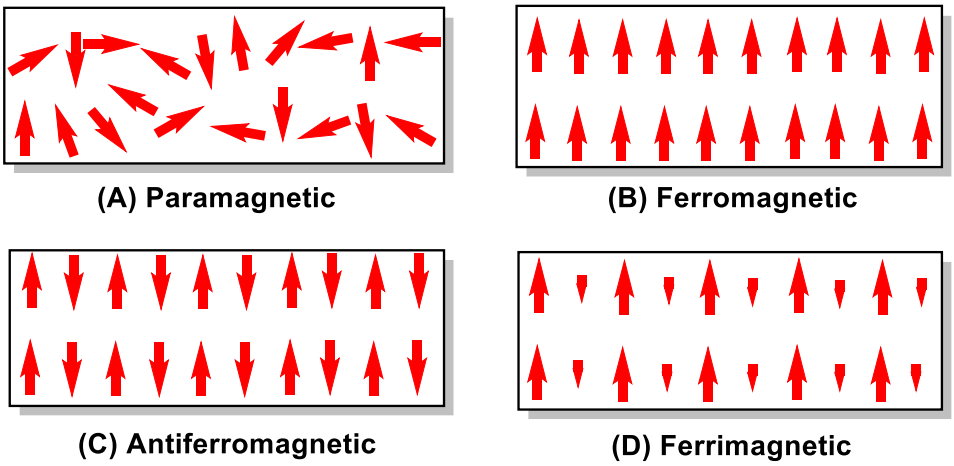

Figure 1.3 *Schematic diagram depicting the alignment of individual magnetic moments (represented as arrows) in (A) paramagnetic, (B) ferromagnetic, (C) antiferromagnetic and (D) ferrimagnetic systems.*[27]

1.2.4 Antiferromagnetism

In materials that exhibit antiferromagnetism, the magnetic moments of the atoms spontaneously align in antiparallel patterns with respect to their neighbouring spins when a magnetic field is applied. Antiferromagnetic substance contains atomic magnetic dipoles that have signs opposite those in ferromagnets. Above a certain critical temperature (the Néel temperature) the material transitions from being antiferromagnetically ordered to exhibiting classic paramagnetic behaviour. That is, the material has then received enough thermal energy to overcome and destroy all antiparallel ordering. This antiparallel alignment is retained when the external field is removed. The Néel temperature was named after Louis Néel, the French physicist who had first identified this type of ordering in 1936 and was awarded the Nobel Prize in Physics in 1970 for his work on the magnetic properties of solid materials. Materials

such as transition metal compounds of chromium, hematite, oxides of nickel and manganese as well as alloys such as iron manganese (FeMn) exhibit antiferromagnetic ordering.

The antiferromagnetic ordering is naturally more complex in nature compared to the ferromagnetic state, since there must be at least two opposite sub lattice moments. If the two opposite sub lattice moments are exactly the same, there is no net spontaneous magnetization on a macroscopic scale. The electronic exchange forces between the magnetic ions in most insulating chemical compounds are of an antiferromagnetic nature.[28] Table 1.1 shows the Néel temperature (T_N) values for some antiferromagnetic substances.

Table 1.1 *Néel temperature (T_N) values for some typical antiferromagnetic substances.*[28]

Metal / Compound	***Neel Temperature (T_N) (K)***
NiO	463
CoNiO	423
CoO	292
FeF_2	79
FeMn	425
MnPt	616

1.2.5 Ferrimagnetism

Ferrimagnetic compounds comprise populations of atoms with unequal opposing magnetic moments meaning that there are more spins held in one direction and so a spontaneous net magnetization remains (Fig. 1.3d). Before the discovery of anti- and ferrimagnetism by Néel in 1948, the oldest known magnetic substance magnetite, which is ferrimagnetic, was originally classified as a ferromagnet. Ferrimagnetism can occur when the material consists of different elements and / or ions as exemplified by the heterovalency in magnetite ($Fe(III)_2Fe(II)O_4$). Akin to ferromagnets, ferrimagnetic materials also retain their magnetization at low temperature and can be removed when the Néel temperature is reached / surpassed as the material enters a paramagnetic phase.

1.2.6 Pauli paramagnetism

Beside the unpaired electrons in atoms, another important contribution to paramagnetism can come through conduction electrons of metals. The tendency of these free electrons in metals to align with an external magnetic field is known as Pauli paramagnetism. The difference between paramagnetism and Pauli paramagnetism is that the latter applies to a metal because it describes the tendency of free electrons in an electron gas to align with an applied magnetic field while the regular paramagnetism arises when there are unpaired electrons after filling up the orbital structure according to Hund's rules. These unpaired electrons are not very mobile. This can happen in some metals such as platinum, osmium, iridium, cerium and yttrium where the conduction electrons are weakly interacting and delocalized in space forming a Fermi gas. Pauli-paramagnetism is much weaker compare to paramagnetism because in paramagnetism, all the magnetic atoms in the material contribute to the magnetic moment where as in case of Pauli paramagnetism only the electrons near the Fermi surface can change its spin to align with the magnetic field.[29]

1.3 Magnetization and magnetic susceptibility

Magnetic susceptibility is a dimensionless proportionality constant that describes the extent that a material will be magnetised in the presence of an external magnetic field. The magnitude of the magnetic field generated by a material may be represented mathematically as the ratio of magnetization *M* to the applied magnetic field *H*, which is a vector quantity since it has both a magnitude and a direction. The formula is given as:

$$Eqn.6 \qquad \chi_v = M/H = \text{volume magnetic susceptibility}$$

Volume magnetic susceptibility (χ_v) is a measure of dipole moment per unit volume. Since it is the ratio of two magnetic fields, susceptibility is a dimensionless number. Two different vectors can be used to represent magnetic fields, one is magnetic field strength or magnetic field intensity *H*, and the other is magnetic field generated by the material itself, which is called the magnetic induction (B) and sometimes called magnetic flux density. These vectors are related by Equation 7:

$$Eqn.\ 7 \quad B = H + 4\pi M$$

M is the magnetization of the material, which represents the magnetic dipole moment per unit volume (measured in amperes per meter). *H* is the applied magnetic field (also measured in

amperes per meter), *B* is the induced magnetic field in a material (Tesla; *T*), in the presence of an external field *H*. Smaller magnetic fields are usually measured in units of Gauss (1 Tesla = 10,000 Gauss).

For experimental convenience this equation if often written as:

$$Eqn.\ 8 \quad B = 1 + 4\pi M = 1 + 4\pi\chi_v H$$

Magnetic susceptibility is occasionally given as magnetic susceptibility per gram (χ_g), however, the most commonly presented form is molar magnetic susceptibility (χ_m) ($\chi_m = \chi_g$ x Mw). The units of measurements are $m^3\ kg^{-1}$ and $m^3\ mol^{-1}$, respectively.

The force exerted on substances in an inhomogeneous magnetic field determines whether a substance is diamagnetic or paramagnetic. At moderate field strengths, the magnetization induced *M* of a substance is linearly related to the magnetizing field (*H*). The degree of induced magnetization is specified by the magnetic susceptibility χ, which is commonly defined by the equation 9:

$$Eqn.\ 9 \quad M = \chi H$$

Magnetic materials may be classified as diamagnetic, paramagnetic, or ferromagnetic on the basis of their magnetic susceptibilities. Diamagnetic substances such as copper, silver, gold, antimony and bismuth have negative susceptibility. They are magnetically attracted toward regions of low magnetic field (their magnetization opposes the applied field). A characteristic feature of diamagnetism is that the magnetic susceptibility in a given field is independent of temperature. However, it changes slightly between solid, liquid and gas due to the change in the number of molecules per unit volume.[16] In a closed shell, the diamagnetic susceptibility from a given electron is proportional to the square of the radius of the shell. This indicates that in larger atoms, the electrons will give a greater contribution to the diamagnetic susceptibility. The magnetic susceptibility of a given molecule can be predicted merely by adding together all the atomic contributions and bonds in the molecule. In the case of paramagnetic and diamagnetic materials, the relative permeability is very close to 1 and the magnetic susceptibility very close to zero. For ferromagnetic materials, these quantities may be very large. Typical magnetic susceptibility values are shown in Table 1.2.

Table 1.2 *Typical magnetic susceptibility (χ) values for a selection of metals, metal salts and metal alloys.*

Metal / Compound	***Magnetic behaviour***	**Magnetic susceptibility (*χ*)** ***(cm^3 mol^{-1})***	**Reference**
SiO_2	*Diamagnetic*	-3×10^{-4}	30,31
Platinum (Pt)	*Pauli paramagnetic*	2×10^{-4}	32,33
$Gd_2(SO4)_3.8H_2O$	*Paramagnetic*	5×10^{-2}	34,35
Ni-Fe alloy (permalloy)	*Ferromagnetic*	$10^4 - 10^6$	36

To correlate χ with the number of unpaired electrons in a compound, we first correct for the small diamagnetic contribution of the core electrons:

$$\textit{Eqn. 10} \quad \chi_{corrected} = \chi_{observed} - \chi_{diamagnetic\ cores}$$

1.3.1 Magnetic susceptibility for paramagnetic substances

In a non-uniform magnetic field, paramagnetic substances exhibit small positive magnetic susceptibilities, less than 1/1,000 g/mol at room temperature. They are magnetically attracted towards high field regions and thus the magnetic field is increased by the induced magnetization. This is because their atoms have small magnetic dipole moments that partly aligned with the applied field. This indicates that the increase in the magnetic field caused by the alignment of magnetic dipoles is relatively small compared with the applied field.[37] The susceptibility of a paramagnetic substance, according to French physicist Pierre Curie in 1895, is inversely proportional to the absolute temperature *T* and is mathematically express in the equation 11 and 12.

$$\textit{Eqn. 11} \quad \chi \propto \frac{1}{T}$$

$$\textit{Eqn. 12} \quad \chi = \frac{C}{T}$$

The inverse relationship between the magnetic susceptibility and T (absolute temperature) is called Curie's Law and C is the Curie constant (Fig. 1.4):

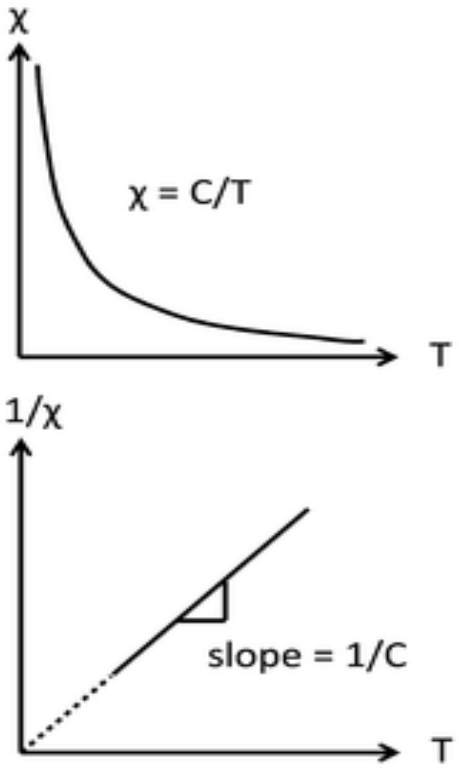

Figure 1.4 *(top) Schematic showing Curie law behaviour of a paramagnet in the form of a χ vs. T plot. (bottom) A plot of 1/χ vs. absolute temperature is a straight line, with a slope of 1/C and an intercept of zero.*[37]

Figure 1.5 shows the number of unpaired electrons per atom, calculated from measured Curie constants, for a number of magnetic elements and 1:1 alloys in the 3d series. The plot reaches a maximum at a value of 2.4 spins per atom, slightly lower than an isolated iron (Fe) atom. This reflects that fact that there is some pairing of d-electrons and that they do contribute somewhat to bonding in this part of the periodic table.

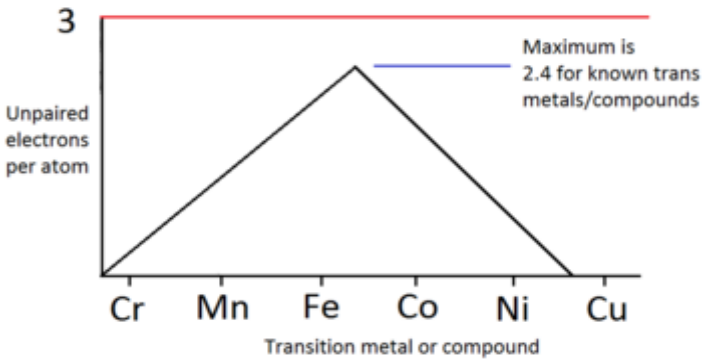

Figure 1.5 *Number of unpaired electrons per atom, determined from Curie constants of transition metals and their 1:1 alloys.*[37]

1.3.2 Magnetic susceptibility of ferro-, ferri- and antiferromagnets

Below a certain critical temperature, the individual spins within a solid paramagnetic substance become ordered and the resultant magnetic susceptibility deviates from simple Curie-law behaviour. Because the ordering depends on the short-range exchange interaction, this critical temperature varies widely. Metals and alloys in the 3d series tend to have high critical temperatures because the atoms are directly bonded to each other and the interaction is strong. For example, iron (Fe) and cobalt (Co) have critical temperatures (also called the Curie temperature (T_c) for ferromagnetic substances) of 1043 and 1400 K, respectively. The Curie temperature is determined by the strength of the magnetic exchange interaction and by the number of unpaired electrons per atom. The number of unpaired electrons peak between Fe and Co as the d-band is filled, and the exchange interaction is stronger for Co than for Fe. In contrast to ferromagnetic metals and alloys, paramagnetic salts of transition metal ions typically have critical temperatures below 1K because the magnetic ions are very weakly coupled electronically. Above the critical temperature T_C, ferromagnetic compounds become paramagnetic and obey the Curie-Weiss law:

$$\textit{Eqn. 13} \quad \chi = \frac{C}{(T - Tc)}$$

This is similar to the Curie law, except that the plot of $1/\chi$ vs. T is shifted to a positive intercept (T_c) on the temperature axis. This reflects the fact that ferromagnetic materials (in their

paramagnetic state) have a greater tendency for spin alignment in a magnetic field than a typical paramagnet in which the spins do not interact with each other. Ferrimagnets follow the same kind of ordering behaviour. Typical plots of χ vs. T and $1/\chi$ vs. T for ferro and ferrimagnets are known as Curie-Weiss plots and should be linear if the Curie-Weiss law is obeyed (Figure 1.6).

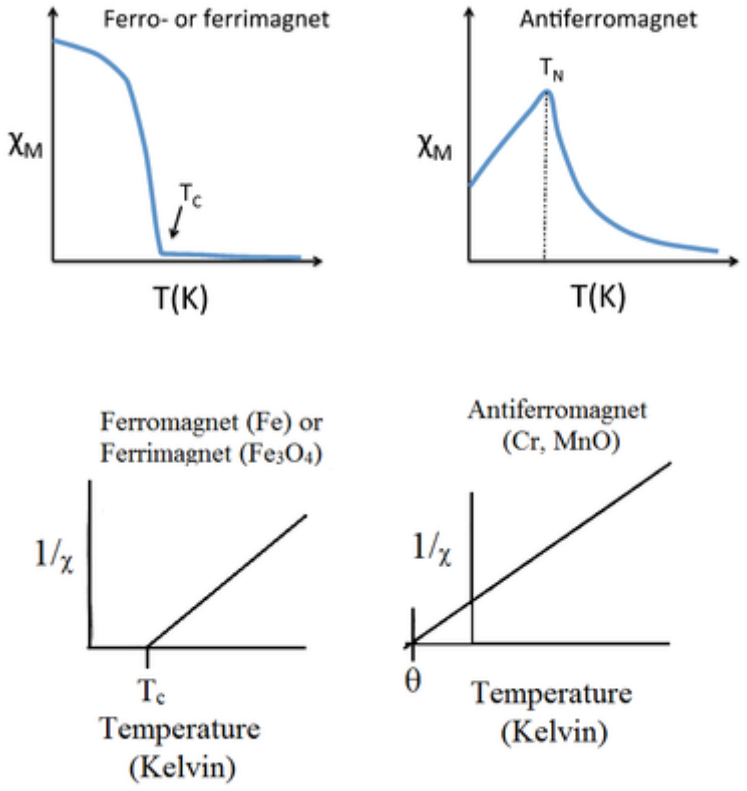

Figure 1.6 *Typical plots of χ vs. T and $1/\chi$ vs. T for ferro-, ferri and antiferromagnet materials.*[37] *T_C and T_N represent the Curie Weiss and Néel temperatures, respectively.*

In the presence of an external magnetic field, antiferromagnetic compounds show an increase in their magnetic susceptibility product with the absolute value of one of the sub-lattice magnetizations differing from that of the other sub-lattice, resulting in a non-zero net magnetization.[6] Above a critical temperature (called the Néel temperature T_N), these compounds also become paramagnetic in nature. In the absence of an applied field, the antiferromagnetic structure corresponds to a vanishing total magnetization.[6] With few exceptions, T_N is found typically to be below room temperature.[9] Antiferromagnets retain some positive susceptibility even at very low temperatures due to of canting of their paired spins. However, the maximum value of χ is much lower for an antiferromagnet than it is for a ferro-

or ferrimagnet.[6] The magnetic susceptibility values decrease inversely with temperature below T_N and increase inversely above this temperature as shown in Figure 6. The more general Curie-Weiss Law gives:

$$Eqn.\ 14 \quad \chi = \frac{C}{(T-\theta)}$$

where C is the Curie constant and θ is the Weiss constant. The latter value can be positive (ferromagnets) or negative (antiferromagnets), depending on the material.[6] This indicates that the material's magnetic susceptibility is a function of temperature and its responsiveness to the applied magnetic field will decrease with an increase in temperature.

In summary, the magnetic susceptibility product (χ) of a solid is temperature dependent and its behaviour upon temperature variation depends on the ordering of spins. Paramagnetic, ferromagnetic, antiferromagnetic, and ferrimagnetic solids all exhibit positive magnetic susceptibility values ($\chi > 0$), however their magnitudes will vary with the kind of ordering observed and with temperature. We will see these kinds of magnetic ordering primarily among the 3d and 4f elements and their alloys and compounds. For example, Fe, Co, Ni, $Nd_2Fe_{14}B$, $SmCo_5$, and YCo_5 are all ferromagnets, Cr and MnO are antiferromagnets, and Fe_3O_4 and $CoFe_2O_4$ are ferrimagnets. Strong paramagnetism decreases with rising temperature because of the de-alignment produced by the greater random motion of the atomic magnets. Weak temperature independent paramagnetism is found in many metallic elements in the solid state, such as sodium and the other alkali metals, because an applied magnetic field affects the spin of some of the loosely bound conduction electrons. Diamagnetic compounds have weak negative susceptibility values ($\chi < 0$).

1.4 Molecular Magnetism

The study of magnetism is mostly concentrated on classical magnetic materials comprised purely of metals (Fe, Co, Ni) or metal oxides.[38,39] They rely on the collective behaviour of the unpaired electron spins of hundreds of thousands of individual metal centers in a particle or bulk material. The disparate but related field of molecular magnetism; discrete and finite paramagnetic architectures that exhibit magnetic behaviour that is molecular in nature, have arisen as a new test ground for several phenomena in quantum behaviour of finite size magnetic systems.[40,41] These relatively new class of magnets include the so-called molecule-based magnets and spin crossover complexes that can mimic the unique magnetic properties exhibited

by the conventional inorganic magnets while incorporating a lot of additional useful properties such as solubility, lightness, transparency as well as magneto-optical property which provide a wide range of applications in many areas of science and technology.[41,42]
Molecular magnets are now of great interest from a coordination chemistry view point as their properties can be designed by careful selection of building blocks in the chemical process.[43] They are magnetic cages of discrete architecture that possess various structures and stability, synthesized from appropriately designed ligands and selected metal ions under specific reaction condition which is usually governed by self-assembly principles.[44]

The term molecular magnet generally refers to a molecular entity containing several magnetic ions whose individual spins couple to generate a collective spin, *S*.[44] This means that the distribution of the magnetization is the sum of contributions of individual magnetic atoms within the molecule, unlike the atom based magnets where the magnetic moments are localised on the metal atoms, with only a small part of the magnetization transferred onto the group of the atoms attached to the metal.[44] The possibility of a rational design of the physicochemical properties of molecular magnets at the synthesis level is their major advantage over classical magnetic materials.[45]

One of the possible criteria that can be used to classify these compounds is the dimensionality of their coordination network.[46] Magnetism in a molecular magnet deals with isolated molecules or assemblies of molecules with one or more magnetic centre in a single molecule (Fig 1.7). As a result, the magnetic building block for a molecular magnet is molecules, instead of an atom, because the magnetization is transferred unto the group of atoms attached.[47,48] Intra-molecular forces in these systems dominate over the intermolecular forces. Because of the fact that the inter-molecular forces are non-covalent (e.g. hydrogen bonding, Van der Waals interactions, donor–acceptor charge transfer) in nature, consequently the crystals are relatively softer than classic metal oxides (for instance) where the ionic cores dominate. These weak inter-molecular forces lead to sometimes-special optical and magnetic properties. The physical properties of molecular magnets are determined by its crystallographic and electronic structure.[46]

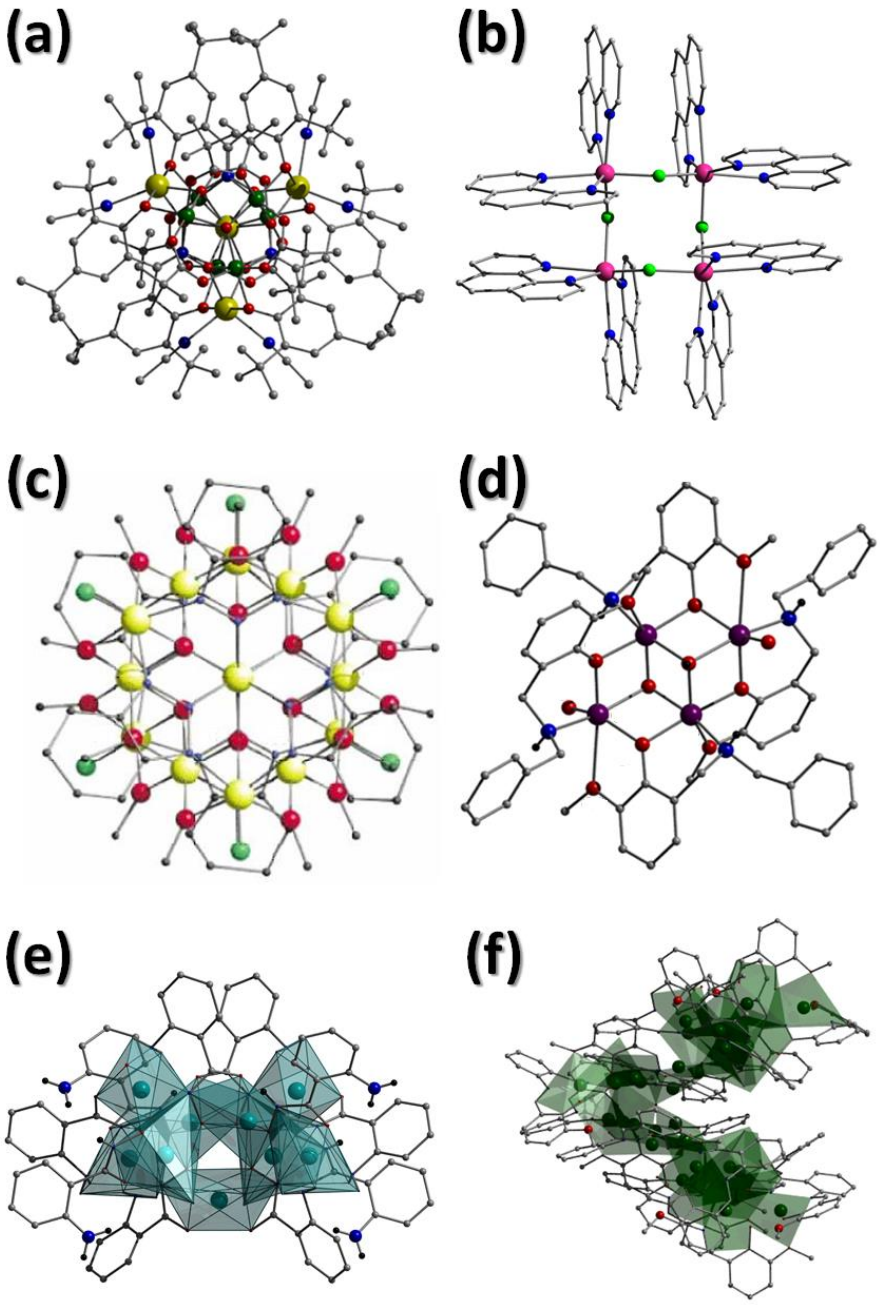

Figure 1.7 *Example of typical polymetallic magnetic cages constructed in the Jones group. These are: (a) $[Na_4Cr(III)_6(O)_2(O_2CC(CH_3)_3)_6(3,5\text{-di-}^tBu\text{-sao})_6(MeCN)_6]$ (3-5-di-tert-Bu-saoH_2 = 3,5-di-tert-Butyl salicyaldoxime), (b) $[Mn(II)_4(\mu\text{-}F)_4(1,10\text{-phen})_8](NO_3)_4$ (1,10-phen = 1,10-phenanthroline), (c) $[Fe(III)_{14}(bta)_6O_6(OMe)_{18}Cl_6]$ (btaH = benzotriazole), (d) $[(NO_3)\subset Co(II)_4(\mu_3\text{-}OH)_2(L)_4(H_2O)_2](NO_3)$ (LH = 2-[(benzylamino)methyl]-6-methoxyphenol), (e) $[Ni(II)_7(LH)_8(L_1)_2(H_2O)_6](SO_4)$ (LH_2 = 2-(dimethylamino)phenylhydroxamic acid) and (f) $[Cu(II)_{30}O(OH)_4(OMe)_2(L)_{16}(MeOH)_4(H_2O)_2](ClO_4)_4$ (LH_3 = o-[(E)-(2-hydroxy3-methoxyphenyl)methylideneamino]benzohydroxamic acid).*[46]

Molecular based magnetism offers the opportunity of being able to 'tune' the transition temperature at which the material will become ferromagnetic via modulation of the chemical structure. Molecular magnets have attracted attention due to their multidisciplinary character which include metal-radical complexes used as photo catalysts; biomimetic models of metalloenzymes with radical cofactors and molecular spintronic devices, which concerns the simultaneous utilisation of electron spin and charge.[47] The long spin coherence times displayed turn molecular based magnets into promising candidates in the context of quantum computing, where the molecule spin is used to encode a qubit.[48]

1.5 Single-Molecule Magnets

The research field of molecular magnetism involves the coupling of a materials magnetic behaviour with other properties towards bi-switchable states or multifunctional materials.[49] Single-Molecule Magnets (SMMs) are a class of nano-sized molecular magnetic materials that have garnered much attention during the last two decades due to their ability to exhibit slow relaxation of their magnetization (e.g. a barrier to magnetisation reversal).[50-55] SMMs also have unique self-assembly processes that allow chemists to both understand and control them.[56] They are polymetallic cages comprising of magnetic cores (akin to metal oxides for instance) surrounded by a sheath of organic ligands with strong intrinsic magnetism.[57,58] Their intrinsic molecular behaviour is due to the presence of an appreciable energy barrier for magnetization reversal that lead to their slow relaxation of magnetization.[59-62] This barrier to magnetisation reversal stems from their non zero ground spin states (S) and significant magnetic anisotropy associated with a negative zero field splitting (D) parameter. Many attempts have been made to enhance the S and D parameters of SMMs towards much improved magnetic bi-stability (as the barrier to magnetisation reversal = S^2D).[63-65] The most efficient way of achieving these properties is through stabilization of a high-spin ground state (S) which comes from ferromagnetic or uncompensated antiferromagnetic coupling between multiple magnetic centers in a molecule.[66] However, controlling both S and D character simultaneously has proved incredibly difficult.[64]

There are many examples of SMMs in the literature, the majority of which are transition metal clusters containing a number of Mn(III) ions, since such complexes often display large spin ground states and large negative D values associated with the present of Jahn-Teller distorted M(III) ions.[67,68] SMMs are neutral entities that form crystals that are molecular in nature bound by weak inter-chain interaction,[69] and regarded as the smallest possible magnetic storage

device, which can be used to preserve information in a single molecule rather than in a range of magnetic particles.[70] The preparation of polynuclear complexes in a rational manner with specific properties remain a formidable challenge to the synthetic chemist.[71] Since it has been establish that the physical properties of crystalline molecular materials can be influence by crystal packing effects and intermolecular interactions, suitable arrangement of the metal ions and bridging ligands in an appropriate manner may enhance the magnetic properties originated from the metal ions.[72] The extensive family of [Mn_6] SMMs reported by Brechin and co-workers is an excellent example of synthetic and magnetic control whereby the magnetic exchange may be fine tuned simply by selecting the correct bridging salicyaldoxime ligand during construction (Fig. 1.8-left).[73] Extensive magneto-structural correlations confirm that the Mn···Mn exchange interactions were governed predominantly by the extent of torsional distortion propagated by the bridging $saoH_2$ ligands.[74]

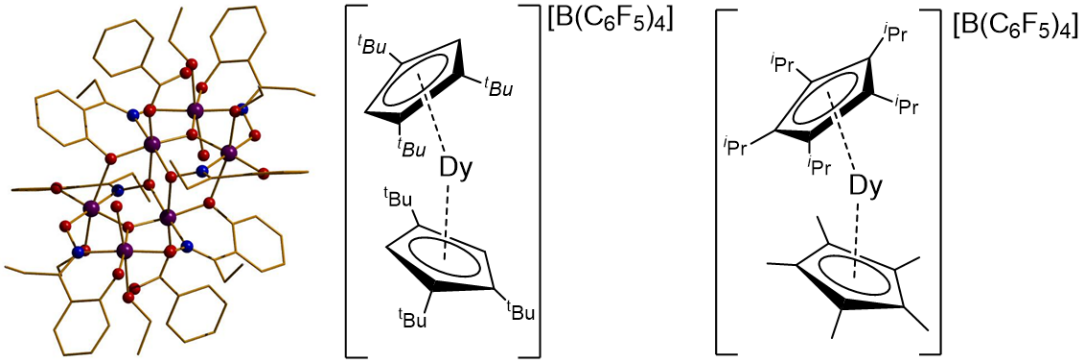

Figure 1.8 *(Left): The molecular structure of the SMM [Mn_6O_2(Et-sao)$_6$(O_2CPh)$_2$(EtOH)$_4$(H_2O)$_2$](bottom), where Et-saoH_2 is 2-hydroxypropiophenone oxime. Colour code: purple (Mn), red (O), blue (N) and light brown (C) (J. Am. Chem. Soc., 2007, 129(41), 12505). (middle) ChemDraw representation of Dysprocenium; the SMM record holder (Nature, 2017, 548, 439) until being superseded by the analogous complex on the right (Science. 2018, 362, 1400-1403).*

Single-Molecule Magnets (SMMs) appear in the centre of interest due to their promising application potential particularly in the design of ultra-dense magnetic memories and quantum computers.[75,76] What is interesting about SMMs is that they are small enough to show quantum effects as well as classic magnetic hysteresis as exhibited by traditional magnets. This peculiar combination may also have many technological implications, especially in the fields of information storage and quantum computation where it is expected to store information at much

higher densities, and to be processed at unprecedented speeds.[77] One of the tough challenge of researchers, is to design SMMs that can operate at higher temperature. These nano-sized cages were until very recently operational only at very low temperature, thus limiting their use in modern information storage technology.[77] Since the discovery of the first Single-Molecule magnet ([Mn_{12}]-with a hysteresis temperature of 4 K),[74] some progress has been achieved in this regard, however, a breakthrough is essentially needed to be made from a practical point of view.[78] To this end, in 2017, David Mills and co-workers reported a new dysprosium molecule that displayed magnetic hysteresis up to 60 K, close to liquid nitrogen temperatures (77 K).[79a] This breakthrough allowed researchers to design even better molecules going forward that could operate at 77 K or higher, which would make SMMs commercially practical for data servers. Indeed, this was the case when in 2018, Layfield and co-workers produced a Dysprocenium analogue showing magnetic hysteresis behaviour at 80 K (Fig. 1.8).[79b] Such an achievement is the equivalent to the development of the first high-temperature superconductors operating at liquid nitrogen temperatures reported in the 1980s.

Among the several benefits of SMMs is their ability to be tuned with respect to their outer organic ligand sheaths. From this, physical properties such as solubility can be (and has been) modulated towards the preparation of thin film. This provides an opportunity to attach SMMs to surfaces or polymers.[80]

1.6 Single-Chain Magnets

Single-Chain Magnets (SCMs) are an interesting class of molecular magnetic materials displaying high relaxation barriers to magnetic reversal directed along their 1-D chains and akin to SMMs, exhibit magnetic hysteresis of molecular origin. This behaviour stems from their large uniaxial magnetic anisotropy, strong intra-chain magnetic interactions between their high spin magnetic units (e.g. monomeric repeating units) and very weak or negligible inter-chain magnetic interactions that hamper the transition to 3-D magnetic ordering.[81] SCM behaviour was first postulated and modelled by Glauber in 1963, however, it was experimentally observed many years later in 2001 by Gatteschi and co-workers.[82]

The field of Single-Chain Magnetism is receiving considerable attention due to their potential applications in quantum computing, spintronics, and high-density memory devices.[83,84] SCM behaviour requires the polymerisation of anisotropic metal ion nodes using appropriate organic bridging ligand units.[85] More specifically, the synthetic approaches employed to design and

prepare SCMs in possession of high relaxation barriers and high blocking temperatures (T_B), requires metal ion building blocks that are spin carriers of large magnetic anisotropy along with appropriate bridging ligands that can connect these magnetic units in a 1-D fashion to ensure magnetic communication between the individual magnetic nodes.[86] The various combinations of intra-chain bridges, metal ions, and organic separators have led to the construction of many SCMs with different spin structures (Scheme 1.1). Although molecule based magnets showing both long-range magnetic ordering and SCM behavior have added new aspects to SCM research, a pure SCM with negligible inter-chain magnetic interaction is still preferred.[87]

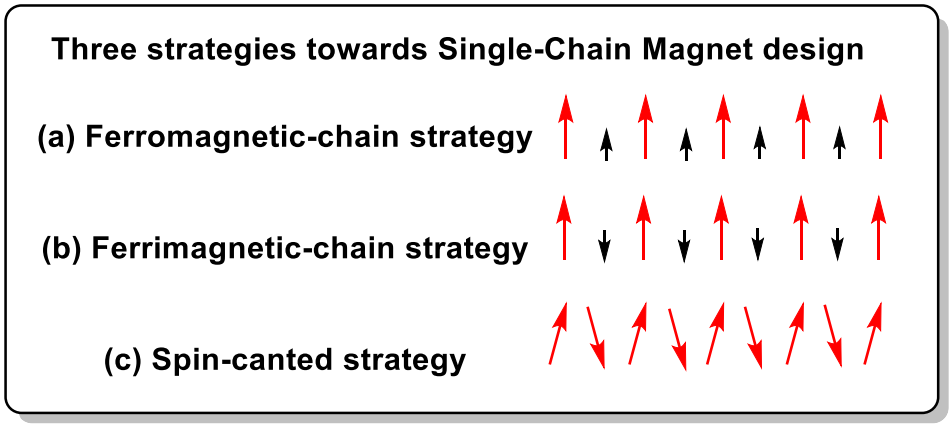

Scheme 1.1 *Three strategies towards the successful construction of a single-chain magnet.*[88]

SCMs are low dimensional polymeric magnetic materials constructed based on an alignment of the spin-carrier component that provide hysteresis behaviour for a single polymeric chain.[89-91] In 2010, Gao and co-workers summarised a successful approach to SCM formation, which is based on control of the intra-chain interaction between building blocks that are not necessarily SMMs, categorising them into three different types: ferromagnetic, ferrimagnetic and spin-centred.[88] It has also been found that spin tunnelling of domain walls and inter-spin exchange interaction play major roles in the relaxation of their magnetization in SCMs.[87] In 2014, Jun Li et al further investigated (using dynamic Monte-Carlo (DMC) methods) the previously reported SCM $[Mn(III)_2(saltmen)_2Ni(II)(pao)_2(py)_2](ClO_4)_2$ ($saltmen^{2-}$ = N,N′-(1,1,2,2-tetramethylethylene) bis(salicylideneiminate); pao = pyridine-2-aldoximate) and py = pyridine) complex by considering both quantum and classical effects. They reported simulated magnetization versus magnetic loops at three different temperatures (2.5, 1.5, and 0.5 K) for five different field-sweeping rates (Fig. 1.9).[90] The strong temperature and field sweeping rate dependent hysteresis loops established single-chain magnet behaviour. It is interesting that the experimental curves correspond to the results for typical temperatures and sweeping rates.[90]

The simulation shows that at 2.5 K, the thermal effects are dominant and spins can easily be reversed, which results in very small hysteresis loops. Similar behaviour is observed at 1.5 K, the spin being reversed, but the chance of reversal is less than that at 2.5 K, and this shows that the coercive fields are considerably greater than at 2.5 K. The data analysis indicated that when the temperature reached 3 K, no hysteresis loops were observed for all the field-sweeping rates. When the temperature was decreased (e.g. down to 0.5 K), the coercive fields became larger due to the very small transverse parameter *E*. This indicated that the coercive fields increase with decreasing temperature and increasing field sweep rate. At very low temperature, the energy barrier between the two states of opposite magnetization was too large and the spin reversal could only be realized through the direct quantum Landau–Zener (LZ) spin tunnelling.[82, 92]

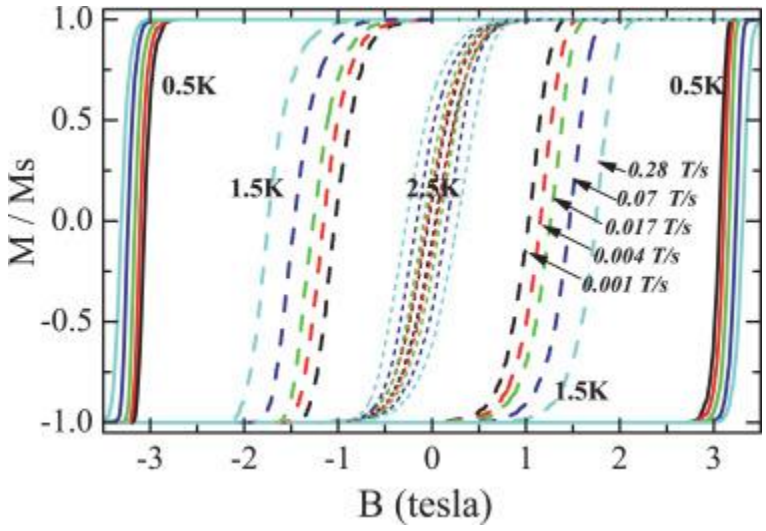

Figure 1.9 *Hysteresis loops for the Single-Chain Magnet $[Mn(III)_2(saltmen)_2Ni(II)(pao)_2(py)_2](ClO_4)_2$ ($saltmen^{2-}$ = N,N'-(1,1,2,2-tetramethylethylene) bis(salicylideneiminate); pao = pyridine-2-aldoximate) and py = pyridine) at three different temperatures: 0.5, 1.5, and 2.5 K. Five magnetization curves are plotted for every temperature using five field-sweep rates (0.001, 0.004, 0.017, 0.07, and 0.28 T/s).*[90] *For a detailed structural and magnetic description see also J. Am. Chem. Soc., 2002, 124, 12844.*

1.7 Spin-crossover complexes

Spin Crossover behaviour (SCO), is a phenomenon that describes the ability of certain complexes to undergo HS ↔ LS spin transitions due to external perturbations such as temperature, pressure, photoexcitation or an influence of a magnetic field.[93-95] The transitions from high spin (HS) to low spin (LS) or vice-versa, is commonly observed with some

octahedral d^4, d^5 and $3d^7$ transition metal complexes.[96] Examples of such metal ions include six-coordinate iron(II),[96] iron(III)[97] and cobalt(II)[98] molecular complexes, depending on the ligands that are coordinated to these metal ions.[99–101]

The extent of the ligand field splitting, and the pairing energy of the complex determines whether it will exhibit a LS or HS electron configuration. The complex would result in a LS if the ligand field splitting (Δ) is greater than the pairing energy of the complex. This mean that the electrons will fill the lower energy t_{2g} orbitals completely before populating the higher energy e_g orbitals. On the other hand, if a weaker ligand field and smaller orbital splitting is observed then a HS electronic configuration would be preferred. In this case the energy required to populate the higher levels is substantially less than the pairing energy and the electrons fill the orbitals according to Hund's Rule by populating the higher energy orbitals before pairing with electrons in the lower lying orbitals. A simplified illustration of the metal's d-orbital splitting in the presence of an octahedral ligand field is shown in Figure 1.10.

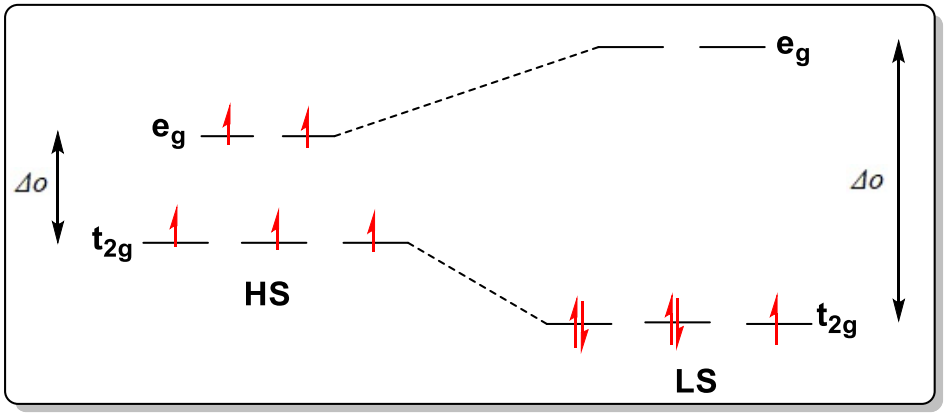

Fig. 1.10 *Diagram illustrating the dependence of the HS or LS state on the octahedral ligand field splitting (Δ_{Oct}) and the corresponding electronic configuration.*

Spin-crossover compounds have potential applications as sensor and in soft materials such as nanoparticles and thin films and conductivity.[102-105] The spin transition curve for most commonly observed types of SCO is presented in Fig. 1.11, which indicates that a HS - LS spin transition has occurred as the temperature is lowered. The temperature at which this occurs is the critical temperature (T_c).

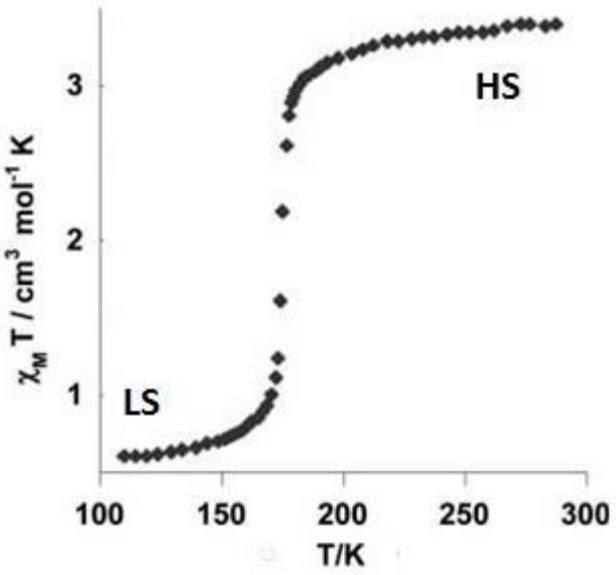

Figure 1.11 *Adapted representation of spin transition curves of χ_{mT} vs temperature (K).*[102-104]

1.8 Coordination polymers

Coordination polymers (CPs) are well defined molecular compounds constructed through an infinite metal-ligand backbone held together by coordination interactions and develop into one, two or three dimensional networks.[106-109] CPs have recorded tremendous progress in the past few decades, especially in the area of inorganic chemistry, material science, crystal engineering and solid state chemistry. This is due to their fascinating crystalline structure and promising functional properties ranging from luminescence,[110,111] magnetism,[111,112] catalysis[113,114] and conductivity.[115]

In recent years, extensive investigations have focused on the design and synthesis of novel metal coordination polymers with diverse topology and multi-dimensional networks.[116,117] As a result, major effort should be focused on the elaborate design and selection of a variety of organic ligands to realize the rational assembly and modulation of CPs. Several effective synthetic strategies such as *'node-and-spacer'* and *'secondary building units; SBUs'* have been successfully established and developed. The structural feature can influence the unusual flexibility in the physio-chemical properties of the synthesized coordination polymers.[118] There are still many challenges in practice to perfectly project and regulate the specific crystal packing of such materials, because structural control may be affected by external factors such as temperature, pressure, solvent and pH as well as by weaker non-covalent secondary interactions such as H-bonding, π–π stacking, and van der Waals forces.[119]

It is well known that di- and multitopic bridging ligands can show flexible and directional binding abilities to metal ions and thus can be applied as effective tectons for constructing a variety of coordination networks.[118,119] One synthetic strategy to design such ligands is through the covalent attachment of two disparate ligand fragments, each able to bind metal nodes in their programmed way. A good example is the employment of the pre-designed ditopic ligands 3,3′- azodibenzoic acid and 4,4′-azodibenzoic acid in the construction of a family of twelve coordination polymers comprising a myriad of metal nodes (e.g. Cu(II), Zn(II), Cd(II) and Co(II) (Fig. 1.12).[120] Indeed, such a strategy has been employed in this work as described in Chapter 3. More specifically, we have successfully coupled the moieties 4-amino-phenylhydroxamic acid and o-vanillin (as well as salicylaldehyde) to give the novel ligands N-hydroxy-4-((2-hydroxy-3-methoxybenzyl)amino)benzamide (L_6H_3) and N-hydroxy-4-((2-hydroxybenzyl)amino)benzamide (L_7H_3). These have been successfully incorporated into the Cu(II) 1-D coordination polymers $[Cu(II)(L_6H_2)_2]_n$ (**11**) and $\{[Cu(II)(L_7H_2)_2].2MeOH\}_n$ (**12**) (Fig. 1.13). Before discussing the specific aims of this project, a brief history of hydroxamic acids along with their metal coordination is provided below.

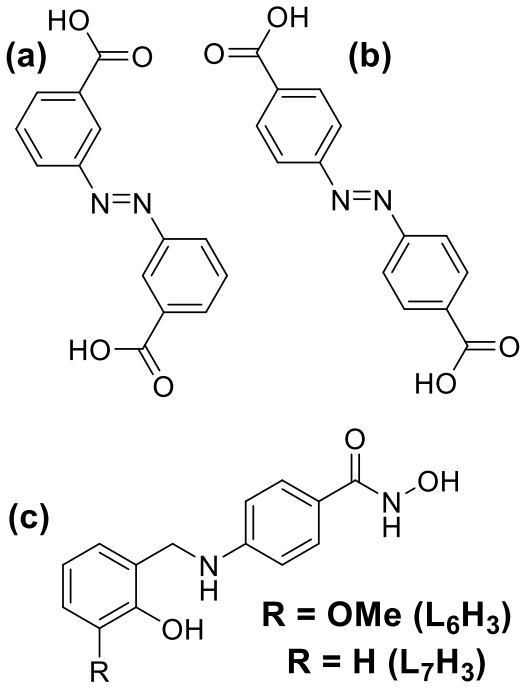

Scheme 1.2 *ChemDraw representations of the ligands 3,3′-azodibenzoic acid (a) and 4,4′-azodibenzoic acid (b) discussed in reference 120 along with the ligands L_6H_3 and L_7H_3 employed in this work.*

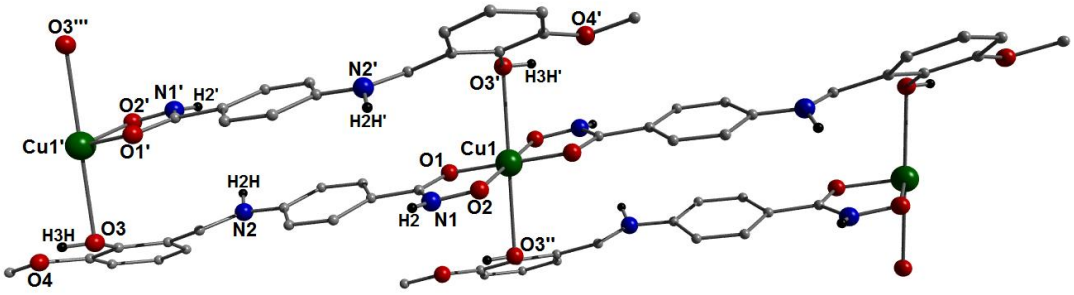

Figure 1.12 *Crystal structure of the coordination polymer* $[Cu(II)(L_6H_2)_2]_n$ ***(11)*** *as described fully in Chapter 3. Colour code: Green (Cu), Grey (C), Blue (N), Red (O) and Black (H). The majority of hydrogen atoms have been omitted for clarity.*

1.9 Magnetocaloric effect (MCE)

The magnetocaloric effect (MCE) is a fascinating feature of molecular-based magnetic materials and is best described as an ability of a material to significantly lower its temperature (adiabatic demagnetisation) upon exposure to rapid switching of an external magnetic field.[121] The magnetocaloric effect (MCE) was first discovered in metallic iron by Warburg in 1881.[122] Here, adiabatic demagnetization was employed to obtained a temperature in the sub-kelvin regime.[123] The ability of paramagnetic materials to exhibit MCE behaviour is depends on isothermal magnetic entropy changes (ΔS_M) or adiabatic temperature changes (ΔT_{ad}) upon a changes in the applied magnetic field.[124] MCE behaviour is an intrinsic attribute of all magnetic molecules but few possess sufficiently large $-\Delta S_M$ or ΔT_{ad} values that make them potential alternatives to the rare and expensive ^3He – ^4He dilution refrigerators.[125]

The intensity depends on peculiar properties of each material. In systems exhibiting long-range magnetic ordering, peak MCE behaviour is observed at the magnetic ordering temperature T_c, while it is more prominent at lower temperatures with respect to molecular nanomagnets.[126] The Gd^{3+} ion is the preferred choice when producing magnetic coolant materials due to its highly paramagnetic and isotropic nature ($4f^7$) as well as weak exchange interactions.[127,128] Previously, systems such as $Gd_5Si_2Ge_2$, MnAs, Tb_5, Si_2Ge_2 and Ni-Mn-In Heusler alloys are regarded as the most suitable candidates for cryogenic magnetic coolants at the lowest

temperature.[129-131] The emergence of molecular based materials in recent years, gave rise to highly competitive 3d, 3d–4f and 4f-type molecular magnetic coolants.[132-141] In the early stages, research focused on temperature lower than that of liquid helium,[142,143] but in recent times an intensive research activity is being undertaken on room temperature applications.[144] Y. C. Chen, et al reported a magneto-caloric study on the inorganic framework material GdF_3 in which the isothermal entropy change was evaluated up to 9 T. An extremely large $-DS_m$ value for GdF_3 was observed up to 528 mJ cm^{-3} K^{-1}, proving it to be an exceptional cryogenic magnetic coolant.[145] Magnetic refrigerators are energy efficient and may be described as an environmentally friendly technique as they do not require gases associated with greenhouse effect or ozone deflection, making them promising candidates as magnetic coolants when working in the ultra-low temperature region.[132,146]

1.10 Hydroxamic acids: A brief history

Hydroxamic acids are weak organic acids of general formula RC(=O)NHR´OH and contain oxime (–N–OH) and carbonyl (C=O) groups along with various organic residues (represented as R and R´ in Scheme 1.3).[147-149] Hydroxamic acids are important metal ion chelators with respect to the elimination of actinides and other hazardous metal ions from radioactive wastewater streams and for the recovery of plutonium and its extraction.[147-151]

Hydroxamic acids are also among the vitally important organic bio-ligands and show a wide range of biological activities such as in the treatment of tuberculosis, hypertension, cardiovascular diseases and fungal infections.[152] Hydroxamic acids are key phamacophores in many important chemotherapeutic agents, pigments and cell-division factors.[153] Much of the activities of these compounds are due to their function as a core binding group for the development of metalloenzyme inhibitors such as Histone deacetylase (HDAC), peroxidases and ureases.[154,155] They have also been considered as potent moieties in the field of cancer therapy and have attracted increasing attention for their potential in combating various etiological factors associated with cancer.[156,157]

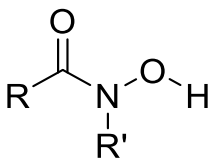

Scheme 1.3 *General structure of a hydroxamic acid with R and R' as organic residues.*[151]

Hydroxamic acids are much weaker acids than the structurally related carboxylic acids RC(=O)OH.[158] Both the naturally occurring and synthetic products generally have low toxicities and as a result are of interest for many therapeutic applications. Deprotonation of hydroxamic acids can take place at the amide nitrogen (to give N acid) or hydroxide oxygen atom (O-acid).[159,160] Hydroxamic acid and its derivatives have been shown to be nitric oxide donors by way of their chemical reactivity.

1.10.1 Synthesis and reactivity of hydroxamic acids

Several methods have been developed for the preparation of hydroxamic acids and are well documented in the literature.[158-162] Hydroxamic acids are commonly prepared through reaction of an N/O protected hydroxylamine or its derivatives with an activated carboxylic acid.[161,163]

Eqn. 15: $RCOX + NH_2OH \rightarrow RCONHOH + HX$

Hydroxamic acids are hydrophilic organic compounds that can exhibit two tautomers: keto-form and enol-form, and both tautomers may exist as Z (zusammen) or E (entgegen) diastereomers (Scheme 1.3).[164-168]

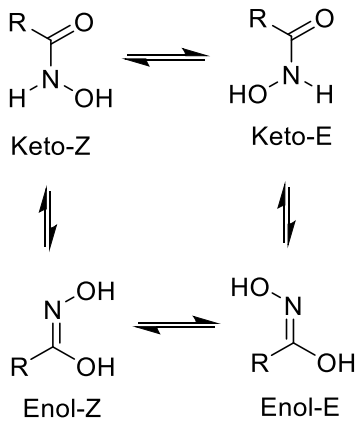

Scheme 1.4 *The Z and E diastereomers commonly observed by hydroxamic acids.*[164-168]

The economical way of making hydroxamic acid derivative is the reaction of hydroxylamine with corresponding carboxylic acid precursor or esters[169-171] For the synthesis of benzohydroxamic acid, the overall equation is:

Eqn. 16: $C_6H_5CO_2Me + NH_2OH \rightarrow C_6H_5C(O)NHOH + MeOH$

The reaction of hydroxylamine with esters does not proceed under neutral conditions (Scheme 1.4); it always needs alkaline conditions (pH > 10). Hence, this method is not suitable if one needs to perform this reaction on ester derivatives that contain halides, esters and other base-sensitive groups.[165]

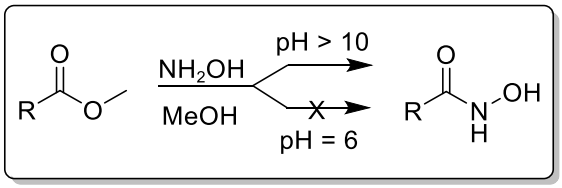

Scheme 1.5 *Synthesis of hydroxamic acid by the reaction hydroxylamine with esters.*[165]

Sekar et al. have also developed a mild and simple one-step approach for the preparation of hydroxamic acids from carboxylic acid derivatives. The carboxylic acid is mostly converted to methyl ester prior to reaction with the hydroxylamine nucleophile as shown in Scheme 1.5.[165]

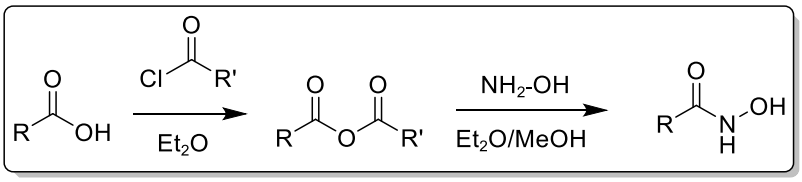

Scheme 1.6 *Preparation of hydroxamic acids from carboxylic acid derivatives.*[172]

Gissot and co-workers also described a simple, efficient and high-yielding one-step method for the synthesis of hydroxamates from various unactivated esters and the anion of *O*-benzyl-hydroxylamine.[172] This simple and efficient method was successfully applied with enolizable esters, including chiral α-amino acid esters and peptides.[173]

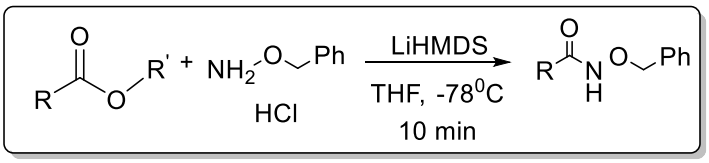

Scheme 1.7 *Preparation of hydroxamic acids from unactivated esters.*[175]

During the last few decades, solid-phase synthesis has emerged as a powerful tool for generating hydroxamic acids. Zhai et al., 2012 describes a convenient method for the direct amidation of methyl and ethyl β-ketoesters to generate solid-supported β-ketohydroxamates.[174] An efficient and convenient procedure for the release of hydroxamic acids from the solid

support through direct hydroxyaminolysis of an ester-linked substrate using aqueous hydroxylamine and KCN as the catalyst has also been reported.[175] The method comprises of treatment of the esterified resins with excess amounts of hydroxylamine to generate the corresponding hydroxamic acids. The hydroxyaminolysis protocol is compatible with a broad range of PEGA-supported peptide and peptidomimetic esters and ultimately affording hydroxamic acid derivatives in high purities.[176]

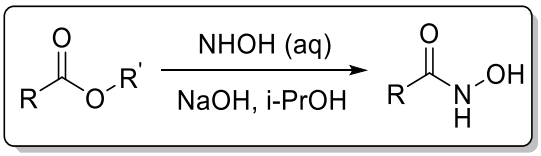

Scheme 1.8 *Hydroxyaminolysis of an esters-link substrate using aqueous NH_2OH.*[175]

Hydroxamic acids have been synthesized in good yield and purity by the reaction of the appropriate esters with hydroxylamine in the presence of a base under microwave activation and by using a modified Angeli-Rimini reaction between an aldehyde and solid-supported *N*-hydroxybenzenesulfonamide.[177,178] Microwave-assisted concepts have also been developed by Massaro and co-workers for the conversion of methyl esters into hydroxamic acids using hydroxylamine as a nucleophile.[178,179] Woodward reported the microwave-assisted preparation of Weinreb amides from N,O-dimethyl hydroxylamine hydrochloride and aliphatic esters in presence of sodium hydride and DABAL-Me_3 catalyst. DABAL-Me_3 which is an adduct of trimethylaluminum and DABCO (1,4-diazabicyclo[2.2.2]octane) is a safer alternative to trimethylaluminium for amide bond formation.[180]

1.10.2 Coordination chemistry of hydroxamic acids

Hydroxamic acids are of great importance in the field of coordination chemistry due to their very strong binding ability towards variety of transition metal ions. They are able to form homo- and heterometallic mono and polynuclear complexes (e.g. metallacrowns), with both O and N types of chelate.[181,182] The predominant binding form for majority of the investigated hydroxamate systems (as well as in this work) revealed that the {O,O} coordinated complexes are the most stable species.[183] {O,O} coordination occurs through deprotonation of hydroxamate NH-OH group and the consequent metal coordination by the carbonyl oxygen atoms (Scheme 1.8b). The bidentate chelating ability of the hydroxamate group towards a variety of metal ions[184,185] makes hydroxamic acids excellent ligands in coordination chemistry. The highly coordinative nature of hydroxamate ligands was also used extensively

to generate nitrile oxides under mild conditions as well as in floatation of rare earth metals and extraction of ores.[186]

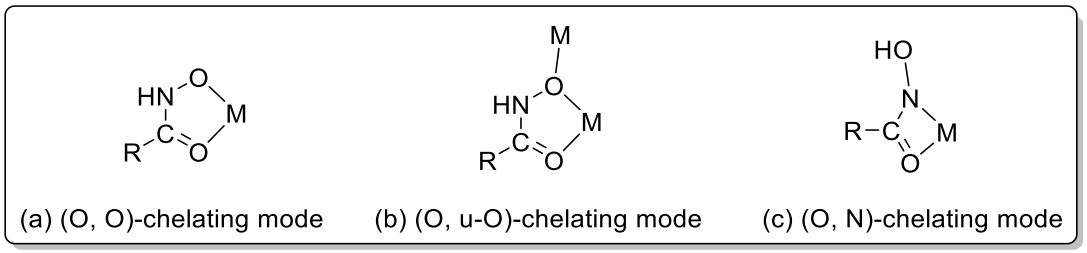

Scheme 1.9 *Schematic representation of common chelating modes of hydroxamate ligands.*[183]

Due to the high affinity between the hydroxamic acid group and Fe(III), their complexation is exploited in the natural world in the form of siderophores; molecules produced by bacteria to solubilize scarce Fe(III) under anoxic and pH neutral conditions.[188] Their biological activity has also been attributed to the strong metal ion chelating ability and the nitric oxide releasing properties. Hydroxamic acids have also been used in solar energy conversion and photocatalysis as rubost anchors for the functionalization of TiO_2 thin films.[189] Their ability to delay the oxidation of other molecules by inhibiting the initiation and / or propagation of chain reactions suggests potential antioxidant applications. They are also able to donate electrons to free radicals to form neutral molecules towards the prevention of cell and tissue damage.[190]

Several researchers have also reported that the interaction of a potent hydroxamate-based histone deacetylase (HDAC) inhibitor with suberoylanilide hydroxamic acid (SAHA), proceeds through the hydroxamate coordinating to metal ions such as Fe(III), Ni(II), Cu(II), and Zn(II) via O,O*'*-bidentate fashion both in solution and solid state.[191-193]

1.11 Aims of the project

This project set out to assess the ability of carefully designed / selected hydroxamic acids to aid the construction of transition metal complexes and extended network architectures. Our strategy to achieve this goal was to *(1)* employ sparsely investigated hydroxamic acids as bridging ligands within transition metal complexes and *(2)* design and synthesise entirely new hydroxamic acids in order to control transition metal coordination and the resultant complex topologies. More specifically and as highlighted in Figure. 1.14, careful functional group selection and positioning (R_1 and R_2) will allow synthetic and binding site control of our resultant complex or (if desired) extended network architecture (e.g. employing binding locations A and C or all three locations). Upon successful ligand design (if required),

production and full characterisation their metal coordinating ability will be investigated with a number of transition metal ions. All complexes would then be assessed both structurally and physically (e.g. Superconducting quantum interference device (SQUID) magnetometry for all paramagnetic complexes) using a myriad of techniques.

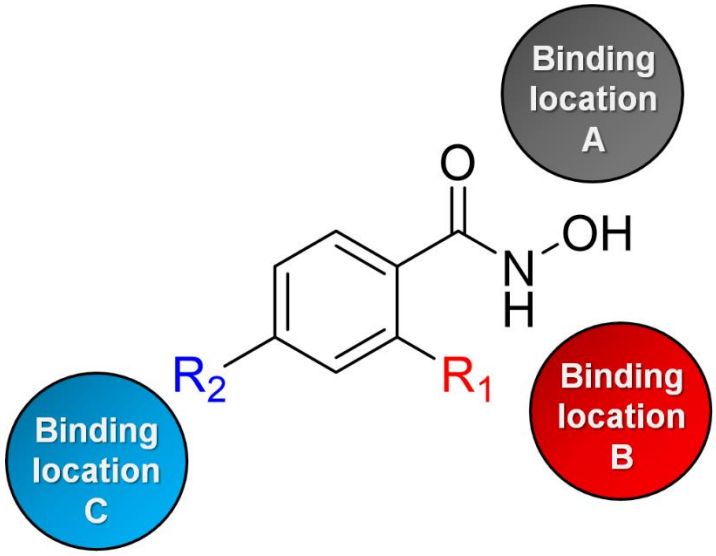

Figure 1.13 *Schematic highlighting the positions (binding locations A-C) situated around a phenylhydroxamic acid backbone that will be exploited in this work towards producing discrete complexes or extended architectures (as desired).*

References

1. E. T. Lacheisserie, D. Gignoux and M. Schlenker. *Springer*, 2005, **2**, 3–6.
2. D. Michael. *Encyclopedia of Chinese History*. Routledge, 2017, 98.
3. W. Lowrie. *Fundamentals of geophysics*, Cambridge University Press, 2007.
4. M. Rochdi, S. A. Kumar and P. P. Mani. *Springer Science & Business Media*, New York, 2012, 403–405.
5. P. M. Smith. *J. Chem. Educ.*, 2005, **82**, 213-214.
6. A. F. Orchard. *Magnatochemistry*, Oxford University Press, New York, 2003.
7. N. H. de V. Heathcote. *Annals of Sci*., 1967, 23(4), 261-275.
8. A. A. Mills. *Annals of Sci*., 2004, **61**, 273–319.
9. K. Helmut, *Handbook of Magnetism and Advanced Magnetic Materials*, John Wiley & Sons Inc, Hoboken, 2007, **5**, 470.
10. R. T. Merril and M. W. McElhinny. *The earth's magnetic field: origin and planetary perspective*, Academic Press, London; New York, 1983.
11. D. C. Giancoli. *Physics for scientists and engineers with modern physics*, Pearson Education, 2008.
12. E. Purcell. *Electricity and Magnetism*. Cambridge University Press, Harvard University, Massachusetts, 2011, 170.
13. R. P. Feynman in *The Feynman Lectures on Physics*, ed. R, B. Leighton, M. L. Sands, Pearson/Addison-Wesley, San Francisco, 2006, Vol. II, pp. 17-2.
14. E. M. Purcell and D. J. Morin. *Electricity and Magnetism*, Cambridge University Press, New York, 2013.
15. B. Michael. *Physics for Engineering and Science*, McGraw Hill/Schaum, New York, 2013.
16. P. J. Nahin. *IEEE Spectrum*, 1992, **29**, 45.
17. W. Stephen. *A New Kind of Science*, Wolfram Media, Inc., Champaign, 2002.
18. J. J. Thomson. *Phil. Mag. Series 5*, 1879, **44,** 293-316.
19. G. Fraser. *Cosmic Anger: Abdus Salam*, Oxford University Press, 2008, 119.
20. S. Glashow. *Nucl. Phys*., 1959, **10**, 107.
21. A. Salam and J. C. Ward. *Nuovo Cimento.*, 1959, **11**, 568–577.
22. S. Weinberg, *Phys. Rev. Lett*., 1967, **19**, 1264–66.
23. E. P. Furlani, *Academic Press*, University of Maryland, 2001, **5**, 518.
24. R. G. Newton. *What Make Nature Tick*, Harvard University Press, Indiana University, 1993.

25. C. J. O'Connor. *Progress in Inorganic Chemistry*, ed. S. J. Lippard, John Wiley & Sons, Inc., Hoboken, NJ, USA, 2007, **29**, 203-283.
26. B. D. Cullity and C. D. Graham. *Introduction to Magnetic Materials* 2nd edn, Wiley Press, Hoboken, NJ, USA, 2008.
27. H. E. Rolf. *Electronic Properties of Materials,* Springer Science and Business Media, LLC, New York, 4th edn, 2011, 339 - 340.
28. X. Y. Lang, W. T. Zheng and Q. Jiang. 2007, *Nanotech.* **18,** 1-6.
29. M. Suzuki, N. Kawamura, H. Miyagawa, J. S. Garitaonandia, Y. Yamamoto and H. Hori. *Phys. Rev. Lett.* 2012, 108, 047201.
30. G. Kopnov, Z. Vager and R. Naaman. *Adv. Mater.*, 2007, **19**, 925–928.
31. V. I. Pavlenko, N. I. Cherkashina and L. N. Demkina. *Mat. Sci. Engr.*, 2018, **327**, 1-5.
32. B. R. Coles. *Platinum Metals Rev*., 1964, **8**, 1.
33. H. J. Albert and L. R. Rubin. *Adv. Chem.*, 1971, **98,** 1-16.
34. J. D. Boer and R. V. Lieshout. *Physica*, 1949, **15**, 569-580.
35. R. C. Richardson and E. N. Smith. *Experimental Techniques in Condensed Matter Physics At Low Temperatures,* New York CRC Press, University Ithaca, 1998.
36. M. W. Jaroszewski, S. Thomas and A. V. Rane. *Advanced Materials for Electromagnetic Shielding: Fundamentals, Properties*, John Wiley & Sons, Hoboken USA, 2018.
37. C. E. Housecroft and A. G. Sharpe. *Inorganic Chemistry*, Pearson Education Limited, 4th Ed., Edinburgh Gate, England, 2012.
38. L. Xu, Y. X. Wang and H. B. Yang. *Dalton Trans*., 2015, **44**, 867-890.
39. T. Chakraborty, T.K. Sen, H.S.D. Das and S. K. Mandal. *C. Mit. Solid State Commun.*, 2012, **152**, 1945–1950.
40. M. J. Santander, A. S. Nunez, A. Roldán-Molina and R. E. Troncoso. *J. Magn. Magn. Mat.*, 2015, **396**, 176–180.
41. R. Lescouezec, J. Vaissermann, C. Ruiz-Perez, F. Lloret, R. Carrasco, M. Julve, M. Verdaguer, Y. Dromzee, D. Gatteschi and W. Wernsdorfer. *Angew. Chem. Int. Ed*., 2003, **42**, 1483 – 1486.
42. J. Ferrando-Soria, J. Vallejo, M. Castellano, J. Martínez-Lillo, E. Pardo, J. Cano, I. Castro, F. Lloret, R. Ruiz-García and M. Julve. *Coord. Chem. Rev.*, 2017, **339**, 17-103.
43. S. Bertaina, T. Gambarelli, B. Mitra, A. Tsukerblat, A. Miller and B. Barbara. *Nature,* 2008, **8,** 453.
44. C. J. Milios, A. Vinslava, W. Wernsdorfer, S. Moggach, S. Parsons, S. P. Perlepes, G.

Christou and E. K. Brechin. *J Am Chem Soc.* 2007, **129**, 2754–2755.

45. P. Konieczny, R. Pełka, P. M. Zieliński, F. L. Pratt, D. Pinkowicz, B. Sieklucka and T. Wasiutyński. *J. Magn. Magn. Mater.*, 2013, **344**, 105–108.

46. (a) E. Houton, P. Comar, M. B. Pitak, S. J. Coles, A. G. Ryder, S. Piligkos, E. K. Brechin and L. F. Jones. *RSC Advances*, 2016, **6**, 73668-73676. (b) S. T. Meally, K. Mason, P. McArdle, E. K. Brechin, A. G. Ryder and Leigh F. Jones. *Chem. Commun.,* 2009, 7024-7026. (c) D. M. Low, L. F. Jones, A. Bell, E. K. Brechin, T. Mallah, E. Rivière, S. J. Teat and E. J. L. McInnes. *Angew. Chem. Int. Ed.*, 2003, 42, 3781-3784. (d) M. E. Slater-Parry, J. P. Durrant, J. M. Howells, M. B. Pitak, P. N. Horton, W. T. Klooster, S. J. Coles, H. M. O'Connor, E. K. Brechin, A.-L. Barra and L. F. Jones. *Dalton Trans.,* 2019, **48**, 1477-1488. (e) C. McDonald, S. Sanz, E. K. Brechin, M. Kumar Singh, G. Rajaraman, D. Gaynor and L. F. Jones. *RSC Advances*, 2014, **4**, 38182-38191. (f) C. McDonald, D. W. Williams, P. Comar, S. J. Coles, T. D. Keene, M. B. Pitak, E. K. Brechin and L. F. Jones. *Dalton Trans.,* 2015, **44**, 13359-13368.

47. J. S. Miller. *Mater. Today*, 2014, **17**, 224-235.

48. D. Lee, D. J. Williams, S. C. Vogel, T. Proffen, J. D. Thompson, L. L. Daemen and S. Park, *Curr. Appl. Phys.*, 2016, **16**, 1100–1104.

49. A. Caneschi, D. Gatteschi and F. Totti. *Coord. Chem. Rev.*, 2015, **289-290**, 357–378.

50. J. Lehmann, A. Gaita-Arino, E. Coronado and D. Loss. *Nature Nanotech.,* 2007, **2(5)**, 312-317.

51. W. Laosiritaworn and Y. Laosiritaworn. *Polyhedron*, 2013**, 66**, 108–115.

52. M. Clemente-León, E. Coronado, C. Martí-Gastaldo and F. M. Romero. *Chem. Soc. Rev*., 2011, **40**, 473.

53. E. Coronado, M. Makarewicz, J. P. Orieto-Ruiz, H. Prima-García and F.M. Romero. *Adv. Mater*., 2011, **23**, 4323.

54. C. J. Milios, A. Vinslava, W. Wernsdorfer, A. Prescimone, P. A. Wood, S. Parsons, S. P. Perlepes, G. Christou and E. K. Brechin. *J. Am. Chem. Soc.,* 2007, **129**, 6547–6561.

55. C. I. Yang, Z. Z. Zhang and S. B. Lin. *Coord. Chem. Rev.*, 2015, **289-290**, 289–314.

56. Y. Liu and A. Garg. *Ann. Phys. (N. Y).*, 2016, **366**, 76–101.

57. N. Ishikawa, M. Sugita and W. Wernsdorfer. *J. Am. Chem. Soc.*, 2005, **127**, 3650-3651.

58. E. K. Brechin, C. Boskovic, W. Wernsdorfer, J. Yoo, A. Yamaguchi, E. C. Sanudo, T. R. Concolino, A. L. Rheingold, H. Ishimoto, D. N. Hendrickson and G. Christou. *J. Am. Chem. Soc*. 2002, **124**, 9710-9711.

59. L. Bogani and W. Wernsdorfer. *Nanoscience and Technology*. 2009, 194-201.

60. L. Zhao, Y. Zhang, J. Hu, C. Jiao, J. Wang, C. Duan and T. Liu. *Inorg. Chem. Comm*, 2016, **66**, 55–58.
61. S. Demir, J. M. Zadrozny, M. Nippe and R. Long. *J. Am. Chem. Soc.*, 2012, **396**, 8–11.
62. D. Gatteschi. *J. Alloys and Compounds.* 2001, **317-318**, 8–12.
63. M. Gregson, N. F. Chilton, A. Ariciu, F. Tuna, I. F. Crowe, W. Lewis, A. J. Blake, D. Collison, E. J. L. McInnes, E. P. Winpenny and S. T. Liddle. *Chem. Sci.*, 2015,**7,** 155–165.
64. O. Waldmann. *Inorg. Chem*., 2007, **46**, 10035-10037.
65. W. Cao, C. Gao, Y.-Q. Zhang, D. Qi, K. Wang, C. Duan, S. Gao and J. Jiang. *Chem Sci.*, 2015, **6**, 5947-5954.
66. I. A. Kühne, G. E. Kostakis, C. E. Anson and A. K. Powell. *Inorg. Chem.*, 2016, **55**, 4072-4074.
67. D. Hamada, T. Fujinami, S. Yamauchi, N. Matsumoto, N. Mochida, T. Ishida, Y. Sunatsuki, M. Tsuchimoto, C. Coletti and N. Re, *Polyhedron*, 2016, **109**, 120–128.
68. L. F. Jones, M. E. Cochrane, B. D. Kovisto, D. A. Leigh, S. P. Perlepes, W. Wernsdorfer and E. K. Brechin. *Inorg. Chim. Acta* 2008, **361**, 3420-3426.
69. R. López-Ruiz, P. T. Almeida, M. G. F. Vaz, M. A. Novak, F. Béron and K. R. Pirota. *J. Magn. Magn. Mater*., 2016, **403**, 188–192.
70. C. J. Milios, R Inglis, A Vinslava, R Bagai, W Wernsdorfer, S. Parsons, S. P. Perlepes, G. Christou and E. K. Brechin. *J. Am. Chem. Soc*., 2007, **129**, 12505–12511.
71. G. Christou, D. Gatteschi, D. N. Hendrickson and R. Sessoli. *MRS Bull.*, 2000, **25**, 66–71.
72. E. K. Brechin, A. D. Katsenis, R. Inglis, A. Prescimone and G. S. Papaefstathiou. *CrystEngComm*, 2012, **14**, 1216-1218.
73. R. Inglis, L. F. Jones, C. J. Milios, S. Datta, A. Collins, S. Parsons, W. Wernsdorfer, S. Hill, S. P. Perlepes, S. Piligkos and E. K. Brechin. *Dalton Trans.*, 2009, 3403-3412.
74. R. Inglis, C. J. Milios, L. F. Jones, S. Piligkos and E. K. Brechin. *Chem. Commun.*, 2012, **48**, 181-190.
75. W. Wernsdorfer, R. Sessoli, A. Caneschi and D. Gatteschi. *Europhys. Lett*., 2010, **50**, 552-558.
76. W. W. Kuang, L.-L. Zhu, Y. Xu and P.-P. Yang. *Inorg. Chem. Commun.*, 2015, **61**, 169–172.
77. C. Rajnák, A. Packová, J. Titiš, J. Miklovič, J. Moncol' and R. Boča, *Polyhedron*, 2016, **110**, 85–92.

78. I. Cimatti, X. Yi, R. Sessoli, M. Puget, B. L. Guennic, J. Jung, T. Guizouarn, A. Magnani, K. Bernot and M. Mannini. *Appl. Surf. Sci*., 2018, **432**, 7-14.
79. (a) C. P. Goodwin, F. Ortu, D. Reta, N. F. Chilton and D. P. Mills. *Nature*, 2017, **548**, 439-442. (b) F. S. Gao, B. M. Day, Y.-C. Chen, M.-L. Tong, A. Mansikkamaki and R. A. Layfield. *Science*, 2018, **362**, 1400-1403.
80. M. Clemente-Leon, H. Soyer, E. Caronado, C. Mingotaud, C. J. Gomez-Garcia and P. Delhaes. Angew. *Chem. Int. Ed.* 1998, **7,** 2842.
81. Y. Z. Zheng, W. Xue, M. L. Tong, X. M. Chen and S. L. Zheng, *Inorg. Chem.,* 2008, **47,** 11202.
82. D. Gatteschi, A. Vindign. *Molecular Magnets; Phy. and Appl.*, ed. J. Bartolom, F. Luis, and J. Fernandez, Springer-Verlag, Berlin, Heidelberg, 2014, vol. 1, ch. 1, pp. 1-31.
83. R. Sessoli. *Angew. Chem., Int., Ed.* 2008, **47**, 5508.
84. D. F. Weng, B. W. Wang, Z. M. Wang and S. Gao. *Coord. Chem. Rev.,* 2013, **257**, 2484-2490.
85. L. Bogani, A. Vindigni, R. Sessoli, and D. Gattesshi. *J. Mater. Chem*., 2008, **18**, 4750–4758.
86. S. Dhers, H. L.C. Feltham and S. Brooker. *Coord. Chem. Rev.,* 2010, **296**, 24-44.
87. K. Bernot, L. Bogani, A. Caneschi, D. Gatteschi and R. Sessoli. *J. Am. Chem. Soc.,* 2006, **128**, 7947–7956.
88. H. L. Sun, Z. M. Whang and S. Gao. *Coord. Chem. Rev.,* 2010, **254**, 1081-1100.
89. V. V. Valkov and M. S. Shustin. *J. Magn. Magn. Mat*., 2017, **440**, 19–22.
90. J. Li and B.-G. Liu. *J. Magn. Magn. Mat*., 2015, **378**, 186-189.
91. V.V. Valkov and M.S. Shustin. *J. Low. Temp. Phys.*, 2016, **185**, 564.
92. G. B. Liu and B.-G. Liu. *Phys. Rev. B,* 2010, **82,** 134-410.
93. M. A. Halcrow. *Chem. Soc. Rev.***,** 2011, **40**, 4119-4142.
94. L. J. Pauling. *J. Am. Chem. Soc.*, 1937, **59**, 633.
95. E. Collet and P. Guionneau. *C. R. Chimie*, 2018, **21**, 1133-1151.
96. M. A. Halcrow. *Polyhedron*, 2007, **26**, 3523.
97. M. Nihei, T. Shiga, Y. Maeda and H. Oshio. *Coord. Chem. Rev*., 2007, **251**, 2606.
98. I. Krivokapic, M. Zerara, M. L. Daku, A. Vargas, C. Enachescu, C. Ambrus, P. Tregenna-Piggott, N. Amstutz, E. Krausz and A. Hauser. *Coord. Chem. Rev*., 2007, **251**, 364.
99. P. Angaridis, F. A. Cotton, C. A. Murillo, D. Villagrán and X. Wang. *J. Am. Chem. Soc.*, 2005, **127**, 5008-5009.

100. G. Balazs, F. G. N. Cloke, L. Gagliardi, J. C. Green, A. Harrison, P. B. Hitchcock, A. R. M. Shahi and O. T. Summerscales. *Organometallics*, 2008, **27**, 2013.
101. A. E. Ashley, R. T. Cooper, G. G. Wildgoose, J. C. Green and D. O'Hare. *J. Am. Chem. Soc.*, 2008, **130**, 15662.
102. H. Li and H. Peng. *Current Opinion in Colloid & Interface Science*, 2018, **35**, 9–16.
103. H. J. Shepherd, G. Molnár, W. Nicolazzi, L. Salmon and A. Bousseksou. *Eur. J. Inorg. Chem*., 2013, 653–61.
104. G. Molnar, L. Salmon, W. Nicolazzi, F. Terki and A. Bousseksou. *J. Mater. Chem. C.*, 2014, **2**, 1360–1366.
105. T. Mallah and M. Cavallini. *C. R. Chimie.*, 2018, **21**, 1270-1286.
106. S. R. Batten, N. R. Champness, X. M. Chen, J. Garcia-Martinez, S. Kitagawa, L. Ohrström, M. O'Keeffe, M. P. Suh and J. Reedijk. *CrystEngComm*, 2012, **14**, 3001.
107. C. Inman, J. M. Knaust and S. W. Keller. *Chem. Commun.*, 2002, **0**, 156–157.
108. L. M. Zheng, P. Yin and Xin. *Inorg. Chem.*, 2002, **41**, 4084–4086.
109. S.R. Batten, N.R. Champness, X.-M. Chen, J. Garcia-Martinez, S. Kitagawa, L. Ohrstrom, M. O'Keeffe, M.P. Suh and J. Reedijk, *Pure Appl. Chem*., 2013, **85**, 1715.
110. J. Heine and K. Müller-Buschbaum. *Chem. Soc. Rev*., 2013, **42**, 9232–9242.
111. D. F. Weng, Z.-M. Wang and S. Gao. *Chem. Soc. Rev*., 2011, **40**, 3157.
112. D. R. Talham and M.W. Meisel. *Chem. Soc. Rev*., 2011 **40**, 3356.
113. A. Corma, H. García and F.X. Llabrés i Xamena, *Chem. Rev*., 2010, **110**, 4606-4655.
114. J. Gascon, A. Corma, F. Kapteijn and, F.X. Llabrés i Xamena, *ACS Catal*., 2013, **4**, 361-378.
115. G. Givaja, P. Amo-Ochoa, C.J. Gómez-García and F. Zamora. *Chem. Soc. Rev*., 2012, **41**,115.
116. C. Pettinari, A. Tabacaru and S. Galli. *Coord. Chem. Rev.*, 2016, **307**, 1-37.
117. J. Sun, M. Zhang, A. Wang and Z. Cai. *Crystals* 2017, **7,** 370.
118. A. Tabacaru, C. Pettinari and S. Galli. *Coord. Chem. Rev.*, 2018, **372**, 1-30.
119. C. Janiak. *Dalton Trans*., 2003, 2781-2804.
120. Z. F. Chen, Z. L. Zhang, Y. H. Tan, Y. Z. Tang, H. K. Fun, Z. Y. Zhou, B. F. Abrahams and Hong Liang. *CrystEngComm.*, 2008, **10**, 217–231.
121. C. A. Zimm, A. Jastrab, A. Sternberg, V. K. Gschneidner Jr., M. G. Osborn and I. E. Anderson. *Adv. Cryog. Eng.*, 1998, **43**, 1759.
122. E. Warburg. *Ann. Phys.*, 1881, **249**, 141.
123. W. F. Giauque. *J. Am. Chem. Soc.*, 1927, **49**, 1864.

124. M. Gajewski, R. Pelka, M. Fitta, Y. Miyazaki, Y. Nakazawa, M. Balanda, M. Reczynski, B. Nowicka and B. Sieklucka. *J. Mag. Mag. Mat.*, 2016, **414**, 25-31.
125. C. Hagmann, D. J. Benford and P. L. Richards. *Cryogenics*, 1994, **34**, 213-219.
126. M. Fitta, W. Sas and T. Korzeniak. *J. Mag. Mag. Mat.*, 2018, **465**, 640-645.
127. K. A. Gschneidner Jr. and V. K. Pecharsky. *Annu. Rev. Mater.Sci.*, 2000, **30**, 387.
128. K. A. Gschneidner Jr., V. K. Pecharsky and A. O. Tsokol. *Rep. Prog. Phys.*, 2005, **68**, 1479-1539.
129. B. Baudun, R. Lagnier and B. Salce. *J. Magn. Magn. Mater.*, 1982, 27, 315.
130. O. Gutfleisch, M. A. Willard, E. Bruck, C. H. Chen, S. G. Sankar and J. P. Liu. *Adv. Mater.*, 2011, **23**, 821.
131. V. Basso, C. P. Sasso, K. P. Skakov, O. Gutfleisch and V. V. Khovaylo. *Phys. Rev.*, 2012, B **58**, 014430.
132. M. Evangelisti and E. K. Brechin. *Dalton Trans.*, 2010, **39**, 4672.
133. S. Nayak, M. Evangelisti, A. K. Powell and J. Reedijk. *Chem. Eur. J.*, 2010, **16**, 12865.
134. J. P. Zhao, R. Zhao, Q. Yang, B. W. Hu, F.-C. Liu and X. H. Bu. *Dalton Trans.*, 2013, **42**, 14509.
135. C. B. Tian, R.-P. Chen, C. He, W. J. Li, Q. Wei, X.-D. Zhang and S. W. Du. *Chem. Commun*., 2014, **50**, 1915.
136. Y. C. Chen, J. L. Liu, J.-D. Leng, F.-S. Guo, P. Vrabel, M. Orendac, J. Prokleska, V. Sechovsky and M. L. Tong. *Chem. Eur. J.*, 2014, **20**, 3029.
137. T. N. Hooper, J. Schnack, S. Piligkos, M. Evangelisti and E. K. Brechin. *Angew. Chem., Int. Ed*., 2012, **51**, 4633.
138. Y. Z. Zheng, M. Evangelisti, F. Tuna and R. E. P. Winpenny. *J. Am. Chem. Soc*., 2012, **134**, 1057.
139. J. B. Peng, Q. C. Zhang, X.-J. Kong, Y. Z. Zheng, Y. P. Ren, L. S. Long, R. B. Huang, L. S. Zheng and Z. Zheng. *J. Am. Chem. Soc.*, 2012, **134**, 3314.
140. E. M. Pineda, F. Tuna, R. G. Pritchard, A. C. Regan, R. E. P.Winpenny and E. J. L. McInnes. *Chem. Commun*., 2013, **49**, 3522.
141. F. S. Guo, Y.-C. Chen, J.-L. Liu, J. D. Leng, Z.-S. Meng, P. Vrabel, M. Orendac and M. L. Tong. *Chem. Commun.*, 2012, **48**, 12219.
142. W. F. Glauque and D. P. MacDougall. *Phys. Rev.*, 1933, **43**, 768.
143. W. F. Glauque and D. P. MacDougall. *J. Am. Chem. Soc.*, 1935, **57**, 1175-1185.
144. A. M. Tishin, Y. I. Spichkin, *The magnetocaloric Effect and its Applications*, Institute of Physics Publishing, Bristol, 2003.

145. Y. C. Chen, J. P. ka, W. J. Xu, J. L. Liu, J. Liu, W. X. Zhang, Jian-Hua Jia, V. Sechovsky and M. L. Tong. *J. Mater. Chem. C*, 2015, **3**, 12206-12211.
146. R. Pelka, P. Konieczny, P. M. Zielinski, T. Wasiutynski, Y. Miyazaki, A. Inaba, D. Pinkowicz and B. Sieklucka. *J. Mag. Mag. Mater.*, 2014, **354**, 359-362.
147. D. Dev, N. B. Palakurthy, K. Thalluri, J. Chandra and B. Mandal. *J. Org. Chem.*, 2014, **79**, 5420-5431.
148. S. T. Heller and R. Sarpong. *Org. Lett.*, 2010, **12,** 4572-4575.
149. B. Vasantha, H. P. Hemantha and V. V. Sureshbabu. *Synthesis*, 2010, **66**, 2990-2996.
150. T. Niu, K.-H. Wang, D. Huang, C. Xu, Y, Su, Y. Hu and Y. Fu. *Synthesis*, 2014, **46,** 320-330.
151. K. Thalluri, S. R. Manne, D. Dev and B. Mandal. *J. Org. Chem.*, 2014, **79**, 3765-3775.
152. H. Vanjari and R. Pande. *J. Pharm. Biomed. Anal*., 2003, **33** 783-788.
153. S. Belvedere, D.J. Witter, J. Yan, J.P. Secrist, V. Richon and T.A Miller. *Med Chem Lett.*, 2007, **17**, 3969–71.
154. A. Fazary, M. Khalil, A. Fahmy and T. Tantawy. *Med. J. Islam. Acad. Sci*, 2001, **14**, 109–116.
155. C. A. Kontogiorgis, P. Papaioannou and D. J. Hadjipavlou-Litina. *Curr. Med. Chem*., 2005, **12**, 339-355
156. J. M. Chalovich and E. Eisenberg, *Biophys. Chem.*, 2005, **257**, 2432–2437.
157. D. Pal and S. Saha. *J. Adv. Pharm. Tech. Res*, 2012, **3**, 92–99.
158. C. J. Marmion, D. Griffith and K. B. Nolan. *Eur. J. Inorg. Chem.*, 2004, 3003-3016.
159. B. J. Colston, G. R, Choppin and R. J Taylor. *Radiochim. Acta*, 2000, **88**, 329–334.
160. S. L. Yedage and B. M. Bhanage. *Synthesis*, 2015, **47**, 526-532.
161. S. P. Gupta and A. Sharma, in *The Chemistry of Hydroxamic Acids*, ed. S. P. Gupta, Springer, Berlin, Heidelberg, 2013, ch. 1, pp. 1–18.
162. C. D. Floyd, C. N. Lewis, S. R. Pate and M. Whittaker. *Tetrahedron Lett.*, 1996, **31**, 8045-8048.
163. P. Guan, F. Sun, X. Hou, F. Wang, F. Yi, W. Xu and H. Fang. *Bioorg. & Med. Chem*., 2012, **20**, 3865-3872.
164. V. M. Patil, S. P. Gupta, in *Hydroxamic Acids: Structure–Activity Relationship Studies of Hydroxamic Acids as Matrix Metalloproteinase Inhibitors*, ed. S. Gupta. Springer, Berlin, Heidelberg, 2013, ch. 1, pp. 71-98.
165. A. S. Reddy, M. S. Kumar and G. R. Reddy. *Tetrahedron Lett.*, 2000, **41**, 6285–6288.
166. E. Adiguzel, F. Yilmaz, M. Emirik and M. Ozil. *J. Mol. Str*., 2017, **1127**, 403-412.

167. A. Beillard, Y. Bhurruth-Alcor, C. Bouix-Peter, K. Bouquet, S. Chambon, L. Clary, C. S. Harris, C. Millois, G. Mouis, G. Ouvry, R. Pierre, A. Reitz and L. Tomas. *Tetrahedron Lett*., 2016, **57**, 2165-2170.
168. G. Zhao, H. Zhong, X. Qiu, S. Wang, Y. Gao, Z. Dai, J. Huang and G. Liu. *Min. Engr*., 2013, **49**, 2013, 54-60.
169. B. Vasanthaa, H. P. Hemantha and V.V. Sureshbabu. *Synthesis*, 2010, 2990-2996.
170. T. Kishore, R.M. Srinivasa, D. Dharm and M. Bhubaneswar. *J. Org. Chem*., 2014, **79**, 3765-3775.
171. L.K. Gediya, P. Chopra, P. Purushottamachar, N. Maheshwari and V.C. Njar, *J. Med. Chem.*, 2005, **48**, 5047-5051.
172. A. Gissot, A. Volonterio and M. Zanda. *J. Org. Chem.*, 2005, **70**, 6925-6928.
173. Giacomelli, A. Porcheddu and M. Salaris, *Org. Lett*., 2003, **5**, 2715-2717.
174. W. Zhai, S. W. Gerritz and M. J. Sofia. *Tetrahedron Lett.*, 2012, **52**, 267-270.
175. N. S. Nandurkar, R. Petersen, K. Qvortrup, V. V. Komnatnyy, K. M. Taveras, S. T. Le Quement, R. Frauenlob, M. Givskov and T. E. Nielsen. *Tetrahedron Lett.*, 2011, **52**, 7121-7124.
176. D. M. Wilson, L. N. Silvermanb, M. Bergauer and K. R. Keshari. *Tetrahedron Lett.*, 2013, **54**, 151-153.
177. *R. Codd. Coord. Chem. Rev*., 2008, **252**, 1387–1408.
178. A. Massaro, A. Mordini, G. Reginato, F. Russo and M. Taddei. *Synthesis*, 2007, 3201-3204.
179. T. Kurz and K. Widyan. *Org. Biomol. Chem*., 2004, **2**, 2023.
180. D. Glynn, D. Bernier and S. Woodward. *Tetrahedron Lett*., 2008, **49**, 5678.
181. R. Arora, U. Issar and R. Kakkar. *J. Mol. Graph Model,* 2018, **83**, 64-73.
182. C. McDonald, S. Sanz, E. K. Brechin, M. K. Singh, G. Rajaraman, D. Gaynor and L. F. Jones. *RSC Adv.*, 2014, **4**, 38182.
183. B. J. Brennan, J. Chen, B. Rudshteyn, S. Chaudhuri, B. Q. Mercado, V. S. Batista, R. H. Crabtree and G. W. Brudvig. *Chem.Commun*.,2016, **52**, 2972-2975.
184. G. Giacomelli, A. Porcheddu and M. Salaris. *Org. Lett.*, 2003, **5**, 2715–2717.
185. D. M. Griffith, B. Szocs, T. Keogh, K. Y. Suponitsky, E. Farkas, P. Buglyo and C. J. Marmion. *J. Inorg. Biochem*., 2011, **105**, 2011, 763-769.
186. Gang Zhao, Hong B. Lou and K. Yang. *Mini Rev. Med. Chem*., 2003, **3**, 609
187. O. A. Phillips, R. D'Silva, T. O. Bahta, L. H. Sharaf, E. E. Udo, L. Benov and D. E. Walters. *Eur. J. Med. Chem*., 2015, **106**,120-131.

188. A. Sarvaramini, D. Azizi, F. Larachi. *Appl. Surf. Sci*., 2016, **387**, 986–995.

189. W. R. McNamara, R. C. Snoeberger III, G. Li, C. Richter, L. J. Allen, R. L. Milot, C. Schmuttenmaer, R. H. Crabtree, G. W. Brudvig and V. S. Batista. *Energy Environ. Sci.*, 2009, **2**, 1173.

190. A. Adewuyi, C. A. Otuechere, Z. O. Oteglolade, O. Bankole, E. Unuabonah. *J. Acute Dis* 2015, **4,** 230–235.

191. S. Minucci, P.G. Pelicci. *Nat. Rev. Cancer*, 2006, **6,** 38-51.

192. S. Cang, Y. Ma, D. Liu. *J. Hematol. Oncol*., 2009, **2**, 22.

193. J. Sille, M. Sramko, V. Garaj, M. Remko. *J. Mol. Str. Theochem*., 2009, **911**, 137-143.

Chapter Two

Binding flexibility of di- and multitopic hydroxamate ligands towards dia- and paramagnetic complexes

2.0 Introduction

The O,O´-bidentate chelating ability of the hydroxamate functional group towards a range of transition metals engenders hydroxamic acids as excellent ligands / bioactive agents in the fields of coordination chemistry, bioinorganic chemistry, chemical biology and medicine. Such properties afford these organic acids rich toxicological, pharmacological and pathological bioactivities, leading to their prominence as selective enzyme inhibitors[1-5] and as vital elements in a variety of therapeutic drugs.[3-8] More specifically, the exceptionally strong binding affinities of hydroxamic acids towards Fe(III) ions in solution[9,10] is best exampled through their integral roles as iron chelators in the treatment of iron overload therapy[11-13] and as prominent building blocks within iron scavenging sidephore architectures.[14,15] Moreover, hydroxamic acids have been extensively employed in the metal extraction and recovery of a number of transition metals,[16] and as expected, have regularly shown an inherent ability to coordinate to a plethora of transition metal ions in the crystalline solid state.[3] Although the O,O´-bidentate chelating binding mode is regularly observed in crystal structures of metal complex and metalloprotein structures alike, more recent investigations into the coordination chemistry of hydroxamic acids tend to focus on the behaviour of their polyfunctional analogues that are employed to transcribe a more diverse range of binding modes upon more elaborate polymetallic architectures such as metallacrowns.[17]

2.1 Results and Discussion

In this chapter we describe the synthesis and full characterisation of the ligands 2-(acetoxy)phenylhydroxamic acid (L_1H_2) and 4-amino-2-(acetoxy)phenylhydroxamic acid (L_2H_2) (Scheme 2.1), along with their employment in the formation of a family of discrete complexes and extended networks as described below.

2.1.1 Ligand preparations

2-(acetoxy)phenylhydroxamic acid (L_1H_2) was synthesised according to literature methods,[18,19] by equimolar reaction of methyl 2-methoxybenzoate and hydroxylamine sulphate. This reaction was carried out under alkaline condition as reported by Reddy et al 2000.[20] A small amount of disodium sulphate was added to accelerate the reaction. The desired product (light pink crystalline powder) was recovered in pure form and in high yield (74%). The reaction is not fast and requires 24 hours for completion in most cases. However, this method can also be successfully applied on a large scale. The compound is stable at room temperature in the solid

state and soluble in the common organic solvents $CHCl_3$, EtOH, MeOH, DMF, and DMSO. Ligand L_1H_2 was subsequently characterised using nuclear magnetic resonance (NMR), infrared spectroscopy (IR) and mass spectrometry (MS) (See experimental section for details).

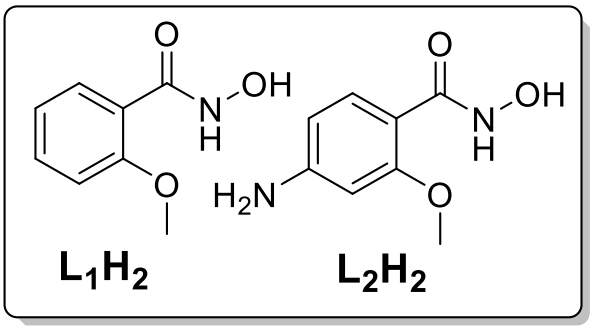

Scheme 2.1 *ChemDraw representations of the ligands 2-(acetoxy)phenylhydroxamic acid (L_1H_2) and 4-amino-2-(acetoxy)phenylhydroxamic acid (L_2H_2) employed in this chapter.*

The ^{1}H NMR spectrum of L_1H_2 showed a singlet signal at 3.83 ppm associated with the OMe group, while two doublets at 7.56 and 7.10 ppm and two triplets at 7.01 and 7.44 ppm were assigned to the aromatic protons. Singlets at 9.07 and 10.61 ppm corresponding to protons belonging to the amide and OH groups, respectively, were also observed. The mass spectrum obtained from L_1H_2 gave rise to peaks at (m/z): 167, 153, 149 and 135 corresponding to the $\{M^+\}$, $\{M\text{-}CH_3\}^+$, $\{M\text{-}OH\}^+$ and $\{M\text{-}OCH_3\}^+$ fragments, respectively. The FT-IR spectrum of L_1H_2 showed a characteristic band at 1812 cm^{-1} which was assigned to the C=O stretching vibration, while bands at 3324 and 3351 cm^{-1} were consistent with the presence of O-H and N-H stretches, respectively.

The ligand 4-amino-2-(acetoxy)phenylhydroxamic acid (L_2H_2) was synthesised in a similar fashion to L_1H_2 by reaction of hydroxylamine with the corresponding methyl ester.[10] As in L_1H_2, L_2H_2 is also air and moisture stable and soluble in organic solvents. Satisfactory microanalysis, ^{1}H NMR, MS and IR spectra were obtained. The ^{1}H NMR spectrum of the ligand L_2H_2 showed a singlet signal at 3.78 ppm due to three protons of the $–OCH_3$ group, and another single at 5.69 ppm associated with the NH_2 functional group. A multiplet at 6.21 ppm and two doublets centred at 7.52 ppm (J = 8.2 Hz) corresponding to the aromatic protons were also observed. Singlets at 8.78 and 10.11 ppm are due to protons belonging to the amide and OH groups, respectively. The mass spectrum obtained from L_2H_2 gave rise to some fragment ions at (m/z): 182, 166 and 150, corresponding to the $\{M^+\}$, $\{M\text{-}NH_2\}^+$ and $\{M\text{-}OCH_3\}^+$ ions,

respectively. The FT-IR spectrum of L_2H_2 showed an absorption band at 1619 cm^{-1} corresponding to the C=O stretching vibration, while absorption bands at 3343 and 3316 cm^{-1} were consistent with the presence of O-H and N-H stretches, respectively.

2.1.2 Metal complexations

Upon completion of ligand synthesis and full characterisation, work then focused on investigating the coordination chemistry of ligands L_1H_2 and L_2H_2. We present here our findings in the form of the monometallic complexes $[Cu(L_1H)_2]$ (**1**) and $[Ni(II)(L_1H)(H_2O)(py)_3](NO_3)\cdot MeCN$ (**5**) along with the dimetallic $[Fe(III)_2(L_1H)_4Cl_2].2MeCN$ (**2**) and heptametallic $[Co(III)Co(II)_6(L_1H)_8(L_1)_2(MeOH)_4(NO_3)_2]NO_3\cdot 3.5H_2O\cdot 14MeOH$ (**3**) species. We also present the synthesis of the hexametallic $[Mn(II)_6(L_3)_{12}].6MeCN$ (**4**) wheel-like cage, where L_3H is the ligand 2-methoxybenzoic acid formed by the unexpected hydrolysis of L_1H_2 (described later in the chapter).

Complex **1**-**3** and **5**-**6** are the first 3d transition metal complexes to contain the ligand 2-(acetoxy)phenylhydroxamic acid (L_1H_2) ligand to date. However, L_1H_2 has been previously used in the construction of a ruthenium(III)-hydroxamate complex ($[Ru(III)(H_2edta)(L_1H_1)].2H_2O$).[21] We also present a new coordination polymer (2-D [4,4]) constructed with L_2H_2 in the form of $\{[Cu(II)(L_2H)(H_2O)(NO_3)]\cdot H_2O\}_n$ (**7**). Crystallographic information for complexes **1**-**7** are given in Tables 2.5 and 2.6.

The reaction of $Cu(NO_3)_2.3H_2O$, L_1H_2 and a suitable base (NaOH) in methanol gave rise to a dark green mother liquor from which needle shaped crystals of $[Cu(II)(L_1H)_2]$ (**1**) were obtained. Complex **1** crystallised in the monoclinic $P2_1/c$ space group and gave the unit cell parameters: a = 3.6987(1) Å, b = 12.6213(4) Å, c = 15.7971(5) Å, α = 90°, β = 93.451(3)° and γ = 90° (Table 2.4). The structure in $[Cu(II)(L_1H)_2]_2$ (**1**) comprises a single square planar Cu(II) ion (O1-Cu1-O1 = 180°) connected to two singly deprotonated L_1H^- ligands, each utilise a chelating coordination mode and giving rise to Cu-O bond lengths of 1.94 Å (Cu1-O1) and 1.91 Å (Cu1-O2) (Fig. 2.1). As illustrated in Fig. 2.1(a), a centre of inversion lies at the metal centre. Both of the hydroxamate ligands in **1** remain protonated at the amide N atom (N1-H1) and are therefore able to partake in intramolecular H-bonds with their neighbouring -OCH_3 groups as shown by the dashed lines in Figure 2.1(a and b) (N1(H1)$\cdots$O3 = 1.98 Å).

The individual {Cu(II)} units in **1** align into superimposable stacks along the *a*-direction of the unit cell (Cu1···Cu1' = 3.7 Å) and these individual rows are arranged in an efficient brickwork pattern along the *bc* cell plane (Fig. 2.2). This packing arrangement is supported by numerous inter-molecular H-bonding interactions (e.g. C6(H6)···O2' = 2.40 Å, C8(H8A)···O2' = 2.51 Å and C5(H5)···O3 = 2.61 Å).

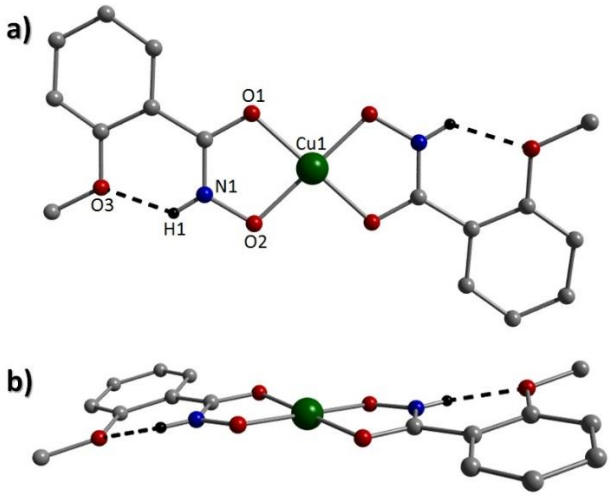

Figure 2.1 *Structure of* ***1*** *as viewed perpendicular (a) and parallel (b) to the plane. Black dashed line represents intramolecular hydrogen bonding (N1(H1)···O3 = 1.98 Å). Colour code (as used throughout the manuscript): Green (Cu), red (O), blue (N), grey (C) and black (H). The majority of hydrogen atoms have been omitted for clarity.*

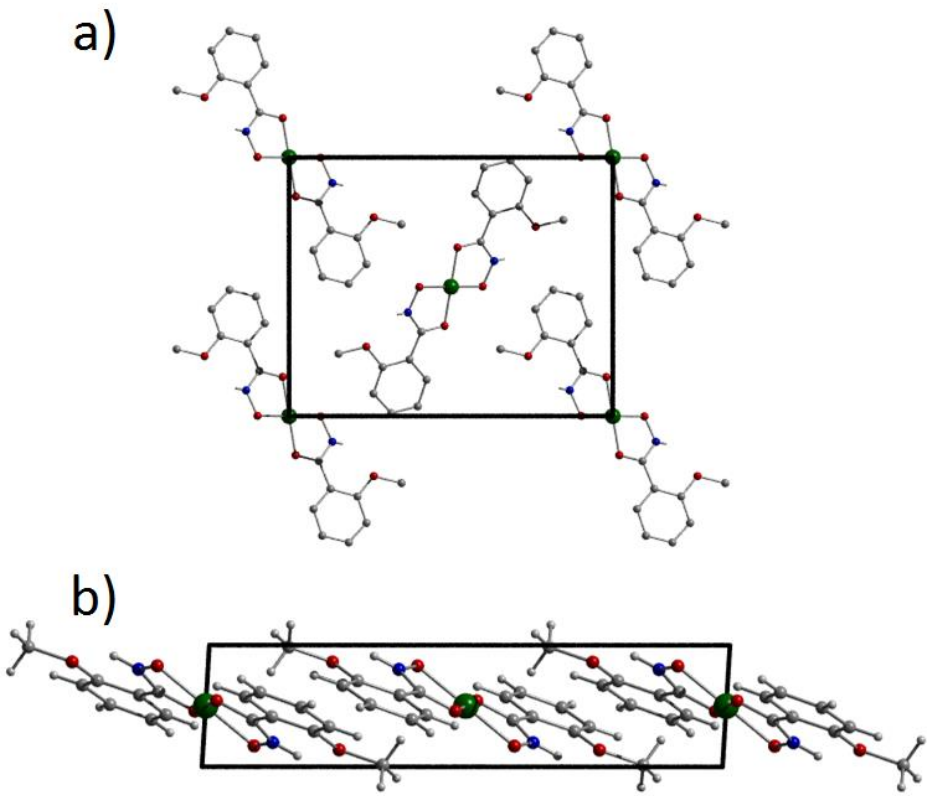

Figure 2.2 *Crystal packing representations of [Cu(II)(L_1H)$]_2$] (**1**) as viewed along the a-(**a**) and the b-axis (**b**) of the unit cell.*

To confirm that our bulk sample was consistent with our single crystal data, powder XRD measurements were carried out on complex **1** and the resultant diffraction pattern is given in (Fig. 2.3). The second (red) pattern represents the simulated pXRD pattern obtained from single crystal XRD data using the Mercury software platform.[22] Using a Johnson Matthey balance, the room temperature magnetic moment (μ_{eff}) of 1 (1.61 BM) was found to be consistent with that expected for a monometallic distorted square planar Cu(II) complex ($\mu_{S.O.}$ = 1.73 BM) (Table 2.1).

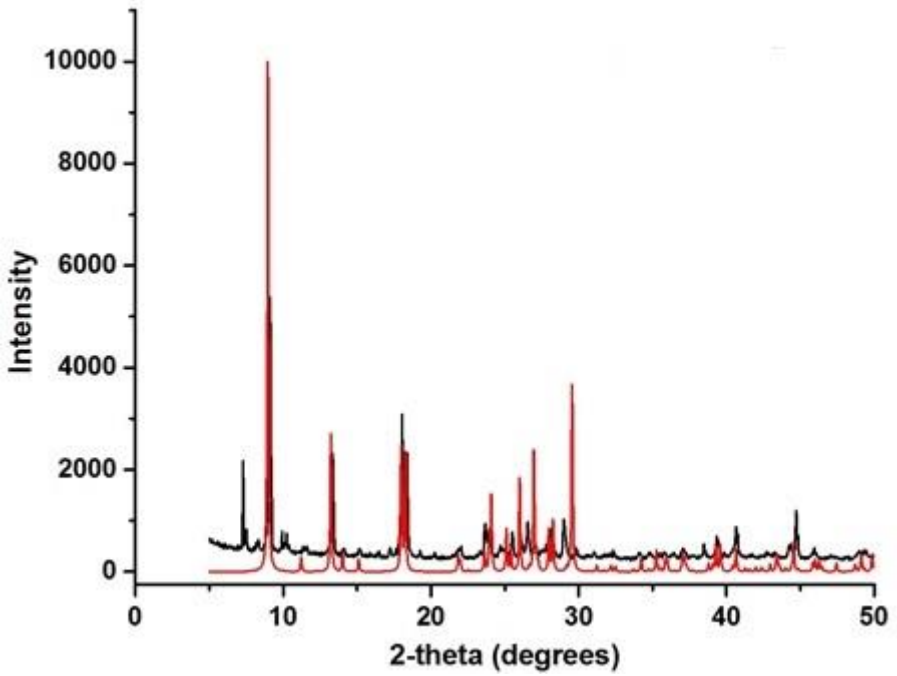

Figure 2.3 *(Black line) Powdered XRD pattern obtained from a crystalline sample of [Cu(II)(L_1H)$_2$] (**1**). (Red line) the diffraction pattern of (**1**) as simulated by the Mercury software package.*[22]

Table 2.1 Magnetic moment data obtained from a polycrystalline sample of **1**.

Sample	[Cu(II)(L_1H)$_2$] (**1**)
C (calibration constant)‡	1.18
T (K)	302
L (sample length; cm)	2.6
MW (g mol^{-1})	395.88
M_0 (g)	0.6990
M_1 (g)	0.8643
M (M_1-M_0) (g)	0.1653
R_0	-0.27
R	145
R-R_0	145.27
μ_{eff}	1.61

‡ Johnson Mathey balance was calibrated using Hg[Co(II)(NCS)$_4$] prior to use.[1] *Magnetic moments calculated using the equations 17-19 below.*

Eqn. 17: $\chi_g = c.L.(R-R_o)/10^9.m$

Eqn. 18: $\chi_m = \chi_g.Mw$

Eqn. 19: $\mu = 2.828.(\chi_m.T)^{1/2}$

The reaction of anhydrous ferric chloride, L_1H_2 and $Bu_4N(OH)$ in acetonitrile produced a red / brown solution from which red X-ray quality crystals of the dinuclear complex $[Fe(III)_2(L_1H)_4Cl_2]\cdot 2MeCN$ (**2**) were obtained. Complex **2** crystallised in the triclinic P-1 space group (Z = 1) with unit cell parameters: *a* = 10.0272(3) Å, *b* = 10.6948(3) Å, *c* = 10.8905(4) Å, α = 76.760(3)°, β = 65.622(3)° and γ = 69.977(3)°. The two Fe(III) centres in **2** are linked by two μ- bridging O donor atoms (O2 and symmetry equivalent (s.e.)) belonging to two singly deprotonated $\eta^1{:}\eta^2$: μ-bonding L_1H^- ligands (Fe1-O2-Fe1′ = 106.85 º) (Fig. 2.4). The Fe(III) oxidation state assignments in **2** were confirmed using BVS calculations, bond length and charge balancing considerations (Table 2.2).[23] The two remaining symmetry related hydroxamate ligands chelate to the metal centres in **2** (O,O′-bidentate), while terminal Cl^- ligands complete their respective coordination spheres (Fe1-Cl1 = 2.31 Å). Intra-ligand H-bonding interactions are observed within all four L_1H^- ligands between the hydroxamate N-H groups (H1 and H2) and the juxtaposed methoxide O atoms (O3 and O6) (N1(H1)···O3 = 1.96 Å; N2(H2)···O6 = 2.00 Å) (Fig. 2). Two MeCN solvent of crystallisation lies at the periphery of the structure in **2** and is held in position through an inter-molecular hydrogen bond between its N donor atom (N3) and a nearby hydroxamate NH group (N2(H2)···N3 = 2.28 Å). This solvent of crystallisation (and s.e.) connects the individual $\{Fe(III)_2\}$ units in **2** through H-bonding with adjacent Cl^- ligands via its $-CH_3$ protons (Cl1···(H18C′)C18′ = 2.82 Å) (Fig. 2-right). These Cl^- ligands also interact with nearby protons belonging to hydroxamate –OMe groups of adjacent $\{Fe(III)_2\}$ complexes (Cl1(H16B)···Cl6 = 2.82 Å) to forge the primitive (P-1) packing arrangement observed in **2**.

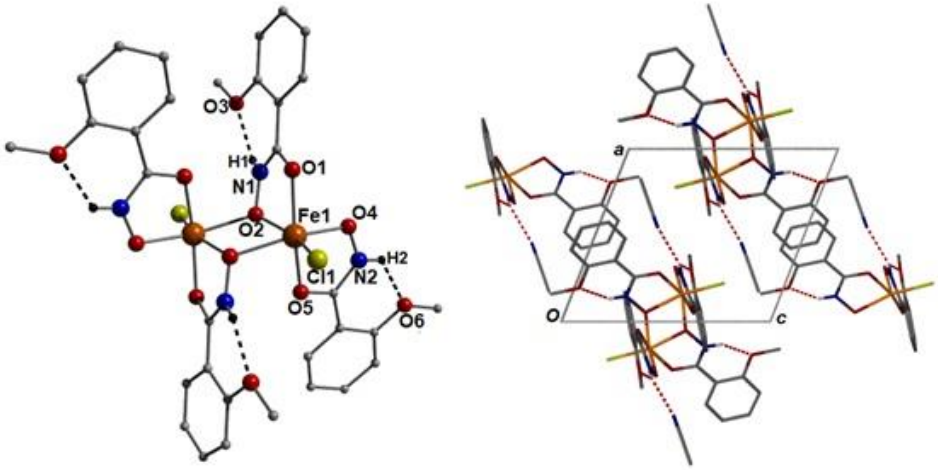

Figure 2.4 *Crystal structure (left) of* $[Fe(III)_2(L_1H)_4Cl_2]\cdot 2MeCN$ ***(2)*** *and its corresponding packing arrangement (right) as viewed along the b unit cell direction. Dashed lines represent intra-molecular H-bonds (N1(H1)···O3 = 1.96 Å; N2(H2)···O6 = 2.00 Å). Colour code: Orange (Fe), Red (O), Blue (N), grey (C), light grey (H), yellow (Cl). The MeCN solvents of crystallisation and the majority of hydrogen atoms have been omitted for clarity.*

Table 2.2: BVS data on $[Fe(III)_2(L_1H)_4Cl_2].2MeCN$ (**2**)

Complex	**Atom label and BVS result**
$[Fe_2]$ (2)	**Fe1**
	2.62

The methanolic reaction of $Co(II)(NO_3)_2.6H_2O$ and L_1H_2 along with the introduction of a suitable base ($NEt_4(OH)$) gives rise to the crystallisation of the heterovalent heptanuclear complex $[Co(III)Co(II)_6(L_1H)_8(L_1)_2(MeOH)_4(NO_3)_2]NO_3\cdot 3.5H_2O\cdot 14MeOH$ (**3**) (Fig. 2.5). Complex **3** crystallised in the triclinic *P*-1 space group and possesses a metallic skeleton describing a bicapped trigonal bipyramid. As highlighted in Figure 2.5c, the centres Co2-Co6 occupy the trigonal bipyramidal core structure, while metal ions Co1 and Co7 act as edge caps to the Co2-4 and Co5-6 vertices, respectively. BVS calculations, bond length and charge balancing considerations reveal that the Co3 is in the +3 oxidation state while all other metal centres are divalent (Table 2.3). The core in **3** is constructed through a combination of eight singly (L_1H^-), and two doubly (L_1^{2-}) deprotonated 2-(acetoxy)phenyl hydroxamate ligands using the $\eta^1{:}\eta^2$ μ- (L_1H^-), $\eta^1{:}\eta^3$ μ_3- (L_1H^-) and $\eta^1{:}\eta^3{:}\eta^1$ μ_4- (L_1^{2-}) bridging modes (Fig. 2.5). All cobalt centres exhibit distorted octahedral geometries. Terminally bonded methanol ligands

complete the coordination spheres at centres Co1, Co4, Co5 and Co7 (Co-O_{MeOH} bond range: 2.05-2.09 Å), while two of the three NO_3^- anions in **3** are bound to the metal ions Co2 and Co6, respectively, at distances of 2.10 Å (Co2-O14) and 2.06 Å (Co6-O25). The eight singly deprotonated L_1H^- ligands remain protonated at their amide N atoms. These protons involved in intra-ligand interactions through their -OCH_3 groups (*e.g.* N2(H2H)···O13 = 1.96 Å; N8(H8H)···O37 = 1.85 Å and N10(H10H)···O7 = 2.15 Å), as well as with O donor atoms of neighbouring hydroxamate ligands (*e.g.* N2(H2H)···O19 = 2.79 Å; N8(H8H)···O24 = 2.64 Å and N10(H10H)···O36 = 2.426 Å) and NO_3^- counter anions (N1(H1)···O15 = 2.14 Å). The terminal MeOH ligands in **3** also partake in intra-molecular hydrogen bonding with nearby nitrate counter anions at distances of (for instance): 2.11 Å (O17(H17)···O14) and 2.39 Å (O34(H34)···O25). The individual {Co(III)$Co(II)_6$} units in **3 c**onnect to one another through strongly directional inter-molecular H-bonds between terminal MeOH protons (H4H) and O donor atoms (O27) from a neighbouring metal bound NO_3^- counter anion (O4(H4H)···O27 = 1.82 Å). Further connections in the form of C-H···π intermolecular interactions are observed between aromatic hydroxamate protons (i.e. H47) and neighbouring aromatic hydroxamate rings (e.g. $[C75\text{-}C80]_{centroid}$···H47 = 2.83 Å).

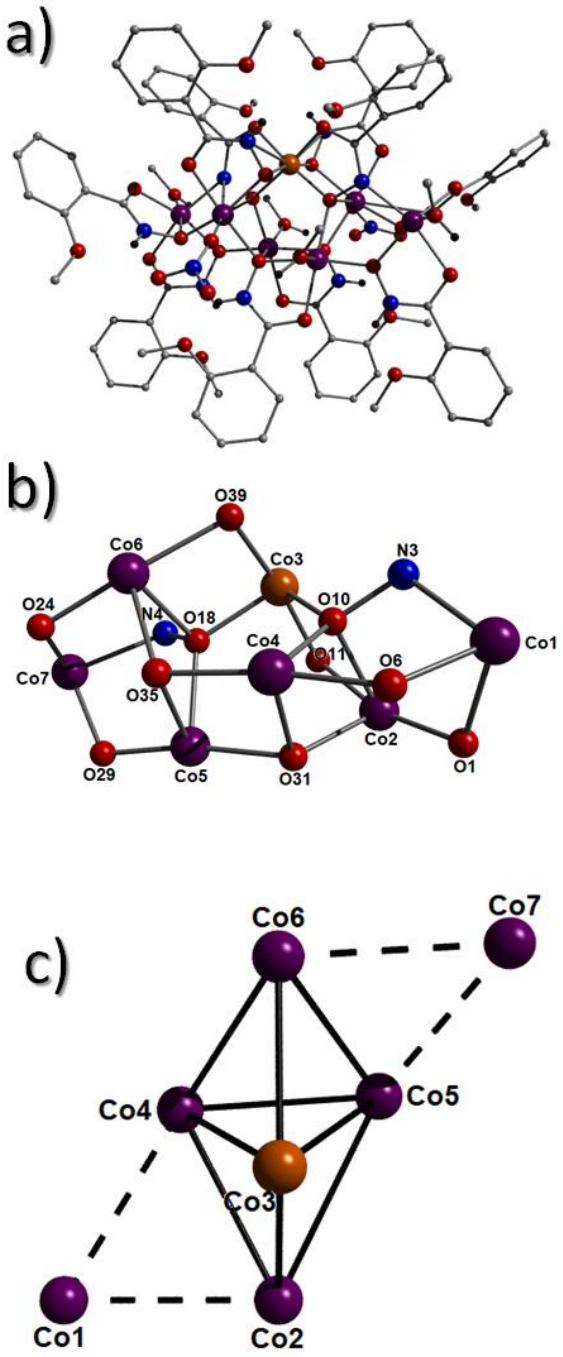

Figure 2.5 *(a) Crystal structure of [Co(III)Co(II)$_6$(L$_1$H)$_8$(L$_1$)$_2$(MeOH)$_4$(NO$_3$)$_2$]NO$_3$.3.5H$_2$O·14MeOH (**3**). Colour code: Purple (Co(II)), Orange (Co(III)), Red (O), Blue (N), grey (C), black (H). The majority of hydrogen atoms have been omitted for clarity. (b) The inorganic core in **3** including the bridging O / N atoms (c) The bicapped trigonal bipyramidal topology in **3**. The solid lines highlight the trigonal bipyramidal core (Co2-6) while the two edge capped metal ions (Co1 and Co7) are connected to the core through dashed lines.*

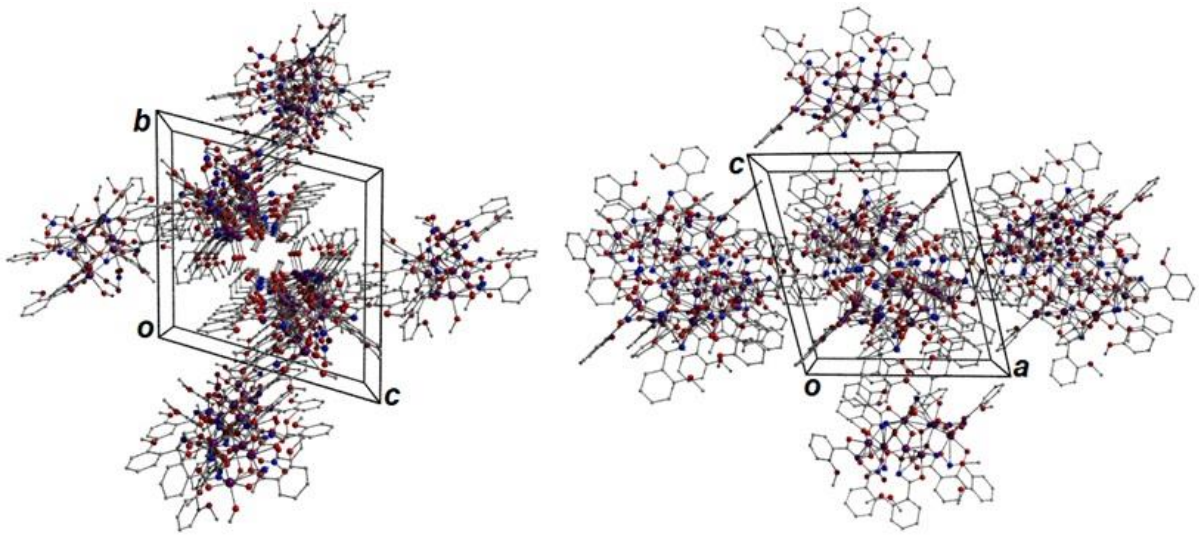

Figure 2.6 *The crystal packing observed in* $[Co(III)Co(II)_6(L_1H)_8(L_1)_2(MeOH)_4(NO_3)_2]NO_3{\cdot}3.5H_2O{\cdot}14MeOH$ (***3***) *as viewed along the a (left) and b (right) unit cell direction.*

Table 2.3: BVS data on $[Co(III)Co(II)_6(L_1H)_8(L_1)_2(MeOH)_4(NO_3)_2]NO_3{\cdot}3.5H_2O{\cdot}14MeOH$ (**3**).

Atom label	BVS result
Co1	1.98
Co2	2.05
Co3	3.29
Co4	2.06
Co5	2.07
Co6	2.10
Co7	2.11

The methanolic reaction of L_1H_2 with $Mn(II)(NO_3)_2.4H_2O$ in the presence of tetrabutylammonium hydroxide (TBAOH) resulted in the formation of the rather unexpected Mn_6 wheel complex $[Mn(II)_6(L_3)_{12}].6MeCN$ (**4**; where L_3H = 2-methoxybenzoic acid). The origin of the 2-methoxybenzoate ligands in **4** is presumably the metal catalysed hydrolysis of the ligand 2-(acetoxy)phenyl hydroxamic acid (L_1H_2). Complex **4** crystallises in the triclinic P-1 space group in low (5%) yield. For the crystallographic data obtained from the pale yellow crystals in **4**, please refer to Table 2.6. The wheel topology in **4** comprises six distorted

octahedral Mn(II) ions (Mn1-3 and s.e.) connected by a combination of six μ-bridging and six $\eta^1:\eta^2:\eta^1$ μ_3-bridging L_3^- ligands (Fig. 2.7b). More specifically, the μ-bridging L_3^- moieties lie approximately parallel to the $\{Mn(II)_6\}$ plane while the six μ_3-bridging ligands sit approximately perpendicular to the $\{Mn(II)_6\}$ wheel in an alternating up down arrangement (Fig. 2.7c). The Mn(II) oxidation states in **4** were determined using charge balancing and bond length considerations coupled with BVS analysis[23] as given in Table. 2.4.

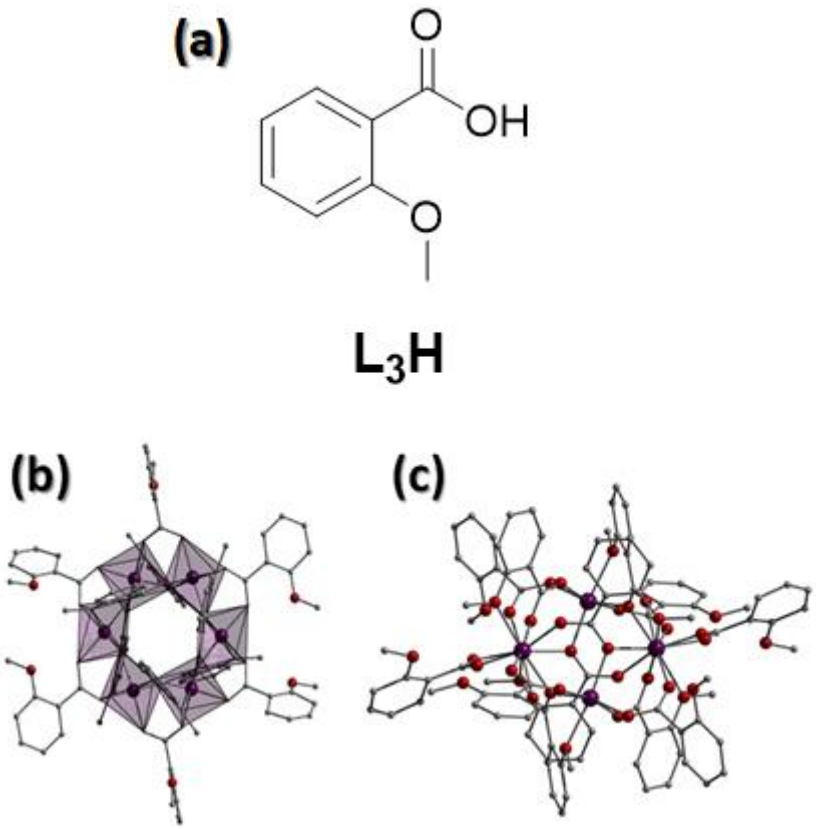

Figure 2.7 *Crystal structure of $[Mn(II)_6(L_3)_{12}]\cdot 6MeCN$ (**4**; where L_3H = 2-methoxybenzoic acid in (a)) as viewed perpendicular (b) and parallel (c) to the $\{Mn(II)_6\}$ plane. All hydrogen atoms and solvate (MeCN) molecules have been omitted for clarity.*

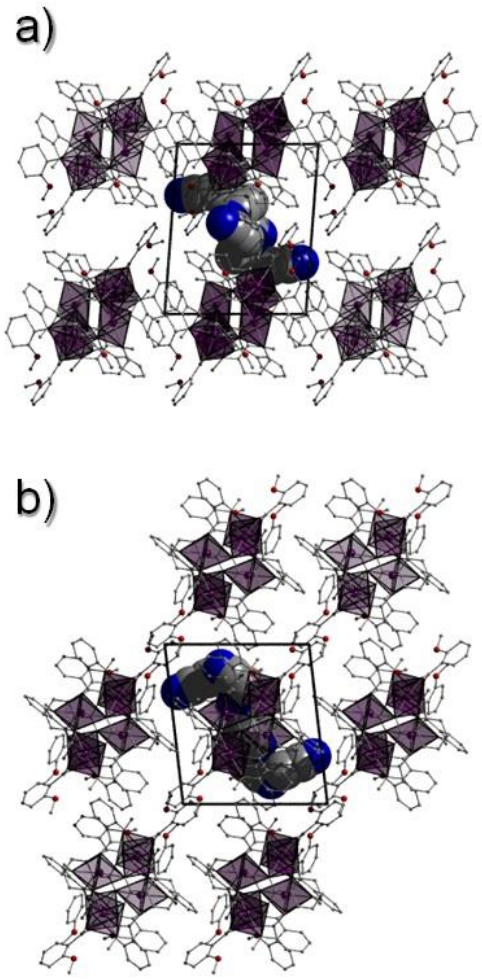

Figure 2.8 *Packing of the individual {Mn(II)$_6$} units in* ***4*** *as viewed along the b direction (a) and c direction of the unit cell. MeCN solvents of crystallisation are space-fill represented. All hydrogen atoms have been omitted for clarity.*

Compound **4** crystallizes with six MeCN molecules of solvation lying at the periphery of the structure and are held in position through inter-molecular hydrogen bonds between their N donor atoms (N1-N3 and s.e.) and –OCH_3 protons belonging to nearby L_3^- ligands (C53(H53B)$\cdots$N1 = 2.42 Å, C8(H8A)$\cdots$N2 = 2.50 Å and C30(H30)$\cdots$N3 = 2.47 Å). The overall topology of the core (Figure 2.7) is analogous to that of hexanuclear ferric wheel {[$Fe_6F_6(edea)_6$]·$10H_2O$} (where H_2mdea = N-methyldiethanol amine) previously reported by Rumberger *et al* along with another wheel-shape topology of [$Mn_{12}(mdea)_8(O_2CCH_3)_{14}$] ·$CH_3CN$ (H_2edea = N-ethyldiethanol amine).[24]

All attempts to resynthesise the compound using commercially available 2-methoxybenzoic acid under numerous reaction condition (using different bases, solvents and stoichiometries) failed to reproduce complex **4**. Surprisingly even the simple metathesis reactions of various Mn(II) salts and the sodium salt of L_3H failed to produce our target complex. Undeterred, work is still ongoing within the Jones group in reliably producing this potentially interesting complex (e.g. potential Magnetic Coolant Effect (MCE) behaviour).

Table 2.4: BVS data on $[Mn(II)_6(L_3)_{12}].6MeCN$ (**4**)

Complex	**Atom label and BVS result**
$[Mn(II)_6]$ (4)	**Mn1**
	2.18
	Mn2
	2.16
	Mn3
	2.14

Despite numerous attempts and synthetic permutations, the equivalent reaction using $Ni(NO_3)_2.6H_2O$ gave no discernible products, however the addition of pyridine to the mixture promoted the crystallisation of the monomeric complex $[Ni(II)(L_1H)(H_2O)(py)_3](NO_3)\cdot MeCN$ (**5**) in the triclinic P-1 space group. The distorted octahedral Ni(II) centre (Ni1) is bound by a chelating L_1H^- ligand whose iminato hydrogen atom (H1) partakes in an intramolecular H-bond with its close by $–OCH_3$ oxygen atom (O1) at a distance of 2.132 Å (N1(H1)···O1; Fig 2.9). The four remaining coordination sites are occupied by three terminal pyridine ligands (Ni1-N bond range: 2.101-2.116 Å) and a single terminally bound water molecule (Ni1-O4 = 2.076 Å). In the unit cell the individual $\{Ni(II)(L_1H)(H_2O)(py)_3\}^+$ units self-assemble into dimeric arrays through self-complementary H-bonding between the terminal water ligands (H4A-O4-H4B) and neighbouring hydroxyl O donor atoms (O3 and s.e.) at a distance of 1.858 Å (O4(H4A)···O3) (Figures 2.9-2.11). The NO_3^- (labelled N5, O5-O7) counter anions and MeCN solvents of crystallisation (labelled N6; C24-C25) effectively act as molecular 'cement' by

connect the {Ni(II)} monomeric 'bricks' in **5** through numerous intermolecular hydrogen bonding interactions (e.g. C7(H7)···N6 = 2.591 Å; N1(H1)···O5 = 2.149 Å; C10(H10)···O6 = 2.481 Å and C11(H11)···O7 = 2.402 Å).

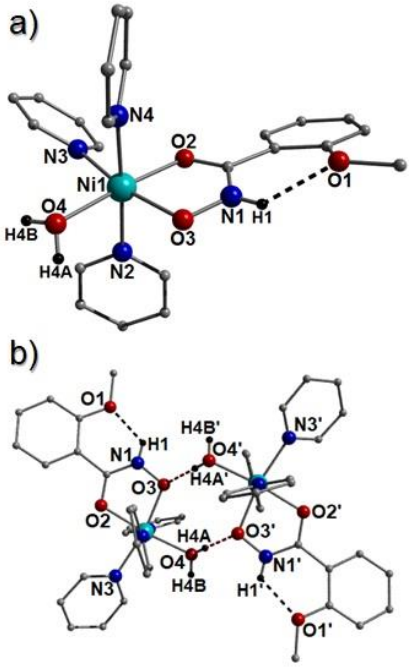

Figure 2.9 *(a) Crystal structure of [Ni(II)(L_1H)(H_2O)($py)_3$](NO_3)·MeCN (**5**). Colour code: Light blue (Ni), red (O), blue (N), grey (C). NO_3^- counter anion and the majority of hydrogen atoms have been omitted for clarity. The dashed black line represents the intramolecular H-bond: N1(H1)···O1 = 2.13 Å. (b) A dimer of {Ni(II)(L_1H)(H_2O)($py)_3$}$^+$ units connected through self-complementary H-bonding at a distance of 1.86 Å (O4(H4A)···O3) as viewed along the axial direction of the Ni(II) metal centre.*

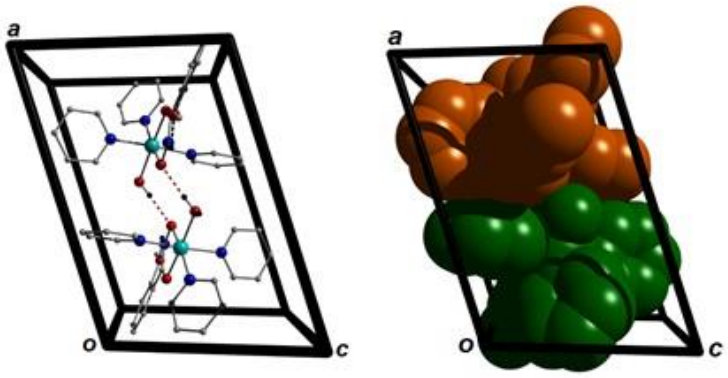

Figure 2.10 *(left) A H-bonded dimer of {Ni(II)(L_1H)(H_2O)($py)_3$}$^+$ units in **5** as viewed along the b unit cell direction along with a space-fill represented view of the same image (right).The red dashed lines represent the intermolecular H-bonding (see main text for details). All NO_3^- counter anions, MeCN solvents of crystallisation and (the majority of) hydrogen atoms have been omitted for clarity.*

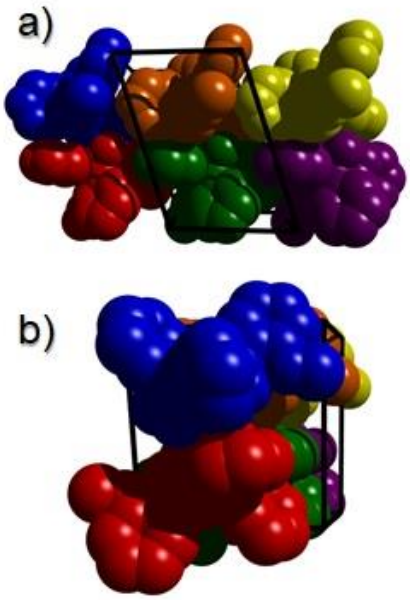

Figure 2.11 *Space-fill represented packing diagram observed in the unit cell of* ***5*** *as viewed along the b (figure a) and a (figure b) unit cell directions, respectively. Each colour represents an individual* $\{Ni(II)(L_1H)(H_2O)(py)_3\}^+$ *unit. The dimeric H-bonded pairings are colour coded as follows: blue ↔ red; orange ↔ green and yellow ↔ purple. All* NO_3^-*, MeCN solvents of crystallisation and hydrogen atoms have been omitted for clarity.*

Reaction of $Zn(II)(NO_3)_2{\cdot}6H_2O$, L_1H_2 and NaOH in methanol gave rise to a pale yellow solution from which (upon filtration and evaporation of the resultant mother liquor) produced crystals of the 1-D coordination polymer $[Zn(II)_2(L_1H)_2(H_2O)_5](NO_3)_2]_n$ (**6**) in 10% yield. The asymmetric unit in **6** comprises three Zn(II) metal centres (Zn1-3), two of which (Zn1 and Zn3) are of half occupancy. The Zn2 centre exhibits a distorted trigonal bipyramidal geometry (τ = 0.55) whereby four of the five coordination locales are occupied by O donor atoms (O1, O2, O4 and O5) belonging to two singly deprotonated L_1H^- ligands (Zn-O bond range: 2.02-2.05 Å). The final spot is occupied by a terminal H_2O ligand (Zn2-O17 = 1.99 Å). Moreover, the L_1H^- ligands effectively connect the Zn(II) nodes via the $\eta^2{:}\eta^1$ μ-bridging mode to produce the polymeric architecture in **6** (Fig. 2.12). The zinc centres labelled Zn1 and Zn3 are of distorted octahedral geometry and are coordinated to their neighbouring metal nodes via the amide O2 and O5 (and s.e.) oxygen donor atoms belonging to the bridging L_1H^- hydroxamate ligands (Zn1-O5 = 2.09 Å and Zn3-O2 = 2.10). The four remaining positions at both metal centres are occupied by terminal water ligands (Zn1-O7 = 2.11 Å; Zn1-O8 = 2.07 Å, Zn3-O9 = 2.09 Å and Zn3-O10 = 2.10 Å).

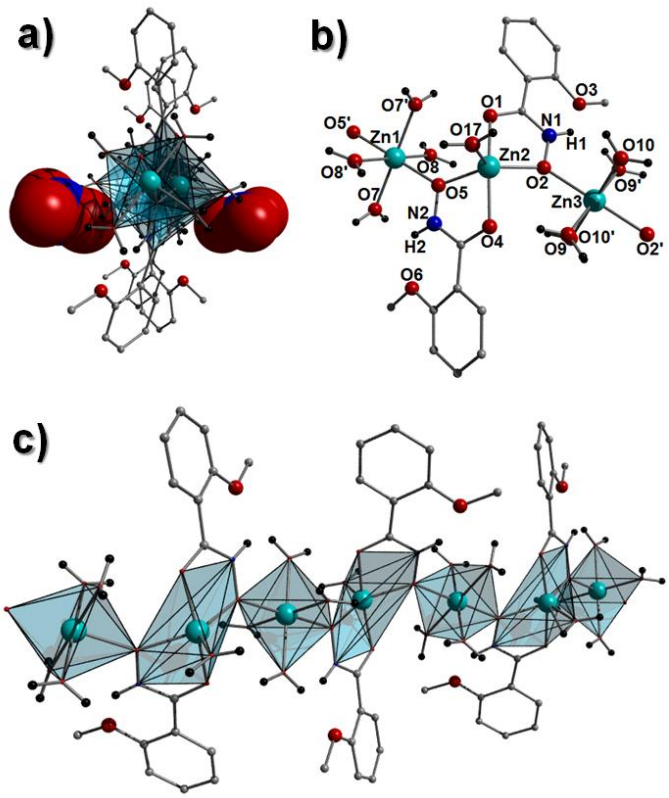

Figure 2.12 *The crystal structure of the 1-D coordination polymer in* $[Zn(II)_2(L_1H)_2(H_2O)_5](NO_3)_2]_n$ *(**6**) as viewed parallel (a) and perpendicular (b and c) to the chain direction. The nitrate counter anions in (a) are space-fill represented. Figure (c) highlights the metal geometries in **6**.*

Intra-ligand H-bonding is observed between the amide protons (N1(H1) and N2(H2)) and O donor atoms of nearby -OCH_3 groups (N1(H1)···O3′ = 2.01 Å and N2(H2)···O6′ = 2.04 Å). A number of intra-chain interactions stabilise the coordination polymer in **6**. More specifically, the terminal water ligands partake in H-bonding with neighbouring O donor atoms belonging to neighbouring L_1H^- ligands (e.g. O9(H9B)···O4′ = 1.88 Å and O9(H9A)···O3′ = 2.29 Å). Furthermore, the two NO_3^- counter anions in **6** lie in-between the 1-D chains and are held in position through numerous H-bonding interactions with terminal H_2O ligand protons (e.g. O7(H7B)···O14′ = 1.81 Å, O8(H8E)···O15′ = 1.90 Å; O10(H10A)···O12′ = 1.92 Å and O17(H17B)···O15′ = 1.84 Å). The individual chains in **6** traverse the *bc* plane of the unit cell and pack in superimposable stacks along the *a* unit cell direction (Fig. 2.13).

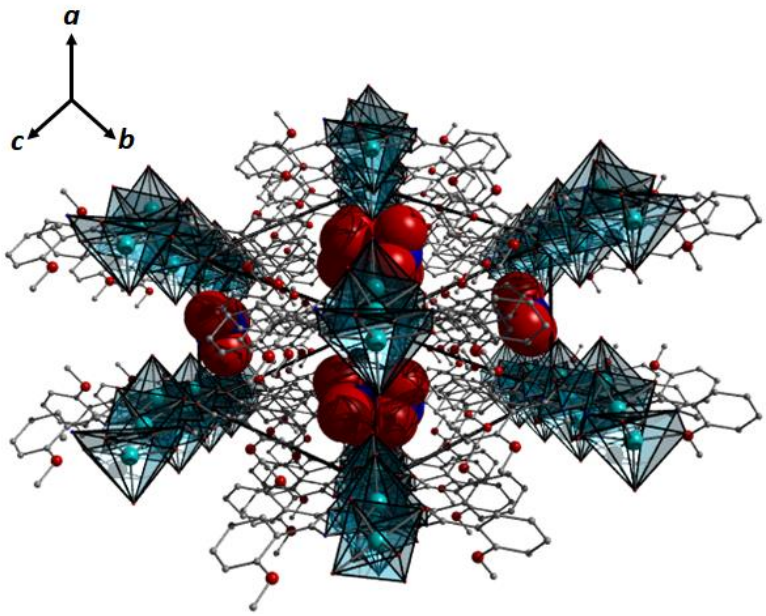

Figure 2.13 *Packing arrangement observed in* ***6****. The coordination spheres around each Zn(II) centre are represented as polyhedra. The* NO_3^- *counter anions are represented in space-fill mode. All hydrogen atoms have been omitted for clarity.*

Due to the redundant nature of the $–OCH_3$ group in L_1H_2 with respect to metal coordination in all the above compounds (bar complex **4**), our next strategy was to introduced $-NH_2$ group at the fourth position which afforded the analogous ligand 4-amino-2-(acetoxy)phenylhydroxamic acid (L_2H_2; Scheme 2.1). Indeed, this proved successful when the methanolic reaction of $Cu(NO_3)_2.3H_2O$ and L_2H_2 in the presence of suitable base (tetrabutylammonium hydroxide) gave a dark green reaction mixture that upon filtration and slow evaporation gave rise to pale yellow crystals of the 2-D extended network $\{[Cu(II)(L_2H)(H_2O)(NO_3)]\cdot H_2O\}_n$ (**7**) (Fig. 2.14). The 2-D architecture in **7** represents the first example of a metal coordination compound built with the L_2H_2 ligand. Crystals of **7** were obtained in the monoclinic $P2_1/c$ space group and its asymmetric unit comprises one Cu(II) centre, one L_2H^- ligand, one NO_3^- anion and a single terminally bonded water ligand. Each hydroxamate (L_2H^-) ligand chelates to a Cu(II) centre through the hydroxyl and carbonyl atoms O1 and O2, respectively, to give bond lengths of 1.92 Å (Cu1-O1) and 1.94 Å (Cu1-O2). The remaining methoxy atom (O3) remains unbound and hydrogen bonds with the juxtaposed amide NH group (N1) (N1(H1)···O3 = 2.03 Å). The Cu1 centre in **7** exhibits distorted, Jahn-Teller elongated octahedral geometry where the basal plane comprises donor atoms from the chelating hydroxamate ligand, a terminal water ligand (Cu1-O4 = 1.96 Å) and a $-NH_2$ group from a neighbouring L_2H^- unit (Cu1-N2′ = 2.03 Å). Moreover, the axial positions are occupied

by NO_3^- anions (via O5 and O6 respectively) at distances of 2.44 Å (Cu1-O5) and 2.703 Å (Cu1-O6′). The symmetry equivalent NO_3^- counter anions in **7** connect the Cu(II) ions (Cu1···Cu1′ = 5.70 Å) to form superimposable zig-zag arrays along the *c* direction of the unit cell. These 1-D rows are connected to one another through the ditopic L_2H^- ligand via their pendant $–NH_2$ groups (N2-Cu1′ = 2.03 Å) to produce a Cu···Cu1′′ distance of 9.25 Å (Fig. 2.14). The result is the formation of 2-D wave-like sheets that propagate along the *ac* plane of the unit cell with an overall [4,4] net topology (Fig. 2.15a). The individual sheets in **7** pack in a space efficient manner along the *b* direction as highlighted using the colour coded space-fill diagram in Figure 2.12c. These waters of crystallisation (O8) lie in the channels forged by the 2-D sheets in **7** and are involved in multiple hydrogen bonding interactions with nearby amide (N1′(H1′)···O8 = 2.21 Å) and ligated water protons (O4(H4A)···O8 = 2.01 Å and O8···O4 = 3.46 Å).

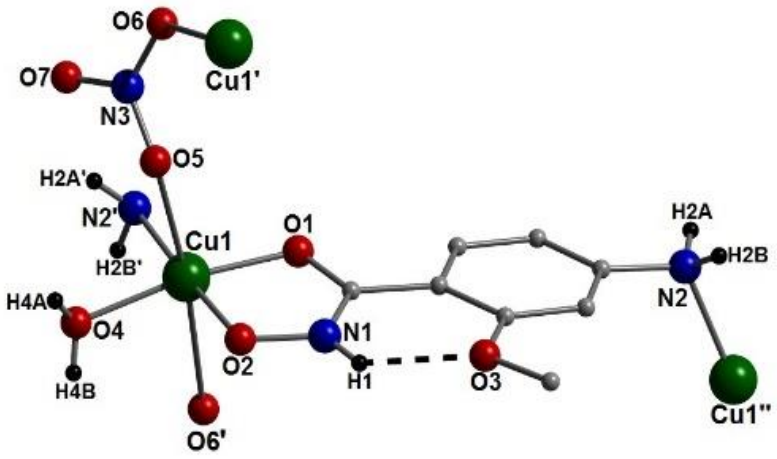

Figure 2.14 *The asymmetric unit in {[Cu(II)(L_2H)(H_2O)(NO_3)]·H_2O}$_n$ (**7**) along with the connector atoms (N2′, O5′, Cu1′ and Cu1′′) that propagate the 2-D extended network in **7**. The majority of H atoms and the water of crystallisation have been omitted for clarity. Intramolecular H-bond represented as a dashed line (N1(H1)···O3 = 2.37Å).*

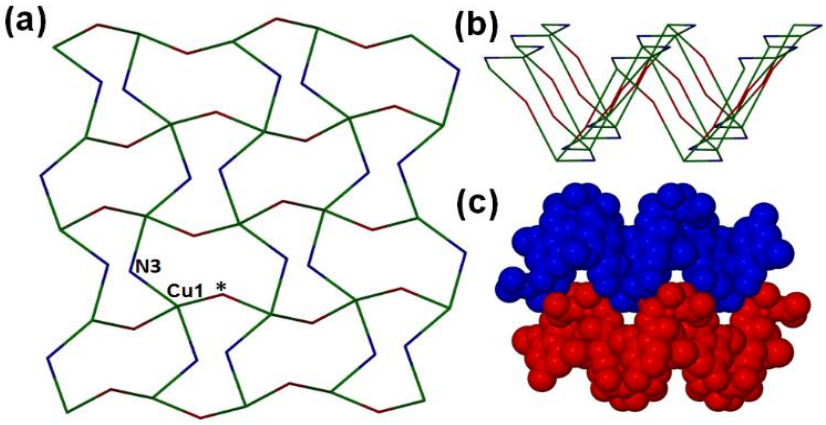

Figure 2.15 *The wave-like [4,4] net topology in **7** as viewed perpendicular (a) and parallel (b) to the plane of the 2-D sheets. Note: The green and dark blue nodes represent the Cu(II) centres and the central N atom (N3) of the connector NO_3^- anions, respectively. The red nodes (*) represent the aromatic centroid positions of the ditopic L_2H^- hydraxamate ligands in **7**. (c) A space-fill representation of the packing motif between two colour coded wave-like sheets in **7** as viewed along the c unit cell direction.*

2.13 Magnetic susceptibility studies

The dc (direct current) molar magnetic susceptibility, χ_M, of polycrystalline samples of $[Fe(III)_2(L_1H)_4Cl_2]\cdot 2MeCN$ (**2**) and $[Co(III)Co(II)_6(L_1H)_8(L_1)_2(MeOH)_4(NO_3)_2]NO_3\cdot 3.5H_2O\cdot 14MeOH$ (**3**) were measured in an applied magnetic field, *B*, of 0.1 T and the *T* = 300-2 K temperature range. The experimental results are shown in Figure 2.16 in the form of the $\chi_M T$ products. For **2**, the $\chi_M T$ product of 9.21 $cm^3\ mol^{-1}$ K at 300 K is close to that expected for two non-interacting Fe(III) ions (8.75 $cm^3\ mol^{-1}$ K), assuming g_{Fe} = 2.0, where g_{Fe} is the *g*-factor of Fe(III). The $\chi_M T$ vs. *T* plot for **2** shows a decrease in the value of $\chi_M T$ upon cooling and is indicative of significant intra-molecular antiferromagnetic exchange interactions between the Fe(III) ions in **2**. The magnetic data for **2** was fitted using the program PHI and the isotropic spin-Hamiltonian of the form: [25, 26]

$$\hat{H} = -2\sum_{i,j>i}^{n} \hat{S}_i J_{ij} \hat{S}_j + \mu_B \sum_{i=1}^{n} \vec{B}\, g_i \hat{S}_i$$

where $\hat{S}$ is a spin operator, J is the pairwise isotropic magnetic exchange interaction between constitutive metal centres, μ_B is the Bohr magneton, $\vec{B}$ the external static magnetic field, g the isotropic g-factor of the metal ions, the indices i and j refer to the two metal ions (n = 2 for **2**). The best fit parameters for **2** are J = -7.34 cm^{-1} and g_{Fe} = 2.00, consistent with previously reported analogues.[27-30]

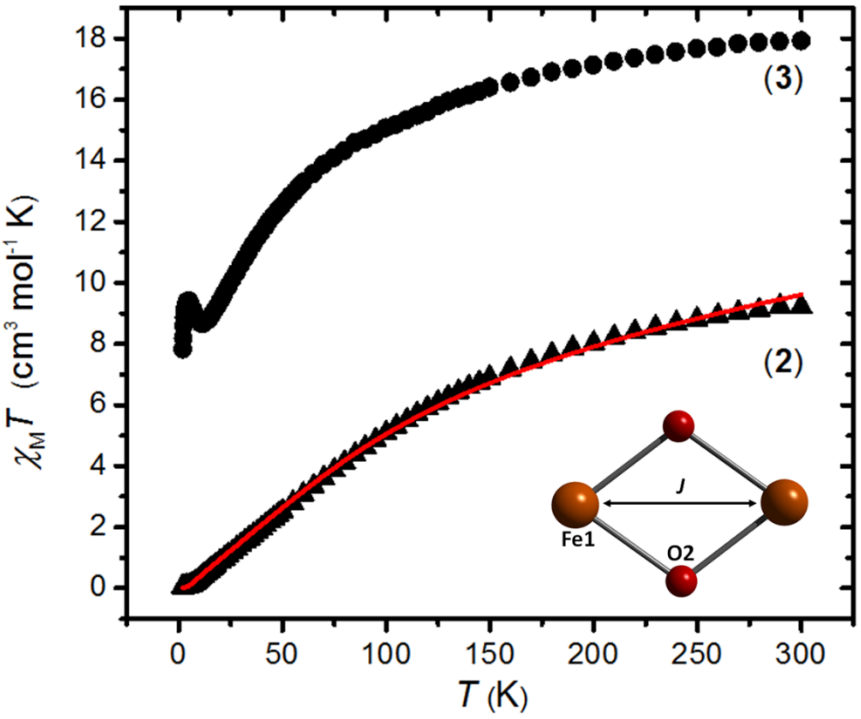

***Figure 2.16**: Overlay $\chi_M T$ versus T plots for polycrystalline sample of **2** and **3**, taken in the T = 300-2 K temperature range in an applied field, B, of 0.1 T. The solid lines represent a simultaneous best-fit of the experimental susceptibility and magnetisation data as described in the main text.*

The $\chi_M T$ value for **3** at 300 K is 17.93 cm^3 mol^{-1} K, higher than that expected for six non-interacting Co(II) ions (S = 3/2, g_{Co} = 2.3, $\chi_M T$ = 14.88 cm^3 mol^{-1} K).[31-35] On cooling, the value of $\chi_M T$ decreases to approximately 8.68 cm^3 mol^{-1} K at 12 K before increasing to 9.41 cm^3 mol^{-1} K at 5 K, and then decreasing to a value of 7.84 cm^3 mol^{-1} K at 2 K. The initial decrease in the value of $\chi_M T$ can be attributed to the large orbital contribution of the high spin, octahedral Co(II) ions and / or antiferromagnetic exchange interactions. The increase between 12-5 K indicates the presence of some ferromagnetic exchange interactions, and the low T decrease due to zero-field splitting effects and / or antiferromagnetic intermolecular interactions. Quantitative analysis of the data is precluded by the large first order spin orbit coupling

contribution associated with the octahedral Co(II) ions. No out-of-phase alternating current (ac) signals were observed for **3**, even in the presence of an applied magnetic field.

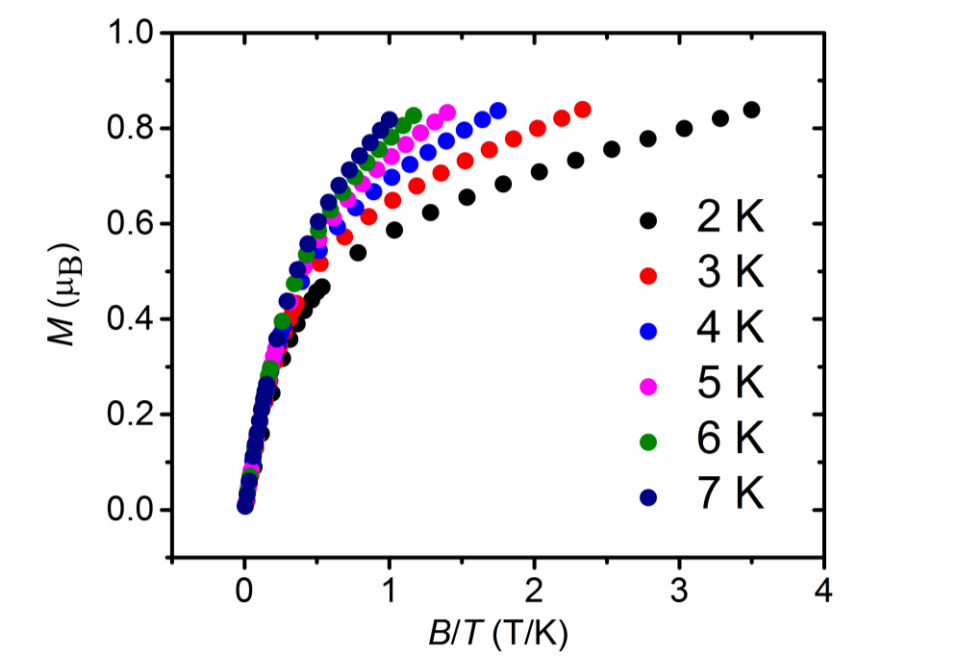

Figure 3.17 *Reduced magnetisation (M/μ_B) vs. B/T (T/K) data obtained from a polycrystalline sample of **3** measured within the 2-7 K temperature range and 0-7 T magnetic field range.*

Table 2.5 Selected crystal data obtained from **1**-**3**.

	1	**2.** 2MeCN	**3**·3.5·14MeOH
Formula[a]	$C_{16}H_{16}N_2O_6Cu_1$	$C_{36}H_{38}N_6O_{12}Cl_2Fe_2$	$C_{98}H_{157}N_{13}O_{60.5}Co_7$
M_W	395.85	929.32	2897.88
Crystal System	Monoclinic	Triclinic	Triclinic
Space group	$P2_1/c$	P-1	P-1
a/Å	3.69870(10)	10.0272(3)	17.7308(7)
b/Å	12.6213(4)	10.6948(3)	19.4055(4)
c/Å	15.7971(5)	10.8905(4)	19.8470(4)
α/°	90	76.760(3)	103.669(2)
β/°	93.451(3)	65.622(3)	101.741(3)
γ/°	90	69.977(3)	96.955(3)
V/Å^3	736.11(4)	994.20(6)	6393.1(3)
Z	2	1	2
T/K	100.0(2)	100.0(2)	100(2)
λ[b]/Å	0.71073	0.71073	0.71073
D_c/g cm^{-3}	1.786	1.552	1.207
μ(Mo-Ka)/ mm^{-1}	1.524	0.934	7.560
Meas./indep.(R_{int}) refl.	14748 / 1670 (0.0331)	12861 / 3554 (0.0516))	24583/12485 (0.1014)
Restraints, Parameters	0, 120	0, 265	0, 1302
wR2 (all data)	0.2127	0.1719	0.1801
$R1^{d,e}$	0.0617	0.0613	0.0643
Goodness of fit on F^2	1.458	1.170	1.015

[a] Includes guest molecules. [b] Mo-Kα radiation, graphite monochromator. [c] $wR2 = [\Sigma w(|F_o^2| - |F_c^2|)^2 / \Sigma w|F_o^2|^2]^{1/2}$. [d]For observed data. [e] $R1 = \Sigma||F_o| - |F_c|| / \Sigma|F_o|$

Table 2.6 Selected crystal data obtained from **4**-**7**.

	4·6MeCN	**5**·MeCN	**6**	**7**·H_2O
Formula[a]	$C_{108}H_{102}N_6O_{36}Mn_6$	$C_{25}H_{28}N_6O_7Ni_1$	$C_{16}H_{26}N_4O_{17}Zn_2$	$C_8H_{13}N_3O_8Cu_1$
M_W	2389.59	583.24	677.15	342.75
Crystal System	Triclinic	Triclinic	Triclinic	Monoclinic
Space group	P-1	P-1	P-1	$P2_1/c$
a/Å	12.2128(7)	9.10480(10)	8.6253(17)	12.2451(4)
b/Å	15.2726(9)	11.74010(10)	12.452(3)	10.0658(2)
c/Å	16.4125(10)	13.16470(10)	13.711(3)	10.9339(3)
α/°	62.321(6)	91.2950(10)	101.95(3)	90
β/°	81.862(5)	107.1730(10)	104.88(3)	114.906(4)
γ/°	80.460(5)	99.7700(10)	109.85(3)	90
V/Å^3	2666.1(3)	1321.00(2)	1266.5(5)	1222.34(6)
Z	1	2	2	4
T/K	100(2)	100(2)	100.0(1)	100(2)
λ[b]/Å	0.71073	0.71073	0.71073	0.71073
D_c/g cm^{-3}	1.488	1.466	1.776	1.852
μ(Mo-Ka)/ mm^{-1}	0.777	0.790	1.982	1.832
Meas./indep.(R_{int}) refl.	50248 / 9682 (0.0934)	41304 / 4713 (0.0273)	9395 / 4592 (0.2378)	13558 / 2233 (0.0232)
Restraints, Parameters	12,662	2, 366	0, 352	4, 193
wR2 (all data)	0.3126	0.0543	0.3572	0.0675
$R1$[d,e]	0.1071	0.0207	0.1097	0.0249
Goodness of fit on F^2	1.065	1.072	1.173	1.071

[a] Includes guest molecules. [b] Mo-Kα radiation, graphite monochromator. [c] $wR2 = [\Sigma w(|F_o^2| - |F_c^2|)^2 / \Sigma w|F_o^2|^2]^{1/2}$. [d] For observed data. [e] $R1 = \Sigma||F_o| - |F_c|| / \Sigma|F_o|$

2.2 Concluding Remarks

We have described the synthesis and characterisation (structural and magnetic) of a family of novel mono-, di- and polymetallic complexes constructed using the ligands 2-methoxyphenylhydroxamic acid (L_1H_2) and 4-amino-2-(acetoxy)phenylhydroxamic acid (L_2H_2). For instance, the ligands 4-amino-2-(acetoxy)phenylhydroxamic acid (L_2H_2) was employed in the construction of the 2-D extended network $\{[Cu(II)(L_2H)(H_2O)(NO_3)].H_2O\}_n$ (**7**). Complex **7** represents the first complex to be constructed with the L_2H_2 ligand. Moreover, the 1-D chain $[Zn(II)_2(L_1H)_2(H_2O)_5](NO_3)_2]_n$ (**6**), the monomer $[Ni(II)(L_1H)(H_2O)(py)_3](NO_3)\cdot MeCN$ (**5**), the ferric dimer $[Fe(III)_2(L_1H)_4Cl_2].2MeCN$ (**2**) and the heterovalent heptanuclear complex $[Co(III)Co(II)_6(L_1H)_8(L_1)_2(MeOH)_4(NO_3)_2]NO_3\cdot 3.5H_2O\cdot 14MeOH$ (**3**) complexes represent extremely rare examples of metal coordination of the ligands 2-(acetoxy)phenylhydroxamic acid (L_1H_2). Variable temperature magnetic susceptibility measurements on **2** indicate dominant antiferromagnetic exchange between the two Fe(III) metal centres (J = -7.34 cm^{-1}).

2.3 Experimental Section

Infra-red spectra were recorded on a Perkin Elmer FT-IR *Spectrum 100* spectrometer (School of Chemistry, Bangor University). ^1H and ^{13}C NMR spectra were obtained at room temperature (298 K) on a Bruker UltrashieldTM 400 Plus with Sample Xpress at 400 MHz. Chemical shifts are reported in ppm and referenced to $CDCl_3$ (^1H: 7.28 ppm, ^{13}C: 77.00 ppm) or DMSO (^1H: 2.50 ppm, ^{13}C: 39.52 ppm). Elemental analysis was carried out at OEA Laboratories (Kelly Bray, Cornwall). Powder XRD was carried out using a PANalytical Philips X`Pert 3040/60 diffractometer at 45 kV and 35 mA between 5 and 60° 2θ using Ni-Filtered Cu-$K_{\alpha 1}$ radiation (λ = 1.5405 Å) at the School of Natural Sciences, Bangor University.

Variable-temperature, solid-state direct current (*dc*) magnetic susceptibility data down to 5 K were collected on a Quantum Design MPMS-XL SQUID magnetometer equipped with a 7 T *dc* magnet. Diamagnetic corrections were applied to the observed paramagnetic susceptibilities using Pascal's constants. All measured complexes were set in eicosane to avoid torqueing of the crystallites. All magnetic samples are collected as single-crystalline products and analysed using microanalysis and IR measurements prior to their magnetic assessment. If necessary, phase purity between cross-batches are

validated using unit cell checks and IR measurements. Yields calculated upon collection of single-crystalline products in order to ensure high quality magnetic data.

2.3.1 Single-crystal X-ray crystallography

Complexes **1-7** were collected on an Rigaku AFC12 goniometer equipped with an enhanced sensitivity (HG) Saturn724+ detector mounted at the window of an FR-E+ Super Bright molybdenum rotating anode generator with HF Varimax optics (100m focus). The cell determination and data collection of each complex was carried out using the CrystalClear-SM Expert package (Rigaku, 2012). Each data reduction, cell refinement and absorption correction were carried out using CrysAlisPro software (Rigaku OD, 2015),[36] while all structures were solved and refined using SHELXT and SHELXL-2014[37] within OLEX-2.[38]

All non hydrogen atoms in complexes **1**, **2**, **4**, **6** and **7** were modelled as anisotropic, while all hydrogen atoms were modelled at calculated positions. Despite numerous attempts, each single crystal data set obtained from **3** were found to consistently diffract poorly at higher angles. The best data set has been supplied in this work. Residual electron densities in solvent accessible voids and channels were observed in **3** (void volume ~ 2105 $Å^3$) so were modelled using the SQUEEZE program (electron count = 639).[39,40] All non-hydrogen atoms were refined anisotropically, while all hydrogen atoms were assigned to calculated positions. All non-hydrogen atoms in **5** were refined anisotropically. The iminato (N1-H1) and terminally bound H_2O ligand protons (H2A and H2B) were located in the difference map. DFIX restraints were imposed on the O-H bond distances of the terminal water ligand. All other hydrogen atoms were assigned to calculated positions.

2.3.2 Organic ligand preparation

All starting materials were used as purchased unless otherwise stated.

Synthesis of 2-(acetoxy)phenylhydroxamic acid (L_1H_2)

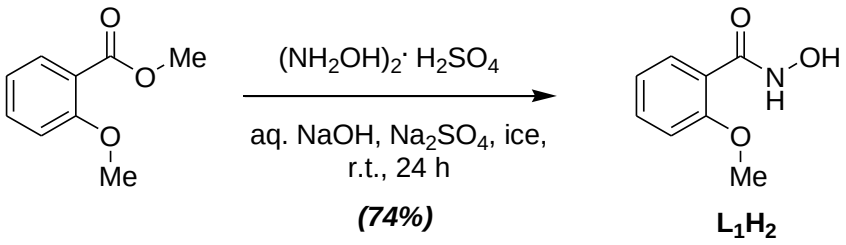

To a stirring solution of NaOH (7.41 g, 185 mmol, 30 cm^3 water) in ice (30 g), hydroxylamine sulphate (6.11 g, 37.0 mmol) and Na_2SO_4 (0.58 g, 4.1 mmol) were added followed by methyl 2-methoxybenzoate (6.14 g, 37.0 mmol) and the solution stirred for 24 hours. After this time the solution was allowed to cool and subsequently pH adjusted to 6 using H_2SO_4, after which the product began to precipitate out. The precipitate was then collected by suction filtration and dried, before recrystallisation from hot water. The remaining solution was left overnight to allow more product to precipitate out which was similarly purified. The remaining solution was then evaporated to dryness under reduced pressure to give a mixture of white and yellow solid, this solid was then dissolved in hot methanol and any remaining solid filtered off. The resultant filtrate was evaporated to dryness under reduced pressure and the solid recrystallised from hot water to form a third batch of the ligand to give a final yield of 74% (4.58 g).

Elemental analysis (%) calculated as L_1H_2 ($C_8H_9N_1O_3$): C 57.48, H 5.43, N 8.38. Found: C 57.39, H 5.35, N 8.23.

^{1}H NMR (DMSO-d_6, 400 MHz): δ (ppm) 3.83 (s, 3H, OCH_3), 7.01 (t, *J* = 7.5 Hz, 1H, CH-Ar) 7.10 (d, *J* = 8.3 Hz, 1H, CH-Ar) 7.44 (dd, *J* = 11.4, 4.3 Hz, 1H, CH-Ar), 7.57 (d, *J* = 7.5 Hz, 1H, CH-Ar), 9.09 (s, 1H, NH-OH), 10.61 (s, 1H, NH-OH).

^{13}C NMR (DMSO-d_6, 100 MHz): δ (ppm) 56.1 (OCH_3), 112.2 (CH-Ar), 120.8 (CH-Ar), 123.0 (C-Ar) 130.2 (CH-Ar), 132.2 (CH-Ar), 157.0 (OC-Ar), 163.6 (C=O).

MS (EI$^+$): *m/z* 167 (26%,{M^+}), 153 (16%,{$M–CH_3$}$^+$), 149 (9%, {$M–OH$}$^+$), 135 (73%, {$M–OCH_3$}$^+$ and/or{$M–NHOH$}$^+$).

FT-IR: ν (cm^{-1}) 3351 (w), 3324 (s), 3119 (m/b), 3012 (w), 2979 (w), 2940 (w), 2842 (w), 2035 (m), 1967 (w), 1935 (w), 1903 (w), 1845 (w), 1812 (w), 1638 (s), 1598 (m), 1571 (w), 1507

(w), 1477 (s), 1434 (m), 1297 (s), 1243 (s), 1183 (s), 1156 (s), 1107 (s), 1056 (m), 1020 (s), 952 (w), 898 (m), 858 (w), 780 (w), 757 (s), 659 (w), 620 (m), 519 (m), 437 (w), 404 (w).
UV-vis (MeOH): λ_{max} (nm) (ε_{max} 10^3, dm^3 mol^{-1} cm^{-1}): 202 (31.9), 206 (33.2), 284 (5.80).
UV-vis (MeCN): λ_{max} (nm) (ε_{max} 10^3, dm^3 mol^{-1} cm^{-1}): 204 (31.6), 228 (10.1), 288 (4.65).

Synthesis of 4-amino-2-methoxyphenylhydroxamic acid (L_2H_2)

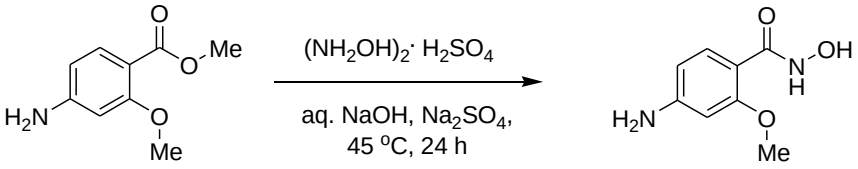

Hydroxylamine sulphate (6.10 g, 37.0 mmol) and Na_2SO_4 (0.58 g, 4.44 mmol) were added to an aqueous solution of NaOH (7.41 g, 185 mmol, 30 cm^3) mixed with 30 g of ice. Methy-4-amino-2-methoxybenzoate (6.70 g, 37.0 mmol) was then added and the solution was subsequently stirred at 45°C for 24 hrs. The resultant solution was allowed to cool and the pH was adjusted to 6 using conc. H_2SO_4 to initiate the precipitation of a pink solid. The solid was then collected via suction filtration and recrystallized from hot water to give L_2H_2 in 69% yield (4.64 g).
Elemental analysis (%) calculated as L_2H_2 ($C_8H_{10}N_2O_3$): C 52.75, H 5.53, N 15.38. Found: C 53.07, H 5.43, N 15.02.
^{1}H NMR (DMSO-d_6, 400 MHz): δ (ppm) 3.78 (s, 3H, OMe), 5.69 (s, 2H, NH_2), 6.21 (m, 1H, Ar), 7.52 (d, *J* = 8.2 Hz, 2H, Ar-H), 8.78 (s, 1H, Ar-H), 10.11 (s, 1H, OH).
^{13}C NMR (DMSO-d_6, 100 MHz): δ (ppm) 55.6 (OMe), 96.3 (C, Ar), 106.4 (CH, Ar), 108.3 (CH, Ar), 132.3 (CH, Ar), 153.3 (CH, Ar), 158.8 (C, Ar), 164.4 (C=O).
MS (EI$^+$): *m/z* 182 (8%,{M^+}), 166 (28%, {M–NH_2}$^+$), 150 (100%, {M–OCH_3}$^+$ and / or{M–NHOH}$^+$).
FT-IR: ν (cm^{-1}) 3343 (s), 3316 (m), 3220 (m), 2831 (w), 1619 (s), 1594 (s), 1527 (s), 1497 (s), 1468 (s), 1459 (s), 1427 (s), 1335 (s), 1278 (s), 1260 (s), 1212 (s), 1192 (s), 1156 (s), 1118 (s), 1025 (s), 955 (s), 889 (s), 849 (s), 828 (m), 771 (s), 738 (s), 717 (w), 644 (s) 611 (s), 546 (s), 525 (s).

2.3.3 Preparation of complexes 1-7.

All reactions were performed under aerobic conditions and all reagents and solvents were used as purchased. *Caution*: Although no problems were encountered in this work, care should be taken when manipulating the potentially explosive nitrate salts.

*Synthesis of [Cu(II)(L_1H)$_2$] (**1**)*

$Cu(NO_3)_2.3H_2O$ (0.25 g, 1.034 mmol), 2-(acetoxy)phenyl hydroxamic acid (L_2H_2) (0.17 g, 1.035 mmol) and NaOH (0.041 g, 1.025 mmol) were dissolved in methanol (25 cm^3) and stirred at room temperature for 4 h. The resultant green solution was subsequently filtered and X-ray quality crystals of **1** were obtained upon slow evaporation after one week in 49% yield. Elemental analysis (%) calculated as [Cu(L_1H)$_2$] ($C_{16}H_{16}N_2O_6Cu_1$): C 48.55, H 4.07, N 7.07. Found: C 48.93, H 4.16, N 7.08. FT-IR (cm^{-1}): 3463 (b), 3258 (m), 2979 (w), 3945 (w), 2843 (m), 2494 (w), 2045 (w), 1965 (w), 1802 (w), 1749 (w), 1606 (s), 1562 (m), 1511 (s), 1467 (s), 1425 (m), 1384 (m), 1314 (m), 1294 (w), 1248 (s), 1186 (m), 1166 (m), 1147 (s), 1108 (s), 1019 (s), 985 (m), 929 (s), 858 (w), 824 (w), 809 (w), 770 (s), 750 (s), 709 (m), 677 (s), 633 (s), 532 (m), 485 (m), 421 (m).

*Synthesis of [Fe(III)$_2$(L_1H)$_4Cl_2$].2MeCN (**2**)*

Anhydrous $FeCl_3$ (0.25 g 1.54 mmol), 2-(acetoxy)phenyl hydroxamic acid (L_1H_2) (0.25 g, 1.54 mmol) and $Bu_4N(OH)$ (0.40 g, 1.54 mmol) were dissolved in MeCN (40 cm^3) and the solution stirred for 4 hours. The resultant red / brown solution was filtered and red X-ray quality of **2** were obtained in 14% yield after 2 weeks. Elemental analysis (%) calculated as **2** ($C_{32}H_{32}N_6O_{12}Cl_2Fe_2$): C 45.37, H 3.81, N 6.61. Found: C 45.38, H 3.86, N 6.49. FT-IR (cm^{-1}): 3436 (br), 3075 (w), 3002 (m), 2941 (m), 2838 (m), 1606 (s sh), 1590 (m), 1561 (s, sh), 1514 (w), 1488 (s), 1464 (w), 1450 (s), 1435 (s), 1396 (s, sh), 1301 (s), 1275 (s), 1250 (s), 1179 (s), 1051 (w), 1042 (s), 1022 (s), 949 (w), 851 (s), 806 (m), 783 (w), 758 (s, sh), 697 (s), 658 (s,),629 (s) 572 (m), 530 (m), 473 (s), 429 (m).

*[Co(III)Co(II)$_6$(L_1H)$_8$(L_1)$_2$(MeOH)$_4$(NO_3)$_2$]NO_3·3.5H_2O·14MeOH (**3**)*

$Co(NO_3)_2.6H_2O$ (0.25 g, 0.86 mmol), *N*-hydroxy-2-methoxybenzamide (L_1H_2) (0.25 g, 1.54 mmol) and tetraethylammoniumhydroxide (NEt_4OH) (0.08 g, 0.08 cm^3, 1.54 mmol) were dissolved in MeOH (30 cm^3) and stirred for 4 hrs at room temperature. The resultant dark purple solution was subsequently filtered and X-ray quality crystals of **3** were obtained upon Et_2O diffusion over a period of three weeks in 20% yield. Elemental analysis (%) calculated as

3·2.5H_2O ($C_{96}H_{150}N_{13}O_{59}Co_7$): C 40.56, H 5.32, 6.41. Found: C 40.33, H 5.38, N 7.33. FT-IR (cm^{-1}): 3327 (br), 2942 (w), 2839 (w), 1597 (s), 1560 (s), 1509 (s), 1477 (s), 1461 (w), 1434 (s), 1373 (s), 1294 (s), 1240 (s), 1180 (s), 1162 (s,), 1149 (s), 1105 (s), 1056 (s), 1013 (m), 957 (s), 911 (w), 865 (s), 774 (s), 751 (s), 725 (s), 689 (w), 667 (w), 622 (s), 603 (s), 562 (s), 522 (s), 500 (s),433 (s).

*Synthesis of [Mn(II)$_6$(L_3)$_{12}$].6MeCN (**4**)*

Mn(II)(NO_3)$_2$.4H_2O (0.25 g, 1.00 mmol), *N*-hydroxy-2-methoxybenzamide (L_1H_2) (0.16 g, 1.00 mmol) and sodium hydroxide (0.039 g, 1.00 mmol) were dissolved in methanol (20 cm^3) and stirred at room temperature for 4 h. The purple solution obtained was filtered and colourless / pale yellow X-ray quality crystals of 4 were obtained upon slow evaporation of the mother liquor in approximately 5% yield over a period of two months. Elemental analysis (%) calculated as **[**Mn(II)$_6$(L_3)$_{12}$].2H_2O ($C_{96}H_{88}O_{38}Mn_6$): C 52.91, H 4.07. Found: C 53.11, H 3.65. FT-IR (cm^{-1}):3430 (br), 3071 (w), 2941 (m), 2840 (m), 2019 (w), 1625 (s, sh), 1599 (s), 1571 (s, sh), 1552 (s), 1485 (s), 1458 (s), 1438 (s), 1398 (s), 1374 (s, sh), 1297 (m), 1273 (s), 1235 (s), 1184 (s), 1164 (m), 1151 (w), 1103 (s), 1051 (s), 1019 (s), 1009 (s), 856 (s), 846 (w), 806 (w), 786 (s), 754 (s, sh), 700 (s), 660 (s, sh), 565 (s) 533 (m), 449 (w), 421(m).

*Synthesis of [Ni(II)(L_1H)(H_2O)($py)_3$](NO_3)·MeCN (**5**)*

Ni(NO_3)$_2$.6H_2O (0.25 g 0.86 mmol), 2-(acetoxy)phenyl hydroxamic acid (L_1H_2) (0.14 g, 0.86 mmol) and NaOH (0.34 g, 0.86 mmol) were dissolved in a methanol / pyridine solvent mixture (25 cm^3: 1 cm^3) and the solution stirred for 4 hours. The resultant green solution was filtered and aqua blue X-ray quality of **5** were obtained in 12% yield after 1 week. Elemental analysis (%) calculated as [Ni(II)(L_1H)(H_2O)($py)_3$](NO_3) ($C_{23}H_{25}N_5O_7Ni_1$): C 50.94, H 4.65, N 12.91. Found: C 47.85, H 4.53, N 9.83. FT-IR (cm^{-1}): 3410 (br), 3274 (s), 3108 (w), 3068 (m), 2999 (m), 2925 (w), 2840 (m), 2426 (s), 2032 (w), 1603 (s, sh), 1590 (s), 1566 (s, sh), 1514 (s), 1488 (s,), 1446 (s, sh), 1406 (m), 1384 (s, sh), 1332 (m), 1272 (s), 1245 (s, sh), 1219 (s), 1182 (s), 1155 (s, sh), 1106 (s, sh), 1071 (s, sh), 1040 (s, sh), 1019 (s), 923 (s, sh,), 849 (s), 839 (w), 768 (w), 757 (s, sh), 698 (s, sh) 663 (s, sh) 629 (s, sh) 575 (s, sh) 522 (m) 431 (s, sh) 413 (s).

*Synthesis of $[Zn(II)_2(LH)_2(H_2O)_5](NO_3)_2]_n$ (**6**)*

$Zn(NO_3)_2.6H_2O$ (0.25 g 0.86 mmol), 2-(acetoxy)phenyl hydroxamic acid (L_1H_2) (0.14 g, 0.86 mmol) and NaOH (0.34 g, 0.86 mmol) were dissolved in a methanol (20 cm^3) and the solution stirred for 4 hours. The resultant solution was subsequently filtered and X-ray quality crystals of **6** were obtained upon slow evaporation after one week in 10% yield. Elemental analysis (%) calculated as **6** ($C_{16}H_{26}N_4O_{17}Zn_2$): C 28.38, H 3.87, N 8.27. Found: C 28.08, H 3.74, N 11.30. FT-IR (cm^{-1}): 3231 (br), 2970 (w), 2920 (w), 2838 (w), 2363 (w), 2197 (w), 2168 (w), 2143 (w), 2026 (w), 1674 (w), 1600 (s, sh), 1571 (m), 1515 (s), 1475 (s), 1461 (m), 1431 (m), 1345 (s), 1294 (w), 1269 (s), 1241 (s, sh), 1182 (m), 1166 (w), 1155 (s), 1111 (s, sh), 1065 (s), 1044 (s), 1018 (s), 927 (s, sh), 826 (s), 770 (s), 745 (s), 703 (m), 654 (s), 565 (s), 524 (m), 437 (s).

*$\{[Cu(II)(L_2H)(H_2O)(NO_3)].H_2O\}_n$ (**7**)*

$Cu(NO_3)_2.3H_2O$ (0.25 g, 1.034 mmol), 4-amino-N-hydroxy-2-methoxybenzamide (L_2H_2) (0.18 g, 1.035 mmol) and tetrabutylammonium hydroxide (0.27 g, 1.025 mmol) were dissolved in methanol (20 cm^3) and stirred at room temperature for 4 h. The resultant green solution was subsequently filtered and X-ray quality crystals of **7** were obtained upon slow evaporation of the mother liquor over a period of two weeks (25% yield). Elemental analysis (%) calculated as $[Cu(II)(L_2H)(H_2O)(NO_3)]_n$ ($C_8H_{11}N_3O_7Cu_1$): C 29.59, H 3.41, N 12.94. Found: C 29.07, H 3.83, N 11.98. FT-IR (cm^{-1}): 3377 (s), 3305 (br), 3219 (s), 3124 (w), 2977 (w), 2838 (w), 22361 (w), 2241 (w), 2201 (w), 2188 (w), 2147 (w), 2100 (w), 2062 (w), 2019 (w), 2008 (w), 1940 (w), 1886 (w), 1601 (s, sh), 1573 (s), 1519 (s), 1472 (s), 1429 (w), 1386 (s), 1330 (w), 1307 (m), 1281 (w), 1260 (s), 1200 (s), 1179 (s), 1151 (s), 1112 (s), 1065 (s), 1025 (s, sh), 951 (s), 904 (s), 851 (s), 838 (m) 821 (m), 753 (w), 734 (s), 704 (m), 654 (s), 583 (s), 553 (s), 535 (w), 461 (s), 431 (s).

2.4 References

1. D. Griffith, M. Devocelle and C. J. Marmion. *Hydroxamic Acids: Their Chemistry, Bioactivity, Solution and Solid Phase Synthesis in Amino Acids, Peptides and Proteins in Organic Chemistry*, Ed. A. B. Hughes, 2009, vol. 2, pp. 93–137.
2. M. Paris, M. Porcelloni, M. Binaschi and D. Fattori. *J. Med. Chem.*, 2008, **51**, 1505.
3. R. Codd. *Coord. Chem. Rev*., 2008, **252**, 1387–1408.
4. Z. Amtul, R. Attaur, R. A. Siddiqui and M. I. Choudhary. *Curr. Med. Chem.*, 2002, **9**, 1323–1348.
5. D. T. Puerta and S. M. Cohen. *Curr. Top. Med. Chem*., 2004, **4**, 1551.
6. E. M. F. Muri, M. J. Nieto, R. D. Sindelar and J. S. Williamson. *Curr. Med. Chem.*, 2002, **9**, 1631–1653.
7. C. J. Marmion, D. Griffith and K. B. Nolan. *Eur. J. Inorg. Chem*., 2004, 3003.
8. B. Kurzak, H. Kozlowski and E. Farkas. *Coord. Chem. Rev.*, 1992, **114**, 169-200.
9. D. S. Kalinowski, D. R. Richardson. *Pharmacol. Rev.*, 2005, **57(4)**, 547-583.
10. M. R. Bedford, S. J. Ford, R. D. Horniblow and C. Tselepis. *J. Clin. Pharmacol.*, 2013, **53(9)**, 885-891.
11. K.N. Raymond, E.A. Dertz, in: J.H. Crosa, A.R. Mey, S. M. Payne (Eds.), *Iron Transport in Bacteria*, ASM Press, Washington, DC, 2004, p. 3.
12. A. Stintzi, K.N. Raymond, in: D.M. Templeton (Ed.), *Molecular and Cellular Iron Transport*, Marcel Dekker, Inc., New York, 2002, p. 273.
13. M. J. Miller. *Chem. Rev.*, 1989, **89**, 1563-1579.
14. A. M. Wilson, P. J. Bailey, P. A. Tasker, J. R. Turkington, R. A. Grant and J. B. Love. *Chem. Soc. Rev.*, 2014, **43**, 123–134.
15. B. K. Tait, K. E. Mdlalose and I. Taljaard. *Hydrometallurgy*, 1995, **38**, 1–6.
16. G. Mezei, C. M. Zaleski and V. L. Pecoraro. *Chem. Rev.*, 2007, **107**, 4933.
17. P. Happ, C. Plenk and E. Rentschler. *Coord. Chem. Rev.*, 2015, **289-290**, 238-260.
18. C. McDonald, S. Sanz, E. K. Brechin, M. K. Singh, G. Rajaraman, D. Gaynor, L. F. Jones. *RSC Advances*, 2014, **4**, 38182-38191.
19. C. McDonald, T. Whyte, S. M. Taylor, S. Sanz, E. K. Brechin, D. Gaynor and L. F. Jones. *CrystEngComm.*, 2013, **15**, 6672-6681.
20. A. S. Reddy, M. S. Kumar and G. R. Reddy. *Tetrahedron Lett.*, 2000, **41**, 6285–6288.
21. J. Comiskey, E. Farkas, K. A. Krot-Lacina, R. G. Pritchard, C. A. McAuliffe and K. B. Nolan. *Dalton. Trans.*, 2003, 4243.

22. C. F. Macrae, I. J. Bruno, J. A. Chisholm, P. R. Edgington, P. McCabe, E. Pidcock, L. Rodriguez-Monge, R. Taylor, J. van de Streek and P. A. Wood. *J. Appl. Cryst*., 2008, **41**, 466-470.
23. I. D. Brown. *Chem. Rev.* 2009, **109**, 6858–6919.
24. E. M. Rumberger, L. N. Zakharov, A. L. Rheingold, and D. N. Hendrickson. *Inorg. Chem.*, 2004, **43**, 6531−6533
25. N. F. Chilton, R. P. Anderson, L. D. Turner, A. Soncini and K. S. Murray. *J. Comput. Chem.*, 2013, **34**, 1164–1175.
26. O. Khan. *Molecular Magnetism*, VCH, New York, 1993.
27. A. K. Powell, S. L. Heath, D. Gatteschi, L. Pardi, R. Sessoli, G. Spina, F. Del Giallo, F. Pieralli. *J. Am. Chem. Soc.*, 1995, **117**, 2491–2502.
28. R. Werner, S. Ostrovsky, K. Griesar and W. Haase. *Inorg. Chim. Acta*, 2001, **326**, 78-88.
29. F. Le Gall, F. Fabrizi de Biani, A. Caneschi, P. Cinelli, A. Cornia, A. C. Fabretti and D. Gatteschi. *Inorg. Chim. Acta*, 1997, **262**, 123–132.
30. T. Weyhermüller, R. Wagner and P. Chaudhuri. *Eur. J. Inorg. Chem.*, 2011, **2011**, 2547–2557.
31. A. A. Kitos, C. G. Efthymiou, C. Papatriantafyllopoulou, V. Nastopoulos, A. J. Tasiopoulos, M. J. Manos, W. Wernsdorfer, G. Christou and S. P. Perlepes. *Polyhedron*, 2011, **30**, 2987–2996.
32. S.-H. Zhang, Y. Song, H. Liang, and M.-H. Zeng. *CrystEngComm*, 2009, **11**, 865–872.
33. V. Tudor, G. Marin, F. Lloret, V. Ch. Kravtsov, Y. A. Simonov, M. Julve and M. Andruh. *Inorg. Chim. Acta*, 2008, **361**, 3446–3452.
34. S. T. Meally, C. McDonald, P. Kealy, S. M. Taylor, E. K. Brechin and L. F. Jones. *Dalton Trans.*, 2012, **41**, 5610-5616.
35. A. Ferguson, A. Parkin, J. Sanchez-Benitez, K. Kamenev, W. Wernsdorfer and M. Murrie. *Chem. Commun.*, 2007, **0**, 3473–3475.
36. Rigaku OD (2015). *CrysAlis PRO*. Rigaku Oxford Diffraction Ltd, Yarnton, England.
37. G. M. Sheldrick. *Acta Crystallogr. Sect. C Struct. Chem.* 2015, **71**, 3.
38. O. V. Dolomanov, L. J. Bourhis, R. J. Gildea, J. A. K. Howard and H. J. Puschmann. *Appl. Crystallogr.* 2009, *42*, 339.
39. A. Spek, *J. Appl. Cryst.* 2003, **36**, 7.
40. P. van der Sluis and A. L. Spek, *Acta Cryst*., 1990, **A46**, 194.

Chapter Three

Multitopic Hydroxamate Ligands aid the Construction of Discrete Polynuclear Complexes and Coordination Polymers

3.1 Introduction

The design of a new ligands is at the core of contemporary coordination chemistry.[1,2] Multi-topic bridging ligands are among the ligands used to produce changes in the structural and reactivity properties of metal complexes especially coordination polymers (CPs).[3-5] CPs are an interesting class of molecular inorganic-organic hybrid compounds, constructed through an infinite metal-ligand backbone held together by coordination interactions.[6-9] The design of CPs using hydroxamate Schiff base ligands and their reduced forms is gaining increased attention due to their ability to covalently couple metal centres and their convenient synthetic methods.[10-12] Hydroxamic acids coupled with aldehydes/ketone and their reduced analogues can be employed to gain more insights into the geometry around the coordinating moiety and modulate the spatial orientation, and the extent of electronic coupling of the attached metals.[13,14] Moreover, they determine the flexibility and effect of different donor atoms on the formation of diverse coordination networks such as 2-D and 3-D network architectures, hydrogen-bonded linear polymers or helical coordination polymers with possible applications in the area of catalysis, gas adsorption, optics, bioactivity, ion recognition and molecular magnetism (among others) due to their unique physicochemical properties.[15-20] In this chapter, we will focus on multi-topic bridging ligands that contain functional groups (such as N-H, O-H and C=O) with effective binding ability to the metal ions to demonstrate their significant role in the synthetic strategies for defining the assemblies, structures, and properties of targeted CPs. [21,22]

3.2 Result and Discussion

Previous investigations by the Jones group into the coordination chemistry of the ligands 2-(amino)phenylhydroxamic acid (2-am-phaH_2) and 2-(dimethylamino)phenylhydroxamic acid (2-dm-phaH_2; Scheme 3.1) initially led to the formation of a family of planar 12-MC-4 [M(II)] (M = Ni, Cu) metallacrowns, which included the complexes: [Cu(II)$_5$(2-dm-pha)$_4$(MeOH)$_4$](ClO$_4$)$_2$, [Ni(II)$_5$(2-dm-pha)$_4$(MeOH)$_4$](ClO$_4$)$_2$·2MeOH[23] and [Cu(II)$_5$(2-am-pha)$_4$(MeOH)$_2$](ClO$_4$)$_2$·H_2O (Scheme. 3.1).[24] Furthermore, the apparent stability of these pentametallic metallacrown architectures was further highlighted upon their successful employment as nodes in the construction of the 1- and 2-D coordination polymers: {[Cu(II)$_5$(2-dm-pha)$_4$(4,4′-bipy)$_3$](ClO$_4$)$_2$·(H_2O)}$_n$ (4,4-bipy = 4,4-bipyridyl*)*, {[Cu(II)$_5$(2-dm-pha)$_4$(4,4′-azp)$_2$(MeOH)$_2$](ClO$_4$)$_2$}$_n$ and {[Cu(II)$_5$(2-am-pha)$_4$(pz)$_2$(MeOH)$_3$](ClO$_4$)$_2$·MeOH}$_n$ (4,4-azp = 4,4-azopyridine; pz = pyrazine).[24]

The Jones group also described a series of ligands constructed from the Schiff base coupling of 2-amino-phenylhydroxamic acid (2-am-phaH_2) and o-vanillin (and its analogues). The planarity of the resulting ligands (e.g. o-[(E)-(2-hydroxy-3-methoxyphenyl)methylideneamino]benzohydroxamic acid; Scheme 3.2), gave rise to a family of layered planar cages ranging in nuclearity from [Cu(II)$_{10}$] to [Cu(II)$_{30}$].[25]

3.2.1 Ligands descriptions

Recognizing their well-established metal binding ability, we decided to modify these aforementioned hydroxamate ligands in order to achieve similar effect upon complexation. Thus 2-(dimethylamino)phenylhydroxamic acid (2-dm-phaH_2) was modified to 2-(methylamino)phenylhydroxamic acid (L_4H_2; Scheme 3.1), and was prepared as reported by Fugu et al in 2019.[26] The ligand L_4H_2 was obtained when dimethyl anthranilate was reacted with equimolar hydroxylamine sulphate in alkaline medium (see experimental section for details). The desired product was recovered in pure form after recrystallization using hot water in yield of 53% (Scheme 3.1).

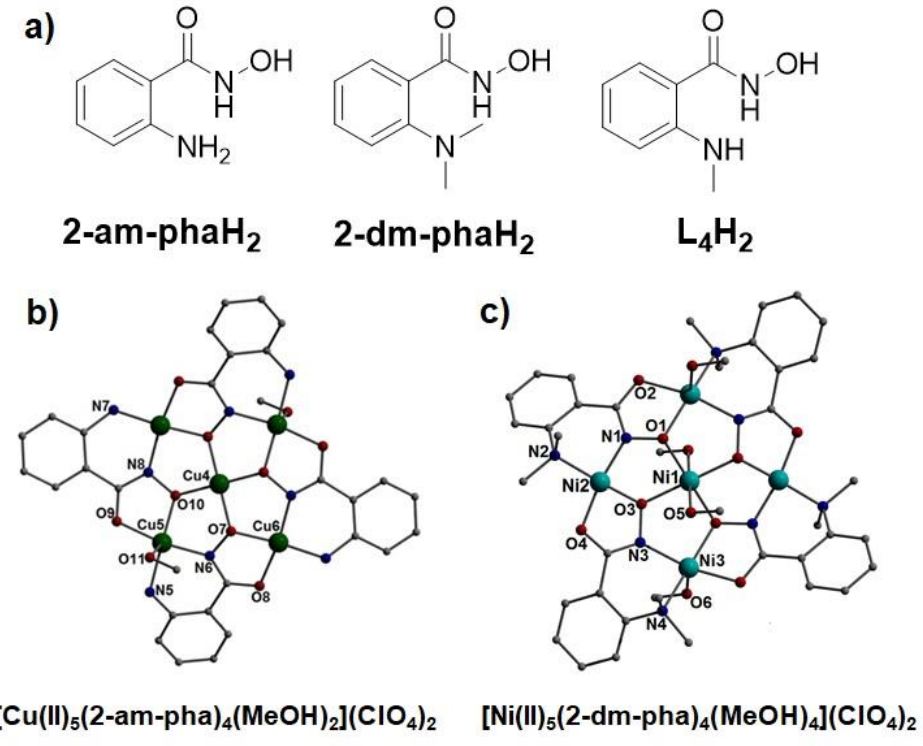

Scheme 3.1 *(a) ChemDraw representations of the ligands 2-(amino)phenylhydroxamic acid (2-am-phaH_2) and 2-(dimethylamino)phenylhydroxamic acid (2-dm-phaH_2) previously used in the production of a series of polynuclear 12-MC-4 [M(II)$_5$] (M = Ni, Cu) complexes and coordination polymers.[23,24] Two examples are given above. (Top right) ChemDraw representation of the ligand 2-(methylamino)phenylhydroxamic acid (L_4H_2) used in this work.*

As highlighted in Scheme 3.2, we also decided to selectively reduce the imine group of the ligand o-[(E)-(2-hydroxy-3-methoxyphenyl)methylideneamino]benzohydroxamic acid to afford the target molecule (*N*-hydroxy-2-((2-hydroxy-3-methoxybenzyl)amino)benzamide (L_5H_3; Scheme 3.2). It was hoped that the introduction of a secondary amine group should render the resultant ligand non-planar and the effect of this structural change would be observable upon subsequent metal complex formation. The target ligand (*N*-hydroxy-2-((2-hydroxy-3-methoxybenzyl)amino)benzamide (L_5H_3) was successfully synthesised by the one-pot Schiff base coupling and selective imine reduction of 2-amino-phenylhydroxamic acid and ortho-vanillin using the reducing agent sodium triacetoxyborohydride.[27] The desired product was recovered in moderate but workable yield (31%), which may be attributed to the hydrolysis of the Schiff base in the presence of water as reported by Pramanik *et al*., in 2018 and Kim *et al*. in 2016.[28,29] The ligand L_5H_2 was also characterised using nuclear magnetic resonance (NMR), infrared spectroscopy (IR) and mass spectrometry (MS) (See experimental section for details).

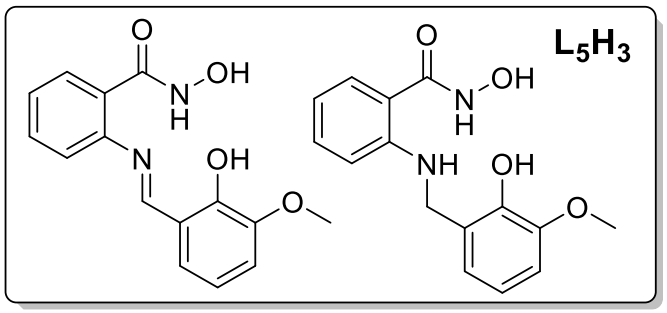

Scheme 3.2 *(Left) The ligand o-[(E)-(2-hydroxy-3-methoxyphenyl)methylideneamino]benzohydroxamic acid previously used in the production of a series of polynuclear Cu(II) complexes ([Cu(II)$_{10}$], [Cu(II)$_{14}$] and [Cu(II)$_{30}$]).[25] (Right): The novel ligand (N-hydroxy-2-((2-hydroxy-3-methoxybenzyl)amino)benzamide (L_5H_3) used in this work.*

Other ligands synthesized in this work include the linear multitopic ligands: N-hydroxy-4-((2-hydroxy-3-methoxybenzyl)amino)benzamide (L_6H_3) and N-hydroxy-4-((2-hydroxybenzyl)amino)benzamide (L_7H_3) (Scheme 3.3). Akin to ligands L_5H_3, ligands L_6H_3 and L_7H_3 are prepared via the Schiff base coupling and subsequent imine reduction of 4-amino-phenylhydroxamic acid and either *o*-vanillin (L_6H_3) or salicylaldehyde (L_7H_3) and differ only in the coupling site (the 2-position in L_5H_3 *cf.* to the 4-position in $L_{6\text{-}7}H_3$).[30-32]

The general reaction in which these Schiff baes were reduced involved the addition of sodium borohydride ($NaBH_4$) to a stirring solution of the Schiff bases (see experimental section). The two-step reduction using sodium borohydride (which is also highly selective reducing agent and will not usually attack any substituent group attached),[33] was adopted on the basis of the low yield experienced from the one-pot imine reduction. The yield of the secondary amines this time were generally better compared to the one-pot reduction. Dry THF proved to be a convenient medium for the reaction in both one and two step cases. All the reactions were accompanied by a colour change (yellow → colourless) which indicates that the reduction was taking placed.

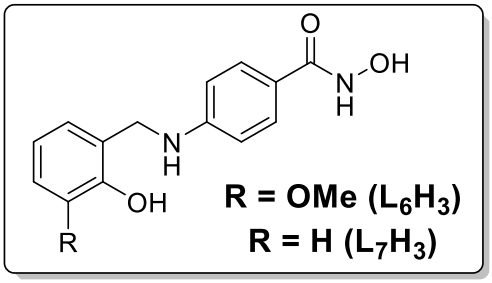

Scheme 3.3 *ChemDraw representation of the ligands N-hydroxy-4-((2-hydroxy-3-methoxybenzyl)amino)benzamide (L_6H_3) and N-hydroxy-4-((2-hydroxybenzyl)amino)benzamide (L_7H_3) used in this work.*

3.2.2 Metal complexation

This chapter describes the first examples of 1st row transition metal complexation of the novel ligands L_4H_2 and $L_{5\text{-}7}H_3$ in the form of the complexes $[Cu(II)_5(L_4)_4(NO_3)_2]\cdot 3H_2O$ (**8**) and $[Cu(II)_5(L_5H)_4(MeOH)_2](NO_3)_2\cdot 3H_2O\cdot 4MeOH$ (**10**), along with the 1-D coordination polymers $\{[Zn(II)(L_4H)_2]\cdot 2MeOH\}_n$ (**9**), $[Cu(II)(L_6H)_2]_n$ (**11**) and $\{[Cu(II)(L_7H_2)].2MeOH\}_n$ (**12**). Crystallographic information for complexes **8**-**10** and **11**-**12** are given in Tables 3.3 and 3.4, respectively.

The methanolic reaction of $Cu(NO_3)_2\cdot 3H_2O$ and L_4H_2 in the presence of NaOH, gave rise to a green solution which after filtration and slow evaporation produced dark green block-like crystals of $[Cu(II)_5(L_4)_4(NO_3)_2]\cdot 3H_2O$ (**8**). The asymmetric unit in **8** comprises two half $\{Cu_5\}$ units (labelled Cu1-Cu3 and Cu4-Cu6, respectively) and are separated by 2.95 Å (Cu4···N4′) at the shortest distance. The inorganic core in **8** comprises a body centred square array of Cu(II) ions joined together through four $\eta^1{:}\eta^2{:}\eta^1{:}\eta^1$ μ_3- bridging L_4^{2-} ligands to forge a 12-MC-4

metallacrown topology (Fig. 3.1).[34] The central Cu(II) ions exhibit distorted octahedral (Cu1) and distorted square planar (Cu6) geometries, respectively. The axial contacts at Cu1 are made by two symmetry equivalent μ-bridging NO_3^- anions (Cu1-O5 = 2.43 Å), that also provide the axial contacts at the two symmetry equivalent Cu3 centres (Cu3-O7 = 2.64 Å). The two NO_3^- anions belonging to the second crystallographically unique {Cu(II)$_5$} moiety are located at the axial positions of the outer (distorted square based pyramidal) Cu(II) ions (Cu5 and s.e.) at a distance of 2.42 Å (Cu5-O12). The remaining metal centres (Cu2 and Cu4) in both pentametallic units exhibit distorted square planar geometries, although the Cu2 centres are provided with long contact at the axial positions with O donor atoms (O10 and s.e.) of the nearby second {Cu(II)$_5$} unit (Cu2···O10′ = 2.91 Å). The waters of crystallisation in **8** (O17-O19) are held in position through numerous H-bonding interactions with O donor atoms and secondary amine and aromatic protons belonging to juxtaposed L_4^{2-} units (e.g. O3···O17 = 2.74 Å; N2(H2)···O17 = 1.99 Å; C3(H3)···O18 = 3.14 Å and C13(H13)···O19 = 2.76 Å). The individual pentametallic units in **8** pack in a space efficient brickwork manner along the *ab* plane of the unit cell and the resultant 2-D sheets stack in parallel and superimposable rows along the *c* axis of the unit cell (Fig. 3.2).

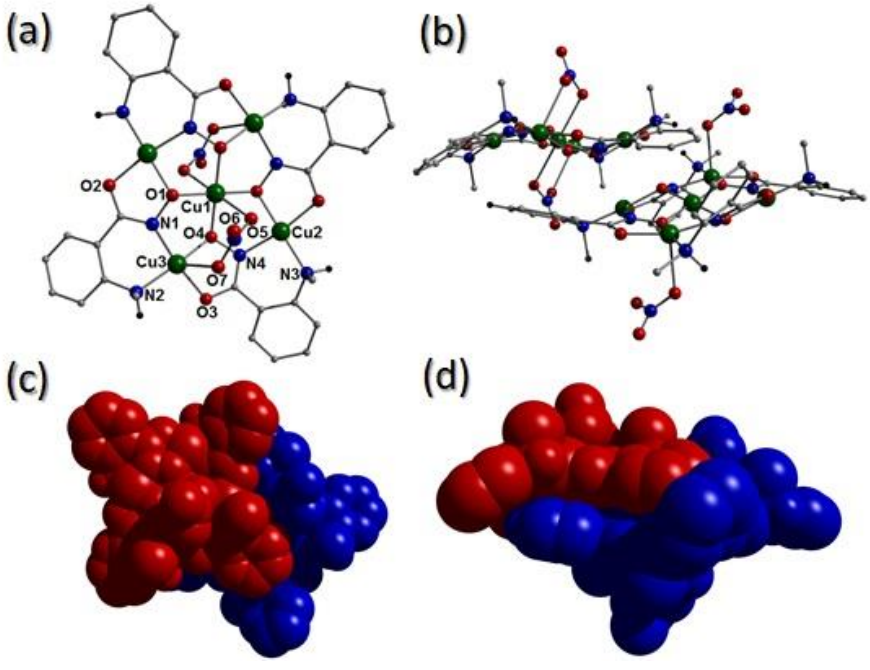

Figure 3.1 *(a) The crystal structure in [Cu(II)$_5$(L$_4$)$_4$(NO$_3$)$_2$]·3H$_2$O (**8**) as viewed perpendicular to the pentametallic core. (b) The two [Cu$_5$] units grown from the asu in **8** represented in traditional (b) and colour coded space-fill modes as viewed perpendicular (c) and parallel (d) to their pentametallic inorganic cores. The majority of hydrogen atoms and all waters of crystallisation have been removed for clarity.*

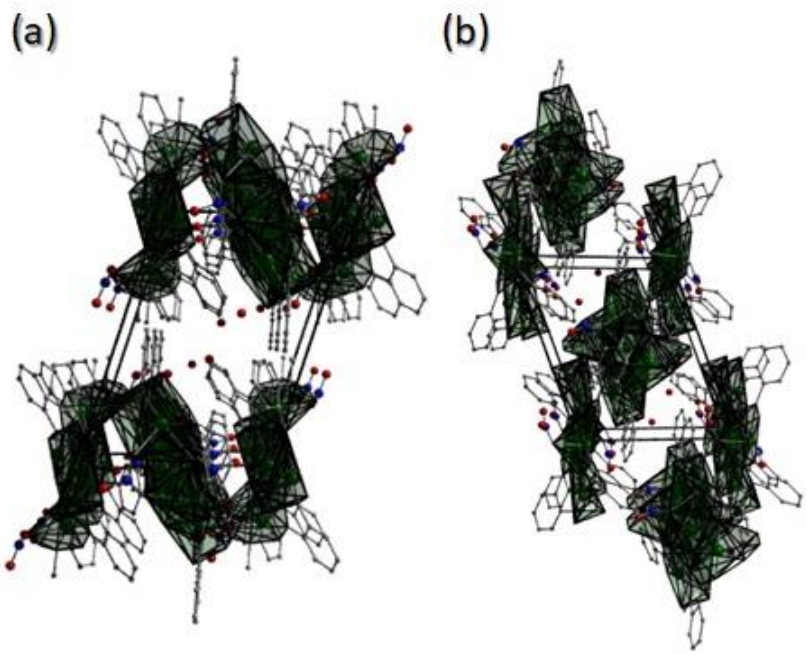

Figure 3.2 *Polyhedral packing arrangement in* ***8*** *as viewed down the b-axis (a) and c-axis (b) of the unit cell. All hydrogen atoms were omitted for clarity.*

The same ligand 2-(methylamino)phenylhydroxamic acid (L_4H_2) upon methanolic reaction with $Zn(II)(NO_3)_2 \cdot 6H_2O$ in the presence of NaOH gave a pale yellow reaction mixture that upon filtration and slow evaporation gave rise to pale yellow crystals of the coordination polymer $\{[Zn(II)(L_4H)_2]\cdot 2MeOH\}_n$ (**9**). The parallelpiped crystals of **9** were obtained in the orthorhombic *Pcc*2 space group and comprise of Zn(II) ions in distorted octahedral geometry connected into superimposable 1-D rows that propagate along the *c* unit cell direction (Figs. 3.3 and 3.4). The metal centres are linked into the polymeric array via the singly deprotonated $\eta^1{:}\eta^2$ μ-bridging L_4H^- ligands. The hydroxamate ligands in **9** sit alternately above and below the Zn1-O1-Zn1′ plane and form both the equatorial (Zn1-O1 = 2.13 Å and Zn1-O1′ = 2.09 Å) and axial (Zn1-O2 = 2.12 Å) bonds to the metal centres. The crystallographically equivalent methanol solvents of crystallisation lie along the channels formed in between the cubic packed $[Zn(II)(L_4H)_2]_n$ chains and are held in position through H-bonds with nearby hydroxamate O donor atoms (O1 and s.e.) at a distance of 1.94 Å (C9-O3(H3)···O1).

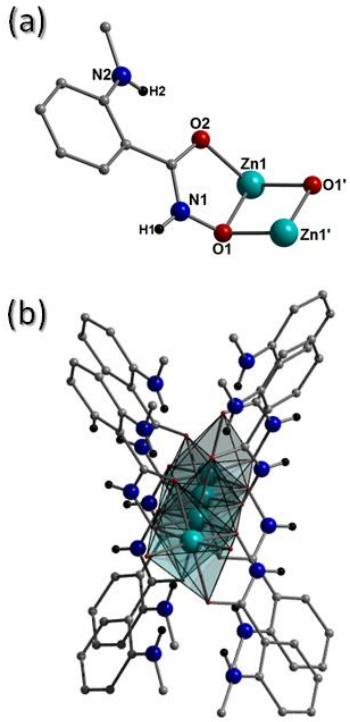

Figure 3.3 *(a) The asymmetric unit in {[Zn(II)(L_4H)$_2$]·2MeOH}$_n$ (**9**) along with the crystallographically related Zn1′ and O1′ atoms. (b) A 1-D row in **9** as viewed off-set along the c unit cell direction.*

The 12-MC-4 metallacrown in **8** along with the Zn(II) coordination polymer in **9** represent the first 1st row transition metal complexes to be constructed using L_4H_2. Lipczynska-Kochany and co-workers have previously synthesised L_4H_2 towards their work on the Lossen rearrangement of hydroxamic acids and more broadly, on the biological activities of hydroxamic acids.[35] Iwamura and co-workers have probed the fluorescence properties of 2-(methylamino)phenylhydroxamic acid.[36] Furthermore, Sianesi and Bonola used L_4H_2 as part of their research into using a series of 3-hydroxy-2,3-dihydro-4(1H)-quinazoline derivatives (produced via the ring closure of certain hydroxamic acids), for potential use as antibacterial and antifungal agents.[37]

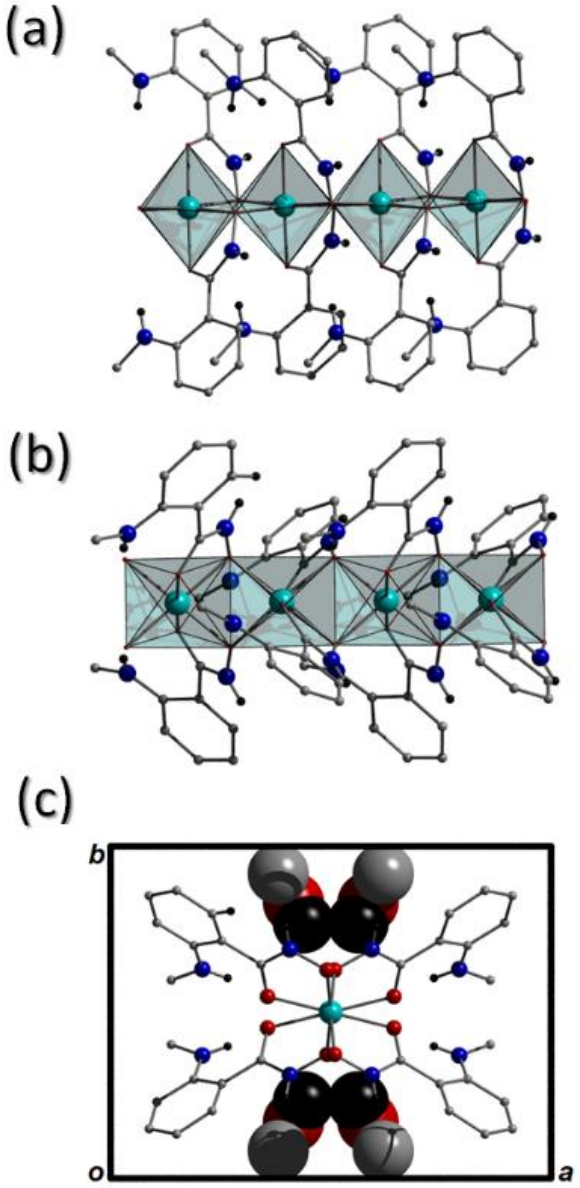

Figure 3.4 *A polyhedral representations of the 1D-chains as viewed along the equatorial (a) and axial (b) planes of the distorted octahedral Zn(II) centres in* ***9****. (c) The unit cell in* ***9*** *as viewed along the c direction. The methanol solvents of crystallisation are shown in space-fill mode.*

After successfully investigating the coordinating power of the L_4H_2 ligand, we then decided to investigate the ligating ability of the more structurally elaborate ligand (*N*-hydroxy-2-((2-hydroxy-3-methoxybenzyl)amino)benzamide (L_5H_3; Scheme 3.2). To this end, upon reaction with $Cu(NO_3)_2{\cdot}3H_2O$ and NaOH gave rise to the pentametallic complex $[Cu(II)_5(L_5H)_4(MeOH)_2](NO_3)_2{\cdot}3H_2O{\cdot}4MeOH$ (**10**), that crystallises in the triclinic *P*-1 space group. The pentametallic core in **10** comprises a planar 12-MC-4 metallacrown topology,

where the central, distorted octahedral Cu centre (Cu1) is surrounded by a square of four other copper ions (Cu2-3 and s.e.) (Fig. 3.5a). The five metal centres in **10** are bound by four doubly deprotonated L_5H^{2-} ligands, each exhibiting an $\eta^1:\eta^2:\eta^1:\eta^1:\eta^1$ μ_3-bonding mode (Fig. 3.5d). More specifically, the planar {Cu(II)$_5$} core in **10** is formed due to metal ligation to the near planar hydroxamate groups of each L_5H^{2-} ligand, as observed in previous 12-MC-4Cu(II) metallacrowns.[9] However, unlike in other analogues, the deliberate introduction of the secondary amine groups provides each ligand with a natural kink, which results in each the four independent ligand phenolic groups to significantly deviate from the {Cu(II)$_5$} plane (Fig. 3.5c).

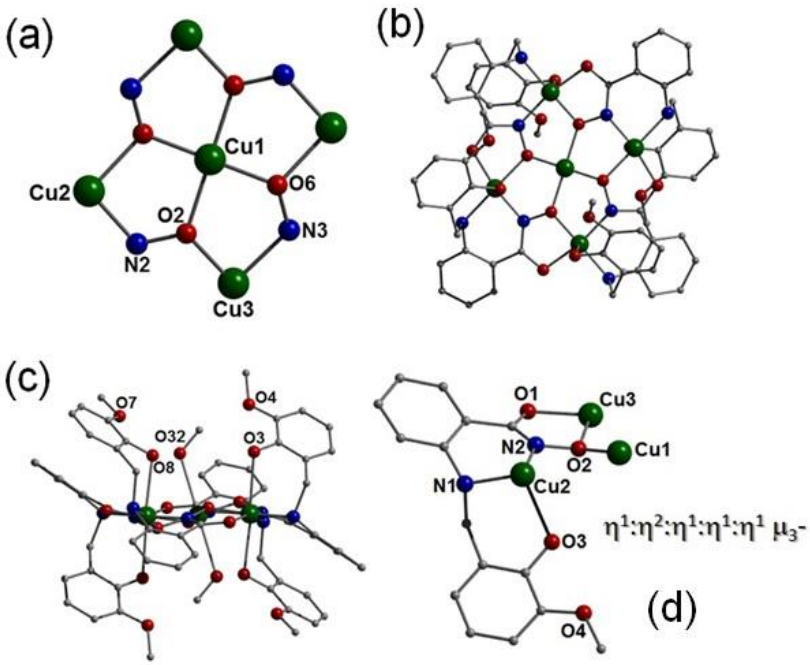

Figure 3.5 *(a) The inorganic core in [Cu(II)$_5$(L$_5$H)$_4$(MeOH)$_2$](NO$_3$)$_2$ (**10**) along with the crystal structure of **10** as viewed perpendicular (b) and parallel (c) to the {Cu(II)$_5$} plane. The terminal MeOH ligands at Cu1 in (b) have been omitted for clarity. All hydrogen atoms have been omitted for clarity. (d) The bonding mode exhibited by the L$_5$H^{2-} ligands in **10**. The bold line represents an elongated axial Cu-O interaction (Cu2-O3 = 2.50 Å).*

As a result, these phenolic units sit in an up-up-down-down arrangement with respect to the planar core in **10** and are therefore able to forge long axial contacts with the four outer Cu centres (Cu2-O3 = 2.502 Å and Cu3-O8 = 2.53 Å). This gives rise to a distorted square based pyramidal geometry at Cu2 (τ_{Cu2} = 0.10) and a distorted octahedral geometry at Cu3 (due to a long sixth contact with a nearby NO_3^- counter anion; Cu3-O10 = 2.719 Å). It should be noted that the aromatic hydroxamate rings also deviate away from the {Cu(II)$_5$} plane but to a lesser

extent. Two terminal ligated MeOH ligands occupy the axial positions at the central distorted octahedral Cu1 site (Cu1-O32 = 2.65 Å) and effectively sit in a pocket forged by the aforementioned phenolic groups of the L_5H^{2-} ligands, while two other unbound methanol solvents of crystallisation lie at the periphery of the structure in **10**. The L_5H^{2-} units remain protonated at the phenolic oxygen sites and these protons (H3H and H8H) partake in H-bonding with the oxygen atoms (O32) of the terminally bound MeOH ligands at Cu1 (O3(H3H)···O32 = 1.79 Å) and with nearby water solvents of crystallisation (O8(H8H)···O31 = 1.78 Å), respectively. These metal ligated methanol units also participate in H-bonding with the $–OCH_3$ groups (O4 and O7) at each hydroxamate site (C46(H46C)···O4 = 2.84 Å and C46(H46B)···O7 = 1.82 Å). The protonated nitrogen atoms (N1(H1H), N4(H4H) and s.e.) at the secondary amine groups at each L_5H^{2-} ligand engage with juxtaposed solvents (MeOH and H_2O) of crystallisation at H-bonding distances of (Å): 1.66 (N1(H1H)···O30) and 2.02 (N4(H4H)···O34), respectively. Moreover, numerous parallel-displaced π-π stacking interactions between the hydroxamate aromatic rings of each L_5H^{2-} moiety aid the space efficient packing observed in the unit cell of **10** (e.g. $[C2\text{-}C7]_{centroid}$···$[C2'\text{-}C7']_{centroid}$ = 3.78 Å) (Fig. 3.6).

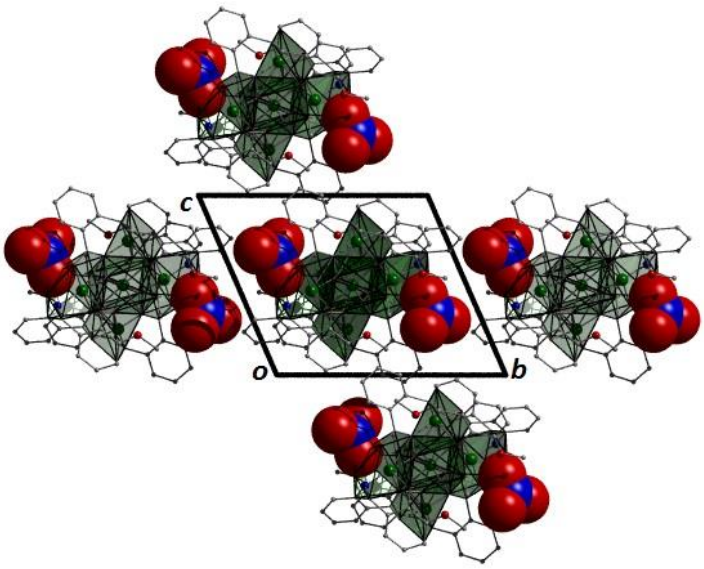

Figure 3.6 *Packing arrangement in **10** as viewed down the a-axis of the unit cell. The NO_3^- counter anions are space-fill represented.*

The production and characterisation of complexes **8-10** highlighted that hydroxamic acid ligands functionalised at the 2-position (L_4H_2 and L_5H_3) are excellent candidates in the construction of both discrete polymetallic cages and 1-D coordination polymers. It was time to

look at the design and synthesis of similar ligands that are functionalised at the 4-position towards their potential use as multitopic ligands in extended network architectures. To this end, we present here the Cu(II) ligation of two multitopic ligands: N-hydroxy-4-((2-hydroxy-3-methoxybenzyl)amino)benzamide (L_6H_3) and N-hydroxy-4-((2-hydroxybenzyl)amino)benzamide (L_7H_3); leading to the construction of the 1-D coordination polymers $[Cu(II)(L_6H_2)_2]_n$ (**11**) and $\{[Cu(II)(L_7H_2)_2].2MeOH\}_n$ (**12**).

$[Cu(II)(L_6H_2)_2]_n$ (**11**) crystallises in the monoclinic $P2_1/c$ space group and the asymmetric unit comprises one Cu(II) centre (Cu1) and one $L_6H_2^-$ ligand. Each axially elongated J-T distorted octahedral Cu(II) centre in **11** is bound at the equatorial positions by two singly deprotonated $L_6H_2^-$ ligands that chelate through their hydroxamate (O2) and carbonyl (O1) oxygen atoms (Cu1-O1 = 1.93 Å, Cu1-O2 = 1.91 Å). The axial sites at each metal centre are occupied through long contacts with O_{phen} oxygen atoms (O3 and s.e.) belonging to neighbouring $L_6H_2^-$ ligands (Cu1-O3 = 2.74 Å and s.e.). Moreover, intra-ligand hydrogen bonding interactions are observed between phenolic protons (H3H), and juxtaposed $–OCH_3$ oxygen atoms (O4) (O3(H3H)$\cdots$O4 = 2.16 Å). The multitopic nature of the $L_6H_2^-$ moieties in **11** results in the formation of the ribbon 1-D chain as shown in Figure 3.7.[38] The individual chains in **11** propagate in superimposable rows along the *ac* plane of the unit cell and produce an intra-chain Cu$\cdots$Cu distance of 11.75 Å. The chains in **11** are stabilised by intra-chain π-π interactions between neighbouring hydroxamate phenyl rings giving a $[C2\text{-}C6]_{centroid}\cdots[C2'\text{-}C6']_{centroid}$ distance of 3.83 Å. The individual chains in **11** form superimposable 2-D stacks through H-bonding interactions (e.g. N1(H2)$\cdots$O2′ = 2.38 Å and N2(H2H)$\cdots$O3′ = 2.95 Å). The resultant H-bonded 2-D sheets arrange in a space efficient herring bone motif along the *b* direction of the unit cell (Fig. 3.8) and are connected through H-bonding (C15(H15A)$\cdots$O3′ = 2.83 Å) and C-H$\cdots$π interactions ($[C9\text{-}14]_{centroid}\cdots$(H12′)C12 = 3.10 Å).

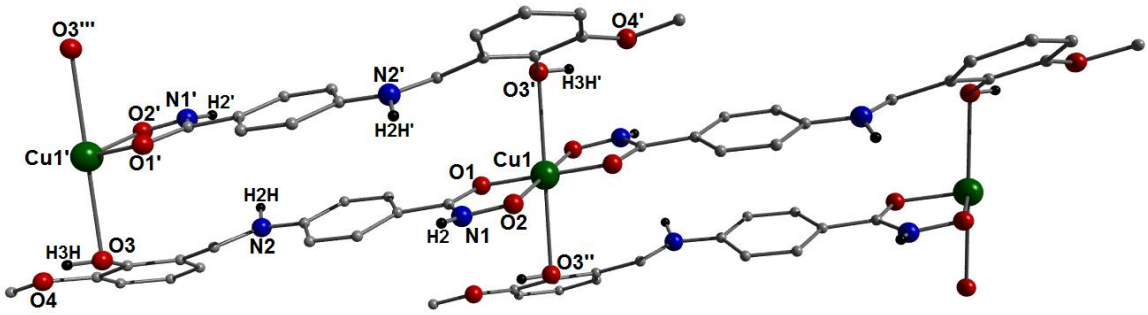

Figure 3.7 *Crystal structure of the coordination polymer in* $[Cu(II)(L_6H_2)_2]_n$ ***(11)****. Colour code: Green (Cu), Grey (C), Blue (N), Red (O) and Black (H). The majority of hydrogen atoms have been omitted for clarity.*

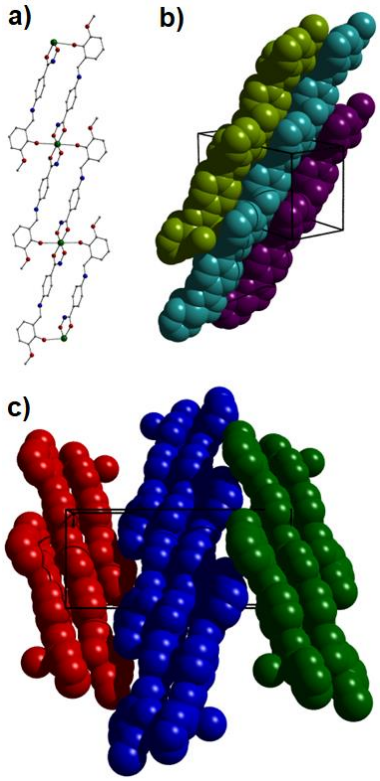

Figure 3.8 *(a) A single ribbon 1-D chain in* ***11****. All hydrogen atoms have been omitted for clarity. (b) Space-fill represented and colour coded H-bonded stacks of chains in* ***11*** *as viewed along the ab plane of the unit cell. (c) Space-fill and colour coded representation of three H-bonded stacks comprising 1-D chains of* ***11****.*

An identical reaction synthon to that employed in the production of **11** (simply replacing L_6H_3 with L_7H_3) gave rise to the formation of the analogue $\{[Cu(II)(L_7H_2)_2].2MeOH\}_n$ (**12**). Akin to **11**, the 1-D coordination polymer **12** crystallises in the monoclinic $P2_1/c$ space group. The asymmetric unit comprises an axially elongated Cu(II) centre, a single $L_7H_2^-$ ligand and a

methanol solvent of crystallisation that sits at H-bonding distance from the amide proton of the hydroxamate section of the ligand (N1(H1N)···O4 = 1.98 Å; Fig. 3.9a). Two $L_7H_2^-$ ligands chelate to the metal centre at distances of 1.91 Å (Cu1-O1) and 1.93 Å (Cu1-O2) to give the {Cu(II)(L_7H_2)$_2$} chair shaped building block in **12** (Fig. 3.9a). The major difference between the structure in **12** *cf.* **11** lies in the axial connectivity at the Cu(II) centres in **12**. Here, the 1-D chains in **12** are propagated by long axial contacts between the metal centres and secondary amine N atoms (N2) located at the junction of the hydroxamate and phenolic units within each $L_7H_2^-$ ligand (Cu1-N2′ = 3.04 Å), as opposed to the O_{phen} oxygen atoms donors in **11** (Fig. 3.7 *cf.* Fig. 3.9b). The result is a much shorter intra-chain Cu1···Cu1′ distance of 8.62 Å in **12** (*cf.* 11.75 Å in **11**; Fig. 3.9b). Interestingly, the deliberate omission of the –OCH_3 group in L_7H_3 allows each ligand to distort to a much greater extent than observed in **11** (Fig. 3.10). More specifically, the phenolic aromatic rings in the $L_7H_2^-$ units in **12** twist away from their phenyl hydroxamate counterparts to produce a torsion angle of -75.1° (C5-N2-C8-C9) compared to the more co-planar value of -164.5° (C5-N2-C8-C9) exhibited by the $L_6H_2^-$ units in **11** (Fig. 3.10b *cf.* 3.10c). The individual chains in **12** propagate in a step-like manner along the *a* direction of the unit cell (Fig. 3.9b) and arrange themselves in a space efficient 2-D arrays along the *ab* plane. These individual sheet-like arrays pack along the *c*-direction in an alternating fashion, as highlighted in Figure 3.9d. The methanol solvents of crystallisation (labelled C15-O4(H4H)) sit at H-bonding distance from $L_7H_2^-$ amide N atoms at a distance of 1.98 Å (N1(H1N)···O4) and act as molecular mortar by forming inter-chain interactions with both nearby phenolic rings ($[C9\text{-}C14]_{centroid}$···O4(H4H) = 2.54 Å) and –OCH_3 oxygen donor atoms (O3) (C15(H15C)···O3(H3H) = 2.86 Å). The $L_7H_2^-$ secondary amine N atoms (N2 and s.e.) also partake in inter-chain H-bonding with neighbouring ligand phenolic aromatic rings (N2(H2N)···$[C9'\text{-}C14']_{centroid}$ = 3.14 Å).

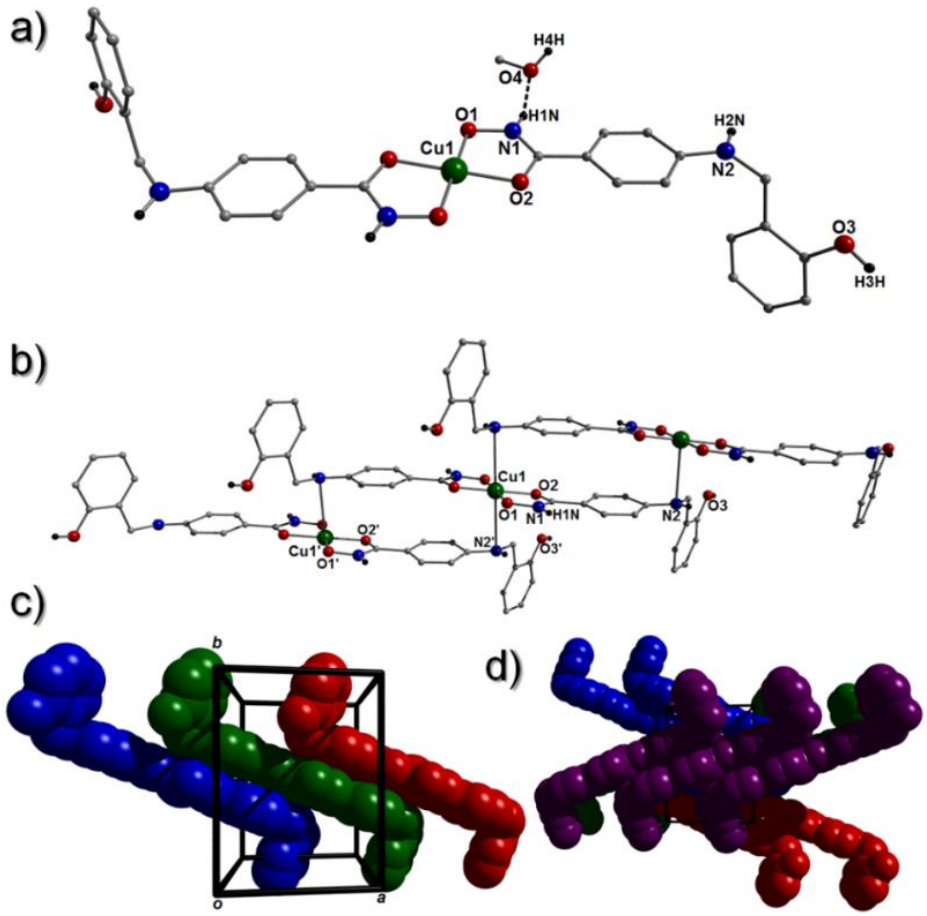

Figure 3.9 *(a) A single {[Cu(II)(L_7H_2)$_2$].2MeOH} unit in* ***12****. The asymmetric unit has been labelled and only one MeOH solvent of crystallisation is shown. The dashes black line shows an inter-molecular H-bond at a distance of 1.98 Å (N1(H1N)···O4). The chain arrangement in* ***12*** *as viewed in normal (b) and space-fill mode (c), where each colour represents an independent {Cu(II)(L_7H_2)$_2$} unit. (d) Space-fill representation of the packing in* ***12****. Each colour represents an H-bonded stack of 1-D chains in* ***12*** *as viewed along the c unit cell direction.*

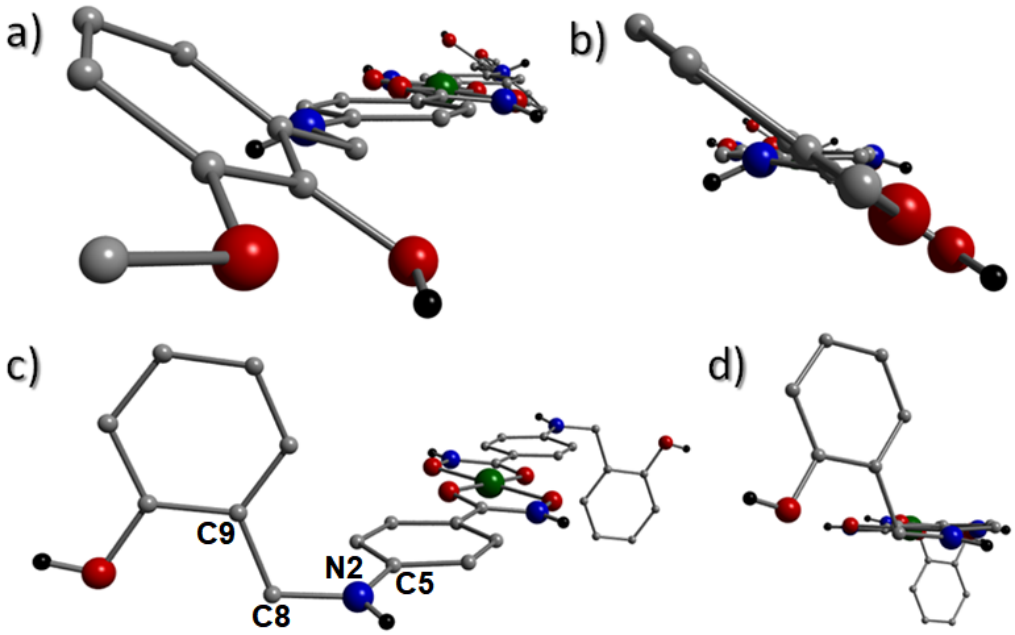

Figure 3.10 *The coordination polymers in* ***11*** *(a and b) and* ***12*** *(c and d) highlighting significant differences in phenolic ring positions in relation to their conjoined hydroxamate fragments. The planes of the phenolic and hydroxamate aromatic rings in* ***11*** *lie at an angle of 144.2 ° from one another as illustrated in Figure b.*

Powder X-ray diffraction studies on **11** and **12** were uses to confirm that their bulk samples were consistent with their single crystal data (Figures 3.11 and 3.12). Using a Johnson Matthey balance the room temperature magnetic moment (μ_{eff}) of **11** (1.69 BM) and 1**2** (1.64 BM) were found to be consistent with that expected for a magnetically dilute Cu(II) chain ($\mu_{S.O.}$ = 1.73 BM) (Table 3.1).[39]

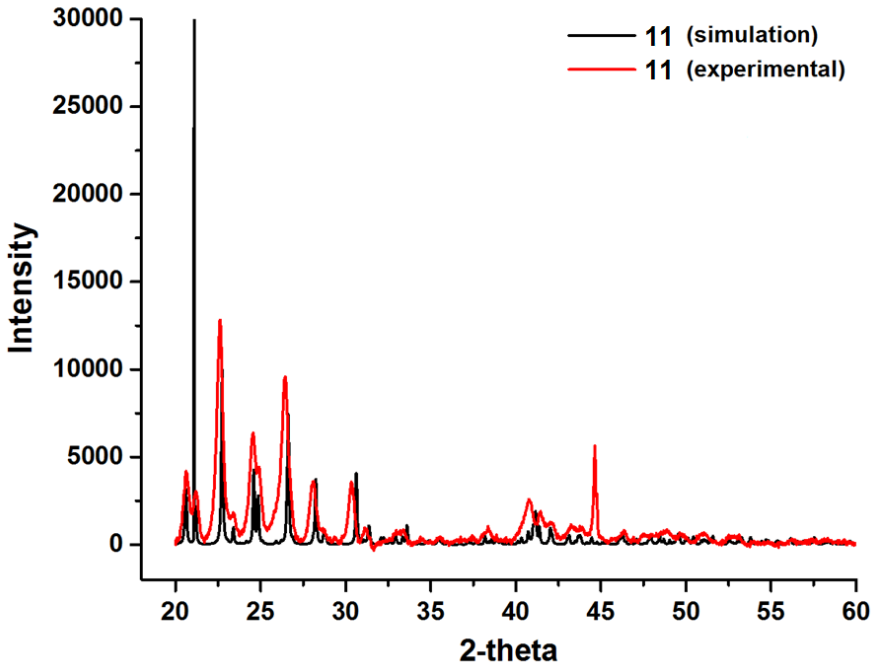

Figure 3.11 *Powdered XRD pattern obtained from a crystalline sample of* $[Cu(II)(L_6H_2)_2]_n$ ***(11)*** *(red line) along with its simulated diffraction pattern (black line) produced using single crystal data via the Mercury software package.*

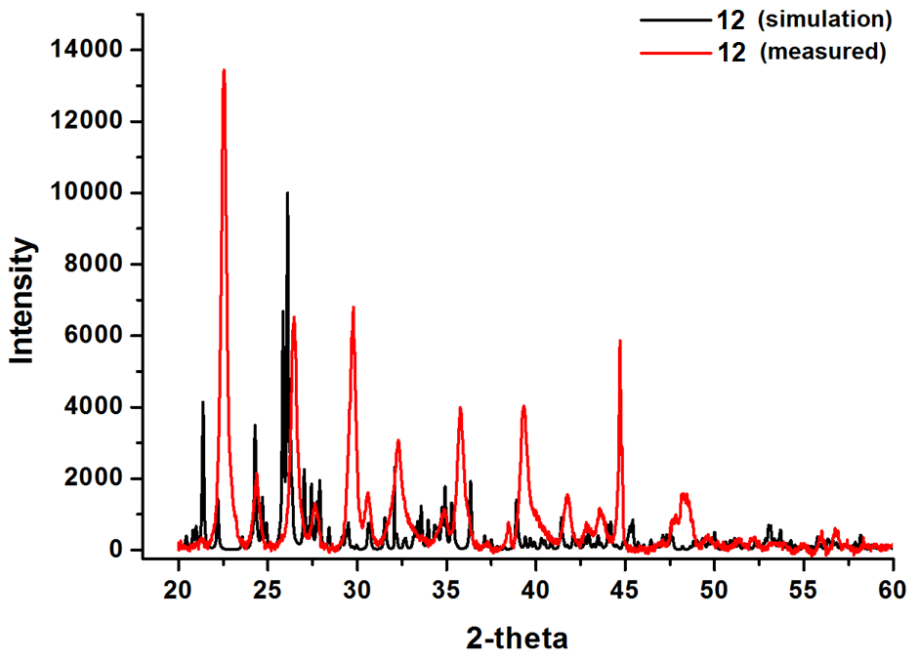

Figure 3.12 *Powdered XRD pattern obtained from a crystalline sample of* $\{[Cu(II)(L_7H_2)].2MeOH\}_n$ ***(12)*** *(red line) along with its simulated diffraction pattern (black line) produced using single crystal data via the Mercury software package.*

Table 3.1 Magnetic moment data obtained from polycrystalline samples of **11** and **12**.

Sample	$[Cu(II)(L_6H_2)_2]_n$ (**11**)	$\{[Cu(II)(L_7H_2)].2MeOH\}_n$ (**12**)
C (calibration constant)‡	1.18	1.18
T (K)	296	296
L (sample length; cm)	2.9	2.0
MW (g mol^{-1})	638.12	642.15
M_0 (g)	0.6511	0.6785
M_1 (g)	0.8144	0.8725
M (M_1-M_0) (g)	0.1633	0.1940
R_0	-0.26	-0.26
R	90	145
R-R_0	90.26	145.26
μ_{eff}	1.69	1.64

‡ Johnson Mathey balance was calibrated using $Hg[Co(II)(NCS)_4]$ prior to use. Magnetic moments calculated using the equations 17-19 (page 73).

3.3 UV-Vis absorption and photoluminescence spectra of complex 9

Complex $\{[Zn(II)(L_4H)_2]\cdot 2MeOH\}_n$ (**9**) showed blue fluorescence upon UV irradiation, which prompted a more detailed UV-Vis absorption and fluorescence study as described below. Absorption spectra demonstrated two distinct maxima at ca. 255 – 258 nm and 341 – 351 nm (Fig. 3.13a and Table 3.2). The longest wavelength absorption maxima are only slightly shifted upon solvent variation, while no correlation with respect to solvent polarity is observed. A Drop-casted film of **9** shows an absorption in the same region (346 nm), thus there is no solid-state effect on the electronic ground state of the complex (Fig. 3.15).

Photoluminescence (PL) spectra show that in all solvents, complex **9** emits in the blue region with PL maxima of λ_{PL} = 421 – 433 nm (Figures 3.13 and 3.14) (Table 3.2). Thus, the solvent effect on the excited state is comparable to that of the ground state. Again, while there are obvious changes (but not large) in PL maxima with solvent change, they do not correlate with the polarity of the solvent, reflecting that while solvation is an important factor, it cannot be assigned just to changes in the intra-chain charge transfer in **9**. We should also mention that for

all solvents, the emission of the complex is bathochromically shifted compared to that of the free ligand L_4H_2 (Table 3.2).

In contrast to the absorption spectra PL spectra for both thin films and powder demonstrate bathochromic shifts (by *ca.* 15 – 30 nm, as estimated at their half maxima) with an appearance of two distinct emission bands. This indicates a stabilisation of the excited state of the complex due to intermolecular interactions. However, no broadening of the PL spectra is observed and the emission bands show only small changes in their fwhm (full width at half maximum) in the range of 0.432 – 0.478 eV (Table 3.2).

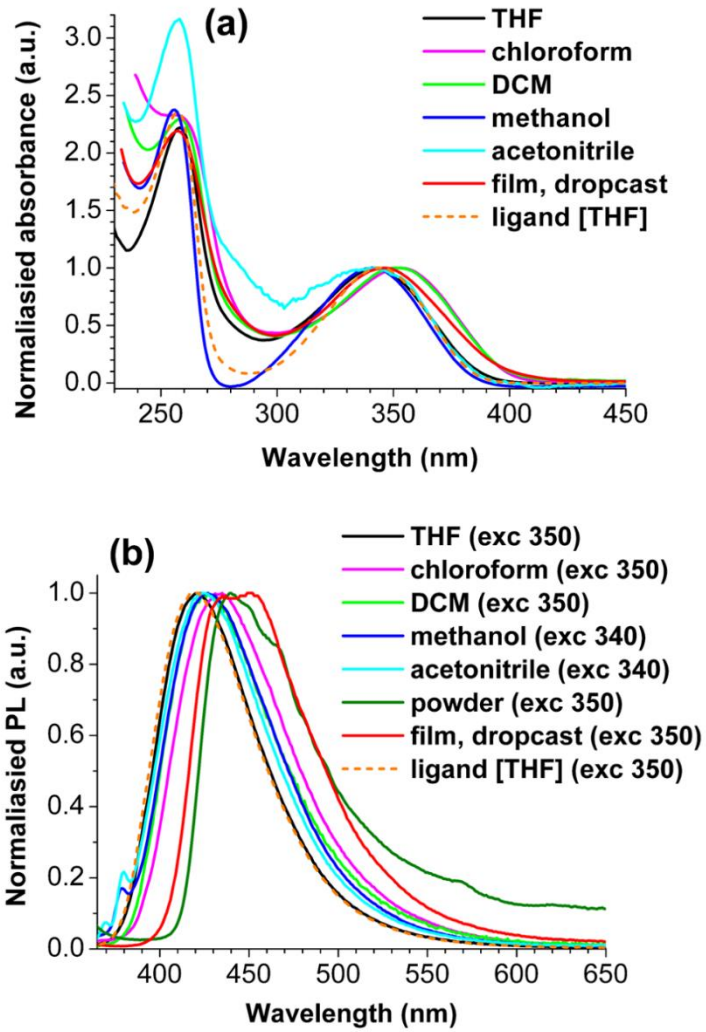

Figure 3.13 *UV-Vis absorption (a) and photoluminescence (b) spectra of complex* ***9*** *and ligand L_4H_2 (labelled as ligand) in different solvents and in the solid state. Excitation wavelengths for PL spectra are given in brackets. UV-Vis absorption spectra are normalised to the longest wavelengths maxima.*

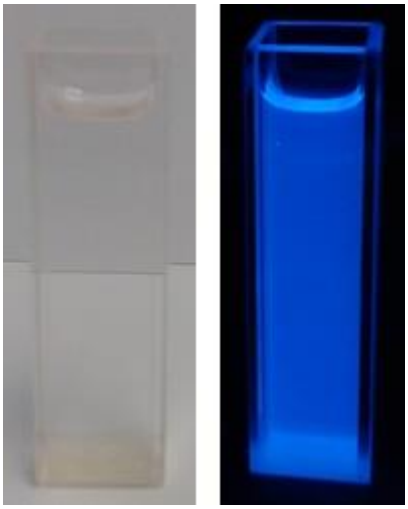

Figure 3.14 *Solution of complex* ***9*** *in dichloromethane under ambient light (left) and under hand-held UV lamp irradiation, λ = 365 nm (right).*

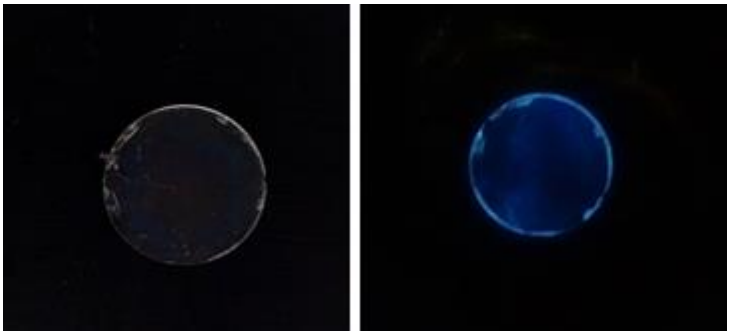

Figure 3.15 *Thin films of complex* ***9*** *drop-casted on quarts disks from chloroform solution, under ambient light (left) and under hand-held UV lamp irradiation, λ = 365 nm (right).*

Table 3.2 Absorption and emission maxima of complex **9** in different solvents and in the solid state, together with data for ligand L_3H_2.

Solvent (or solid state)	**ε[a]**	**λ_{abs} (nm)**	**λ_{PL} (nm)[b]**	**Fwhm (eV)[c]**
Ligand L_4H_2 (in THF)	37.5	257, 344	419	0.448
Chloroform	4.81	256sh, 353	433	0.473
Tetrahydrofuran	7.58	258, 342	421	0.446
Dichloromethane	8.93	258.5, 351	426	0.474
Methanol	32.7	255.5, 341	427	0.478
Acetonitrile	37.5	258, 342	425	0.475
Film (drop-casted)	–	257, 346	436, 450	0.465
Powder	–	–	440, 460sh	0.432

[a] Dielectric permittivity of the solvent. [b] Excitation maxima are shown on Fig. 11b. [c] Full width at half maximum of the emission spectra.

Table 3.3 Selected crystal data obtained from **8 - 10**.

	8.3H_2O	**9**·2MeOH	**10**·3H_2O·4MeOH
Formula[a]	$C_{32}H_{38}N_{10}O_{17}Cu_5$	$C_{18}H_{26}N_4O_6Zn_1$	$C_{66}H_{86}N_{10}O_{31}Cu_5$
M_W	1152.37	459.80	1833.17
Crystal System	Triclinic	Orthorhombic	Triclinic
Space group	P-1	Pcc2	P-1
a/Å	11.3704(6)	14.3459(4)	11.464(2)
b/Å	13.3009(7)	10.8600(3)	12.740(3)
c/Å	14.8558(8)	6.3652(2)	14.419(3)
α/°	91.179(4)	90	109.97(3)
β/°	106.814(5)	90	97.74(3)
γ/°	108.726(5)	90	106.55(3)
V/Å^3	2020.8(2)	991.68(5)	1833.3(8)
Z	2	2	1
T/K	100(1)	100(2)	100.0(2)
λ[b]/Å	0.71073	0.71075	0.71073
D_c/g cm^{-3}	1.884	1.540	1.668
μ(Mo-Ka)/ mm^{-1}	2.676	1.282	1.524
Meas./indep.(R_{int}) refl.	33372/9598 (0.0770)	17587 / 1787 (0.0335)	25169 / 8673 (0.0252)
Restraints, Parameters	0, 569	1, 135	17, 486
wR2 (all data)	0.1287	0.1165	0.1781
$R1$[d,e]	0.0494	0.0457	0.0577
Goodness of fit on F^2	1.076	1.043	1.072

[a] Includes guest molecules. [b] Mo-Kα radiation, graphite monochromator. [c] wR2= [Σw(IF$_o^2$I-IF$_c^2$I)^2/ ΣwIF$_o^2$I^2]$^{1/2}$. [d]For observed data. [e] R1= ΣIIF$_o$I- IF$_c$II/ ΣIF$_o$I

Table 3.4 Selected crystal data obtained from **11** and **12**.

	11	**12.**2MeOH
Formula[a]	$C_{30}H_{30}N_4O_8Cu_1$	$C_{30}H_{34}N_4O_8Cu_1$
M_W	638.12	642.15
Crystal System	Monoclinic	Monoclinic
Space group	$P2_1/c$	$P2_1/c$
a/Å	6.7098(2)	8.61560(10)
b/Å	21.4689(8)	11.31420(10)
c/Å	9.4280(2)	14.8436(2)
α/°	90	90
β/°	91.889(2)	100.8870(10)
γ/°	90	90
V/Å^3	1357.38(7)	1420.89(3)
Z	2	2
T/K	100.0(2)	100.0(2)
λ[b]/Å	0.71073	0.71073
D_c/g cm^{-3}	1.561	1.501
μ(Mo-Ka)/ mm^{-1}	0.867	0.828
Meas./indep.(R_{int}) refl.	26867 / 9697 (0.0487)	12946 / 11113 (0.0206)
Restraints, Parameters	0, 205	0, 199
wR2 (all data)	0.1113	0.1406
R1[d,e]	0.0481	0.0424
Goodness of fit on F^2	1.303	1.138

[a] Includes guest molecules. [b] Mo-Kα radiation, graphite monochromator. [c] wR2= [Σw(IF$_o^2$I-IF$_c^2$I)^2/ ΣwIF$_o^2$I^2]$^{1/2}$. [d]For observed data. [e] R1= ΣIIF$_o$I- IF$_c$II/ ΣIF$_o$I

3.4 Magnetic studies

The dc (direct current) molar magnetic susceptibility, χ_M, of polycrystalline samples of $[Cu(II)_5(L_4H)_4(MeOH)_2](NO_3)_2 \cdot 3H_2O \cdot 4MeOH$ (**10**) was measured in an applied magnetic field, *B*, of 0.5 T, in the *T* = 300-2 K temperature range. The experimental results are shown in Figures 3.16 and 3.17 in the form of the $\chi_M T$ products, where $\chi = M/B$, and *M* is the magnetisation of the sample, respectively. The $\chi_M T$ product of 1.49 $cm^3\ mol^{-1}$ K for **10** is significantly lower than the expected value for five Cu(II) ions (2.17 $cm^3\ mol^{-1}$ K, when g_{Cu} = 2.14) and suggests strong antiferromagnetic interactions between Cu(II) ions, even at room temperature. As shown in Figure 3.16, the $\chi_M T$ vs. *T* plot shows a decrease in the value of $\chi_M T$ upon cooling and are indicative of significant intramolecular antiferromagnetic exchange interactions between the Cu(II) ions in **10**. The magnetic data for **10** were fit using the program PHI and the isotropic spin-Hamiltonian of the form: [40,41]

$$\hat{H} = -2 \sum_{i,j>i}^{n} \hat{S}_i J_{ij} \hat{S}_j + \mu_B \sum_{i=1}^{n} \vec{B}\, g_i \hat{S}_i$$

where $\hat{S}$ is a spin operator, *J* is the pairwise isotropic magnetic exchange interaction between constitutive metal centres, μ_B is the Bohr magneton, $\vec{B}$ the external static magnetic field, *g* the isotropic *g*-factor of the metal ions, the indices *i* and *j* refer to the two metal ions (n = 5 for **10**). There are two separate magnetic exchange interactions between the constituent Cu(II) centres in **6** (Fig. 3.16-inset), $Cu(II)_{outer}$-$Cu(II)_{inner}$ (comprising 1 x Cu-O_{oxime}-Cu bridge; J_1) and $Cu(II)_{outer}$-$Cu(II)_{outer}$ (comprising 1 x Cu-N-O-Cu bridge; J_2). A simultaneous fit of the susceptibility and magnetisation data affords best-fit parameters g_{Cu} = 2.14, J_1 = -115.33 cm^{-1} and J_2 = -83.03 cm^{-1}. The *J*-values obtained are in line with those observed in other similarly bridged Cu(II) complexes[24,42,43] and give rise to an isolated *S* = ½ ground spin state. As shown in Figure 3.17, magnetisation saturation is only beginning to develop even at the lowest temperature recorded (2 K) and this is indicative of low lying excited spin states in **10**. Its saturation value (~1.1 μβ) is consistent with an *S* = ½ ground spin state.

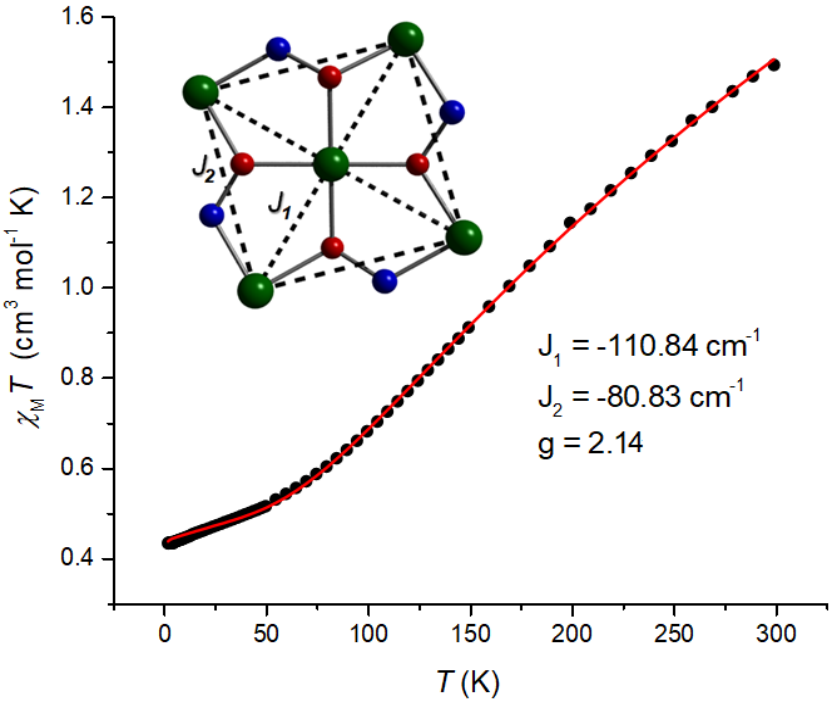

Figure 3.16 *Variable temperature $\chi_M T$ vs. T plot obtained from a polycrystalline sample of* ***10****. The solid red line represents the best-fit to the experimental data (black dots). Inset: The exchange coupling scheme used to fit the data; $\hat{H}$ = -2J_1($\hat{S}_1$·$\hat{S}_5$ + $\hat{S}_2$·$\hat{S}_5$ + $\hat{S}_3$·$\hat{S}_5$ + $\hat{S}_4$·$\hat{S}_5$) -2J_2($\hat{S}_1$·$\hat{S}_2$ + $\hat{S}_2$·$\hat{S}_3$ + $\hat{S}_3$·$\hat{S}_4$ + $\hat{S}_4$·$\hat{S}_1$). The solid lines represent a simultaneous best-fit of the experimental susceptibility and magnetisation data as described in the main text.*

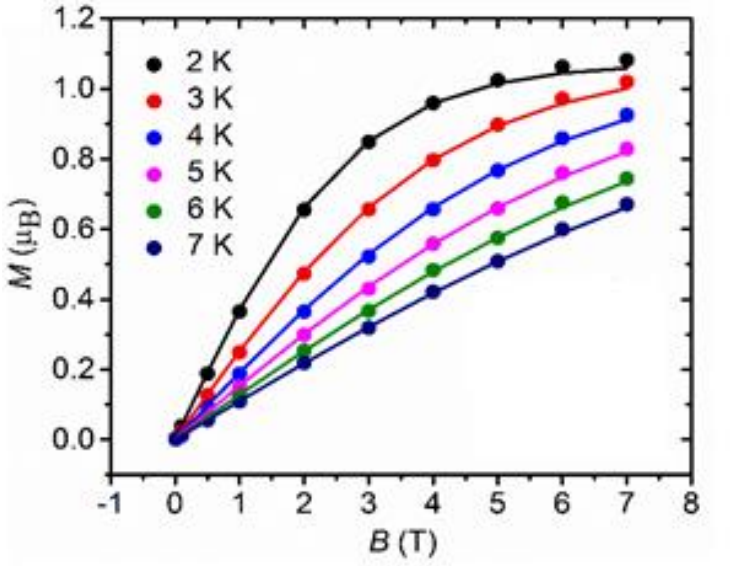

Figure 3.17 *Magnetisation (M / μB vs B (T) data obtained from a polycrystalline sample of* ***10*** *measured in the 2-7 K temperature range and 0-7 T magnetic field range.*

3.5 Conclusions

We have described in this chapter the synthesis and physical characterisations of a number of novel polymetallic complexes and 1-D coordination polymers using pre-designed multi-topic hydroxamate bridging ligands. For instance, the ligands 2-(methylamino)phenyl hydroxamic acid (L_4H_2) and *N*-hydroxy-2-[(2-hydroxy-3-methoxybenzyl)amino]benzamide (L_5H_3) were employed in the construction of the discrete 12-MC-$4_{Cu(II)}$ metallacrowns $[Cu(II)_5(L_4)_4(NO_3)_2]\cdot 3H_2O$ (**8**) and $[Cu(II)_5(L_5H)_4(MeOH)_2](NO_3)_2\cdot 3H_2O\cdot 4MeOH$ (**10**), respectively. Complex **10** represents the first complex to be constructed with the L_5H_3 ligand. The self-assembly of the 1-D chains $[Cu(II)(L_6H_2)_2]_n$ (**11**) and $\{[Cu(II)(L_7H_2)].2MeOH\}_n$ (**12**) were obtained through Cu(II) ligation of the novel multitopic ligands N-hydroxy-4-((2-hydroxy-3-methoxybenzyl)amino)benzamide (L_6H_3) and N-hydroxy-4-((2-hydroxybenzyl)amino)benzamide (L_7H_3), respectively. Slight differences in the functionality of ligands L_6H_3 vs. L_7H_3, namely the omission of an $–OCH_3$ group in the latter, give rise to significant topology changes when closely inspecting chains **11** and **12**. Moreover, the H-bonded 1-D coordination polymer $\{[Zn(II)(L_4H)_2].2MeOH\}_n$ (**9**) represent extremely rare examples of metal coordination of the ligand 2-(methylamino)phenylhydroxamic acid (L_4H_2). Variable temperature magnetic susceptibility measurements on **10** indicate dominant antiferromagnetic exchange, with best-fit-data J_1 = -115.33 cm^{-1}, J_2 = -83.03 cm^{-1}. In solution, coordination polymer complex **9** exhibits an emission in the blue region with $\lambda_{PL} \approx 421 – 433$ nm depending on the solvent. While very small effects are observed upon absorption and PL spectra of **9** in solution, a bathochromic shift of ≈ 15 – 30 nm is observed for its photoluminescence in the solid state, underlying the importance of inter-chain interactions on the excited state of the complex.

3.6 Experimental Section

Infra-red spectra were recorded on a Perkin Elmer FT-IR *Spectrum 100* spectrometer (School of Natural Sciences, Bangor University). ^1H and ^{13}C NMR spectra were obtained at room temperature (298 K) on a Bruker Avance 400 Plus spectrometer with Sample Xpress, operating at 400 MHz (for ^1H) or 100 MHz (for ^{13}C). Chemical shifts are reported in ppm and referenced to DMSO-d_6 (δ_H: 2.50 ppm, δ_C : 39.52 ppm). Elemental analysis was carried out at OEA Laboratories (Kelly Bray, Cornwall). Room temperature magnetic moment measurements were taken on a Johnson Matthey balance (reference material: $HgCo(NCS)_4$). Variable-temperature, solid- state direct current (*dc*) and alternating current (ac) magnetic susceptibility data down to 2 K were collected on a Quantum

Design MPMS-XL SQUID magnetometer and a Quantum Design PPMS magnetometer fitted with an ac measurement system, respectively. Diamagnetic corrections were applied to the observed paramagnetic susceptibilities using Pascal's constants. All measured complexes were set in eicosane to avoid torqueing of the crystallites. All magnetic samples are collected as single-crystalline products and analysed using microanalysis and IR measurements prior to their magnetic assessment. If necessary, phase purity between cross-batches was validated using unit cell checks and IR measurements. Yields calculated upon collection of single-crystalline products in order to ensure high quality magnetic data.

UV-Vis spectra on $\{[Zn(II)(L_4H)_2].2MeOH\}_n$ (**9**) were recorded on a Shimadzu (UV-3600) UV-Vis-NIR spectrophotometer at room temperature. Solution measurements in solvents of different polarities (hexane, chloroform, dichloromethane, tetrahydrofyran, acetonitrile, methanol) were carried out in 10 mm path length square quartz cells. For solid state measurements, the solutions in chloroform were drop-casted onto a quartz circular window, allowed to evaporate slowly and dried *in vacuo.* Photoluminescence spectra (PL) were recorded on a Horiba Jobin-Yvon Fluoromax-4 spectrofluorometer at room temperature. The solution spectra were measured in 10 mm path length quartz cells for diluted solutions (with absorption at longest wavelength of < 0.1 a.u.). Solid-state PL measurements were performed either for drop-casted film on a quartz substrate or for powder (in a d = 3 mm cylindrical quartz cell, using an integrating sphere Horiba F-3018 on the spectrofluorometer). The samples were excited at λ_{exc} = 340 – 350 nm, close or equal to the maxima of their longest wavelength absorption.

3.6.1 Single-crystal X-ray crystallography

Complexes **8-12** were collected on an Rigaku AFC12 goniometer equipped with an enhanced sensitivity (HG) Saturn724+ detector mounted at the window of an FR-E+ Super Bright molybdenum rotating anode generator with HF Varimax optics (100m focus). The cell determination and data collection of each complex was carried out using the CrystalClear-SM Expert package (Rigaku, 2012). Each data reduction, cell refinement and absorption correction were carried out using CrysAlisPro software (Rigaku OD, 2015),[44] while all structures were solved and refined using SHELXT and SHELXL-2014[45] within OLEX-2.[46]

In complexes $\{[Zn(II)(L_4H)_2].2MeOH\}_n$ (**9**), $[Cu(II)(L_6H_2)_2]_n$ (**11**) and $\{[Cu(II)(L_4H_2)].2MeOH\}_n$ (**12**), all hydrogens were assigned to calculated positions while all non-hydrogen atoms were refined anisotropically. All non-hydrogen atoms in $[Cu(II)_5(L_4)_4(NO_3)_2]\cdot 3H_2O$ (**8**) was refined as anisotropic. The waters of crystallisation in both complexes were refined isotropically. All hydrogen atoms in **8** was assigned to calculated positions. Disorder was observed when refining the crystal structure in $[Cu(II)_5(L_5H)_4(MeOH)_2(NO_3)_2]\cdot 3H_2O\cdot 4MeOH$ (**10**). More specifically, one of the phenolic units belonging to one of the crystallographically unique L_5H^- ligands in **10** required modelling over two sites (50:50 occupancy). These disordered atoms required isotropic refinement and DFIX and FLAT restraints, while all other non-hydrogen atoms belonging to the $[Cu_5]$ unit were refined anisotropically. Moreover, the bound (C46-O32) and unbound MeOH ligands (C45-O30 and C47-O33) in **10** were each restrained using the DFIX restraints. The unbound MeOH labelled C47-O33 required isotropic refinement, while all others were refined anisotropically.

3.6.2 Organic ligand preparation

All starting materials were used as purchased unless otherwise stated.

Synthesis of 2-(methylamino)phenylhydroxamic acid (L_4H_2)

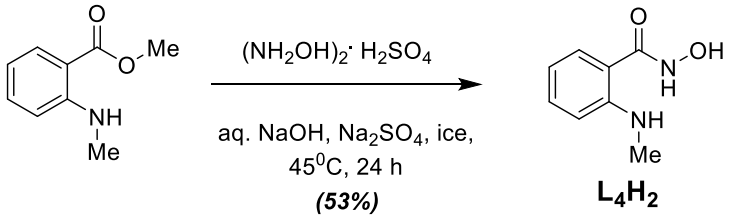

To a stirring solution of NaOH (7.41 g, 185 mmol, 30 cm^3 water) in ice (30 g), hydroxylamine sulphate (6.11 g, 37.0 mmol) and Na_2SO_4 (0.58 g, 4.1 mmol) were added followed by dimethyl anthranilate (5.7 cm^3, 35 mmol), and the solution stirred for 24 hours. After this time the solution was allowed to cool and subsequently pH adjusted to 6 using H_2SO_4, after which the product began to precipitate out. The precipitate was then collected by suction filtration and dried, before recrystallisation from hot water to give a final yield of 53% (3.25 g).

^{13}C NMR (DMSO-d_6, 100 MHz): δ (ppm) 29.3 (CH_3), 110.9 (CH-Ar), 114.0 (C-Ar), 114.5 (CH-Ar), 128.0 (CH-Ar), 132.7 (CH-Ar), 150.2 (NH-C-Ar), 167.5 (C=O).

MS (EI$^+$): *m/z* 166 (57%, {M$^+$}), 134 (100%, {M–NHOH}$^+$).

FT-IR: ν (cm^{-1}): 3409 (s), 3295 (m/b), 3076 (w), 3033 (w), 2911 (w), 2819 (m), 1937 (w), 1910 (w), 1815 (w), 1788 (w), 1622 (s), 1581 (s), 1511 (s), 1445 (m), 1417 (m), 1327 (m), 1282 (m), 1252 (w), 1173 (s), 1153 (s), 1102 (w), 1069 (m), 1028 (s), 969 (w), 942 (w), 897 (s), 846 (m), 803 (m), 782 (m), 748 (s), 706 (m), 668 (m), 599 (m), 565 (w), 552 (m), 515 (w), 474 (w), 409 (w).

UV-vis (MeOH): λ_{max} (nm) (ε_{max} 10^3, dm^3 mol^{-1} cm^{-1}): 218 (sh), 255.5 (5.53), 341 (1.78).

UV-vis (MeCN): λ_{max} (nm) (ε_{max} 10^3, dm^3 mol^{-1} cm^{-1}): 215 (26.93) 258 (14.01), 342 (7.73).

Preparation of 2-(amino)phenylhydroxamic acid {Precursor 1 (PC1)}

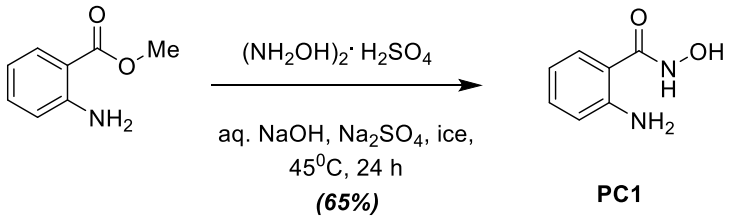

The preparation of 2-(amino)phenylhydraxamic acid was carried out according to literature procedure.[59] To an aqueous solution of NaOH (7.40 g, 185 mmol, 30 cm^3) and 30 g of ice, hydroxylamine sulphate (6.10 g, 37 mmol) and $NaSO_4$ (0.58 g, 4.44 mmol) were added folloed by methyl 2-aminobenzoate (5.60 g, 4.8 cm^3, 37 mmol). The reaction mixture was stirred at 45^{o}C for 24 h. The solution was then allowed to cool and the pH was adjusted to 6 using 10% H_2SO_4. At this point a light pink solid precipitate out of the solution and stirring continued for another 15 mins. The solid was then filtered and dried via suction filtration to give a yield of 65.4% (3.69 g).

Elemental analysis (%) calculated as PC1 ($C_7H_8N_2O_2$): C 55.26, H 5.30, N 18.41. Found: C 54.52, H 5.36, N 17.77.

*^{1}H NMR (400 MHz d_6-DMSO):*δ 2.5 ($(CD_3)_2SO$ residual solvent peak), 3.40 (s, H_2O), 6.20 (s, 2H, NH_2), 6.5-7.4 (m, 4H, Ar-H), 8.85 (s, 1H, NH), 10.90 (s, 1H, OH).

^{13}C NMR (400 MHz, DMSO): δ (ppm) = 170.0 (CO), 152.0 (C, Ar), 134.2 (CH, Ar), 131.6 (CH, Ar), 116.8 (CH, Ar), 115.0 (CH, Ar), 110.1 (CH, Ar).

MS: m/z (% Rel. Ab.): 152 (48) [M$^+$], 136 (40) [M$^+$– OH], 120 (100) [M$^+$– NH_2OH].

FT-IR (cm^{-1}): 3403(sh), 3323 (w), 3171 (m), 2972 (w), 2863(m), 1636(sh), 1562(w), 1495(w), 1450(w), 1348(w), 1250(w), 1131(sh, s), 1021 (m, sh), 947 (w), 901 (w), 872 (w), 683 (w), 639 (w), 617 (m, sh), 419 (m).

Synthesis of (N-hydroxy-2-((2-hydroxy-3-methoxybenzyl)amino)benzamide (L_5H_3)

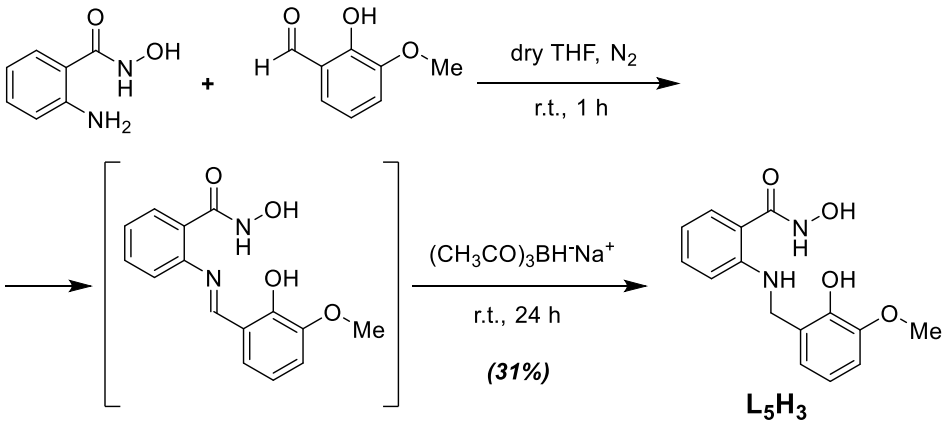

Equimolar amounts of 2-aminophenylhydroxamic acid (2.00 g, 13.00 mmol) and *ortho*-vanillin (1.99 g, 13.00 mmol) were dissolved in dry tetrahydrofuran (30 cm^3) under a nitrogen atmosphere and the solution was stirred at room temperature for 1 hour. The reaction mixture was then treated with sodium triacetoxyborohydride (4.16 g, 19.50 mmol) and the solution stirred under nitrogen conditions at room temperature for 24 h. The progress of the reaction was monitored by TLC. Upon completion the reaction was quenched with saturated sodium bicarbonate solution and the organic layer was subsequently extracted with ethyl acetate (30 cm^3) and subsequently washed with water (3 x 30 cm^3) followed by brine (3 x 30 cm^3) until all traces of sodium triacetoxyborohydride were removed. The organic layer was then dried with anhydrous magnesium sulphate and the solvent evaporated to dryness under reduced pressure. The product (L_5H_3) was purified by column chromatography using a methanol: chloroform (10:90 v/v) solvent mixture to give the solid L_5H_3 in 31% yield (1.17 g).

^{1}H NMR (DMSO-d$_6$ 400 MHz): δ (ppm) 3.79 (s, 3H, OCH_3), 4.51 (s, 2H, CH_2), 6.93 (dt, *J* = 7.6, 1.9 Hz, 1H, Ar-H), 6.84 (dd, *J* = 8.1, 1.6 Hz, 1H, Ar-H), 6.76 (dd, *J* = 7.7, 1.4 Hz, 1H, Ar-H), 8.32 (s, 1H, NH), 8.50 (s, 1H, NH), 10.2 (s, 1H, OH), 11.2 (s, 1H, OH).

^{13}C NMR (DMSO-d$_6$, 100 MHz): δ (ppm) 163.1 (CO), 148.0 (C, Ar), 146.5 (C, Ar), 144.3 (C, Ar), 133.5 (CH, Ar), 127.4 (C, Ar), 126.8 (CH, Ar), 118.9 (CH, Ar), 118.8 (CH, Ar), 117.5 (CH, Ar), 114.8 (C, Ar), 112.1 (CH, Ar), 69.7 (CH_3, OMe), 56.4 (CH_2, CHO).

MS (EI$^+$): *m/z* 286.04 (100%; {M$^+$}), 269.22 (30%, {M–OH}$^+$), 255.24 (18%, {M–OCH$_3$}$^+$). FT-IR: ν (cm^{-1}) 3379 (br), 3069 (w), 2938 (w), 2839 (w), 2341 (w), 1905 (w), 1722 (w), 1611 (s, sh), 1592 (w), 1515 (m), 1484 (m), 1462 (w), 1442 (w), 1371 (m), 1328 (w), 1272 (m), 1163 (w), 1083 (m), 1056 (w), 988 (m), 988 (m), 912 (w), 829 (w), 747 (s, sh) 686 (m), 539 (w), 411 (w).

Synthesis of 4-(amino)phenyl hydroxamic acid (PC2)

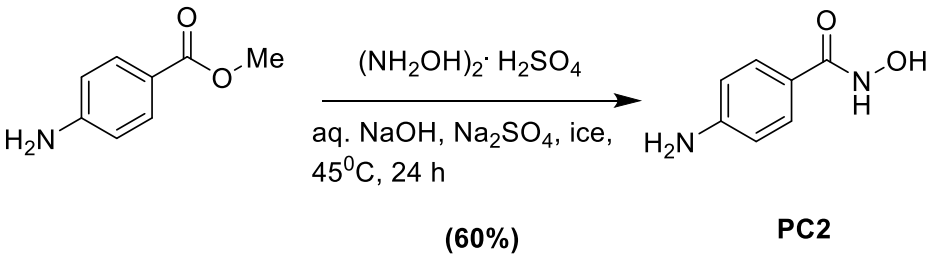

Hydroxylamine sulphate (6.10 g, 37mmol) and 30.03 g of ice were added to an aqueous solution of NaOH (7.41 g, 185 mmol, 30 cm^3). Na_2SO_4 (0.58 g, 4.44 mmol) and methy-4-aminobenzoate (5.70 g, 37 mmol) were then added to the solution. The mixture was subsequently stirred at 45^{o}C for 24 hrs. The resultant solution was allowed to cool and the pH was adjusted to 6 using H_2SO_4. When the pH reached 6, a solid precipitated out of the solution. When the pH reached 6, a beige colour solid precipitated out of the solution. The solid was then collected via filtration and recrystallized from hot water and cooled with ice to give PC2 in 60 % yield (3.39 g). Elemental analysis (%) calculated as L_5H_2 ($C_7H_8N_2O_2$): C 55.26, H 5.30, N 18.42. Found: C 55.24, H 5.53, N 18.10.

^{1}H NMR (400 MHz d_6-DMSO): δ 2.5 ($(CD_3)_2SO$ residual solvent peak), 3.4 (s, H_2O), 5.5 (s, 2H, NH_2), 6.5 (d, *J* =8.5 Hz, 2H, Ar-H), 7.4 (d, *J* = 8.6 Hz, 2H, Ar-H), 8.6 (s, 1H, NH), 10.7 (s, 1H, OH).

^{13}C NMR (400 MHz, DMSO): δ (ppm) = 165.5 (CO), 152.0 (C, Ar), 128.7 (2CH, Ar), 119.6 (C, Ar), 113.1 (2CH, Ar).

FT-IR (cm^{-1}): 3410(s, sh), 3332 (m), 3274 (br), 3025(m), 2789(m), 1645(s, sh), 1589 (s, sh), 1556 (s, sh), 1535 (s, sh), 1502 (s, sh), 1405 (s, sh), 1321 (sh, s), 1292 (sh, s), 1188 (sh, s), 1157 (sh, s), 1094 (sh, s), 1023 (sh, s), 895 (sh, s), 832 (sh, s), 746 (sh, s), 694 (sh, s), 638 (m, sh), 567 (s), 520 (sh), 469 (s, sh), 422 (sh).

MS-EI: mz (% Rel. Ab.): 152 (8,{M$^+$}), 134 (8, {M- OH}$^+$), 120 (100, {M- NHOH}$^+$).

Synthesis of (E)-N-hydroxy-4-((2-hydroxy-3-methoxybenzylidene)amino)benzamide (PC3).

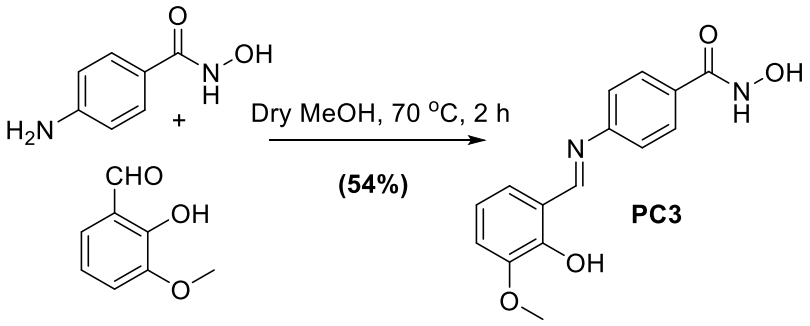

Equimolar amounts of 4-(amino)phenylhydroxamic acid (0.50 g, 3.20 mmol) and *ortho* vanillin (0.50 g, 3.20 mmol) were dissolved in dry methanol (30 cm^3) and the solution refluxed at 70 ˚C for 2 hours to give a red precipitate. The solution was then allowed to cool and the resultant precipitate filtered under suction to give a yield of 54% (0.51 g). Elemental analysis (%) calculated as PC3 ($C_{15}H_{14}N_2O_4$): C 62.93, H 4.93, N 9.73. Found: C 63.46, H 4.81, N 9.52.

^{1}H NMR (400 MHz d_6-DMSO): δ 2.51 ($(CD_3)_2SO$ residual solvent peak), 3.83 (s, 3H, OCH_3), 6.53 (d, *J* = 8.4 Hz, 1H), 6.93 (t, *J* = 7.9 Hz,1H, Ar-H), 7.16 (d, *J* = 8.0 Hz, 1H, Ar-H), 7.26 (t, *J* = 9.9 Hz, 1H, Ar-H), 7.48 (d, *J* = 8.4 Hz, 2H, Ar-H), 7.86 (d, *J* = 8.3 Hz, 2H, Ar-H), 8.99 (s, 1H, CH=N), 9.07 (s, 1H, NH), 11.28 (s, 1H, OH), 12.95 (s, 1H, OH).

^{13}C NMR (400 MHz, DMSO-d_6): δ (ppm) = 165.0 (CO), 151.0 (C, Ar), 150.8.3 (C, Ar), 148.4 (C, Ar), 131.3 (C, Ar), 128.7 (2CH, Ar), 124.4 (CH, Ar), 121.8 (2CH, Ar), 119.7 (C, Ar), 119.2 (CH, Ar), 116.3 (CH, Ar), 113.1 (CH, Ar), 56. (CH_3, OMe).

FT-IR (cm^{-1}): 3326 (s), 3066 (w), 2957 (w), 2931 (w), 2899 (w), 2832 (w), 1623 (s), 1595 (s), 1570 (s), 1533 (m), 1513 (m), 1474 (s, sh), 1387 (s, sh), 1367 (w), 1332 (s), 1257 (s, sh), 1202 (s), 1173 (m), 1148 (s), 1111 (s), 1020 (w), 1009 (s), 976 (s, sh), 906 (s), 869 (s), 849 (s), 834 (s), 771 (s, sh), 745 (s), 708 (s, sh), 578 (m), 525 (s), 488 (s), 448 (s), 409 (s).

MS-EI: m/z (% Rel. Ab.): 286.07 (44; M^+), 254.15 (100; $\{M - H_2NO\}^+$), 224.29 (25, $\{M - CH_2NO_2\}^+$), 135.25 (26, {Phenylhydroxamic acid $\{C_7H_7NO_2\}^+$), 136.22 (20, $\{M - C_8H_{10}NO_2\}^+$)

Synthesis of 4-((2-hydroxy-3-methoxybenzyl)amino)-N-hydroxybenzamide (L_6H_3).

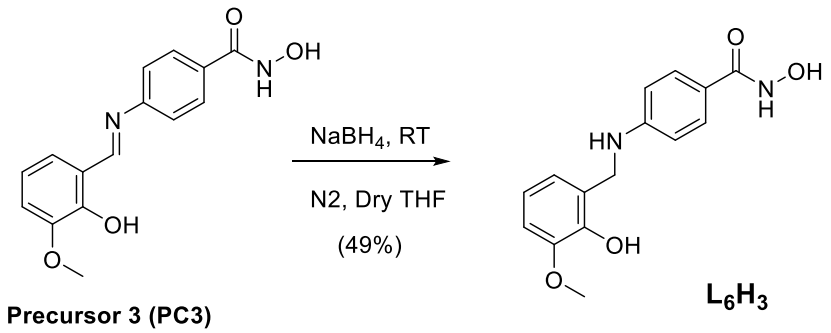

Precursor 3 (PC3) **L_6H_3**

(E)-4-((2-hydroxy-3-methoxybenzylidene)amino)-N-hydroxybenzamide ((2.00 g, 6.98 mmol) and sodium borohydride (0.40 g, 10.48 mmol) were dissolved in 40 cm^3 dry tetrahydrofuran (THF), and the red solution was stirred under nitrogen at room temperature for 4 hrs. After reduction, a pale yellow solution is formed which was quenched with saturated sodium bicarbonate solution (30 cm^3). The reaction was extracted with ethyl acetate (3 x 30 cm^3) and the combined extract washed repeatedly with brine water until a clear organic layer was obtained. The organic layer was dried with anhydrous magnesium sulphate and the solvent evaporated to dryness to give L_6H_3 in 49% yield (0.99 g). Elemental analysis (%) calculated as $L_5H_3.H_2O$ ($C_{15}H_{18}N_2O_5$): C 58.82, H 5.92, N 9.15. Found: C 59.95, H 5.71, N 8.89.

^{1}H NMR (400 MHz d_6-DMSO): δ 2.51 ($(CD_3)_2SO$ residual solvent peak), 3.83 (s, 3H, OCH_3), 4.25 (s, 2H, CH_2), 6.54 (d, 2H, Ar-H), 6.62 (d, 1H, Ar-H), 6.68 (s, 1H, NH), 6.70 (t, 1H, Ar-H), 6.80 (d, 1H, Ar-H), 6.84 (d, 1H, Ar-H), 7.49 (d, 2H, Ar-H), 8.75 (s, 1H, NH), 10.75 (s, 1H, OH), 11.20 (s, 1H, OH).

^{13}C NMR (400 MHz, DMSO-d_6): δ (ppm) = 161.3 (CO), 151.6 (C, Ar), 147.7 (C, Ar), 144.3 (C, Ar), 128.6 (CH, Ar), 127.7 (CH, Ar), 126.1 (C, Ar), 120.6 (CH, Ar), 119.5 (C, Ar), 119.1 (CH, Ar), 112.1 (CH, Ar), 111.4 (CH, Ar), 110.7 (CH, Ar), 56.2 (CH_3, OMe), 40.6 (CH_2, CHO).

MS-EI: m/z (% Rel. Ab.): 288.11 (05; $\{M^+\}$), 270.30 (05; $\{M - OH\}^+$), 256.41 (36; $\{M – H_2NO\}^+$), 134.28 (35; {4-aminobenzamide $[M – C_8H_{10}O_2]^+$}), 120.28 (100, {benzamide $[M – C_8H_{10}NO_2]^+$}).

FT-IR (cm^{-1}): 3400 (s), 3311 (m), 3209 (m), 2870 (m), 2815 (m), 1608 (s, sh), 1573 (m), 1538 (s), 1502 (s), 1476 (s, sh), 1457 (m), 1434 (m), 1411 (m), 1360 (s), 1335 (s), 1317 (s), 1275

(w), 1262 (s), 1231 (w), 1193 (s), 1181 (w), 1152 (s), 1134 (w), 1081 (s, sh), 1043 (m), 1023 (w), 1005 (w), 987 (w), 894 (s, sh), 877 (w), 823 (s, sh), 759 (s), 727 (m), 717 (m), 617 (w), 568 (w), 529 (w), 511 (s), 535 (s).

Synthesis of (E)-N-hydroxy-4-((2-hydroxybenzylidene)amino)benzamide (PC4).

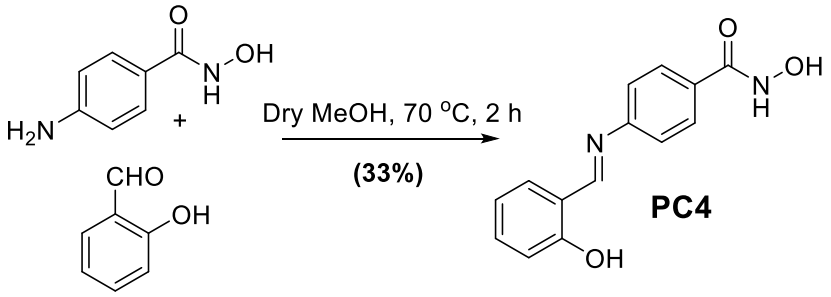

.

4-(amino)phenylhydroxamic acid (1.00 g, 6.57 mmol) and salicylaldehyde (0.80 g, 6.57 mmol) were dissolved in dry methanol (30 cm^3) and refluxed at 70^0C for 3 hours to give yellow precipitate. The solution was allowed to cool and the precipitate filtered and air dried under suction to give yield of 33% (0.56 g). Elemental analysis (%) calculated as PC4 ($C_{14}H_{12}N_2O_3$): C 65.62, H 4.72, N 10.93. Found: C 65.67, H 4.57, N 10.58.

^{1}H NMR (400 MHz d_6-DMSO): δ 2.51 ($(CD_3)_2SO$ residual solvent peak), 7.00 (t, 2H, Ar-H), 7.44 (d, 1H, Ar-H), 7.49 (d, 2H, Ar-H), 7.70 (d, 1H, Ar-H), 7.88 (d, 2H, Ar-H), 8.99 (s, 1H, CH=N), 9.08 (s, 1H, NH), 11.28 (s, 1H, OH), 12.85 (s, 1H, OH).

^{13}C NMR (400 MHz, DMSO-d_6): δ (ppm) = 164.9 (C, Ar), 164.1 (CO), 160.7 (C, Ar), 151.0 (C, Ar), 134.2 (CH, Ar), 130.1 (CH, Ar), 131.3 (C, Ar), 128.7 (2CH, Ar), 121.8 (2CH, Ar), 119.7 (C, Ar), 119.7 (CH, Ar), 117.1 (CH, Ar).

MS-EI: m/z (% Rel. Ab.): 256.08 (20; $\{M\}^+$), 240.23 (24; $\{M - OH\}^+$), 224.32 (100, $\{M – H_2NO\}^+$), 196.43 (16, $\{M – CH_2NO_2\}^+$), 77.37 (04, $\{C_6H_6\}^+$).

FT-IR (cm^{-1}): 3275 (s), 3026 (br), 2699 (br), 1644 (m), 1617 (w), 1598 (s), 1559 (s, sh), 1489 (s, sh), 1455 (m), 1437 (w), 1409 (m), 1363 (m), 1330 (m), 1309 (w), 1283 (s, sh), 1190 (s), 1181 (w), 1157 (s), 1033 (s), 1011 (s), 982 (s), 910 (w), 899 (s), 848 (s, sh), 779 (m), 750 (s, sh), 740 (w), 698 (m), 683 (m), 541 (w), 525 (s), 481 (s), 442 (s).

Synthesis of N-hydroxy-4-((2-hydroxybenzyl)amino)benzamide (L_7H_3).

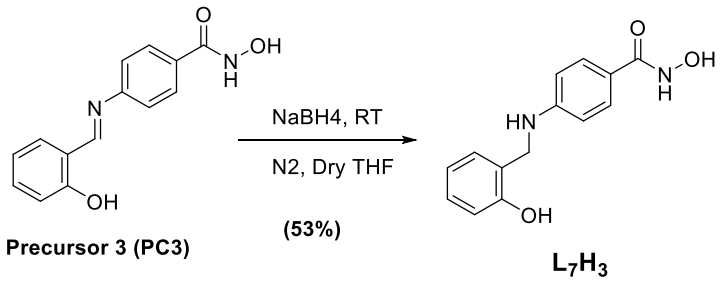

(E)-N-hydroxy-4-((2-hydroxybenzylidene)amino)benzamide (2.00 g, 7.80 mmol) and sodium borohydride (0.44 g, 11.72 mmol) were dissolved in 40 cm^3 dry tetrahydrofuran (THF), and the red solution was stirred under nitrogen at room temperature for 4 hrs. After reduction, an amber coloured solution was formed which was quenched with saturated sodium bicarbonate solution (30 cm^3). The reaction was extracted with ethyl acetate (3 x 30 cm^3) and the combined extract washed repeatedly with brine water until a clear organic layer was obtained. The organic layer was dried with anhydrous magnesium sulphate and the solvent evaporated to dryness to give L_6H_3 in 53% yield (1.06 g). Elemental analysis (%) calculated as L_6H_3 ($C_{14}H_{14}N_2O_3$): C 62.91, H 5.05, N 7.24. Found: C 62.81, H 5.65, N 10.14.

^{1}H NMR (400 MHz d_6-DMSO): δ 2.51 ($(CD_3)_2SO$ residual solvent peak), 4.23 (s, 2H, CH_2), 6.54 (d, 2H, Ar-H), 6.59 (s, 1H, NH), 6.73 (t, 1H, Ar-H), 6.82 (d, 1H, Ar-H), 7.05 (t, 1H, Ar-H), 7.15 (d, 1H, Ar-H), 7.50 (d, 1H, Ar-H), 8.68 (s, 1H, NH), 9.57 (s, 1H, OH), 10.75 (s, 1H, OH).

^{13}C NMR (400 MHz, DMSO-d_6): δ (ppm) = 155.5 (CO), 151.7 (C, Ar), 128.6 (C, Ar), 128.6 (2CH, Ar), 128.1 (C, Ar), 125.6 (C, Ar), 119.6 (CH, Ar), 119.2 (CH, Ar), 119.1 (CH, Ar), 115.3 (CH, Ar), 111.4 (2CH, Ar), 41.3 (CH_2, CHO).

MS-EI: m/z (% Rel. Ab.): 240.26 (10; $\{M - OH\}^+$), 224.13 (10, $\{M - 2OH\}^+$), 198.25 (04; $\{M - CH_2NO_2\}^+$), 134.13 (100, $\{M - C_7H_8NO\}^+$), 120.14 (92, $\{M - C_7H_6NO_2\}^+$).

FT-IR (cm^{-1}): 3194 (br), 2974 (m), 2872 (m), 1604 (s, sh), 1509 (s), 1454 (s, sh), 1416 (w), 1384 (s), 1334 (s), 1275 (m), 1232 (m), 1183 (w), 1152 (w), 1124 (s), 1079 (s), 1045 (m) 987 (w), 886 (s), 828 (s), 751 (s, sh), 682 (w), 617 (w), 511 (s), 438 (m).

3.6.3 Preparation of complexes 8-12.

All reactions were performed under aerobic conditions and all reagents and solvents were used as purchased. ***Caution:*** Although no problems were encountered in this work, care should be taken when manipulating the potentially explosive nitrate salts.

*$[Cu(II)_5(L_4)_4(NO_3)_2]\cdot 3H_2O$ (**8**)*

$Cu(NO_3)_2.3H_2O$ (0.25 g, 1.034 mmol), 2-(methylamino)phenyl hydroxamic acid (L_4H_2) (0.17 g, 1.035 mmol) and NaOH (0.041 g, 1.025 mmol) were dissolved in methanol (25 cm^3) and stirred at room temperature for 4 h. The resultant dark green solution was subsequently filtered and X-ray quality crystals of **8** were obtained upon slow evaporation after one week in a 44% yield. Elemental analysis (%) calculated as $[Cu(II)_5(L_3)_4(NO_3)_2]$ ($C_{32}H_{32}N_{10}O_{14}Cu_5$): C 34.99, H 2.94, N 12.75. Found: C 35.31, H 3.20, N 12.99. FT-IR (cm^{-1}): 3430 (w), 3135 (m) 2925 (m), 1635 (m), 1593 (s), 1551 (s), 1467 (m), 1383 (s), 1160 (m), 1137 (m), 1091 (s), 1039 (s), 937 (m), 777 (m), 753 (m), 689 (s), 653 (s).

*$\{[Zn(II)(L_4H)_2].2MeOH\}_n$ (**9**)*

$Zn(NO_3)_2.6H_2O$ (0.25 g, 0.85 mmol), *N*-hydroxy-2-(methylamino)benzamide (L_4H_2) (0.14 g, 0.85 mmol and NaOH (0.033 g, 0.85mmol) were stirred in methanol (30 cm^3) for 4 hrs. The resultant pale yellow solution was then filtered and X-ray quality crystals of **9** were obtained upon slow evaporation of the mother liquor in 18% yield. Elemental analysis (%) calculated as **9** ($C_{18}H_{26}N_4O_6Zn_1$): C 47.02, H 5.70, N 12.18. Found: C 47.08, H 4.78, N 12.71. FT-IR (cm^{-1}): 3378 (s), 3270 (br), 3073 (w), 2936 (w), 2814 (m), 2166 (w), 2123 (w), 2010 (w), 1942 (w), 1612 (s, sh), 1572 (s, sh), 1505 (s, sh), 1475 (m), 1452 (m), 1420 (s), 1354 (m), 1324 (s), 1283 (s), 1221 (s), 1173 (s), 1146 (s), 1101 (s), 1066 (s, sh), 1024 (w), 940 (s), 902 (s), 842 (s), 803 (s), 776 (m), 748 (s, sh), 697 (s), 666 (s), 627 (m), 604 (m) 556 (m), 528 (m), 501 (m), 460 (s) 432 (m), 410 (m).

*$[Cu(II)_5(L_5H)_4(MeOH)_2(NO_3)_2]\cdot 3H_2O\cdot 4MeOH$ (**10**).*

$Cu(NO_3)_2.3H_2O$ (0.25 g, 1.04 mmol), *N*-hydroxy-2-((2-hydroxy-3-methoxybenzyl)amino benzamide (L_5H_3) (0.38 g, 1.04 mmol) and NaOH (0.042 g, 1.04 mmol) were dissolved in MeOH (30 cm^3) and stirred for 4 hrs at room temperature. The resultant dark green solution was then filtered and X-ray quality crystals of **10** were obtained upon slow evaporation of the mother liquor in 20% yield. Elemental analysis (%) calculated as $[Cu(II)_5(L_3H)_4(H_2O)_2(NO_3)_2]\cdot 7H_2O$ ($C_{60}H_{74}N_{10}O_{31}Cu_5$): C 41.20, H 4.27, N 8.01. Found: C

40.91, H 4.07, N 7.86. FT-IR (cm^{-1}): 3375 (br), 3071 (w), 2938 (m), 2839 (m), 1907 (w), 1732 (m), 1611 (s, sh), 1592 (w), 1515 (w), 1482 (s, sh), 1442 (m), 1371 (m), 1328 (m), 1272 (s), 1163 (m), 1083 (s), 1058 (m), 986 (m), 913 (w), 829 (w), 747 (s), 687 (m), 538 (m).

$[Cu(II)(L_6H_2)_2]_n$ ***(11)***

To a solution of $Cu(NO_3)_2.3H_2O$ (0.025 g, 0.10 mmol), 4-((2-hydroxy-3-methoxybenzyl)amino)-N-hydroxybenzamide (L_6H_3) (0.030 g, 0.10 mmol) and tetraethylammonium hydroxide (TEAOH) (0.015 g, 0.10 mmol) were dissolved in methanol (20 cm^3) and the resultant solution stirred for 4 hrs at room temperature. The resultant yellow-green solution was then filtered and X-ray quality crystals of **11** were obtained upon slow evaporation of the mother liquor in 18% yield. Elemental analysis (%) calculated as **11**$\cdot H_2O$ ($C_{30}H_{32}N_4O_9Cu_1$): C (54.91), H (4.92), N (8.54); Found: C (54.25), H (4.83), N (8.76). FT-IR (cm^{-1}): 3498 (m), 3313 (w), 3189 (w), 2955 (w), 2837 (w), 1608 (s, sh), 1588 (w), 1562 (m), 1543 (w), 1477 (s), 1452 (m), 1439 (m), 1393 (w), 1358 (m), 1335 (w), 1271 (m), 1257 (w), 1211 (m), 1188 (m), 1141 (s), 1130 (w), 1064 (s), 1021 (s), 915 (s, sh), 854 (m), 828 (s), 800 (m), 774 (s), 767 (s), 735 (s), 640 (m), 615 (m) 581 (m), 550(m), 503(s), 453 (s).

$\{[Cu(II)(L_7H_2)_2].2MeOH\}_n$ ***(12)***

$Cu(NO_3)_2.3H_2O$ (0.025 g, 0.10 mmol), N-hydroxy-4-((2-hydroxybenzyl)amino)benzamide (L_7H_3) (0.03 g, 0.10 mmol) and tetraethylammonium hydroxide (TEAOH) (0.015 g, 0.10 mmol) were dissolved in methanol (20 cm^3) and stirred at room temperature for 4 h. The resultant yellowish green solution was then filtered and X-ray quality crystals of **12** were obtained upon slow evaporation of the mother liquor in 15% yield. Elemental analysis (%) calculated as **12** ($C_{30}H_{34}N_4O_8Cu_1$): C (56.11), H (5.34), N (8.73); Found: C (56.02), H (4.75), N (8.78). FT-IR (cm^{-1}): 3624 (m), 3538 (s), 3391 (m), 3208 (w), 3132 (m), 3062 (w), 2940 (m), 2839 (w), 2723 (m), 2611 (m), 2233 (w), 2107 (w), 1899 (w), 1606 (w), 1592 (s, sh), 1533 (m), 1501 (s, sh), 1453 (s, sh), 1414 (w), 1395 (w), 1354 (w), 1333 (m), 1311 (w), 1273 (s), 1242 (s), 1195 (w), 1177 (s, sh), 1157 (w), 1110 (w), 1072 (m), 1033 (s, sh), 1013 (s), 920 (s, sh), 861 (w), 826 (s, sh), 762 (s, sh), 715 (m), 661 (s), 636 (s), 582 (s), 525 (w) 506 (s), 436(s), 414 (s).

3.7 References

1. A. J. Blake, N. R. Champness, P. A. Cooke, J. E. B. Nicolson and C. Wilson. *J. Chem. Soc. Dalt. Trans.*, 2000, 3811–3819.
2. J. Zhao, D.-S. Li, X.-J. Ke, B. Liu, K. Zou and H.-M. Hu. *Dalton Trans.*, 2012, **41**, 2560.
3. E. Peris and R. H. Crabtree. *Chem. Soc. Rev.***,** 2018, **47**, 1959-1968.
4. D. Intrieri, D. M. Carminati and E. Gallo. *Dalton Trans.*, 2016, **45**, 15746-15761.
5. J.-L. Dong, K.-H. He, D.-Z. Wang, Y.-H. Zhang and D.-H. Wang. *J. Solid State Chem.*, 2018, **263**, 164–171.
6. S. R. Batten, N. R. Champness, X.-M. Chen. J. Garcia-Martinez, S. Kitagawa, L. Öhrström, M. O'Keeffe, M. P. Suh and J. Reedijk. *CrystEngComm*, 2012, **14**, 3001.
7. C. Inman, J. M. Knaust and S. W. Keller. *Chem. Commun.*, 2002, 156–157.
8. L. M. Zheng, P. Yin and Xin. *Inorg. Chem.*, 2002, **41**, 4084–4086.
9. C. Di Nicola, E. Forlin, F. Garau, M. Gazzano, A. Lanza, M. Monari, F. Nestola, L. Pandolfo, C. Pettinari, A. Zorzi and F. Zorzi. *Cryst. Growth Des.*, 2013, **13**, 126–135.
10. A.R. Moosavi-Zare, H. Goudarziafshar and Z. Jalilian. *Applied Organometallic Chemistry*, 2018, **33**, 1.
11. L. Kafi-Ahmadi and L. Shirmohammadzadeh. *J. Nanostruct Chem.*, 2017, 7, 179–190.
12. M. Tyagi, S. Chandra, P. Tyagi. *Spectrochimica Acta*, 2014, **117,** 1–8.
13. J.-W. Wen, W.-T. Chen, Z.-X. Zhang, W.-J. Tao and C. Liu. *J. Solid State Chem.*, 2018, **263**, 30–35.
14. P. Falcaro, R. Ricco, C. M. Doherty, K. Liang, A. J. Hill and M. J. Styles. *Chem. Soc. Rev.*, 2014, **43**, 5513–5560.
15. M. Rakibuddin and R. Ananthakrishnan. *Appl. Surf. Sci.*, 2016, **362**, 265–273.
16. C. C. Li, L. Mei, L. B. Chen, Q. hong Li and T. H. Wang. *J. Mater. Chem.*, 2012, **22**, 4982.
17. M. Rakibuddin and R. Ananthakrishnan. *RSC Advances* 2015, **5**, 68117–68127.
18. J. Heine and K. Müller-Buschbaum. *Chem. Soc. Rev.*, 2013, **42**, 9232.
19. G. Givaja, P. Amo-Ochoa, C. J. Gómez-García and F. Zamora. *Chem. Soc. Rev.*, 2012, **41**, 115–147.
20. V. V. Komarchuk, V. V. Ponomarova, H. Krautscheid and K. V. Domasevitch. *Zeitschrift für Anorg. und Allg. Chemie*, 2004, **630**, 1413–1418.
21. S. Q. Bai, D. J. Young and T. S. A. Hor. *Chem. - An Asian J.*, 2011, **6**, 292–304.

22. S. Contaldi, C. Di Nicola, F. Garau, Y. Y. Karabach, L. M. D. R. S. Martins, M. Monari, L. Pandolfo, C. Pettinari and A. J. L. Pombeiro. *Dalton Trans.*, 2009, 4928.
23. C. McDonald, S. Sanz, E. K. Brechin, M. K. Singh, G. Rajaraman, D. Gaynor, L. F. Jones. *RSC Advances*, 2014, **4**, 38182.
24. C. McDonald, T. Whyte, S. M. Taylor, S. Sanz, E. K. Brechin, D. Gaynor and L. F. Jones. *CrystEngComm*, 2013, **15**, 6672.
25. C. McDonald, D. W. Williams, P. Comar, S. J. Coles, T. D. Keene, M. B. Pitak, E. K. Brechin, L. F. Jones. *Dalton Trans*., 2015, **44**, 13359.
26. M. B. Fugu, R. J. Ellaby, H.M. O'Connor, M. B. Pitak, W. Klooster, P. N. Horton, S. J. Coles, M. H. Al-mashhadani, I. F. Perepichka, E. K. Brechin, L. F. Jones. *Dalton Trans.*, 2019, **48**, 10180–10190.
27. A. F. Abdel-Magid, K. G. Carson, B. D. Harris, C. A. Maryanoff, R. D. Shah. *J. Org. Chem.*, 1996, **61**, 3849.
28. B. Pramanik, D. Das. *J. Phys. Chem. C*, 2018, **122**, 3655−3661.
29. W. Y. Kim, H. Shi, H. S. Jung, D. Cho, P. Verwilst, J. Y. Lee, J. S. Kim. *Chem. Commun.*, 2016, **52**, 8675-8678.
30. A. E. Taggi, A. M. Hafez, H. Wack, B. Young, D. Ferraris, T. Lectka. *J. Am. Chem. Soc.* 2002, **124**, 6626-6635.
31. Z. H. Chohan, M. Arif, Z. Shafiq, M. Yaqub, and C. T. J. Supuran. *Enzyme. Inhib. Med. Chem.*, 2006, **21**, 95-103.
32. A. Xavier and N. Srividhya. *IOSR-JAC*, 2014, **7**, 06-15.
33. S. Rayatia, E. Bohloulbandia and S. Zakavib. *Inorg. Chem. Comm.* 2015, **54**, 38–40.
34. P. Happ, C. Plenk and E. Rentschler. *Coord. Chem. Rev.*, 2015, **289-290**, 238.
35. Z. Eckstein, T. Jadach, and E. Lipczynska-Kochany. *J. Chem. Eng. Data*, 1983, **28**, 279.
36. E. Lipczynska-Kochany and H. Iwamura. *Chem. Lett.*, 1982, **11**, 1825.
37. G. Bonola and E. Sianesi. *J. Med. Chem.*, 1970, **13**, 329.
38. W. L. Leong and J. J. Vittal. *Chem., Rev.*, 2011, **111**, 688-764.
39. B. N. Figgis and R. S. Nyholm. *J. Chem. Soc.*, 1958, 4190.
40. N. F. Chilton, R. P. Anderson, L. D. Turner, A. Soncini and K. S. Murray. *J. Comput. Chem.*, 2013, **34**, 1164.
41. O. Khan. *Molecular Magnetism*, VCH, New York, 1993.
42. A. V. Pavlishchuk, S. V. Kolotilov, M. Zeller, L. K. Thompson, I. O. Fritsky, A. W. Addison and A. D. Hunter. *Eur. J. Inorg. Chem.*, 2010, 4851-4858.

43. P. Happ and E. Rentschler. *Dalton Trans.*, 2014, **43**, 15308.
44. Rigaku OD (2015). *CrysAlis PRO*. Rigaku Oxford Diffraction Ltd, Yarnton, England.
45. G. M. Sheldrick. *Acta Crystallogr. Sect. C Struct. Chem.*, 2015, **71**, 3.
46. O. V. Dolomanov, L. J. Bourhis, R. J. Gildea, J. A. K. Howard and H. J. Puschmann. *Appl. Crystallogr.*, 2009, **42**, 339.

Chapter Four

Concluding remarks and future work

4.1 General conclusion and summary

In this thesis we aimed to expand the coordination chemistry of hydroxamic acids by firstly developing a family of novel (or rarely investigated) di- and multitopic hydroxamate ligands as shown in Scheme. 4.1. The second phase of this project was to study the interaction of this family of related ligands with some of the most relevant and common cations in biological, industrial and environmental fields, such as Mn(II), Fe(III) Co(II), Ni(II), Cu(II) and Zn(II). The third and final phase would encompass the complete structural and (when appropriate) magnetic characterization of all synthesized complexes and to highlight any potential applications in the fields of molecular magnetism and photo-physics.

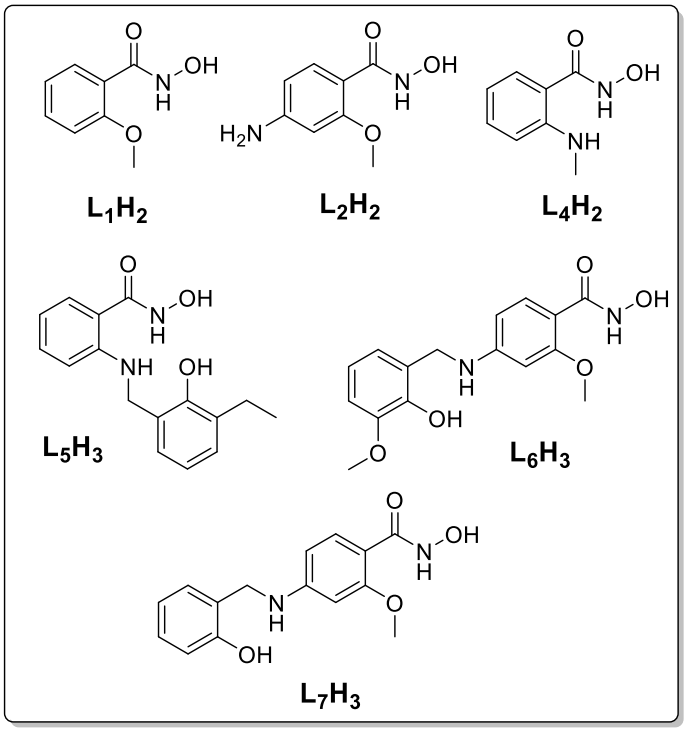

Scheme 4.1 *ChemDraw representations of the ligands employed in this thesis. These are: 2-methoxyphenylhydroxamic acid (L_1H_2); 4-amino-2-(acetoxy)phenylhydroxamic acid (L_2H_2); 2-(methylamino)phenylhydroxamic acid (L_4H_2); N-hydroxy-2-[(2-hydroxy-3-methoxybenzyl)amino]benzamide (L_5H_3); N-hydroxy-4-((2-hydroxy-3-methoxybenzyl)amino)benzamide (L_6H_3) and N-hydroxy-4-((2-hydroxybenzyl)amino)benzamide (L_7H_3).*

To this end we have presented in this thesis fourteen new complexes (**1**-**14**). Five members are extended networks in the form of the 1-D coordination polymers: $[Zn(II)_2(L_1H)_2(H_2O)_5](NO_3)_2]_n$ (**6**), $\{[Zn(II)(L_4H)_2].2MeOH\}_n$ (**9**), $[Cu(II)(L_6H_2)_2]_n$ (**11**) and

{[Cu(II)(L_7H_2)].2MeOH}$_n$ (**12**), along with the 2-D [4,4]- net {[Cu(II)(L_2H)(H_2O)(NO_3)].H_2O}$_n$ (**7**). All other members are discrete cages and include the monometallic complexes [Cu(II)(L_1H)$_2$] (**1**) and [Ni(II)(L_1H)(H_2O)(py)$_3$](NO_3)·MeCN (**5**) and the polynuclear species [Co(III)Co(II)$_6$(L_1H)$_8$(L_1)$_2$(MeOH)$_4$(NO_3)$_2$]NO_3·3.5H_2O·14MeOH (**3**), [Cu(II)$_5$(L_4)$_4$(NO_3)$_2$]·3H_2O (**8**) and [Cu(II)$_5$(L_5H)$_4$(MeOH)$_2$](NO_3)$_2$·3H_2O·4MeOH (**10**). The remaining members are dimeric in nature and are [Fe(III)$_2$(L_1H)$_4$$Cl_2$].2MeCN (**2**) and the very recently produced lanthanide complexes [Dy$_2$(L_1H)$_2$(H_2O)$_4$(NO_3)$_4$] (**13**) and [Gd$_2$(L_1H)$_2$(H_2O)$_4$(NO_3)$_4$] (**14**). The latter two complexes are described in detail below (section 4.2.1).

Complexes **1**, **2**, **3**, **5**, **6**, **13** and **14** represent extremely rare examples of metal coordination of the ligand 2-(acetoxy)phenylhydroxamic acid (L_1H_2). Similarly, complex **7** ({[Cu(II)(L_2H)(H_2O)(NO_3)].H_2O}$_n$) represents the first complex to be constructed with the ligand 4-amino-2-(acetoxy)phenylhydroxamic acid (L_2H_2). Likewise, the 12-MC-Cu(II) metallacrown [Cu(II)$_5$(L_5H)$_4$(MeOH)$_2$](NO_3)$_2$·3H_2O·4MeOH (**10**) showcases the effective bridging ability of the novel ligand *N*-hydroxy-2-[(2-hydroxy-3-methoxybenzyl)amino]benzamide (L_5H_3). Furthermore, the planar {Cu(II)$_5$} core in **10** differ from the other analogues of 12-MC-4Cu(II) metallacrowns[7] due to the deliberate introduction of the secondary amine groups which provides each ligand with a natural kink and results in each of the four independent phenolic groups to significantly deviated from the {Cu(II)$_5$} plane.

The self-assembly of the 1-D chains [Cu(II)(L_6H_2)$_2$]$_n$ (**11**) and {[Cu(II)(L_7H_2)].2MeOH}$_n$ (**12**) was successful through Cu(II) ligation of the novel multitopic ligands N-hydroxy-4-((2-hydroxy-3-methoxybenzyl)amino)benzamide (L_6H_3) and N-hydroxy-4-((2-hydroxybenzyl)amino)benzamide (L_7H_3) respectively. Slight differences in the functionality of ligands (L_6H_3 vs. L_7H_3), give rise to significant topology changes when closely inspecting the 1-D chains in **11** and **12**. Tables A1-3 in the appendices provide information on all mono-, di- and polynuclear hydroxamate containing complexes and coordination polymers to date (total = 153 complexes to date). At the time of writing this work has described the synthesis and characterization of 13 such complexes (**1**-**3** and **5**-**14**), representing an 8.5% increase in the data set. More importantly, we have further explained the coordination chemistry of under employed hydroxamic acid ligands and designed entirely new hydroxamic acid ligands towards the same goal. Future work within the Jones group will pursue the synthesis of heteometallic 3d-4f hydroxamate complexes (towards potential SMM or MCE behaviour). Heteroleptic analogues will also be investigated fully.

4.2 Recent results and future work

As discussed in Chapter 2, upon close inspection of the monomeric complex [Ni(II)(L_1H)(H_2O)($py)_3$](NO_3)·MeCN (**5**), it becomes apparent that the individual {Ni_1} actually self-assemble into dimeric topologies through self-complementary hydrogen bonding (Fig. 4.1). Work is currently underway in probing any potential Ni(II)···Ni(II) magnetic exchange using SQUID magnetometry in collaboration with Professors Mark Murrie (University of Glasgow) and Euan Brechin (University of Edinburgh). During this study, we will also look into tuning this magnetic exchange through high pressure SQUID magnetometry. Any perturbations will be followed using high pressure single crystal X-ray diffraction studies (both high pressure studies will be carried out at the Centre for Science under Extreme Conditions (CSEC) at the University of Edinburgh).

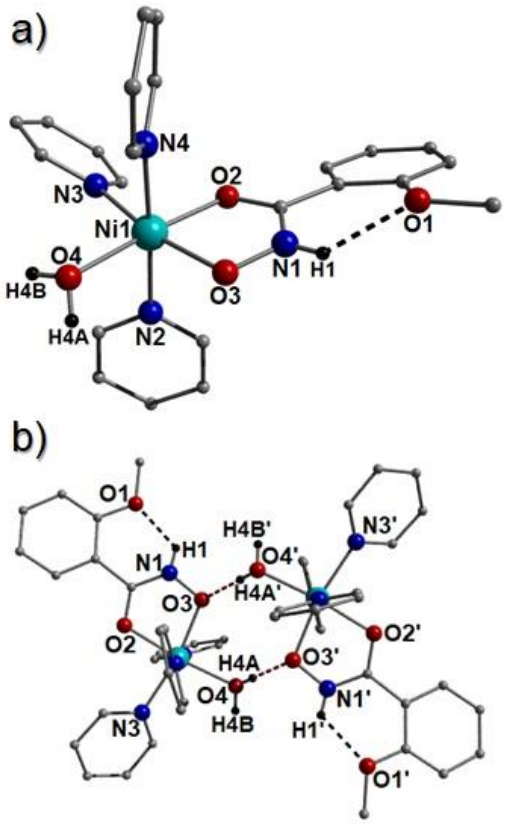

Figure 4.1 *(a) Crystal structure of [Ni(II)(L_1H)(H_2O)($py)_3$](NO_3)·MeCN (**5**). Colour code: Light blue (Ni), red (O), blue (N), grey (C). NO_3^- counter anion and the majority of hydrogen atoms have been omitted for clarity. The dashed black line represents the intramolecular H-bond: N1(H1)···O1 = 2.13 Å. (b) A dimer of {Ni(II)(L_1H)(H_2O)($py)_3$}$^+$ units connected through self-complementary H-bonding at a distance of 1.86 Å (O4(H4A)···O3) as viewed along the axial direction of the Ni(II) metal centre.*

4.2.1 Hydroxamate bridged dimeric lanthanide complexes

Towards the very end of this study, we produced two extremely interesting analogous dinuclear complexes $[Dy(III)_2(L_1H)_2(H_2O)_4(NO_3)_4]$ (**13**) and $[Gd(III)_2(L_1H)_2(H_2O)_4(NO_3)_4]$ (**14**) using the trusted ligand 2-methoxyphenylhydroxamic acid (L_1H_2). X-ray quality crystals of **13** and **14** are obtained in the triclinic P-1 space group (Table 4.2). The asymmetric units in **13** and **14** each comprise half a dimeric unit and thus possess an inversion centre at the midpoint between the two lanthanide centres (Fig. 4.2). The Gd1 and Dy1 (and s.e.) centres are nine coordinate and exhibit distorted tricapped trigonal prismatic geometries. The two Ln(III) centres in **13** and **14** are connected through two $\eta^2{:}\eta^1$ μ-bridging L_1H^- ligands, while the coordination spheres at each metal centre are completed by a combination of two chelating NO_3^- anions and two terminally bound H_2O ligands. For comparison, selected bond lengths and angles in compounds **13** and **14** are listed in Table 4.1. Intra-ligand H-bonding interactions are observed in both complexes between the hydroxamate N-H groups (N1) and the juxtaposed methoxide O atoms (O3) at distances of N1(H1)···O3 = 1.92 Å in **13** and N1(H8)···O3 = 1.94 Å in **14**. The terminal water ligand protons in both analogues partake in extensive inter-molecular H-bonding with the O donor atoms of neighbouring NO_3^- anions (e.g. O10(H10B)···O9′ = 1.90 Å, O11(H11B)···O5′ = 2.45 Å and O11(H11B)···O8′ = 2.16 Å in **13** and O10(H10B)···O6′ = 2.23 Å, O10(H10B)···O9′ = 1.92 Å and O11(H11B)···O7′ = 2.15 Å in **14**) (Fig. 4.3).

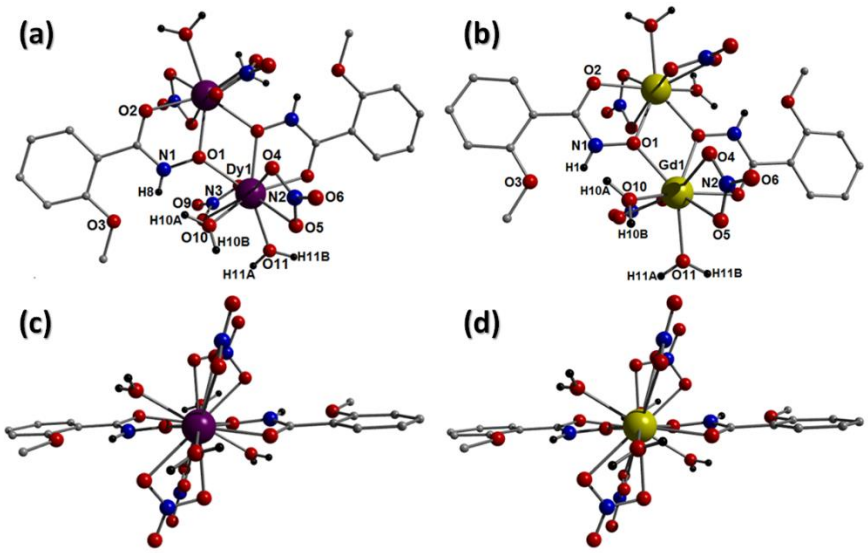

Figure 4.2 *(a) Crystal structures of* $[Dy(III)_2(L_1H)_2(H_2O)_4(NO_3)_4]$ ***(13)*** *and* $[Gd(III)_2(L_1H)_2(H_2O)_4(NO_3)_4]$***(14)*** *as viewed perpendicular (a and b) and parallel (c and d) to the Ln···Ln directions, respectively. Colour code: Purple (Dy), yellow (Gd), grey (C), blue (N), red (O) and black (H).*

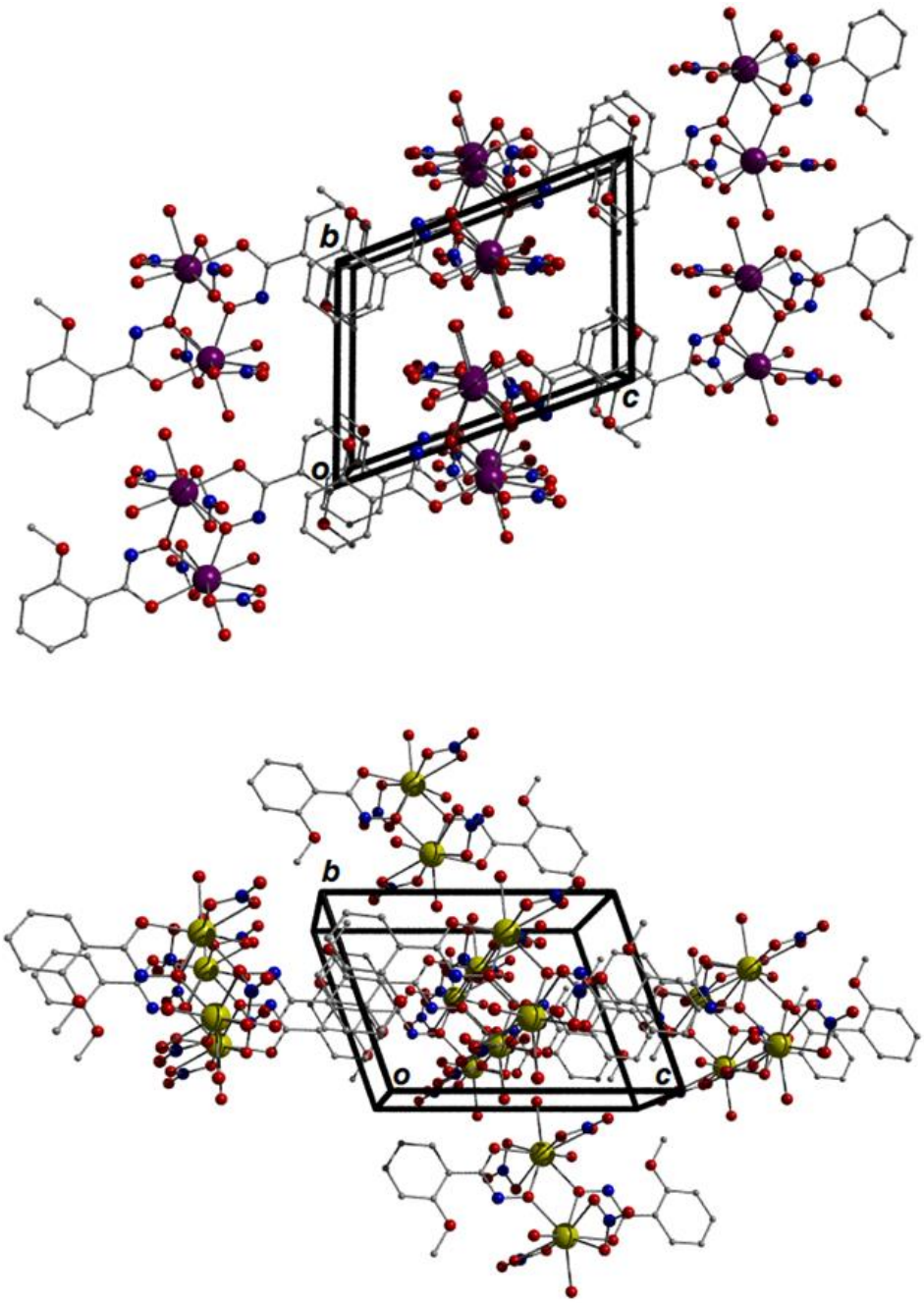

Figure 4.3 *Packing arrangement in* $[Dy(III)_2(L_1H)_2(H_2O)_4(NO_3)_4]$ ***(13)*** *(top) and* $[Gd(III)_2(L_1H)_2(H_2O)_4(NO_3)_4]$***(14)*** *(bottom) as viewed along a unit cell direction. All hydrogen atoms were omitted for clarity.*

Complexes **13** and **14** represent the first lanthanide complexes constructed with the ligand 2-methoxyphenylhydroxamic acid (L_1H_2). The Jones group will utilize and expand upon these promising results by producing more Ln(III) analogues of complexes **13** and **14**. All members of this family will then be magnetically evaluated for potential Single-Molecule Magnet (e.g.

$[Dy(III)_2(L_1H)_2(H_2O)_4(NO_3)_4]$ (**14**)) or Magnetic Coolant Effect (MCE) behaviour (e.g. $[Gd(III)_2(L_1H)_2(H_2O)_4(NO_3)_4]$ (**13**)). Work will also extend to ligand modification towards producing 3d-4f heterometallic complexes and homo- and heterometallic extended network architectures towards potential Single-Chain Magnetic behaviour.

Table 4.1 Selected bond lengths and angles observed in compounds **13** and **14**.

Selected bond lengths and angles	$[Dy_2(L_1H)_2(H_2O)_4(NO_3)_4]$ (**13**)	$[Gd_2(L_1H)_2(H_2O)_4(NO_3)_4]$ (**14**)
Ln-O1 (NH-OH) (Å)	2.336	2.368
Ln-O2 (C=O) (Å)	2.364	2.395
Ln-O5 (NO_3) (Å)	2.547	2.569
Ln-O11 (H_2O) (Å)	2.370	2.394
Ln-O-Ln (°)	118.05	117.72
O-Ln-O (°)	61.95	62.28
Ln-Ln (Å)	3.989	4.031

Table 4.2 Selected crystal data obtained from **13** and **14**.

	14	**13**
Formula[a]	$C_{16}H_{24}N_6O_{22}Dy_2$	$C_{16}H_{24}N_6O_{22}Gd_2$
M_W	977.41	966.91
Crystal System	Triclinic	Triclinic
Space group	P-1	P-1
a/Å	7.3242(2)	7.3575(2)
b/Å	8.7036(3)	8.7641(4)
c/Å	12.0951(3)	12.1090(5)
α/°	109.004(3)	109.212(4)
β/°	99.617(2)	99.355(3)
γ/°	95.903(2)	96.170(3)
V/Å^3	708.46(4)	716.58(5)
Z	1	1
T/K	100.0(2)	100.0(6)
λ[b]/Å	0.71073	0.71073
D_c/g cm^{-3}	2.291	2.241
μ(Mo-Ka)/ mm^{-1}	5.340	30.587
Meas./indep. (R_{int}) refl.	12013 / 10044 (0.0640)	12025 / 9482 (0.0449)
Restraints, Parameters	0, 209	0, 209
wR2 (all data)	0.1217	0.0976
R1[d,e]	0.0435	0.0363
Goodness of fit on F^2	1.122	1.069

[a] Includes guest molecules. [b] Mo-Kα radiation, graphite monochromator. [c] wR2= [Σw(IF$_o^2$I- IF$_c^2$I)^2/ ΣwIF$_o^2$I^2]$^{1/2}$. [d]For observed data. [e] R1= ΣIIF$_o$I- IF$_c$II/ ΣIF$_o$I

4.3 Experimental Section

Infra-red spectra were recorded on a Perkin Elmer FT-IR *Spectrum 100* spectrometer (School of Chemistry, Bangor University). Elemental analysis was carried out at OEA laboratories (Kelly Bray, Cornwall).

4.3.1 Single-crystal X-ray crystallography

Complexes **13** and **14** were collected on a Rigaku AFC12 goniometer equipped with an enhanced sensitivity (HG) Saturn724+ detector mounted at the window of an FR-E+ Super Bright molybdenum rotating anode generator with HF Varimax optics (100m focus). The cell determination and data collection of each complex was carried out using the CrystalClear-SM Expert package (Rigaku, 2012). Each data reduction, cell refinement and absorption correction were carried out using CrysAlisPro software (Rigaku OD, 2015),[1] while all structures were solved and refined using SHELXT and SHELXL-2014[2] within OLEX-2.[3] All non hydrogen atoms in **13** and **14** were refined as anisotropic, while all hydrogens were modelled at calculated positions.

4.3.2 Preparation of complexes 13 and 14.

*Synthesis of [Dy(III)$_2$(L_1H)$_2$(H_2O)$_4$(NO_3)$_4$] (**13**).*

$Dy(NO_3)_3.H_2O$ (0.25 g, 0.72 mmol), 2-metoxyphenylhydroxamic acid (L_1H_2) (0.12 g, 0.72 mmol) and triethylamine (NEt_3) (0.073 g, 0.72 mmol) were dissolved in methanol (30 cm^3) and stirred at room temperature for 4 h. The resultant solution was filtered and the solution was left to evaporate to dryness. The residual solid was then re-dissolved in a minimum amount of acetonitrile, from which X-ray quality crystals of **13** were obtained upon slow evaporation in 23% yield. Elemental analysis (%) calculated as [Dy(III)$_2$(L_1H)$_2$(H_2O)$_2$(NO_3)$_4$] ($C_{16}H_{20}N_6O_{20}Dy_2$): C (20.41), H (2.14), N (8.93). Found: C (20.51), H (2.44), N (8.46). FT-IR (cm^{-1}): 3393 (s), 3311 (s), 3257 (w), 3014 (w), 2949 (w), 2879 (w), 2842 (w), 2488 (w), 2038 (w), 1648 (s), 1610 (s, sh), 1599 (w), 1577 (s), 1508 (s), 1463 (w), 1445 (s), 1336 (s, sh), 1308 (s), 1266 (s), 1247 (s), 1184 (s, sh), 1152 (s), 1105 (s), 1081 (s), 1041 (s), 1020 (s), 919 (s), 855 (m), 814 (s), 773 (m), 752 (w), 743 (s), 718 (w), 670 (s), 601 (s), 551 (w), 514 (w) 430 (w).

*Synthesis of [Gd(III)$_2$(L_1H)$_2$(H_2O)$_4$(NO_3)$_4$] (**14**)*

$Gd(NO_3)_3.6H_2O$ (0.25 g, 0.55 mmol), 2-metoxyphenylhydroxamic acid (L_1H_2) (0.09 g, 0.55 mmol) and triethylamine (NEt_3) (0.073 g, 0.55 mmol) were dissolved in methanol (30 cm^3) and stirred at room temperature for 4 h. The resultant solution was filtered and the solution was left to evaporate to dryness. The residual solid was then re-dissolved in a minimum amount of acetonitrile, from which X-ray quality crystals of **14** were obtained upon slow evaporation in 25% yield. Elemental analysis (%) calculated as **14** ($C_{16}H_{24}N_6O_{22}Gd_2$): C (19.88), H (2.50), N (8.69). Found: C (20.27), H (2.42), N (8.48). FT-IR (cm^{-1}): 3389 (s), 3310 (s), 3254 (w), 3013 (w), 2947 (w), 2843 (w), 2480 (w), 2345 (w), 1958 (s), 1925 (s), 1782 (w), 1648 (w), 1609 (m), 1599 (s), 1577 (w), 1506 (s, sh), 1461 (w), 1333 (m), 1304 (s, sh), 1266 (w), 1246 (m), 1182 (s), 1152 (s), 1105 (s), 1078 (s), 1040 (s), 1020 (s), 917 (s, sh), 855 (w), 814 (s), 772 (w), 752 (w), 741 (m), 718 (s), 670 (w), 587 (s), 546 (m) 509 (w), 445 (w), 426 (w).

4.4 References

1. Rigaku OD (2015). *CrysAlis PRO*. Rigaku Oxford Diffraction Ltd, Yarnton, England.
2. G. M. Sheldrick. *Acta Crystallogr. Sect. C Struct. Chem.,* 2015, **71**, 3.
3. O. V. Dolomanov, L. J. Bourhis, R. J. Gildea, J. A. K. Howard and H. J. Puschmann. *Appl. Crystallogr.,* 2009, **42**, 339.

Appendix A

Table A1 Mononuclear complexes constructed with hydroxamic acids (valid at the time of writing).

No.	Complex	Meanings of abbreviated ligand(s)	Refs.
1	$[B(bha)_2]^-$	bha = benzohydroxamic acid	1
2	fac-$[Si(aha)_3]^{2-}$	aha = acetohydroxamic acid	2
3	fac-$[Si(bha)_3]^{2-}$	bha = benzohydroxamic acid	2
4	mer-$[Si(bha)_3]^{2-}$	bha = benzohydroxamic acid	2
5	$[(Me_2NH)CH_2Si(aha)_2]$	aha = acetohydroxamic acid	3
6	$[(Me_2NH)CH_2Si(bha)_2]$	bha = benzohydroxamic acid	3
7	fac-$[Cr(bhaH)_3]$	bha = benzohydroxamic acid	4
8	fac-$[Cr(bha)_3]^{3-}$	bha = benzohydroxamic acid	5
9	Mer-$[Cr(bha)_3]^{3-}$	bha = benzohydroxamic acid	5
10	$[Fe(bhaH)_3]$	bha = benzohydroxamic acid	6
11	$[Fe(mpaha)_3]$	mpaha = N-(4-methylphenyl)acetohydroxamic acid	7
12	$[Fe(p\text{-}cpaha)_3]$	*p*-cpahaH = *N*-(4-Cyanophenyl)acetohydroxamic acid	8
13	$[Fe(mmbha)_3]$	mmbhaH = *N*-Methyl-4-methylbenzohydroxamic acid	6
14	$[Fe(oep)(bhaH)]\cdot bhaH_2$	oep = octaethylporphyrin bha = benzohydroxamic acid	9
15	*fac*-$[Fe(ahaH)_3]$	aha = acetohydroxamic acid	6
16	*mer*-$[Co(bha)_3]^{3-}$	bha = benzohydroxamic acid	10
17	$[Co(tpa)(ahaH)](ClO_4)$	tpa = tris(2-methylpyridyl)amine aha = acetohydroxamic acid	11
18	$[Co(tpa)(aha)](ClO_4)$	tpa = tris(2-methylpyridyl)amine aha = acetohydroxamic acid	11
19	$[Co(tpa)(phaH)](ClO_4)$	tpa = tris(2-methylpyridyl)amine $phaH_2$= propanohydroxamic acid	11
20	$[Co(tpa)(bhaH)](Cl)$	bha = Benzohydroxamic acid tpa = tris(2-methylpyridyl)amine	11
21	[Co(tpa)(mmst)]	tpa = tris(2-methylpyridyl)amine $mmstH_2$ = marimastat.	12
22	$[Co(tpa)(ahaH)](ClO_4)_2$	tpa = tris(2-methylpyridyl)amine	11

		aha = acetohydroxamic acid	
23	$[Co(tpa)(phaH)](ClO_4)_2$	tpa = tris(2-methylpyridyl)amine $phaH_2$ = propanohydroxamic acid.	11
24	$[Co(6\text{-}Ph_2tpa)(ahaH)]^+$	6-Ph_2tpa = N,N-bis((6-phenyl-2-pyridyl)methyl)-N-((2-pyridyl)methyl)amine. aha = acetohydroxamic acid	13
25	$[Ni([12]aneN_3\text{-}mc2)(ahaH)]^+$	[12]aneN_3-mc2 = 2,4,4,9-tetramethyl-1,5,9-triazacyclododec-1-ene. aha = acetohydroxamic acid	14
26	$[Ni(6\text{-}Ph_2tpa)(ahaH)]^+$	6-Ph2tpa =N,N-bis((6-phenyl-2-pyridyl)methyl)-N-((2-pyridyl)methyl)amine. aha = acetohydroxamic acid	13
27	$[Ni(bppa)(ahaH_2)]^{2+}$	bppa = *N*,*N*-bis[(6-phenyl-2-pyridyl)methyl]-*N*-[(6-pivaloylamido-2-pyridyl)methyl]amine. aha = acetohydroxamic acid	15
28	$[PPh_4]_2[Ni(pydhaH_2)_2]$	$pydhaH_4$= pyridine-2,6-dihydroxamic acid.	16
29	$[Cu(mmmbha)_2]$	mmmbhaH =N-methyl-(3-methoxy-4-methyl)benzohydroxamic acid.	17
30	$[CuL_2].2H_2O$	L = glycinehydroxamic acid	18
31	$[Cu(4\text{-}NH_2\text{-}bhaH)_2]\cdot H_2O$	4-NH2-bha = 4-amino-benzohydroxamic acid	19
32	$[Zn(6\text{-}Ph_2tpa)(ahaH)]^+$	6-Ph2tpa = N,N-bis((6-phenyl-2-pyridyl)methyl)-N-((2-pyridyl)methyl)amine. aha = acetohydroxamic acid	13
33	$[Cu(pivHA)_2]$	$pivHA^-$ = pivaloyl hydroxamate	20
34	$[Zn(en)(bhaH)_2]$	en = 1,2-diaminoethane. bha = benzohydroxamic acid	21
35	$Zn(BA)_2\cdot H_2O$	BA = benzohydroxamic acid	22
36	[Zn(TpMe,Ph)(ahaH)]	TpMe,Ph = hydrotris(5,3-methylphenylpyrazolyl)borate. aha = acetohydroxamic acid	23
37	fac-$[Ga(bhaH)_3]$	bha = benzohydroxamic acid	24
38	$[Ga(mmbha)_3]$	Mmbha = N-Methyl-4-methylbenzohydroxamic acid	7
39	fac-$[Ge(bha)_3]^{2-}$	bha = benzohydroxamic acid	2
40	mer-$[In(bhaH)_3]$	bha = benzohydroxamic acid	25

41	[Hf(pbha)$_4$]	pbhaH = N-phenylbenzohydroxamic acid.	26
42	[Th(ipdmbha)$_4$]	ipdmbhaH =N-isopropyl-3,3-dimethylbutanohydroxamic acid.	27
43	[VO(bhaH)$_2$Cl]	bha = benzohydroxamic acid	28
44	[VO(O^{i}Pr)(L(2−))]$_2$	O^{i}Pr = isopropoxy; L(2−) = *N,N′*-dihydroxy-*N,N′*-diisopropylheptanediamido	28
45	[VO(OMe)(pthaH)$_2$]	pthaH$_2$ = p-toluylohydoxamic acid.	29
46	[VO(pbha)(aabhz)]	pbhaH = *N*-phenylbenzohydroxamic acid. Aabhz = acetylacetone benzoylhydrazonao-*O,N,O′*.	30
47	[VO(shedH)(shiH)]	shedH$_2$ = N-(salicylideneaminato)-N′-(2-hydroxyethyl)ethylenediamine. shiH$_3$ = salicylhydroxamic acid	31
48	[VO(pbha)(mmsal)]	pbhaH = N-phenylbenzohydroxamic acid. mmsalH$_2$ = meta-methoxysalicylaldehyde	32
49	VO(ShiH)(H$_2$O)]·1.58H$_2$O	shiH$_3$ = salicylhydroxamic acid	33
50	cis-[Mo(O)$_2$(paha)$_2$]	pahaH = N-phenylacetohydroxamic acid.	34
51	cis-[Mo(O)$_2$(epaha)$_2$]	epahaH = N-(4-ethoxyphenyl)acetohydroxamic acid.	34
52	cis-[Mo(O)$_2$(phxha)$_2$]	phxhaH = N-phenylhexanohydroxamic acid.	35
53	cis-[Mo(O)$_2$(glyhaH)$_2$]	glyhaH$_2$ = glycinehydroxamic acid.	36
54	cis-[Mo(O)$_2$(ahaH)(aha)]$^-$	aha = acetohydroxamic acid	37
55	[MoO(L″(1−))(bha)(bhaH)]	bha = benzohydroxamic acid L″(1−) = N,N-dimethylhydroxylaminato	38
56	cis-[Mo(O)$_2$(bha)$_2$]$^{2-}$	bha = benzohydroxamic acid	38
57	[Ru(edtaH$_2$)(ombhaH)]	ombhaH$_2$ = 2-methoxybenzohydroxamic acid.	39
58	[Rh(pbha)$_2$Cl(PPh$_3$)]	pbhaH = N-phenylbenzohydroxamic acid.	40
59	[(CH$_3$)$_2$Sn(mbhaH)$_2$]	mbhaH$_2$ = 4-methoxybenzohydroxamic acid.	41
60	[(Ph)$_3$Sn(pbha)]	pbhaH = N-phenylbenzohydroxamic acid	42
61	cis-[W(O)$_2$(bhaH)$_2$]	bha = benzohydroxamic acid	43
62	[Os(tfaha)(tfa)(NO)(PPh$_3$)$_2$]	tfaH = trifluoroacetic acid; tfahaH$_2$ = trifluoroacetohydroxamic acid.	44

63	[Pt(shiH)(DMSO)$_2$]	shiH$_3$ = salicylhydroxamic acid	45
64	[Pt(bha)(DMSO)$_2$]	bha = benzohydroxamic acid	45, 46
65	[Pt(shiH)(PPh$_3$)2]	shiH$_3$ = salicylhydroxamic acid	45, 46
66	[{cis-Pt(NH$_3$)$_2$}$_2$(-piha)](ClO$_4$)$_2$·H$_2$O	pihaH$_2$ = 2-pyridinehydroxamic acid	47
67	trans-[U(O)$_2$(MeOH)(pbha)$_2$]	pbhaH = N-phenylbenzohydroxamic acid	48
68	[Pd(shiH$_2$)$_2$]	shiH$_3$ = salicylhydroxamic acid	46
69	[Cu(L$_1$H)$_2$] (**1**)	L$_1$H$_2$ = 2-(acetoxy)phenyl hydroxamic acid	**This work**
70	[Ni(II)(L$_1$H)(H$_2$O)(py)$_3$](NO$_3$)·MeCN (**5**)	L$_1$H$_2$ = 2-(acetoxy)phenyl hydroxamic acid	**This work**

Table A2 Dinuclear and polynuclear complexes constructed with hydroxamic acids (valid at the time of writing).

No.	**Complex**	**Meanings of abbreviated Ligand(s)**	**Reference**
1	[Ni$_2$(shiH)(shiH$_2$)(py)$_4$(OAc)]	shiH$_3$ = salicylhydroxamic acid	49
2	[Ni$_2$(OAc)$_2$(AA)(urea)(tmen)$_2$][OTf]	Tmen = *N*,*N*,*N*‘,*N*‘-tetramethylethylenediamine; AA = acetohydroxamate anion	50
3	[Ni$_2$(OAc)(AA)$_2$(tmen)$_2$][OAc]	Tmen = *N*,*N*,*N*‘,*N*‘-tetramethylethylenediamine; AA = acetohydroxamate anion	50
4	[Ni$_5$(L$_1$)$_4$(MeOH)$_4$](ClO$_4$)$_2$·2MeOH	L$_1$H$_2$ = 2-(dimethylamino)phenylhydroxamic acid	51
5	([Ni$_5$(L$_1$)$_4$(py)$_5$](ClO$_4$)$_2$·H$_2$O	L$_1$H$_2$ = 2-(dimethylamino)phenylhydroxamic acid	51
6	[Ni$_7$(L$_1$H)$_8$(L$_1$)$_2$(H$_2$O)$_6$](SO$_4$)·15H$_2$O	L$_1$H$_2$ = 2-(dimethylamino)phenylhydroxamic acid	51
7	[Ni$_9$(μ-H$_2$O)$_2$(L$_2$)$_6$(L$_2$H)$_4$(H$_2$O)$_2$](SO$_4$)·29H$_2$O	L$_2$H$_2$ = 2-(amino)phenylhydroxamic acid	51
8	and [Ni$_9$(μ-H$_2$O)$_2$(L$_2$)$_6$(L$_2$H)$_4$(H$_2$O)$_2$](ClO$_4$)$_2$·2MeOH·18H$_2$O	L$_2$H$_2$ = 2-(amino)phenylhydroxamic acid	51
9	[Ni$_7$(2-dmAphaH$_{-1}$)2(2-dmApha)$_8$(H$_2$O)$_2$]SO$_4$·15H$_2$O	2-dmAphaH = 2-(dimethylamino)phenylhydroxamic acid	52
10	[Zn$_2$(μ-OAc)$_2$(OAc)(μ-bha)(tmen)]	tmen =N,N,N′N′-tetramethylethylenediamine bha = benzohydroxamic acid	22
11	[Zn$_3$(tfAcO)$_4$(tmen)$_2$(bhaH)$_2$]	tfAcO = trifluoroacetate tmen =N,N,N′N′-tetramethylethylenediamine bha = benzohydroxamic acid	53

12	$[Zn_2(4\text{-}Apha)_4(H_2O)_2]\cdot 2H_2O$	4-AphaH = 4-aminophenylhydroxamic acid	54
13	$[Co_2(\mu\text{-}OAc)_2(\mu\text{-}AA)(urea)(tmen)_2][OTf]$	Tmen = *N*,*N*,*N*‘,*N*‘-tetramethylethylenediamine; OTf = CF_3SO_3; AA = acetohydroxamate anion	55
14	$[Co_2(\mu\text{-}OAc)(\mu\text{-}AA)_2(tmen)_2][OTf]$	,,	55
15	$[Co^{II}_{16}O\text{-}(OH)_2(bha)_{12}(PhCO_2)_4(Phen)_2(MeOH)_4]\cdot 2MeOH$	bha = Benzohydroxamic acid Phen = 1,10-phenanthroline	56
16	$\{Mn^{II}[Mn^{III}(L)]_4(acetate)_2(DMF)_6\}$	L = salicylhydroximate	57
17	$[Mn_6(tolf)_2(shi)_5(py)_6].0\cdot 5H_2O$,	Tolf = tolfenamic acid H_2sal = salicylic acid	58
18	$[Mn_6(nap)(Hsal)(shi)_5(py)_6]$	nap = naproxen	58
19	$[Cu_5L_5H\text{-}5]$	LH = α-aminohydroxamic acids	59
20	$([Cu_5L_4H\text{-}4]^{2+})$	LH = β-aminohydroxamic acids	59
21	$[Cu_5(L_1)_4(MeOH)_4](ClO_4)_2$	L_1H_2 = 2-(dimethylamino)phenyl-hydroxamic acid	60
22	$[Cu_5(L_1)_4(py)_2](ClO_4)_2.py$	L_1H_2 = 2-(dimethylamino)phenyl-hydroxamic acid	60
23	$[Cu_5(L_1)_4(py)_6](ClO_4)_2$	L_1H_2 = 2-(dimethylamino)phenyl-hydroxamic acid	60
24	$[Cu_5(L_2)_4(MeOH)_4](ClO_4)_2.H_2O$	L_2H_2 = 2-(amino)phenylhydroxamic acid)	60
25	$[Cu(II)_{10}(L_1)_4(2\text{-}aph)_2(H_2O)_2](ClO_4)4.5MeOH$	L_1H_3 = o-[(E)-(2-hydroxy-3-methoxyphenyl)methylideneamino] benzohydroxamic acid	61
26	$[Cu_{14}(L_1)_8(MeOH)_{2.5}(H_2O)_{7.5}](NO_3)4\cdot 3MeOH\cdot 7H_2O$	L_1H_3 = o-[(E)-(2-hydroxy-3-methoxyphenyl)methylideneamino] benzohydroxamic acid	61
27	$[Cu(II)_{14}(L_2)_8(MeOH)_4(H_2O)_6](NO_3)_4.6H_2O$	L_2H_3 = o-[(E)-(2-hydroxy-3-methoxy-5-bromophenyl)methylideneamino]benzohydroxamic acid	61
28	$[Cu(II)_{14}(L_3)_8(MeOH)_6(H_2O)_2](NO_3)_4\cdot 4MeOH\cdot 8H_2O$	L_3H_3 = o-[(E)-(2-hydroxyphenyl)methylideneamino] benzohydroxamic acid	61
29	$[Cu(II)_{30}O(OH)_4(OMe)_2(L_1)16(MeOH)_4(H_2O)_2](ClO_4)_4\cdot 2MeOH\cdot 30H_2O$	L_1H_3 = o-[(E)-(2-hydroxy-3-methoxyphenyl)methylideneamino] benzohydroxamic acid	61
30	$[Cu_5(2\text{-}NH_2\text{-}bha)_4\text{-}(SO_4)(H_2O)_2]_2\cdot 10H_2O$	2-NH_2-bha = 2-amino-benzohydroxamic acid	19
31	$[V_3O_3(5\text{-}Cl_{shiH})_3(H_2O)_3]\cdot 3CH_3COCH_3$	$shiH_3$ = salicylhydroxamic acid	33
32	$Sm\ (H_2O)_3\ \{Cu(pyzha)\}_5\ (H_2O)_2\ (MeOH)\ (HSO_4)_2]\cdot (H_2O)_2\cdot (HSO_4)$	H_2Pyzha = pyrazinohydroxamic acid	62
33	$[Nd(H_2O)_2\ (MeOH)\ \{Cu(pyzha)\}_5\ (ClO_4)_2$	H_2Pyzha = pyrazinohydroxamic acid	62

	$(H_2O)_5(NO_3)]$		
34	$[Eu(H_2O)_2(MeOH)\{Cu(pyzha)\}_5(ClO_4)_2(H_2O)_5(NO_3)]$	H_2Pyzha = pyrazinohydroxamic acid	62
35	$Eu(III)[15\text{-}MC_{Ni(II),picHA}\text{-}5](NO_3)_3]$	picHA = picoline hydroxamic acid	63
36	Eu(NO(3))(3)[15-MC(Cu(II)N(picha))-5]	Picha = picoline hydroxamic acid	64
37	Eu(NO(3))(3)[15-MC(Cu(II)N(glyha))-5]	Glyha = glycine hydroxamic acid	64
38	$Eu(OAc)[15\text{-}MC_{Cu(II)Glyha}\text{-}5](NO_3)_2$	Glyha = glycinehydroxamic acid	65
39	$Ce(H_2O)_4[15MC_{CuGlyha}\text{-}5]Cl_3$	Glyha = glycinehydroxamic acid	66
40	$Ce_2(H_2O)_8[15\text{-}MC_{CuPhalaha}\text{-}5]_2Cl_6\cdot 23.5H_2O$	Phalaha = L-α-Phenyl-alaninehydroxamic acid	67
41	$LaZn_4(pheHA)_2(HpheHA)_2(NO_3)_5(pyridine)_7$	pheHA = phenylalanine hydroxamic acid	68
42	La(NO(3))(3)[15-MC(Cu(II)N(picha))-5]	Picha = picoline hydroxamic acid	63
43	Gd(NO(3))(3)[15-MC(Cu(II)N(picha))-5]	Picha = picoline hydroxamic acid	63
44	$Tb^{III}[12\text{-}MC_{Zn^{II},N,picHA}\text{-}4]_2[24\text{-}MC_{ZnII,N,picHA}\text{-}8]\cdot(pyridine)_8\cdot(triflate)_3$	picHA = picoline hydroxamic acid	69
45	$Ln(III)[15\text{-}MC_{Cu(II),pheHA}\text{-}5]$(adipate) Ln = Gd, La, Dy.	pheHA = phenylalanine hydroxamic acid	70
46	$Ga(H_2O)_4[15MC_{CuGlyha}\text{-}5](Cl)_3$	Glyha = glycinehydroxamic acid	71
47	$Ln(III)[15\text{-}MC_{Zn(II),picHA}\text{-}5](NO_3)_3$ Ln = Gd, Nd, Eu or La.	Picha = picoline hydroxamic acid	62
48	$Ln(III)[12\text{-}MC_{Zn(II),quinHA\text{-}4}]_2[24\text{-}MC_{Zn(II),quinHA}\text{-}8]$ Ln(III) = Y, Nd, Eu, Gd, Tb, Dy, Er, Yb.	quinHA = quinaldichydroxamic acid	72
49	$K[NiL_2H_{-1}]\cdot 5/3\ H_2O$	LH = α-aminohydroxamic acids	58
50	$[\{Pt(en)\}_2(\mu\text{-bha})]ClO_4\cdot H_2O$	en = ethane-1,2-diamine bha = benzohydroxamic acid	73
51	$[\{Pt(\textit{R},\textit{R}\text{-chxn})\}_2(\mu\text{-bha})]NO_3\cdot 2H_2O$	chxn = cyclohexane-1,2-diamine bha = benzohydroxamic acid	73
52	$[Fe(II)_2(L_1H)_4Cl_2]$.2MeCN (**2**)	L_1H_2 = 2-(acetoxy)phenyl hydroxamic acid	**This work**
53	$[Co(III)Co(II)_6(L_1H)_8(L_1)_2(MeOH)_4(NO_3)_2]NO_3\cdot 3.5H_2O\cdot 14MeOH$ (**3**)	L_1H_2 = 2-(acetoxy)phenyl hydroxamic acid	**This work**
54	$[Cu(II)_5(L_4)_4(NO_3)_2]\cdot 3H_2O$ (**8**)	L_4H_2 = 2-(methylamino)phenyl hydroxamic acid	**This work**
55	$[Cu(II)_5(L_5H)_4(MeOH)_2](NO_3)_2.3H_2O\cdot 4$ MeOH (**10**)	L_5H_3 = *N*-hydroxy-2-[(2-hydroxy-3-methoxybenzyl)amino]benzamide	**This work**
56	$[Dy(III)_2(L_1H)_2(H_2O)_4(NO_3)_4]$ (**13**)	L_1H_2 = 2-(acetoxy)phenyl hydroxamic acid	**This work**
57	$[Gd(III)_2(L_1H)_2(H_2O)_4(NO_3)_4]$ (**14**)	L_1H_2 = 2-(acetoxy)phenyl hydroxamic acid	**This work**

Table A3 Coordination polymers constructed with hydroxamic acids (valid at the time of writing).

No.	Complex	Meanings of abbreviated Ligand(s)	Reference
1	$[Cu_3(3\text{-}NH_2\text{-}bhaH)_4(H_2O)SO_4]_n \cdot 8H_2O$	3-NH_2-bha = 3-amino-benzohydroxamic acid	19
2	$\{[C^{II}(AcO)Py]_2\{Cu^{II}[12\text{-}MC_{Cu^{II},hinHA}\text{-}4]\}\}_n$	H_3hinHA = 3-hydroxy isonicotine hydroxamic acid	74
3	$[Cu(3\text{-}HPicHA)_2(ClO_4)_2]$	3-HPicHA = 3-picolinehydroxamic acids	75
4	$[\{Cu(4\text{-}HPicHA)(bpy)(ClO_4)\}_2](ClO_4)_2$	4- HPicHA = 4-picolinehydroxamic acids	75
5	$[Cu(3\text{-}PicHA)(phen)]_n(ClO_4)_n$	3-HPicHA = 3-picolinehydroxamic acids	75
6	$[Cu(4\text{-}PicHA)(bpy)]_n(OH)_n \cdot 3.25nH_2O$	4- HPicHA = 4-picolinehydroxamic acids	75
7	$[Cu(4\text{-}PicHA)(DMSO)_2]_{2n}(ClO_4)_{2n}$,	4- HPicHA = 4-picolinehydroxamic acids	75
8	$[Cu(3\text{-}PicHA)(DMSO)(ClO_4)]_{nm} \cdot nm$DMSO,	3-HPicHA = 3-picolinehydroxamic acids	75
9	$[\{Cu(4\text{-}PicHA)(phen)\}_2]_n(ClO_4)_{2n.}$	4- HPicHA = 4-picolinehydroxamic acids	75
10	$\{[Cu(II)_5(2\text{-}dm\text{-}pha)_4(4,4'\text{-}bipy)_3](ClO_4)_2 \cdot (H_2O)\}_n$	2-dm-phaH_2 = 2-(dimethylamino)phenylhydroxamic acid 4,4-bipy = 4,4-bipyridyl	59
11	$\{[Cu(II)_5(2\text{-}dm\text{-}pha)_4(4,4'\text{-}azp)_2(MeOH)_2](ClO_4)_2\}_n$	2-dm-phaH_2 = 2-(dimethylamino)phenylhydroxamic acid 4,4-azp = 4,4-azopyridine	59
12	$\{[Cu(II)_5(2\text{-}am\text{-}pha)_4(pz)_2(MeOH)_3](ClO_4)_2 \cdot MeOH\}_n$	2-am-phaH_2 = 2-(amino)phenylhydroxamic acid pz = pyrazine	59
13	$[Cu(en)_2(H_2O)_2]_n[Cu(en)_2(H_2O)(m\text{-}H_2O)\{Cu_5(L_4H_4)(H_2O)_3\}_2]_n 20_n H_2O$	H_2L = malonomonohydroxamic acid en = 1,2-diaminoethane	76
14	$[Zn(4\text{-}Apha)(CH_3COO)]_n$	4-AphaH = 4-aminophenylhydroxamic acid	53
15	$[Zn_4(4\text{-}Apha)_4(CH_3COO)_4(H_2O)]_n \cdot 2nCH_3OH$	4-AphaH = 4-aminophenylhydroxamic acid	53
16	$[Mn(Hbha)_2]_n \cdot (2MeOH)_n$	H_2bha = benzohydroxamic acid;	56
17	$\{cis\text{-}[Pt(NH_3)_2(l\text{-}3\text{-}pyha)M(l\text{-}3\text{-}pyha)] \cdot SO_4 \cdot xH_2O\}_n$ M = Cu(II), Ni(II) or Zn(II)	3-pyhaH = 3-pyridinehydroxamic acid	77

18	{cis-[Pt(NH_3)$_2$-(l-4-pyha)M(l-4-pyha)]·SO_4·xH_2O}$_n$	4-pyhaH = 4-pyridinehydroxamic acid M = Cu(II), Ni(II) or Zn(II)	77
19	{cis-[Pt-(NH_3)$_2$(l-3-pyha)Cu(l-3-pyha)]SO_4·8H_2O}$_n$	3-pyhaH = 3-pyridinehydroxamic acid	77
20	[Cd(4-Apha)$_2$]$_n$	4-AphaH = 4-aminophenylhydroxamic acid	53
21	[{Sm(NO_3)}{15-MC$_{Cu^{II}N(L\text{-}pheHA)}$-5}]($NO_3$)$_2$	L-H_2pheHA = L-phenylalanine hydroxamic Acid	78
22	[Ln(TREN-1,2-HOIQO)(H_2O)].MeOH Ln = Ce, Eu, Gd, Lu	1,2-HOIQO = 2-hydroxy-2*H*-isoquinolin-1-one TREN = Tris(2-aminoethyl)amine	79
23	{[Zn(II)$_2$(L_1H)$_2$(H_2O)$_5$](NO_3)$_2$}$_n$ (**6**)	L_1H_2 =2-(acetoxy)phenyl hydroxamic acid	**This work**
	{[Cu(II)(L_2H)(H_2O)(NO_3)]·H_2O}$_n$ (**7**)	L_2H_2 = 4-amino-2-(acetoxy)phenylhydroxamic acid	**This work**
24	{[Zn(II)(L_4H)$_2$]·2MeOH}$_n$ (**9**)	L_4H_2 = 2-(methylamino)phenyl hydroxamic acid	**This work**
25	[Cu(II)(L_6H_2)$_2$]$_n$ (**11**)	L_7H_3 = N-hydroxy-4-((2-hydroxy-3-methoxybenzyl)amino)benzamide	**This work**
26	{[Cu(II)(L_7H_2)$_2$].2MeOH}$_n$ (**12**)	L_7H_3 = N-hydroxy-4-((2-hydroxybenzyl)amino)benzamide	**This work**

Appendix B

^{1}H NMR of 2-(amino)phenylhydroxamic acid (PC1)

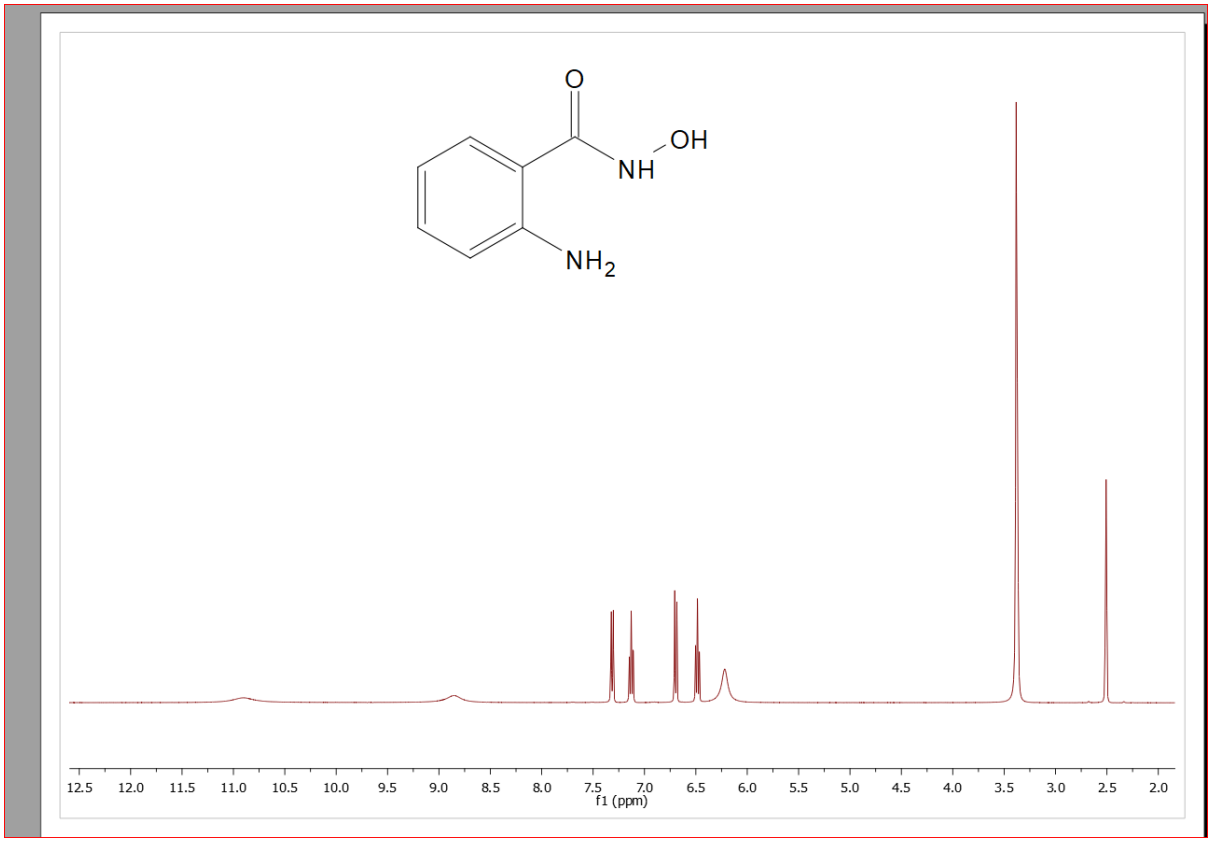

^{13}C NMR of 2-(amino)phenylhydroxamic acid (PC1)

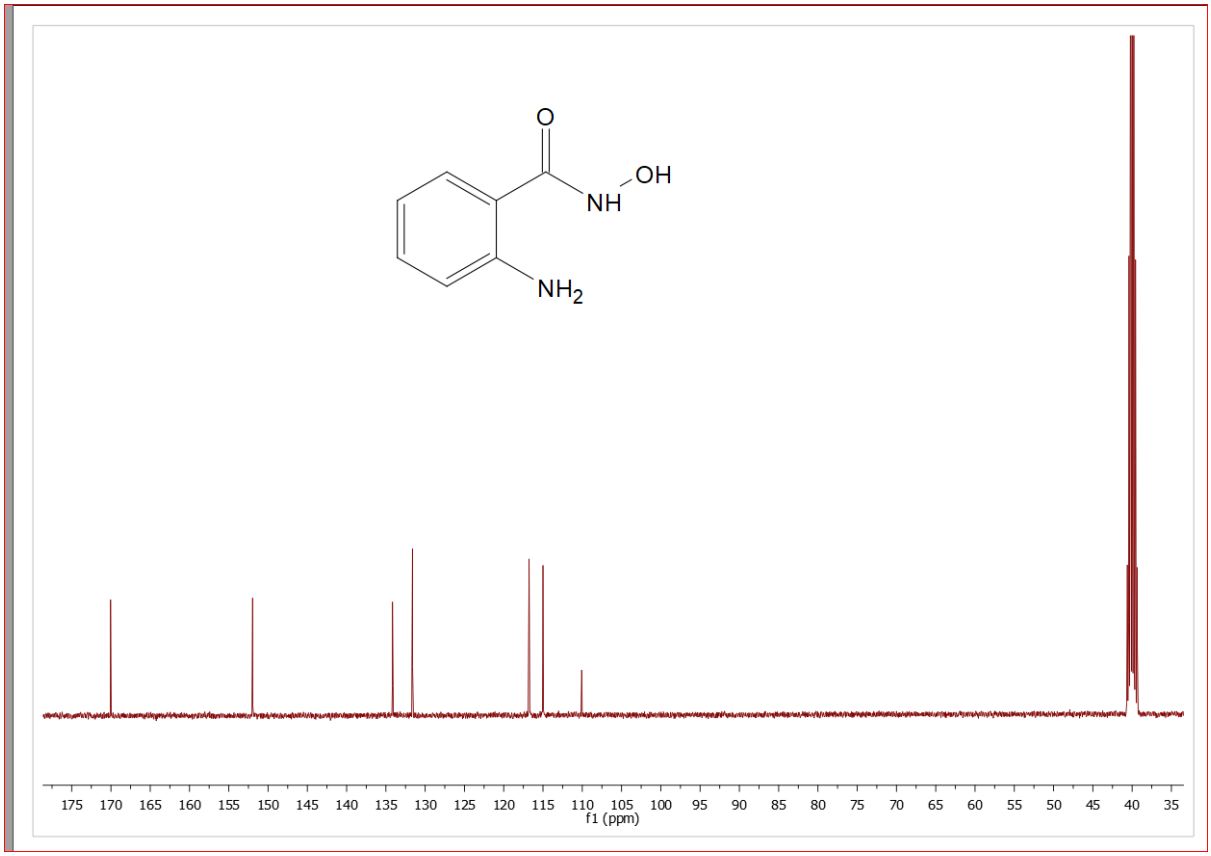

^{1}H NMR of 4-(amino)phenylhydroxamic acid (PC2)

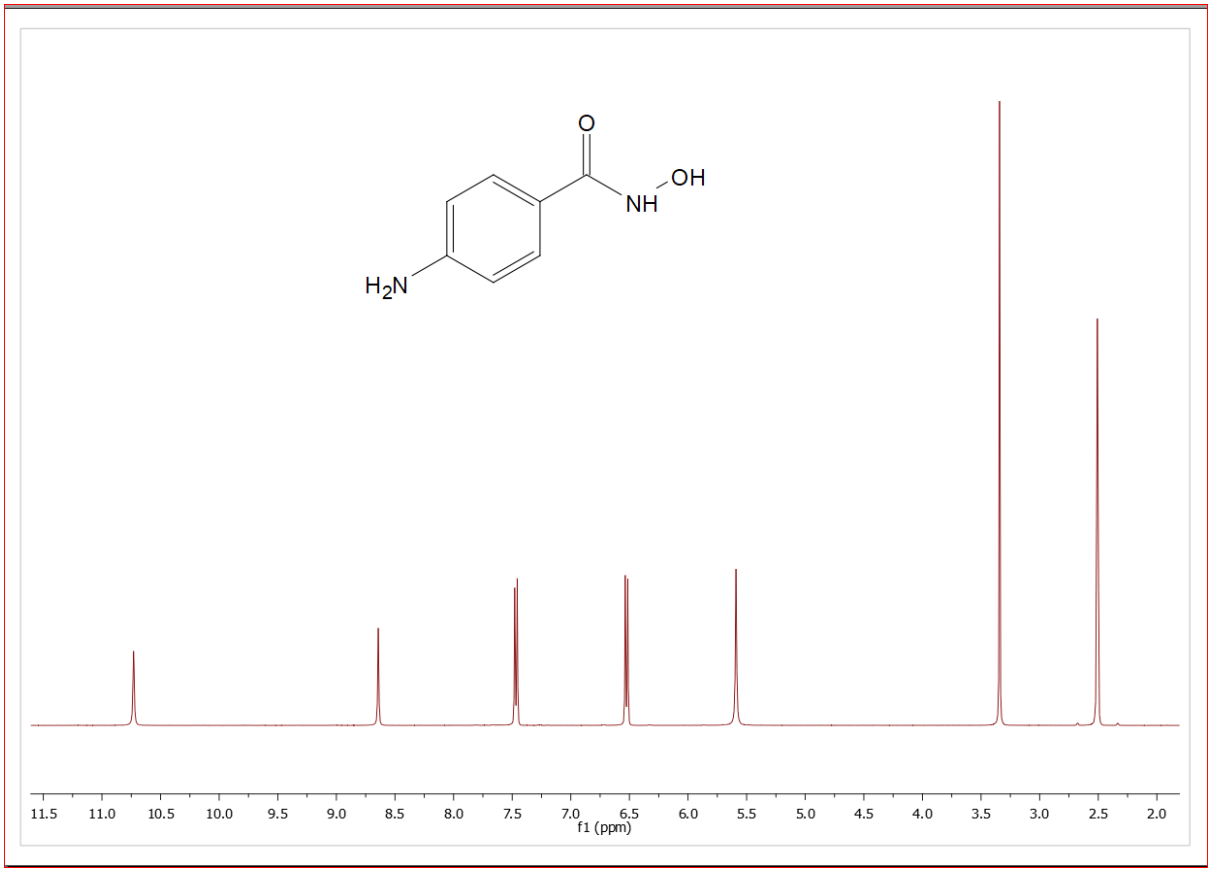

^{13}C NMR of 4-(amino)phenylhydroxamic acid (PC2)

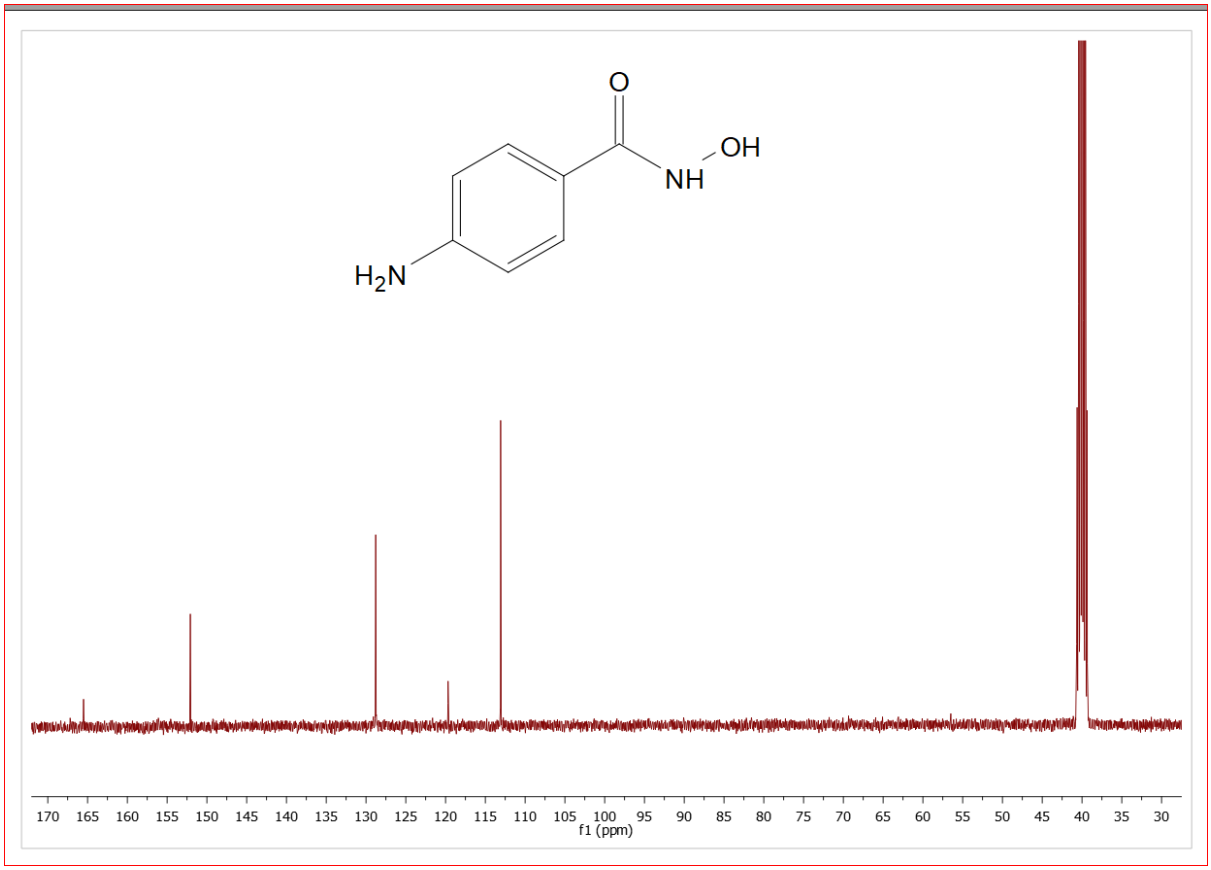

^{1}H NMR of 2-(acetoxy)phenyl hydroxamic acid (L_1H_2)

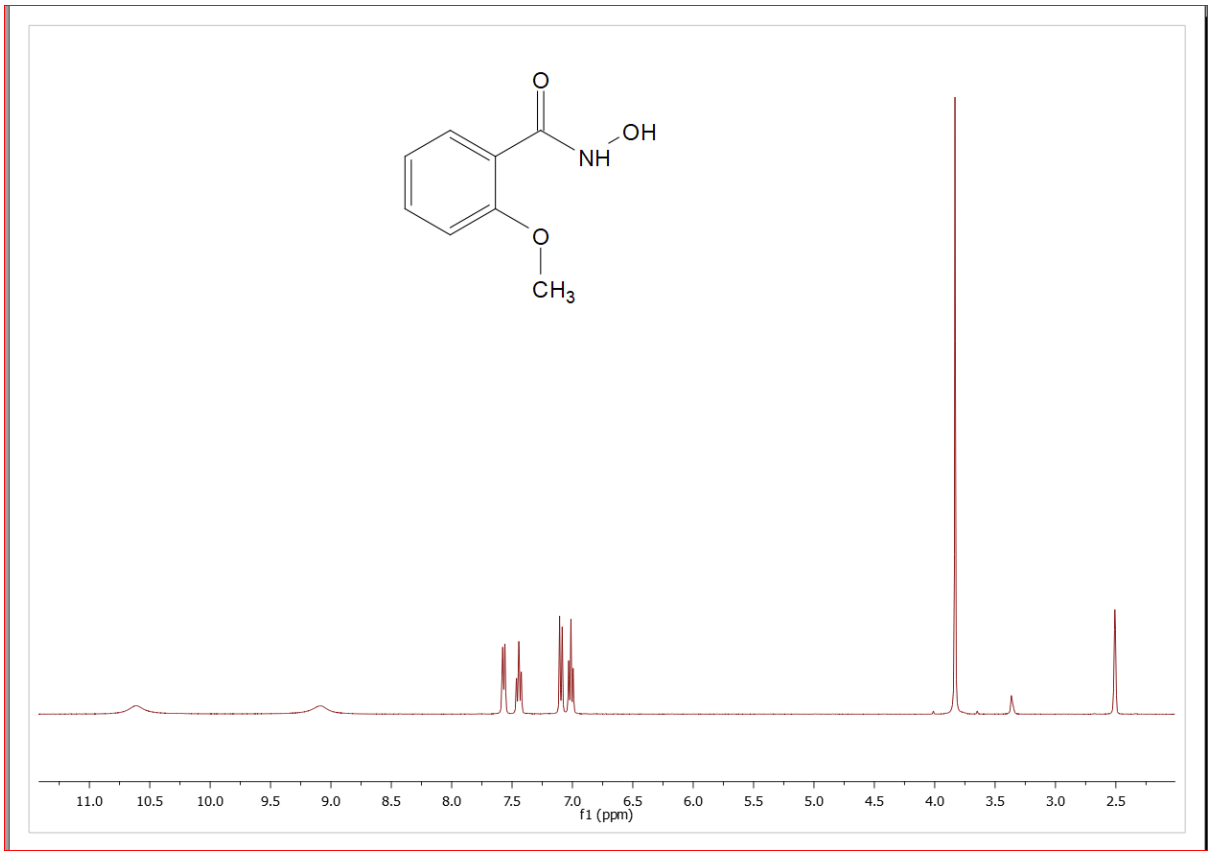

^{13}C NMR of 2-(acetoxy)phenyl hydroxamic acid (L_1H_2)

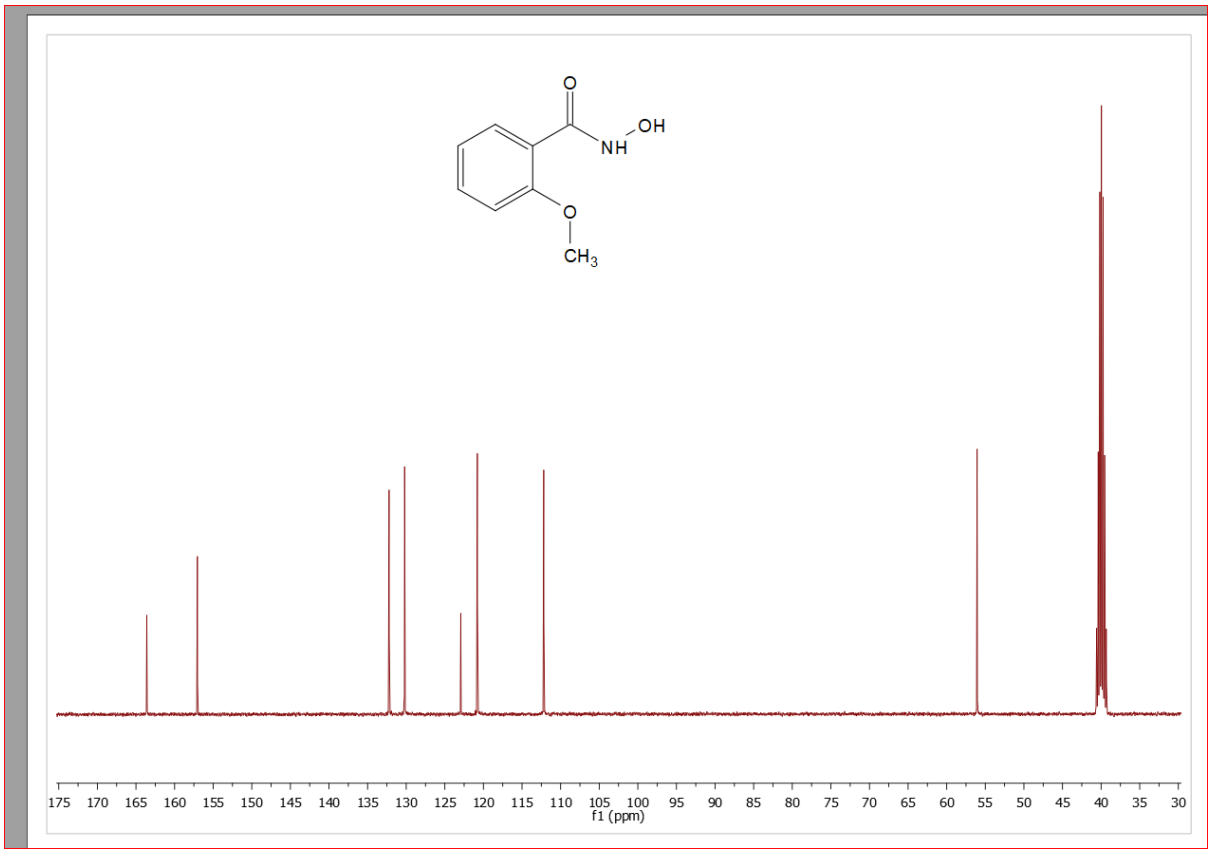

^{1}H NMR of 4-amino-2-methoxyphenylhydroxamic acid (L_2H_2)

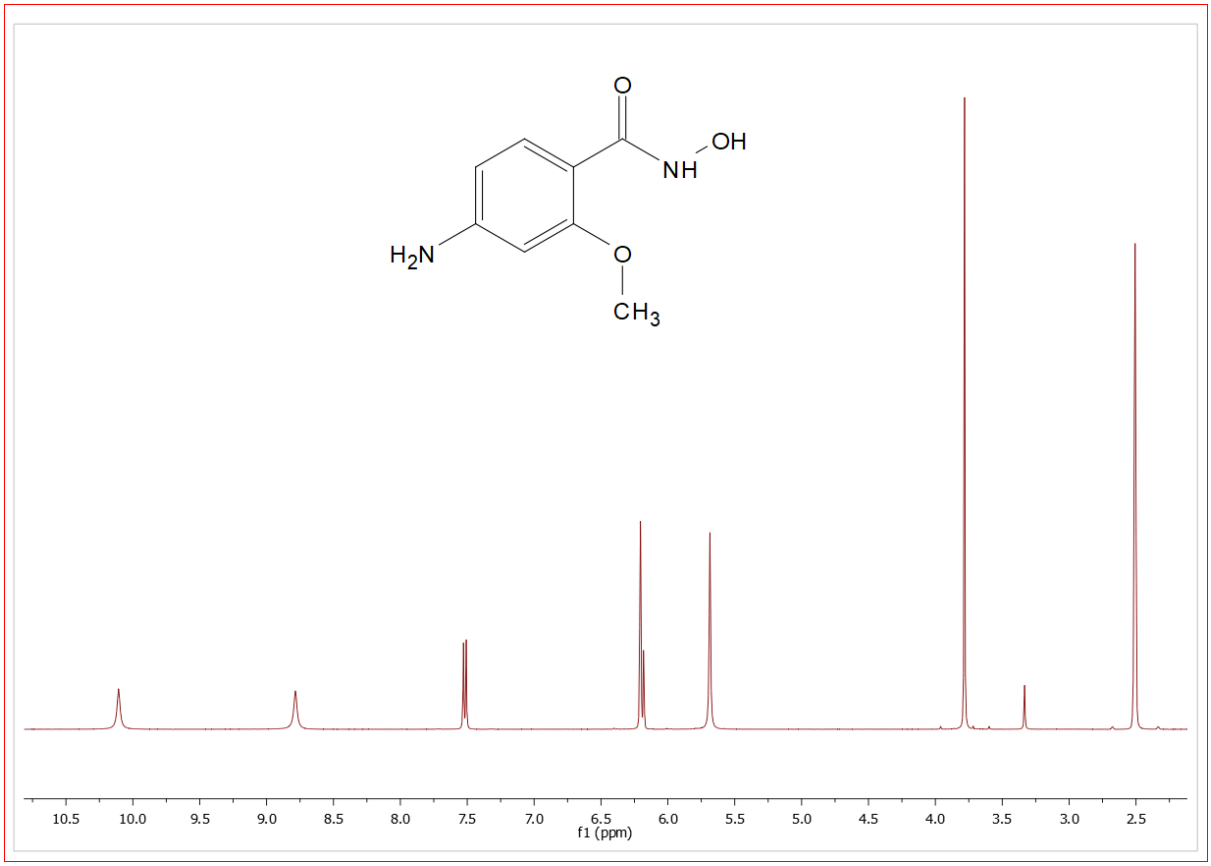

^{13}C NMR of 4-amino-2-methoxyphenylhydroxamic acid (L_2H_2)

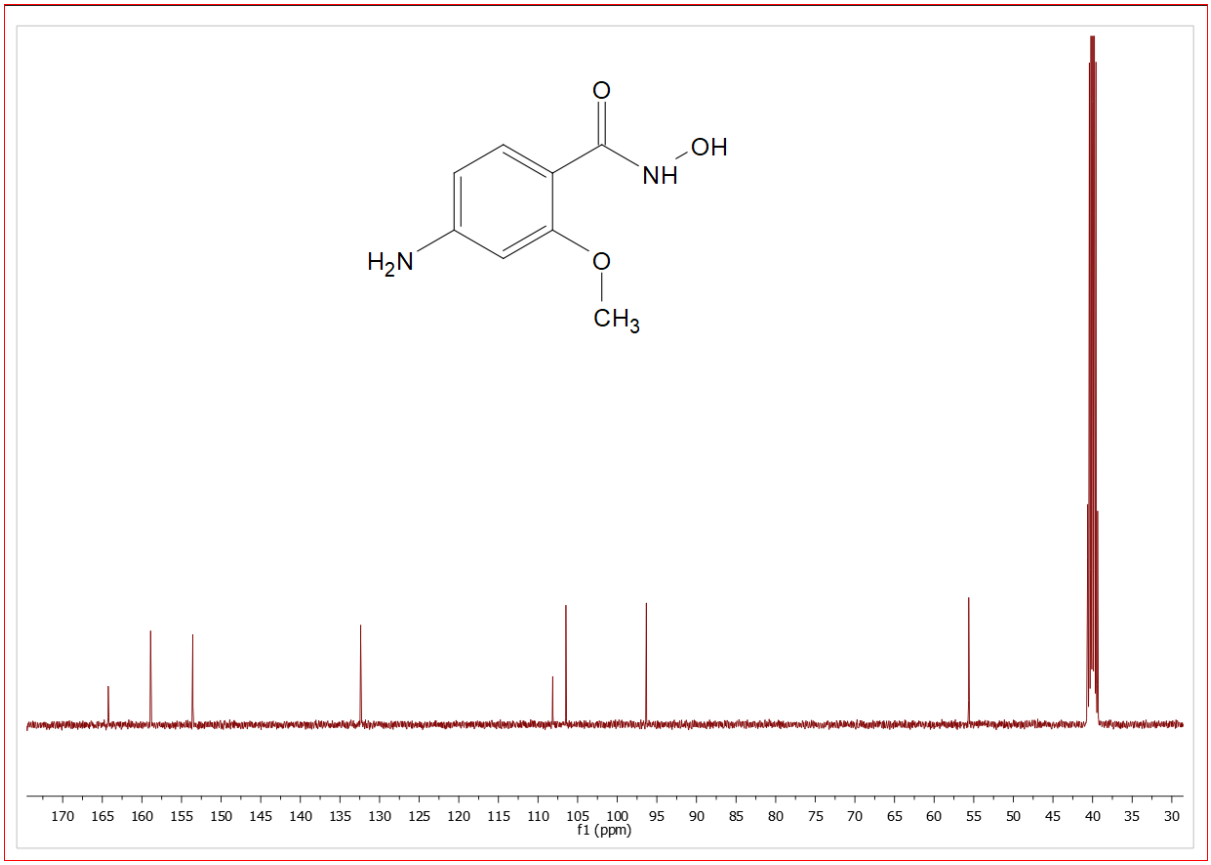

^{1}H NMR of 2-(methylamino)phenylhydroxamic acid (L_4H_2)

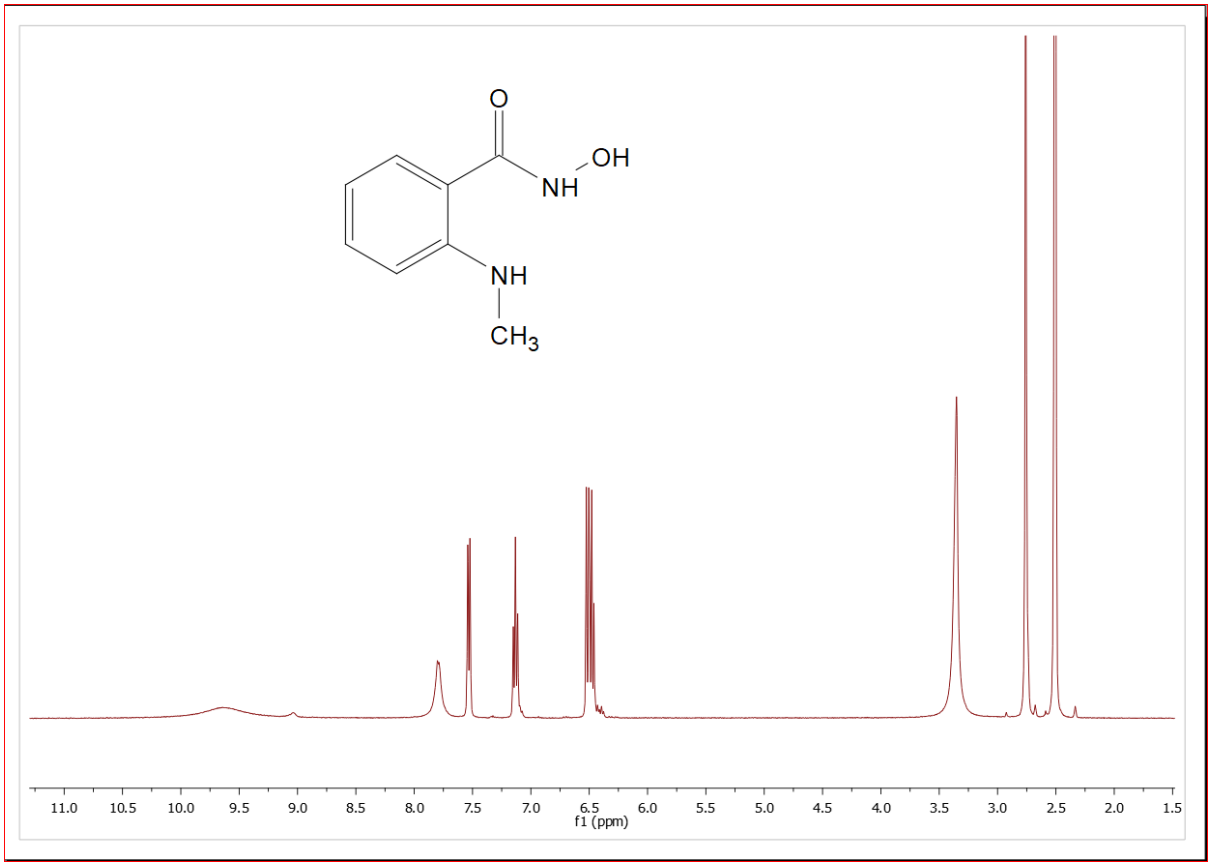

^{13}C NMR of 2-(methylamino)phenylhydroxamic acid (L_4H_2)

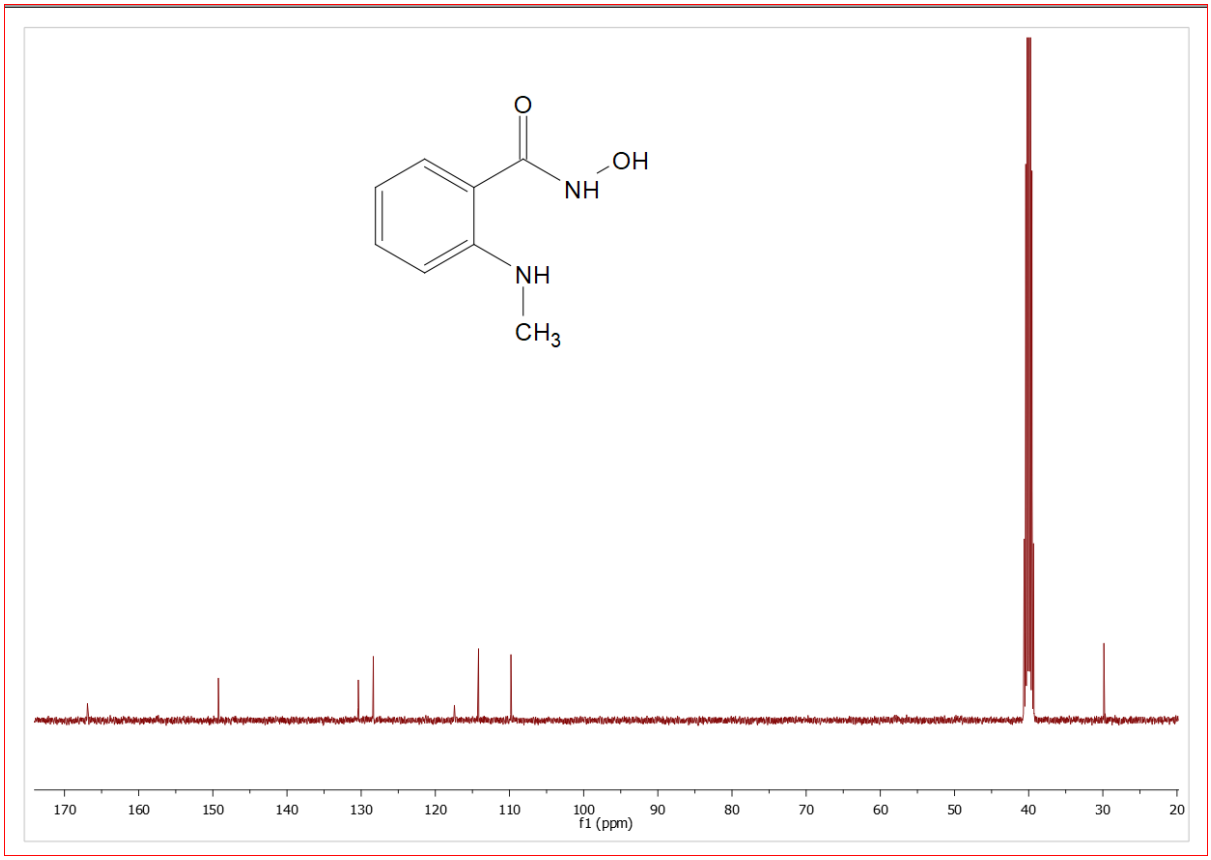

^{1}H NMR of (N-hydroxy-2-((2-hydroxy-3-methoxybenzyl)amino)benzamide (L_5H_3)

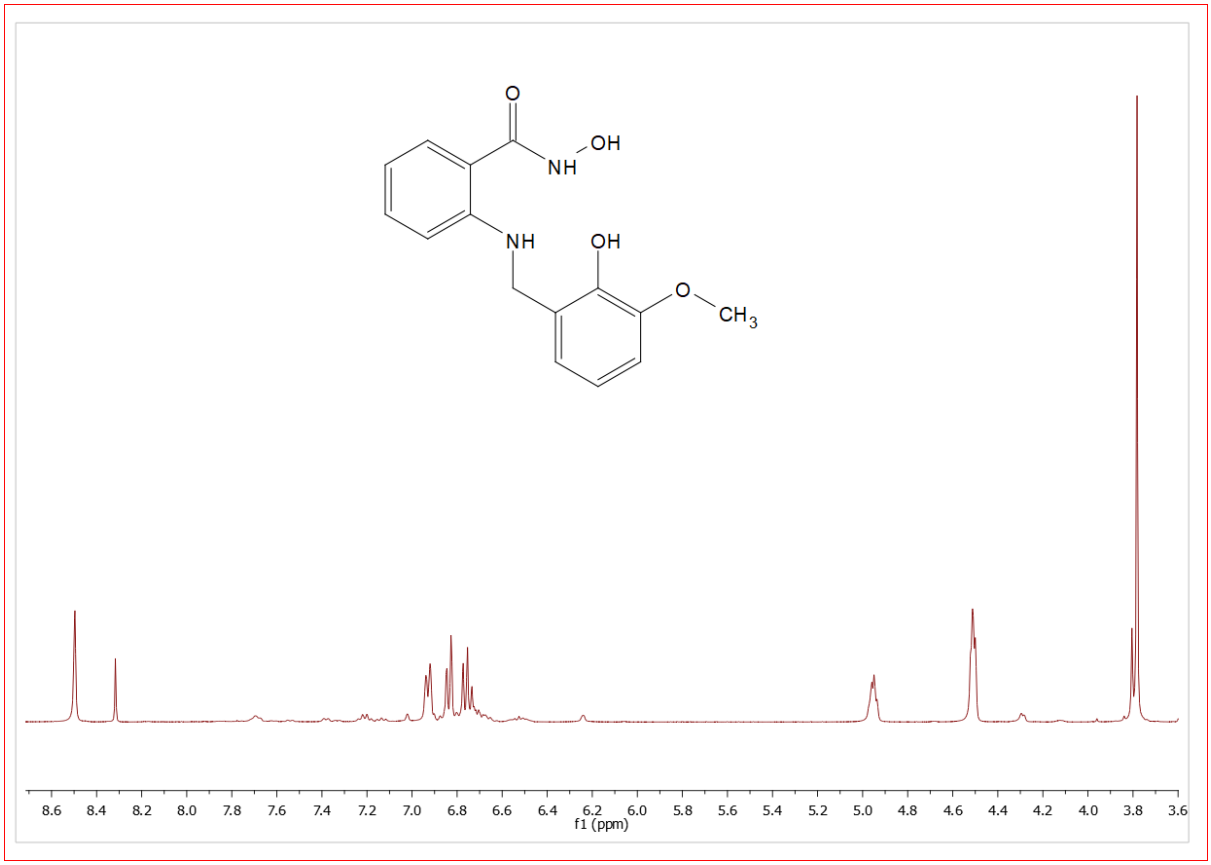

^{13}C NMR of (N-hydroxy-2-((2-hydroxy-3-methoxybenzyl)amino)benzamide (L_5H_3)

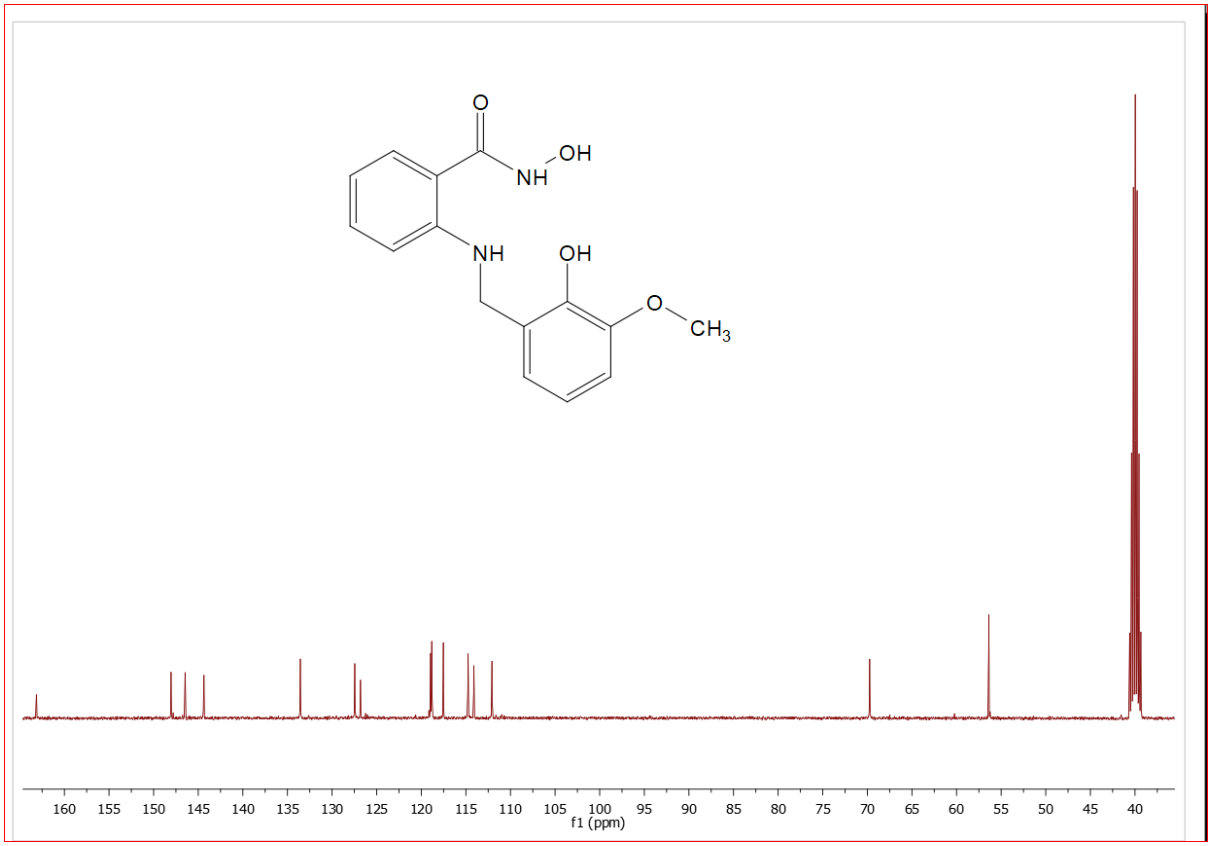

^{1}H NMR of 4-((2-hydroxy-3-methoxybenzyl)amino)-N-hydroxybenzamide (L_6H_3)

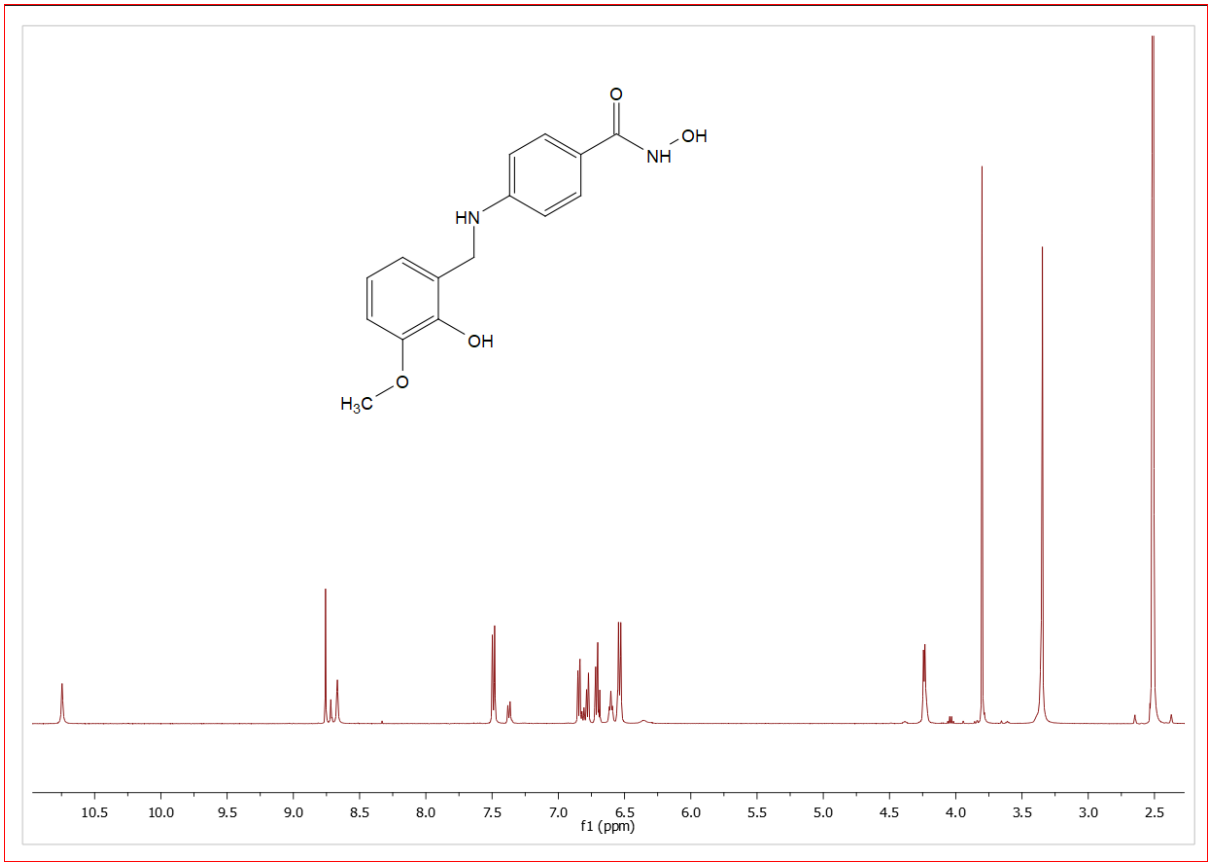

15minDEPTQb of 4-((2-hydroxy-3-methoxybenzyl)amino)-N-hydroxybenzamide (L_6H_3)

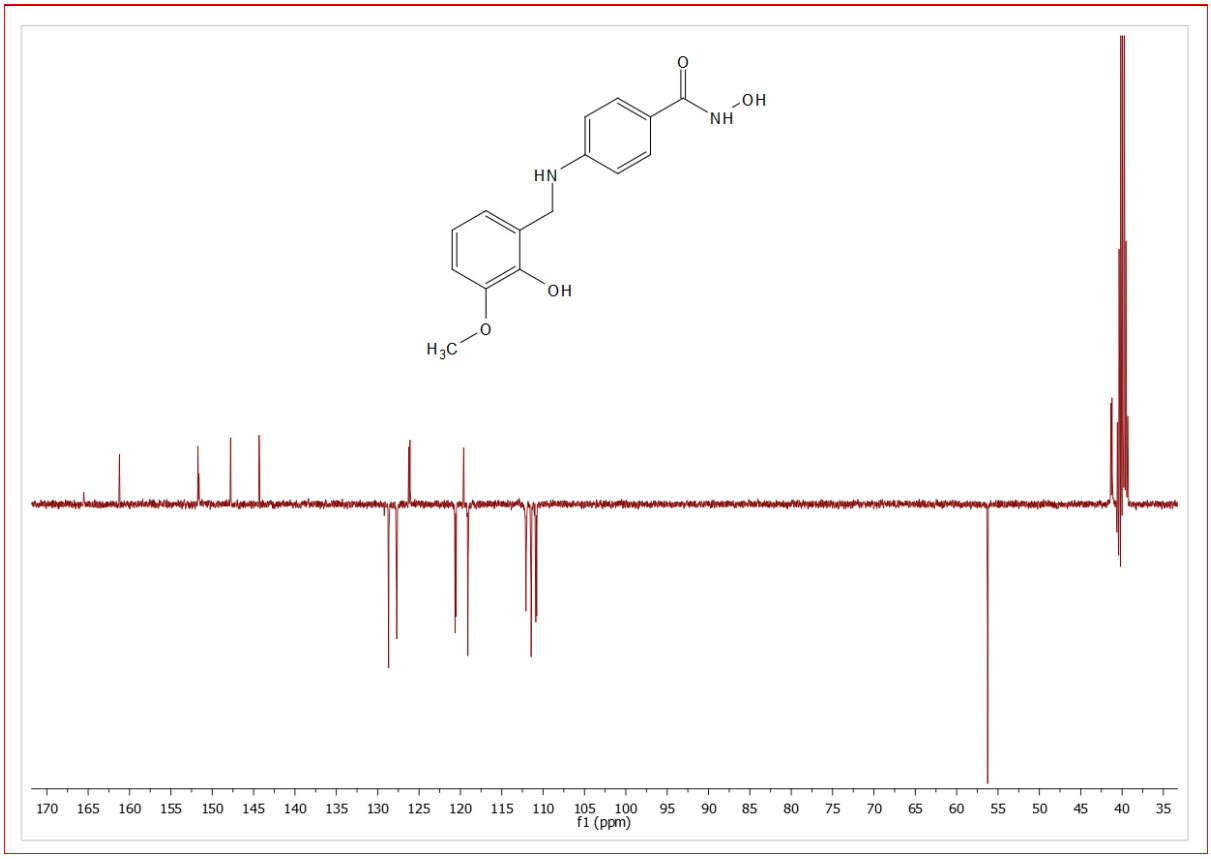

^{1}H NMR of N-hydroxy-4-((2-hydroxybenzyl)amino)benzamide (L_7H_3)

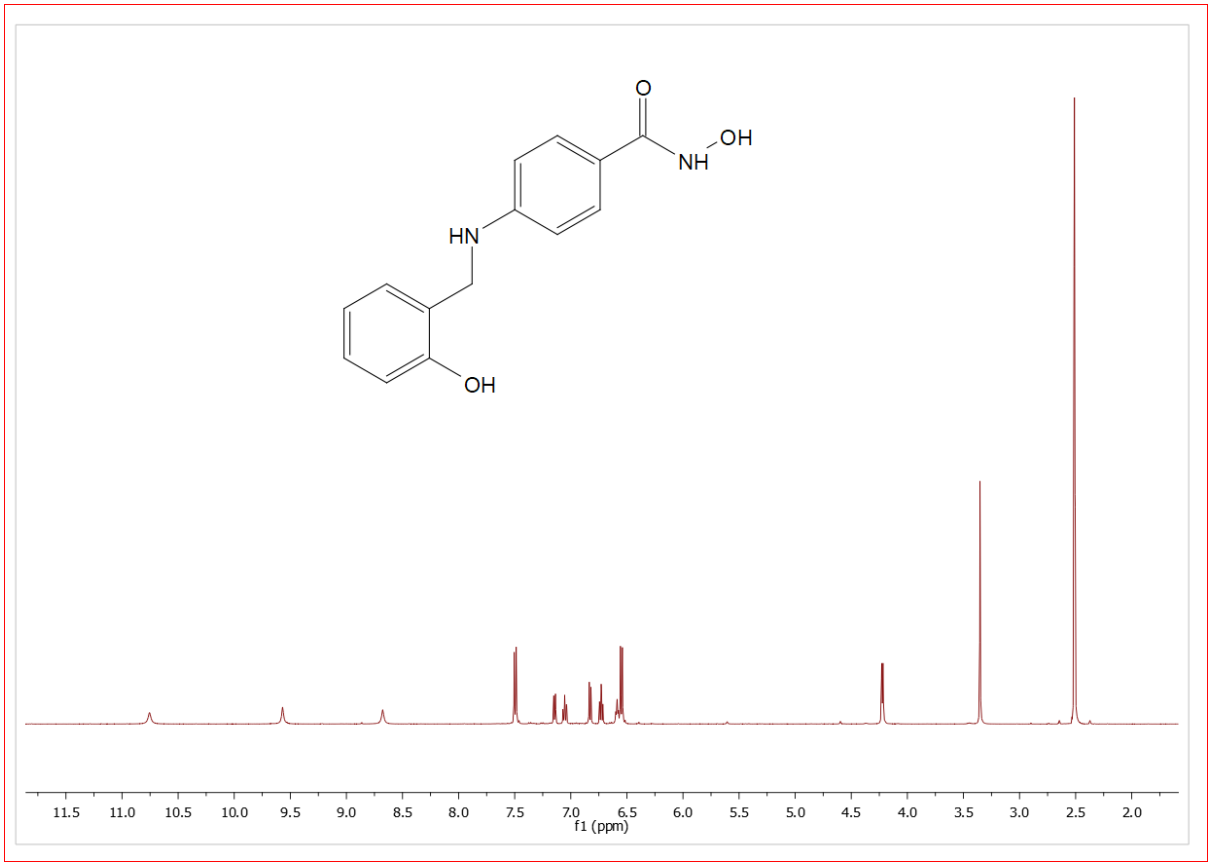

15minDEPTQb of N-hydroxy-4-((2-hydroxybenzyl)amino)benzamide (L_7H_3)

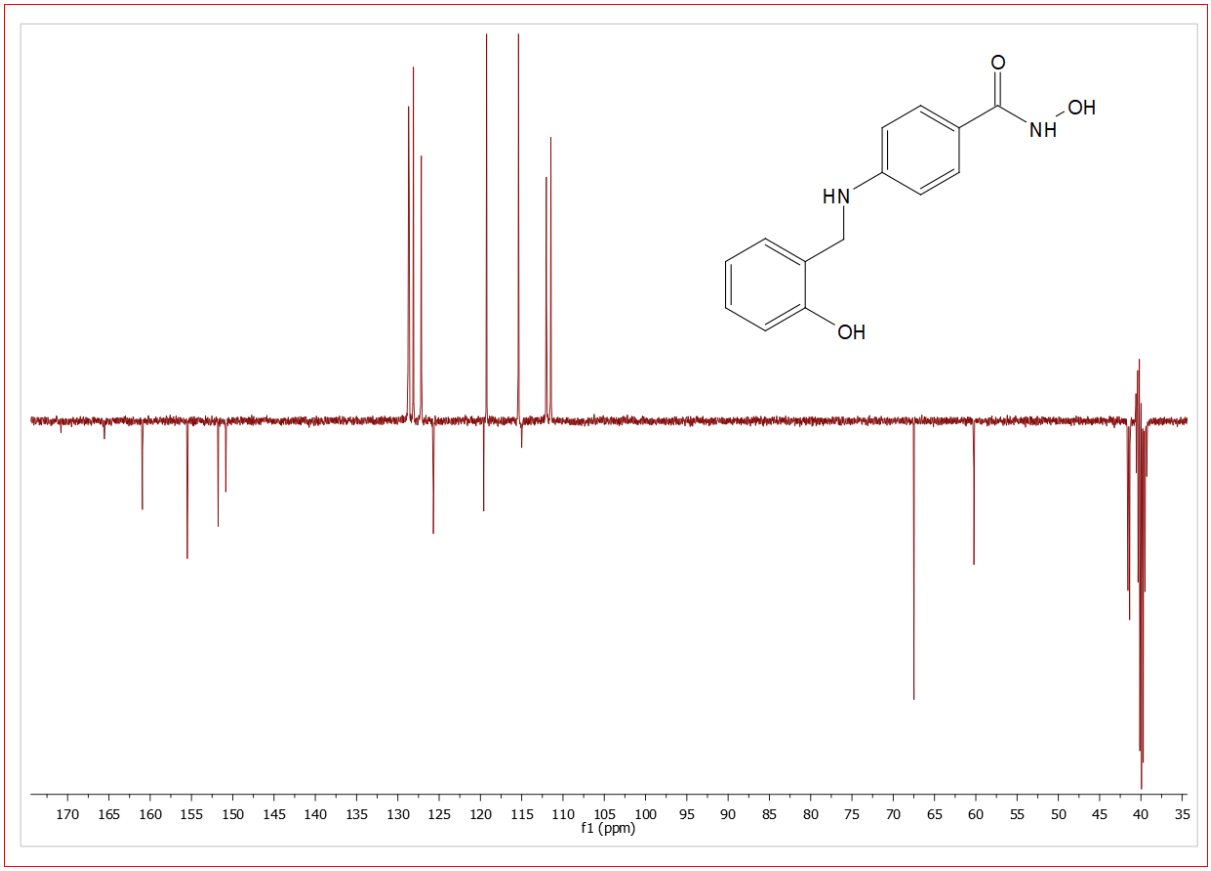

4.5 References (appendices)

1. A.T. de Figueiredo, V.M. Deflon, K.E. Bessler, C. Maichle-Mossmer and U. Abram. *Polyhedron*, 2002, **21**, 2351.
2. A. Biller, C. Burschka, M. Penka and R. Tacke. *Inorg. Chem*., 2002, **41**, 3901.
3. R. Tacke, R. Bertermann, A. Biller, O. Dannappel, M. Penka, M. Pulm and R. Willeke. *Z. Anorg, Allg. Chem*., 2000, **626**, 1159.
4. K. Abu-Dari, J.D. Ekstrand, D.P. Freyberg and K.N. Raymond. *Inorg. Chem.*, 1979, **18**, 108-112.
5. K. Abu-Dari and K. N. Raymond. *Inorg. Chem.*, 1980, **19**, 2034.
6. T. W. Failes and T. W. Hambley. *Aus. J. Chem.*, 2000, **53**, 879-881.
7. A. Dietrich, K. A. Fidelis, D. R. Powell, D. van Der Helm and D. L. Eng-Wilmot. *J. Chem. Soc., Dalton Trans.* 1991, 231.
8. R. R. Mocherla, D. R. Powell, C. L. Barnes and D. van der Helm. *Acta Crys-tallogr*., 1983, **39**, 868.
9. L. Cheng, M. A. Khan, R. W. Taylor, G. B. Richter-Addo and D. R. Powell. *Chem. Commun.*, 1999, 1941.
10. K. Abu-Dari, S. J. Barclay, P. E. Riley and K. N. Raymond. *Inorg. Chem.*, 1983, **22**, 3085.
11. T. W. Failes and T. W. Hambley. *Dalton Trans*., 2006, 1895.
12. T. W. Failes, C. Cullinane, C. I. Diakos, N. Yamamoto, J. G. Lyons and T. W. Hambley. *Chem. Eur. J.*, 2007, **13**, 2974.
13. M. M. Makowska-Grzyska, E. Szajna, C. Shipley, A. M. Arif, M. H.Mitchell, J. A. Halfen and L. M. Berreau. *Inorg. Chem.*, 2003, **42**, 7472.
14. M. D. Santana, G. Garcia, J. Perez, E. Molins and G. Lopez. *Inorg.Chem*., 2001, 40, 5701.
15. K. Rudzka, M. M. Makowska-Grzyska, E. Szajna, A. M. Arif and L. M. Berreau. *Chem. Commun.*, 2005, 489.
16. J. Świątek-Kozlowska, E. Gumienna-Kontecka, A. Dobosz, I. A. Golenya and I. O. Fritsky. *J. Chem. Soc., Dalton Trans.*, 2002, 4639-4643.
17. R. G. Baughman, D. J. Brink, J. M. Butler and P. R. New. *Acta Crystallogr.*, 2000, **56**, 528.
18. C. Otilla, B. Miranda-Pinto, E. B. Paniago, S. Carbalho, M. Tabak and Y. P. Mascarenhas. *Inorg. Chimica Acta,* 1987, **137**, 145-149.

19. D. Gaynor, Z. A. Starikova, W. Haase and K. B. Nolan. *Dalton Trans.*, 2001, 1578-1581.
20. K. Goleva, D. Naumova, A. Paylishchuk, A. W. Addison and M. Zeller. *Acta Cryst. E. Commun*., 2018, **74**, 1384–1387.
21. S. G¨ottlicher and H. Paulus. *Chem. Berl.*, 1982, **115**, 393.
22. D. A. Brown, W. Errington, N. J. Fitzpatrick, W. K. Glass, T. J. Kemp, H. Nimir and A. T. Ryan. *Chem. Commun.*, 2002, 1210.
23. D. T. Puerta and S. M. Cohen. *Inorg. Chem.*, 2002, 41, 5075.
24. B. A. Borgias, S. J. Barclay and K. N. Raymond. *J. Coord. Chem.*, 1986, **15**, 109.
25. C. A. Matsuba, S. J. Rettig and C. Orvig. *Can. J. Chem*., 1988, **66**, 1809.
26. D. Tranqui, J. Laugier, P. Boyer and P. Vulliet. *Acta Crystallogr*. 1978, **4**, 767.
27. W. L. Smith and K. N. Raymond. *J. Am. Chem. Soc*., 1981, **103**, 3341.
28. D. C. Fisher, S. J. Barclay-Peet, C. A. Balfe and K. N. Raymond. *Inorg. Chem.*, 1989, **28**, 4399.
29. M. Haratake, M. Fukunaga, M. Ono and M. Nakayama. *J. Biol. Inorg. Chem.*, 2005, **10**, 250.
30. W. Chen, S. Gao and S.-X. Liu. *Acta Crystallogr.*, 1999, 55, 531.
31. C. R. Cornman, G. J. Colpas, J. D. Hoeschele, J. Kampf and V. L. Pecoraro. *J. Am. Chem. Soc*., 1992, **114**, 9925.
32. S. Gao, J. W. Liu, L. H. Huo and H. Zhao. *Acta Crystallogr*., 2004, 60, 1722.
33. M. Ostrowska, I. O. Fritsky, E. Gumienna-Kontecka and A. V. Pavlishchuk. *Coord. Chem. Rev.*, 2016, **327**, 304-332.
34. G. A. Brewer and E. Sinn. *Inorg. Chem.*, 1981, **20**, 1823.
35. D. A. Brown, H. Bogge, R. Coogan, D. Doocey, T. J. Kemp, A. Müller and B. Neumann. *Inorg. Chem*., 1996, **35**, 1674.
36. E. Farkas, H. Csóka, G. S. Bell, D. A. Brown, L. P. Cuffe, N. J. Fitzpatrick, W. K. Glass, W. Errington and T. J. Kemp. *J. Chem. Soc., Dalton Trans.*, 1999, 2789.
37. S. P. Lin, M. A. Khan and K. M. Nicholas. *J. Chem. Soc., Chem. Commun.*, 1994, 2425.
38. K. Wieghardt, W. Holzbach, E. Hofer and J. Weiss. *Inorg. Chem*., 1981, **20**, 1343.
39. J. Comiskey, E. Farkas, K. A. Krot-Lacina, R. G. Pritchard, C. A. McAuliffe and K. B. Nolan. *Dalton Trans.*, 2003, 4243-4249.
40. A. Das, F. Basuli, S. M. Peng and S. Bhattacharya. *Inorg. Chem.*, 2002, **41**, 440.
41. Q. Li, M. F. C. Guedes Da Silva and A. J. L. Pombeiro. *Chem. Eur. J*., 2004, **10**, 1456.
42. T. J. King and P. G. Harrison. *J. Chem. Soc., Chem. Commun.*, 1972, 815.

43. P. Zheng, M. Cui, Y. Gu and X. Jin. *Acta Chim. Sin*., 1985, **43**, 389.
44. B. Haymore, J. C. Huffman, A. Dobson and S. D. Robinson. *Inorg. Chim. Acta*., 1982, **65**, 231.
45. T. W. Failes and T. W. Hambley. *Aust. J. Chem.*, 2003, **56**, 45.
46. M. D. Hall, T. W. Failes, D. E. Hibbs and T. W. Hambley. *Inorg. Chem.*, 2002, **41**, 1223.
47. D. Griffith, K. Lyssenko, P. Jensen, P. E. Kruger and C. J. Marmion. *Dalton Trans.*, 2005, 956.
48. U. Casellato, P. A. Vigato, S. Tamburini, R. Graziani and M. Vidali. *Inorg.Chim. Acta.*, 1984, **81**, 47.
49. A. J. Stemmler, J. W. Kampf, M. L. Kirk and V. L. Pecoraro. *J. Am. Chem. Soc.*, 1995, **117**, 6368.
50. M. Arnold, D. A. Brown, O. Deeg, W. Errington, W. Haase, K. Herlihy, T. J. Kemp, H. Nimir and R. Werner. *Inorg. Chem*., 1998, **37**, 2920.
51. C. McDonald, S. Sanz, E. K. Brechin, M. K. Singh, G. Rajaraman, D. Gaynor and L. F. Jones. *RSC Advances*, 2014, **4**, 38182.
52. D. Gaynor, Z. A. Starikova, S. Ostrovsky, W. Haase and K. B. Nolan. *Chem. Commun*., 2002, 506–507.
53. D. A. Brown, N. J. Fitzpatrick, H. Müller-Bunz and A. T. Ryan. *Inorg. Chem*., 2006, 45, 4497.
54. Y. Chen, Q. Gao, Y. Liu, Y. Cao, D. Gao, J. Liu, J. Zhao, Y. Li, W. Liu and W. Li. *RSC Adv.*, 2014, **4**, 147–153.
55. D. A. Brown, W. Errington, W. K. Glass, W. Haase, T. J. Kemp, H. Nimir, S. M. Ostrovsky and R. Werner. *Inorg. Chem*., 2001, **40**, 5962.
56. Y. Cao, Y. Chen, L. Li, D. Gao, W. Liu, H. Hu, W. Li and Y. Li. *Dalton Trans*, 2013, **42**, 10912–10918.
57. M. S. Lah and V. Pecoraro. *J. Am. Chem. Soc*. 1989, **11**, 7258-7259.
58. A. Tarushi, M. Zampakou, S. Perontsis, K. Lafazanis, A. A. Pantazaki, A. G. Hatzidimitriou and G. D. Geromichalos. *Inorg. Chim. Acta*., 2018, **483**, 579–592.
59. D. Bacco, V. Bertolasi, F. Dallavalle, L. Galliera, N. Marchetti, L. Marchio, M. Remelli and M. Tegon. *Dalton Trans.***,** 2011, **40**, 2491-2501.
60. C. McDonald, T. Whyte, S. M. Taylor, S. Sanz, E. K. Brechin, D. Gaynor and L. F. Jones. *Cryst. Eng. Comm*, 2013, **15**, 6672.

61. C. McDonald, D. W. Williams, P. Comar, S. J. Coles, T. D. Keene, M. B. Pitak, E. K. Brechin and L. F. Jones. *Dalton Trans.*, 2015, **44**, 13359-13368.
62. Y. Wang,W. Wu and M. LingHuang. *Chin. Chem. Lett*., 2016, **27**, 423–427.
63. J. Jankolovits, J. W. Kampf and V. L. Pecoraro. *Polyhedron*, 2013, **52**, 491–499.
64. A. J. Stemmler, J. W. Kampf, M. L. Kirk, B. H. Atasi and V. L. Pecoraro,. *Inorg. Chem*., 1999, **38**, 2807-2817.
65. M. A. Katkova, G. S. Zabrodina, M. S. Muravyeva, A. A. Khrapichev, M. A. Samsonov, G. K. Fukin and S. Y. Ketkov. *Inorg. Chem. Comm*. 2015, **52**, 31–33.
66. K. V. Kremlev, M. A. Samsonov, G. S. Zabrodina, A. V. Arapova, P. A. Yunin, D. A. Tatarsky, P. E. Plyusnin, M. A. Katkova and S. Y. Ketkov. *Polyhedron*, 2016, **114**, 96-100.
67. M. A. Katkova, G. S. Zabrodina, K. V. Kremlev, S. A. Gusev, B. S. Kaverin, A. M. Obiedkov, I. G. Fomina, K. A. Lyssenko and I. L. Eremenko, *Mendeleev Commun*., 2017, **27**, 402–404.
68. J. Jankolovits, J. Kampf and V. Pecoraro, *Chin. Chem. Lett*., 2015, **26**, 444-448.
69. J. Jankolovits, C. M. Andolina, J. W. Kampf, K. N. Raymond and V. L. Pecoraro. *Angew. Chem. Int. Ed*., 2011, **50**, 9660-9664.
70. J. Jankolovits, A. D. Cutland Van-Noord, J. W. Kampf and V. L. Pecoraro. *Dalton Trans*., 2013, **42**, 9803–9808.
71. M. S. Muravyeva, G. S. Zabrodina, M. A. Samsonov, E. A. Kluev, A. A. Khrapichev, M. A. Katkova and I. V. Mukhina, *Polyhedron*, 2016, **114**, 165–171.
72. E. R. Trivedi, S. V. Eliseeva, J. Jankolovits, M. M. Olmstead, S. Petoud and V. L. Pecoraro, *J. Am. Chem. Soc.*, 2014, **136**, 1526−1534.
73. T. W. Failes, M. D. Hall and T. W. Hambley, *Dalton Trans.*, 2003, 1596-1600.
74. C. Atzeri, L. Marchiò, C. Y. Chow, J. W. Kampf, V. L. Pecoraro and M. Tegoni. *Chem. Eur. J.*, 2016, **22**, 6482–6486.
75. I. A. Golenya, E. Gumienna-Kontecka, M. Haukka, O. M. Korsun, O. N. Kalugin and I. O. Fritsky. *Cryst. Eng. Com*., 2014, **16**, 1904–1918.
76. E. Gumienna-Kontecka, I. A. Golenya, N. M. Dudarenko, A. Dobosz, M. Haukka, I. O. Fritsky and J. Swiatek-Kozlowska. *New J. Chem*., 2007, **31**, 1798–1805.
77. C. Mulcahy, F. M. Dolgushin, K. A. Krot, D. Griffith and C. J. Marmion. *Dalton Trans*., 2005, 1993–1998.
78. A. D. Cutland-Van Noord, J. W. Kampf and V. L. Pecoraro. *Angew. Chem. Int. Ed.*, 2002, **41**, 4667-4670.

79. M. Seitz, M. D. Pluth, K. N. Raymond, *Inorg. Chem*., 2017, **56**, 351-353.